University of Glasgow | College of Medical, Veterinary & Life Sciences

Microwaves: a potential new therapy for HPV-positive anogenital lesions?

An investigation into the molecular mechanism of microwave treatment on human papillomavirus replication, cellular transcription and innate immunity.

Anna Kirk, BA (Hons)

Submitted in fulfilment of the requirements for the Degree of Doctor of Philosophy

MRC-Centre for Virus Research
Institute of Infection and Immunity
College of Medical, Veterinary & Life Sciences
University of Glasgow

September 2024

Abstract

Human papillomavirus (HPV) is the most common viral sexually transmitted infection (STI) globally with almost the entire population coming into contact with the virus within a few months to a few years of becoming sexually active. HPV infection at the mucosal epithelium of the anogenital tract is common and infection with a high-risk virus can result in anogenital lesions, which can progress into cervical and other anogenital cancers. Infection with a low-risk HPV type in the anogenital tract can result in genital warts. The incidence of many of these diseases and cancers, for example, anal and oropharyngeal cancers, has increased significantly over the last two decades. The current treatment options for pathologies caused by both high and low-risk HPV have associated side effects including high pain, recurrence rate and risk of complications. Therefore, better treatment options are required. Hyperthermia is a well-documented adjunct to cancer therapy, which is also gaining traction in the treatment of HPV-driven pathologies. Microwaves offer a precise and targeted approach to deliver hyperthermia, and the Emblation Limited Swift® Microwave Tissue Ablation system is currently in use for clinical treatment of plantar warts: cutaneous lesions associated with HPV infection. Microwave ablation is a promising solution to overcome some of the limitations associated with the current treatment options for HPV-positive anogenital lesions but before implementation, an understanding of the molecular mechanisms behind microwave therapy, particularly how it impacts the HPV replication cycle, and the infected host cell must be carried out.

To analyse how microwave-delivered hyperthermia affected the host cell, we examined transcriptional changes following treatment. Microwave treatment rapidly altered the keratinocyte transcriptome, with 59 genes differentially expressed 4 hours post-treatment. Of these genes, 56 were upregulated and 3 were downregulated. At later time points post-treatment, 150 genes were differentially expressed and all of these were upregulated. Microwave treatment triggered a heat shock response and resulted in the upregulation of many chaperones and co-chaperones, which are important in preventing proteolysis following temperature rises. Many of these genes remained significantly upregulated at later time points. Genes involved in immune pathways, including interleukins (*IL8*, *IL20*, *IL24*), interferons (*IFNκ*) and chemokines

(*CCL24*, *CCL26*) were also upregulated following microwave treatment. Analysis of the mRNA expression of IL-6, IL-1β and TNF-α confirmed an upregulation of innate immunity following microwave treatment. The magnitude of this increase was greater in HPV-positive tissues. Microwave-treated tissues secreted a higher concentration of Th-1 cytokines (IL-1β, IL-8, IL-2, TNF-α, IFN-ɣ) in comparison to mock-treated tissues. Th-1 mediated immunity is important for HPV clearance, so this has important implications for the recurrence of pathologies following microwave treatment.

The HPV genome is associated with histones and uses host RNA polymerase II for viral transcription. Therefore, it was hypothesised that HPV transcription may also be affected by microwave treatment. In models containing HPV16 episomes, there was a transient increase in the expression of transcripts encoding the HPV16 early (E6/E7 and E4 containing) and late (E4^L1 and L1 containing) viral transcripts. The magnitude of this increase was greater for transcripts encoding the viral late proteins. An increase in the differentiated compartment of these tissues following microwave treatment was evident through increased transcription of the late epithelial differentiation markers including transglutaminase, keratins (*KRT37* and *KRT75*), corneodesmosomes and late cornified envelope proteins (*LCE3A*, *LCE3C*, LCE3D, *LCE6A*). Following the transient increase, the levels of early and late viral transcripts decreased by 72 hours post-treatment, to levels below that of untreated proteins. Spatial analysis using RNA Scope in situ hybridisation revealed this decrease in viral transcripts occurring first within the treated area and then spreading out radially into the neighbouring tissue. Microwave treatment could also inhibit viral genome replication up to 24 hours post-treatment.

Finally, we sought to investigate if microwave treatment could disrupt virion production. The L1 protein is the structural determinant of the human papillomavirus capsid but its localisation within the nucleus, and how this enables virion assembly in natural models of infection is poorly understood. Using immunofluorescent staining and confocal microscopy, the subcellular localisation of L1 within differentiated keratinocytes from organotypic rafts was examined. Over time, L1 accumulated in the nucleus, the site of virion assembly. The majority of nuclei positive for L1 showed diffuse nuclear staining but as rafts were grown in culture for extended periods, more

cells contained L1 that was localised to subnuclear foci domains. This is similar to previous reports that have identified these sites as promyelocytic leukaemia nuclear bodies (PML-NBs) and proposed that L2, the minor structural protein, directs L1 to these sites once it is expressed at a high level. Electron microscopy analysis of keratinocytes grown in organotypic raft cultures revealed clusters of viral-like particles within the upper, differentiated cells of the tissues. We propose that these clusters may represent the foci of L1 staining observed by confocal microscopy, suggesting that papillomaviruses assemble in subnuclear domains. The intracellular localisation of L1 was disrupted following microwave treatment, which may restrict virion assembly. Further experiments to confirm the presence of viral-like particles with immunogold labelling will validate these findings.

Overall, this thesis builds on previous work that suggests that microwaves are a safe and effective form of treatment for HPV-associated lesions. The data suggests that microwave treatment inhibits human papillomavirus replication and induces an immune response within HPV-infected cells. This provides an argument for the extension of microwaves as a novel treatment option for HPV-positive anogenital lesions. Future research will determine the regrowth of lesions to predict the effectiveness and recurrence rates following treatment.

Table of Contents

List of Tables

List of Figures

List of Supplementary Figures

Acknowledgement

First and foremost, I would like to thank my primary supervisor Professor Sheila Graham for the wealth of knowledge and experience she has brought to the project. I have often heard the phrase ‘a good supervisor is more important to a PhD than a good project’ and I consider myself incredibly fortunate to have had both. Thank you for all of your advice, granting me the flexibility to direct some of the projects myself and for fostering a fantastic lab environment to work in. Thank you also to my secondary supervisor Alfredo Castello for the keen insights he has provided to the project. I am incredibly grateful to Dr Swetha Vijayakrishnan for collaborating with me on the confocal and structural work, for her selfless giving up of time and for contributing her knowledge and enthusiasm to the project.

I would like to acknowledge the current and past members of the Graham group including Andy, Harry, Ilaria, Chris and Maddie. I feel very lucky to have been able to work with so many friendly and supportive individuals. A heartfelt thank you to Andy for going above and beyond as a lab manager and to Harry for being by my side for all the ups and downs that the project contained. I have been lucky to collaborate with many wonderful individuals and facilities during my PhD. Thank you to the histopathology team especially Lynn, Lynn, Fraser and Jess, and Colin and Mark at the Beatson for their help with the RNAScope work. A huge thank you to Colin for his endless help and enthusiasm with microscopy. Thank you to James for helping me to persuade the EM to work (sometimes with difficulty), Quan for his advice with the RNA Sequencing analysis and Julie and Csilla for performing the Illumina sequencing. I am grateful to Hollie for helping me with flow cytometry and Dianne for access to and running the Luminex assays. Thank you to our collaborators at Emblation, particularly Matt Kidd, for providing the Swift® device and the temperature probe and for the insight they have provided.

I am incredibly grateful for the friends that I have met throughout the project. Having such a supportive and friendly cohort to begin a PhD with, in a new city during the pandemic, helped me more than I can put into words. I am glad that so many of us share the same hobbies and I will cherish our memories spent up hills and swimming in lochs. Thank you to my friends outside of the PhD for their endless support and to Ruari for having an unwavering belief in me and who I appreciate more every day.

Finally, thank you to my family. To my sister, for always being at the end of the phone to support me, and to my parents for being the first people to encourage me to do a PhD and for their unlimited kindness and support whilst I have been carrying out the project.

Author's declaration

I declare that, except where explicit reference is made to the contribution of others, this Thesis is a result of my own work carried out at the University of Glasgow. This work has not been submitted for any other degree at the University of Glasgow or any other institution. All external sources have been accordingly referenced.

Printed Name: Anna Kirk

Abbreviations

$\Delta\Delta C_T$: Delta delta cycle threshold
AIN: Anal intraepithelial neoplasia
AK: Actinic keratoses
ANKRD1: Ankyrin repeat domain 1
ANOVA: Analysis of variance
AP-1: Activator protein 1
APC: Antigen presenting cell
ARC: Activity regulated cytoskeleton associated protein
ATP: Adenosine triphosphate
C/EBPβ: CCAAT enhancer binding protein beta
CCL: Chemokine ligand
cDNA: Complementary DNA
CDSN: Corneodesmosomes
CIN: Cervical Intraepithelial neoplasia
CIN: Vulval intraepithelial neoplasia
CLEM: Correlative light and electron microscopy
CLU: Clusterin
CNV: Copy number variant
CRAYB: Crystallin alpha B
CRTAM: Cytotoxic and regulatory T cell molecule
cSCC: Cutaneous squamous cell carcinoma
CTCF: CCCTC-Binding factor
CXCL: C-X-C motif chemokine ligand
DAPI: 4’. 6-diamidino-2-phenylindole
Daxx: Death domain associated protein
ddPCR: Droplet digital polymerase chain reaction
DDR: DNA damage response
DEG: Differentially expressed gene
DMBA: 7,12-Dimethylbenzathracene
DMEM: Dulecco’s modified eagle medium
DNA-PK: DNA-dependent protein kinase
E2BS: E2 binding site
EGF: Epidermal growth factor
EGR: Early growth response
EM: Electron Microscopy
ERCC: External RNA controls consortium
EV: Epidermodysplasia verruciformis
FBS: Fetal bovine serum
FFPE: Formalin-fixed paraffin-embedded
GEM: GTP binding protein overexpressed in skeletal muscle
GM-CSF: Granulocyte-macrophage colony-stimulating factor
GO: Gene ontology
GSEA: Gene set enrichment analysis
H&E: Haematoxylin and eosin
HPV: Human papillomavirus
hrHPV: High-risk Human papillomavirus
HSD: Honestly significant difference

HSE: Heat shock element
HSF: Heat shock transcription factor
HSIL: High-grade squamous intraepithelial lesions
HSP: Heat shock protein
HDI: Human development index
IARC: International agency for research on cancer
IEG: Immediate early gene
IF: Immunofluorescence
IFIT: Interferon-induced protein with tetratricopeptide repeats
IFN: Interferon
IHC: Immunohistochemistry
IL: Interleukin
ISG: Interferon stimulated gene
ISH: In situ hybridization
ITG: Integrin
Jak: Janus kinase
KLF4: Kruppel-like factor 4
KRT: Keratin
LAP: Liver-enriched transcriptional activator protein
LCE: Late cornified envelope protein
LCR: Long control region
LCs: Langerhans cells
LEAP2: Liver enriched antimicrobial peptide 2
LLETZ: Large loop excision of the transformation zone
LM: Light microscopy
LMIC: Low and middle-income countries
lrHPV: Low-risk human papillomavirus
LSIL: Low-grade squamous intraepithelial lesions
MCODE: Molecular complex detection
MFI: Mean fluorescence intensity
MICA: Major histocompatibility complex class I chain-related protein A
MHC: Major histocompatibility complex
MMP: Matrix metalloproteinases
MmuPV1: Mouse papillomavirus type 1
moDC: Monocyte-derived dendritic cell
MSM: Men who have sex with men
NBF: Neutral buffered formalin
NC: Negative control
ND10: Nuclear domain 10
NFκB: Nuclear factor kappa B
NGF: Nerve growth factor
NIKS: Normal immortalised keratinocytes
NK: Natural killer cells
NLS: Nuclear localisation signal
NS: Non-significant
OPSCC: Oropharyngeal squamous cell carcinoma
ORF: Open reading frame
pA_E: Early polyadenylation site
pA_L: Late polyadenylation site

PAMPs: Pathogen-associated molecular patterns
PBMC: Peripheral blood mononuclear cell
PBS Phosphate buffered saline
PFA : Paraformaldehyde
PIN: Penile intraepithelial neoplasia
PML-NBs: Promyelocytic leukaemia nuclear bodies
PPI: Protein-protein interaction
PRR: Pattern recognition receptor
PsV: Pseudovirion
PV: Papillomavirus
RASD1: Ras-related dexamethasone induced 1
Rb: Retinoblastoma protein
RFA: Radiofrequency ablation
RIN: RNA integrity number
RPA: Replication protein A
RPP30: Ribonuclease P protein subunit 30
RT-qPCR: Reverse transcription-quantitative polymerase chain reaction
SA: Splicing acceptor
SCC: Squamous cell carcinoma
SD: Splicing donor
SFV: Semliki forest virus
SIRV: Spike-In RNA variant controls
SRF: Serum response factor
STAT: Signal transducer and activator of transcription
STI: Sexually transmitted infection
SV40: Simian virus 40
TEM: Transmission electron microscopy
TLR: Toll-like receptor
TNF: Tumour necrosis factor
TP53/p53: Tumour protein 53
TR: Treated
TRE: TPA-responsive element
TRRUST: Transcription Regulatory Relationships Unraveled by Sentence-based Text mining
URR: Upstream regulatory region
UV: Ultraviolet
VAIN: Vaginal intraepithelial neoplasia
VEGF: Vascular endothelial growth factor
VLPS: Virus-like particles
WHO: World health organisation

Chapter 1 Introduction

1.1 A brief introduction to HPV

Human papillomaviruses (HPV) are a large family of epitheliotropic, small, non-enveloped viruses ~50 nm in size, which contain a double-stranded DNA virus genome of approximately 8,000 base pairs. HPV is the most common sexually transmitted viral infection globally and is one of the most consequential carcinogens to humans, accounting for around 5% of cancers worldwide including cancers of the anogenital and oropharyngeal regions (Berman and Schiller, 2017; IARC, 2012). Globally, cervical cancer is the fourth most common cancer in women and causes an estimated 350,000 deaths annually (WHO, 2024). Over 90% of cervical cancer cases are caused by HPV (Cubie, 2013). This chapter will introduce the life cycle of HPV, how infection with HPV can result in disease and the current treatment options that exist.

1.2 HPV evolution

1.2.1 Mucosal and cutaneous types of HPV

To date, more than 300 papillomavirus (PV) genomes, including 229 that infect humans, have been identified and classified (or are pending classification by the International Committee on Taxonomy of Viruses (ICTV) (McBride, 2017; Doorslaer *et al.*, 2018) (https://pave.niaid.nih.gov/). These are organised into alpha, beta, gamma, mu and nu phylogenetic genera based on L1 nucleotide sequence homology (Figure 1.1). Papillomavirus types with less than 60% homology in L1 are classified into different genera (de Villiers *et al.*, 2004; Bernard *et al.*, 2010). Within genera, a greater than 10% difference in the L1 sequence identifies different genotypes (de Villiers *et al.*, 2004; Bernard *et al.*, 2010). Evolution of PVs is extremely slow, with the mutational rate only 5-10 times that of their mammalian hosts (Ong *et al.*, 1993; Rector *et al.*, 2007; Shah, Doorbar and Goldstein, 2010). Papillomaviruses are highly host-restricted and mostly cause benign infections, leading to the hypothesis of host-linked evolution (Bernard, 1994; Doorslaer, 2013). However, the observation of HPV types within five different genera demonstrates that other influences must have contributed to papillomavirus evolution (Figure 1.1). Therefore, it has been proposed that ancestral papillomaviruses specialised in infecting distinct ecological niches on the host

followed by extensive co-speciation (Bravo and Alonso, 2007). HPV types can be separated by the epithelial site the virus infects. HPV types that infect the mucosal epithelium reside within the alpha genus (Figure 1.1). Mucosal sites of infection include the cervix, vagina, vulva, anus and oropharynx (Cubie, 2013). Infections at these sites are common with 80% of the population infected with an anogenital α-HPV over their lifetime (Chesson *et al.*, 2014). The majority of the Beta, mu and nu genera and some of the alpha and gamma genera infect the cutaneous epithelia, where they persist (Egawa *et al.*, 2015). In immunocompetent individuals, this infection is often very well controlled by the immune system and these infections remain largely asymptomatic (Gheit, 2019). Immunosuppression can result in a large reactivation of these cutaneous HPV types, particularly Beta HPV types, which are the most well-studied and can result in an increased risk for skin cancer (Egawa and Doorbar, 2017).

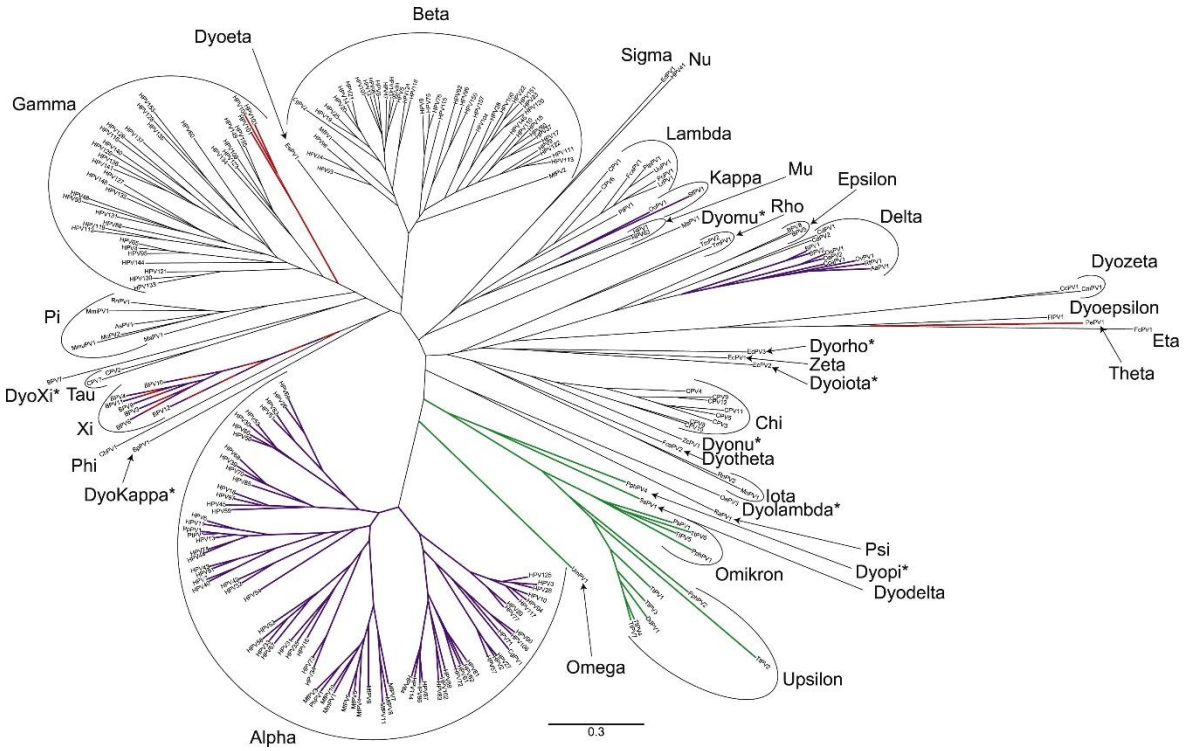

Figure 1.1 Papillomavirus phylogenetic tree. The DNA coding sequences for E1, E2, L1 and L2 for 241 PVs available on PaVE were downloaded and aligned. The maximum likelihood reconstruction of the phylogenetic tree was based on partitioned gene alignment. Genera were named according to previous reports (de Villiers *et al.*, 2004; Bernard *et al.*, 2010) and those with an asterisk are awaiting official recognition. Branch colours indicate viruses lacking an E6 (red) or E7 (green) open reading frame (ORF) and those that code for E5 (purple). Figure adapted from (Doorslaer, 2013).

1.2.2 HPV evolution: high and low-risk Viruses

The mucosal HPV types can be further classified into high- and low-risk viruses. Twelve of the mucosal HPV types are considered high-risk HPV types (hrHPV) (HPV16, 18, 31, 33, 35, 39, 45, 51, 52, 56, 58 and 59), based on an International Agency for Research on Cancer (IARC) working group classifying them as carcinogenic to humans due to their association with cervical cancer (IARC, 2012). HPV68 is categorised as 'probably carcinogenic to humans', with an attributable fraction of 0.2% of cervical cancers, but is not currently defined as a high-risk type (Figure 1.2). HPV16 and HPV18 are the two most prevalent subtypes (Li *et al.*, 2011). HPV16 is uniquely carcinogenic, responsible for around 60% of squamous cell carcinoma cases (SCC) of the cervix (Li *et al.*, 2011; IARC, 2012; IARC, 2022) and HPV18 causes around 15% of cervical SCC cases (Figure 1.2) (Li *et al.*, 2011; IARC, 2012; IARC, 2022). HPV45 is responsible for around 5% of cervical SCC cases and the closely related HPV31, 32, 33, 35, 52 and 58 together account for around 15% of cases (Figure 1.2, yellow). The remaining high-risk types (shown in dark green in the table) are much less carcinogenic (Figure 1.2).

HPV type	HPV species	IARC Group[a]	% HPV type prevalence in cancer	% HPV type prevalence in normal	Odds ratio	% Attributable (etiological) fraction
HPV16	**α-9**	**Group 1**	**55.8**	**2.6**	**47.6**	**62.4**
HPV18	**α-7**	**Group 1**	**14.3**	**1**	**15.7**	**15.3**
HPV45	**α-7**	**Group 1**	**4.8**	**0.6**	**8.3**	**4.8**
HPV33	**α-9**	**Group 1**	**4**	**0.6**	**7.1**	**3.9**
HPV58	**α-9**	**Group 1**	**4**	**0.8**	**5.1**	**3.7**
HPV31	**α-9**	**Group 1**	**3.5**	**1**	**3.7**	**2.9**
HPV52	**α-9**	**Group 1**	**3.2**	**1**	**3.3**	**2.6**
HPV35	**α-9**	**Group 1**	**1.6**	**0.4**	**3.9**	**1.4**
HPV59	**α-7**	**Group 1**	**1.2**	**0.4**	**2.9**	**0.9**
HPV39	**α-7**	**Group 1**	**1.3**	**0.6**	**2.0**	**0.8**
HPV68	**α-7**	**Group 2A**	**0.6**	**0.4**	**1.5**	**0.2**
HPV51	**α-5**	**Group 1**	**1**	**0.9**	**1.2**	**0.2**
HPV56	**α-6**	**Group 1**	**0.8**	**0.6**	**1.3**	**0.2**
HPV73	α-11	Group 2B	0.5	0.3	1.8	0.2
HPV26	α-5	Group 2B	0.2	0.1	4.1	0.2
HPV30	α-6	Group 2B	0.2	0.1	2.6	0.1
HPV69	α-5	Group 2B	0.2	0.1	1.4	0.1
HPV67	α-9	Group 2B	0.3	0.2	1.2	< 0.1
HPV82	α-5	Group 2B	0.2	0.1	1.2	< 0.1
HPV34	α-11	Group 2B	0.1	0.1	1.0	Not attributable
HPV66	**α-6**	**Group 2B**	**0.3**	**0.6**	**0.4**	**Not attributable**
HPV70	α-7	Group 2B	0.2	0.8	0.3	Not attributable
HPV53	α-6	Group 2B	0.5	1.1	0.4	Not attributable

Figure 1.2 The relative importance of the carcinogenic HPV Types. The table shows the attributable fraction of cervical cancer cases caused by each HPV type. A five-level grouping in attributable fraction is shown by the coloured bands. The IARC definitions for the groups given in the third column are carcinogenic to humans (Group 1);

probably carcinogenic to humans (Group 2A) and possibly carcinogenic to humans (Group 2B) Figure adapted from (IARC, 2022).

1.3 HPV and disease:

1.3.1 HPV disease in the mucosal epithelium

Although most individuals acquire an HPV infection, the majority of infections (~90%), with even high-risk viruses, are resolved by the immune system within 1 or 2 years without overt clinical disease (Schiffman, 2007; Bulkmans *et al.*, 2007). These infections are typically productive, releasing progeny virions, which trigger the immune system to respond (Maglennon, McIntosh and Doorbar, 2011; Bourgault *et al.*, 2004). Persistence of infection can result in pathology and pre-malignant lesions can be formed. HPV-associated pre-cancers occur as intraepithelial neoplasia, named after the site of occurrence. Cervical intraepithelial neoplasia (CIN) is the most extensively studied consequence of persistent HPV infection, but other neoplasms at the anogenital region include vulval (VIN), vaginal (VAIN), penile (PIN) and anal intraepithelial neoplasia (AIN) (Cubie, 2013). These intraepithelial neoplasias can progress to cancer due to dysregulation of HPV infection which is often associated with a loss in the production of new virions (Section 1.8) (Doorbar *et al.*, 2012). Therefore, cancer has no evolutionary benefit for the virus and is a rare and inadvertent consequence of HPV infection (Krump *et al.*, 2018).

Anal lesions have a similar association with HPV as cervical lesions, with more than 90% of anal carcinoma cases attributable to HPV infection (Assarzadegan, Brooks and Voltaggio, 2022). These cases have previously been overlooked due to low numbers of incidence, but rates are currently rising by 1 to 3% a year in developed countries, particularly in men who have sex with men (MSM) (Grulich *et al.*, 2012; Deshmukh *et al.*, 2020). Vaginal, vulval and penile cancers are rare, which is thought to be due to the lack of a transformation zone in these sites (Section 1.6.1) (Cubie, 2013). Infection with hrHPVs can also result in oropharyngeal squamous cell carcinomas (OPSCC). The incidence of OPSCC has increased over the past two decades, with evidence suggesting that the incidence of HPV+ OPSCC is rising more rapidly (Taberna *et al.*, 2017). This has resulted in the incidence of oropharyngeal cancer in men surpassing that of cervical cancer in women in both the UK and USA (Lechner *et al.*, 2022).

HPV is also responsible for other diseases at the mucosal epithelium besides cancers including genital warts (condylomata acuminata) and recurrent respiratory papillomatosis, the majority of which are caused by HPV types 6 and 11 (Cubie, 2013). Genital warts are common pathologies, with reports of around 10% of women in Scandinavia developing genital warts before the age of 45, that affect the anogenital site (Kjær *et al.*, 2007). Whilst they do not carry with them the same malignancy risk as intraepithelial neoplasia, they can cause significant psychosocial stress (Cubie, 2013) and have a high rate of transmission between partners (60%) (Woodhall *et al.*, 2008). Recurrent respiratory papillomatosis is a difficult-to-manage disease with high morbidity. Most pathologies arise from HPV6 or HPV11 infection of the larynx, which results in exophytic warty lesions (Goon *et al.*, 2007). In juveniles, these can be life-threatening due to the possibility of lesions blocking the airway and they require surgical intervention, which can be required monthly due to frequent recurrence, to remove the lesion (Cubie, 2013).

1.3.2 HPV disease in the cutaneous epithelium

Infection with the cutaneous HPV types can result in the development of common warts, most commonly caused by HPV2 or HPV4 (Jablonska *et al.*, 1985; Orth, Favre and Croissant, 1977) and plantar warts (verrucas), commonly caused by HPV 1, 2, 27 and 57 (Egawa and Doorbar, 2017). Epidermodysplasia verruciformis (EV) is a rare autosomal recessive condition, which, through mutation of *EVER1* or *EVER2,* can result in the selective depletion of T cell clones (Youssefian *et al.*, 2019; Ramoz *et al.*, 2002). This makes individuals susceptible to extensive cutaneous infection with a subset of the β-HPV types and can result in lifelong development of warts and lesions (Orth *et al.*, 1978). HPV5 and HPV8 are responsible for the majority of warts and these lesions can result in SCC development on sun-exposed sites (Orth, 1987). The immune deficiency in these patients is proposed to be responsible for this enhanced propensity to infection and similar cutaneous lesions have been observed in other immunosuppressed individuals, such as HIV-positive individuals or graft recipients (Moore, Rady and Tyring, 2022).

1.4 Progression of disease

The progression from infection with HPV to cervical cancer development is a rare, long-term process that involves the accumulation of DNA alterations in the host genome. Persistent infection, caused by an inadequate mounting of the immune response to eradicate infection, and dysregulation of the viral life cycle are risk factors for malignancy (Stanley, 2012). Determinants of persistence may involve the viral genotype, tobacco smoking and the use of hormonal contraceptives (del Pino *et al.*, 2024). Moreover, coinfections with sexually transmitted bacterial or viral infections, such as *chlamydia trachomatis* (Silins *et al.*, 2005; Kumari and Bhor, 2022) and HIV (Malagón *et al.*, 2024) respectively, can result in increased likelihood for persistence. In the cervix, pathologies can progress from CIN grades 1 to 3 (Figure 1.3). CIN3 lesions can subsequently progress to cervical SCC (Leeson *et al.*, 2021). The grading of CIN is determined by the proportion of the epithelium that has undergone disruption from normal epithelial fate (Figure 1.3). CIN1 denotes mild dysplasia, where the lower one-third of the epithelium shows dysplasia. In CIN2, the lower two-thirds of the epithelium is affected and once over two-thirds of the epithelium is affected, lesions are graded CIN3 (Figure 1.3) (IARC, 2022). Cervical pathologies can also be classified as low- or high-grade squamous intraepithelial lesions (LSIL, HSIL). LSIL is a similar grading to CIN1 lesions and below whilst HSIL represents CIN2 and CIN3 lesions (IARC, 2022). The majority of CIN1 and CIN2 lesions regress (Schiffman *et al.*, 2011). A recent meta-analysis showed a 50% regression rate for CIN2 lesions over 24 months, which was increased to 60% in women under 30 (Tainio *et al.*, 2018). Even if lesions progress to CIN3, only one-third of cases are predicted to subsequently progress to cancer within 10-20 years (Gravitt, 2011) (Figure 1.4). Moreover, the development of invasive cancer from CIN3 is much slower than the development of CIN3 following a new HPV infection, which allows for detection and intervention (Schiffman and Rodriguez, 2008) (Figure 1.4). Overall, the ability of the immune system to suppress or eradicate HPV infection is one of the most important factors for disease progression. This is particularly apparent when considering the progression rate in women living with HIV. These individuals have a 2.5-fold higher incidence of HSIL and a 4-fold higher incidence of invasive cervical cancer than HIV-negative women (De Vuyst *et al.*, 2008; Denslow *et al.*, 2013; Liu *et al.*, 2018). Moreover, they have an increased risk of

developing invasive cervical cancer 7 to 15 years earlier than HIV-negative women (Sharma *et al.*, 2023).

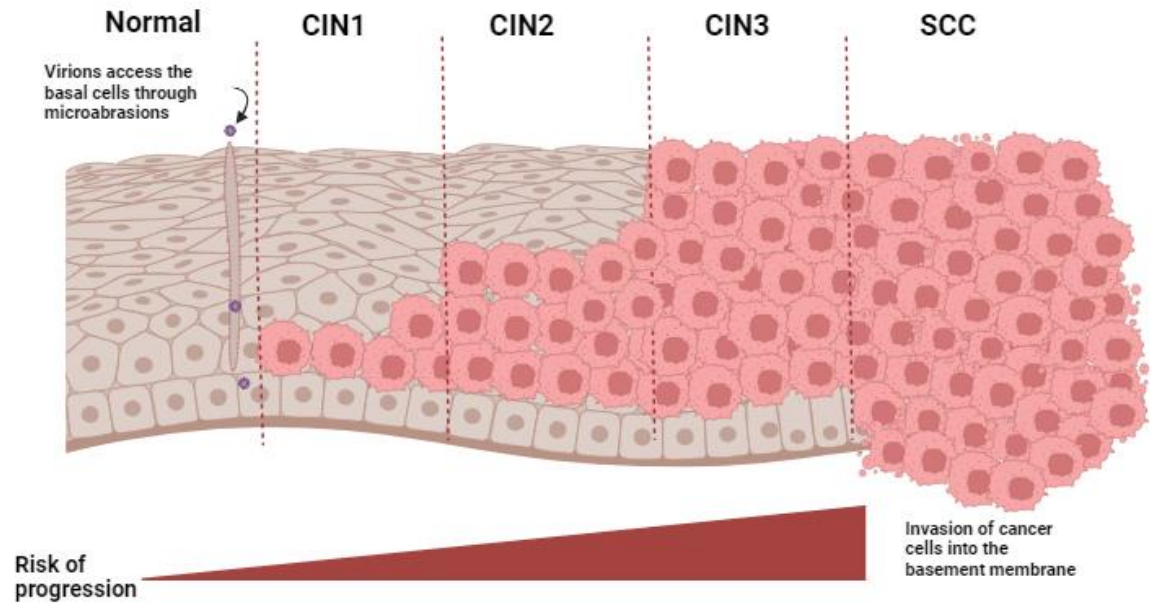

Figure 1.3. Progression of HPV infection to cervical squamous cell carcinoma. Following infection with a high-risk human papillomavirus, persistent infection can result in the appearance of abnormal cells (pink circular cells) and the progression of cervical intraepithelial neoplasms (CIN) towards squamous cell carcinoma (SCC). CIN lesions are graded based on the proportion of the epithelium that contains disrupted cells. Dysplasia of the lower 1/3rd, 2/3rd or over 2/3rds of the epithelium is graded as CIN1, CIN2 and CIN3 respectively. A large proportion of CIN1 and CIN2 lesions will clear naturally and even many CIN3 lesions will revert. The invasion of dysplastic cells into the basement membrane denotes the condition as squamous cell carcinoma. Figure created on Biorender.com

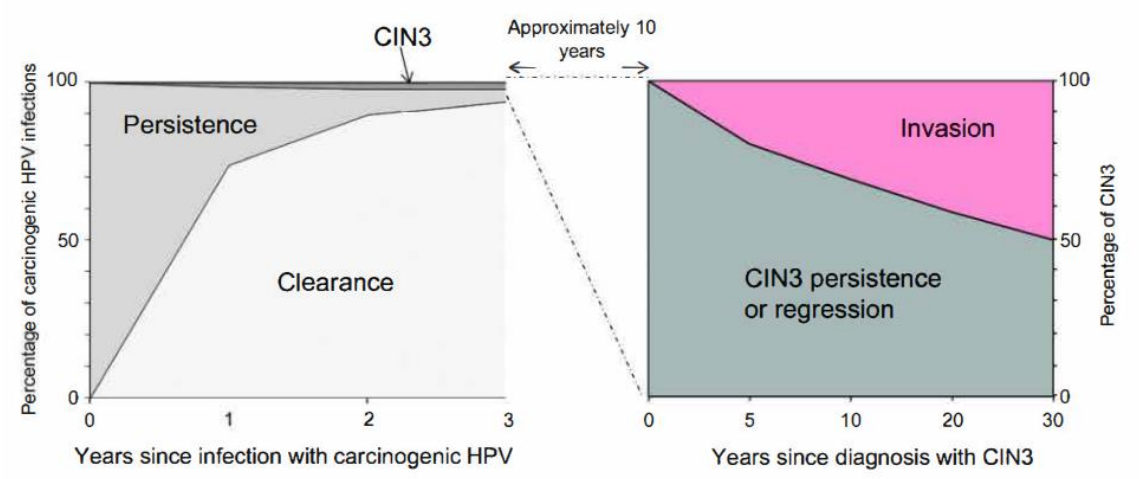

Figure 1.4 Risk of HPV persistence and progression. The graph on the left shows the proportion of carcinogenic HPV infections that clear, persist or progress to CIN3 in the first 3 years after detection. The graph on the right shows the proportion of untreated CIN3 lesions that progress to cancer within 30 years following initial diagnosis. Adapted from (Schiffman *et al.*, 2011). Based on data from (Rodríguez *et al.*, 2008; McCredie *et al.*, 2008).

1.5 The HPV genome

All HPVs contain a circular ~8 kb double-stranded DNA genome (Van Doorslaer *et al.*, 2017). Genomes are composed of an 'early' region, which contains open reading frames (ORFs) for seven viral non-structural proteins (E1, E2, E4, E5, E6, E7, E8^E2) and a 'late' region, which contains ORFs for two viral structural proteins (L1 and L2). The genome also contains a long control region (LCR), also denoted the upstream regulatory region (URR) (Figure 1.5) (Van Doorslaer *et al.*, 2017; Nelson and Mirabello, 2023). The LCR contains the origin of replication and binding sites for the viral E1 and E2 proteins for the initiation of viral replication (Figure 1.5) (Yu, Majerciak and Zheng, 2022). There are four E2 binding sites within the LCR and the most distal of these is upstream of the transcriptional enhancer (Figure 1.5). The LCR also contains *cis*-acting control regions and binding sites for many cellular and viral transcription factors for transcriptional regulation (Graham, 2010; O'Connor, Chan and Bernard, 1995). The 5' end of the LCR contains a late regulatory element, which can interact with several cellular proteins to control viral late gene expression post-transcriptionally (Kennedy, Haddow and Clements, 1990; Kennedy, Haddow and Clements, 1991; Koffa *et al.*, 2000; Cumming *et al.*, 2002; Cumming *et al.*, 2003; McPhillips *et al.*, 2004).

Due to the relatively small genome, papillomaviruses employ multiple strategies to encode the proteins required for the viral life cycle (IARC., 2007). The *in vitro* models used in this thesis contain HPV16 so an in-depth introduction to its transcription will be provided here, however many of the features are shared between the high-risk HPV types (Graham, 2017; Yu, Majerciak and Zheng, 2022). Early and late promoters and polyadenylation sites allow HPV to temporally regulate the expression of genes with distinct phases of the viral life cycle (Kirk and Graham, 2024). HPV16 uses a major early and late (p97 and p670 respectively) transcriptional start site (Figure 1.5). Recruitment of host RNA polymerase II is required for transcription, which takes place in a unidirectional manner with all the ORFs contained on the same strand of the double-stranded genome (Yu, Majerciak and Zheng, 2022). HPV pre-mRNAs are polycistronic and encode overlapping ORFs in three coding frames (Figure 1.5) (Kajitani and Schwartz, 2022). Alternative splicing results in the production of the HPV mRNAs, which are capped at the 5' terminus and cleaved at early or late polyadenylation sites for polyA tail addition using host machinery (Figure 1.5) (Graham and Faizo, 2017).

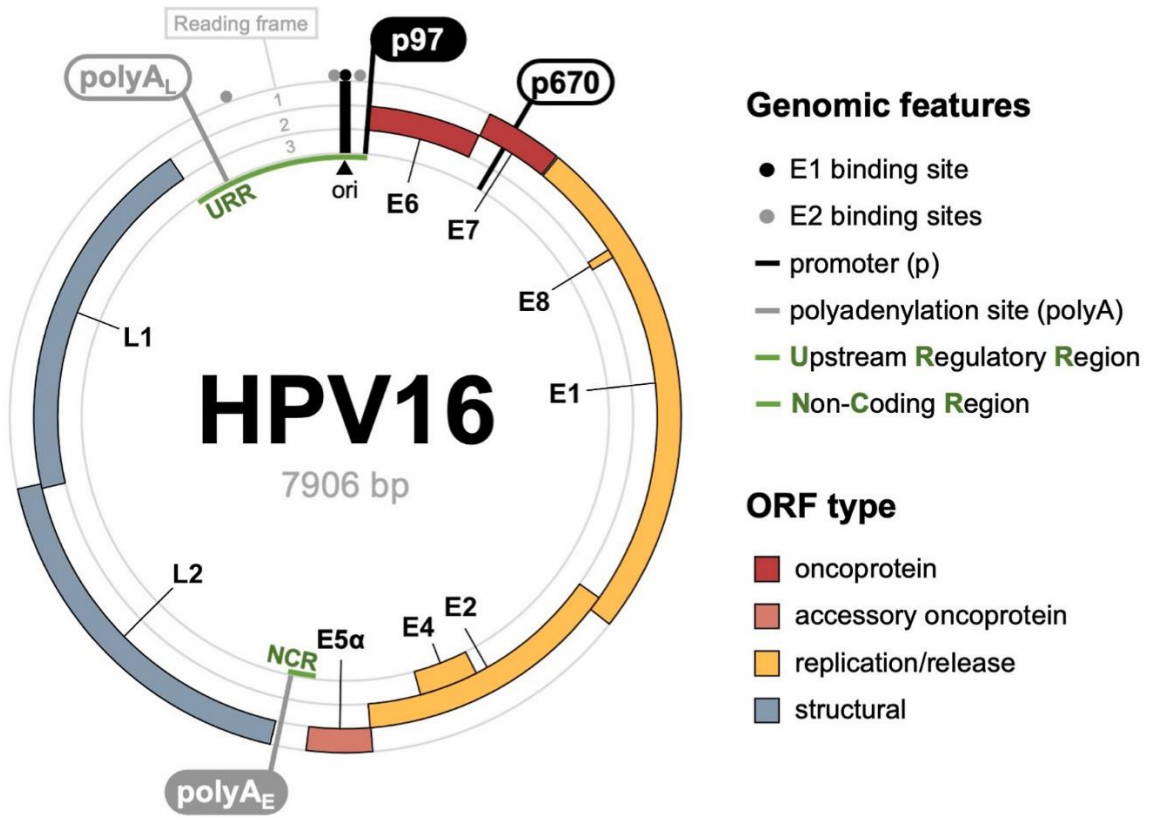

Figure 1.5: The genome organisation of HPV16. Other high-risk HPV genomes are very similar in organisation. The circular ~ 7.9 kb double-stranded DNA genome is depicted as three codon reading frames: 1 (outside track), 2 (middle track) and 3 (inside track). The genome comprises a long control region (LCR) or upstream regulatory region (URR) and protein-coding frames depicted as coloured rectangles in the appropriate reading frame. The major early and late promoters are denoted p97 and p670 respectively and the early and late polyadenylation sites labelled in grey (polyA$_E$ and polyA$_L$). Black and grey circles within the URR represent E1 and E2 binding sites respectively and the origin of replication is labelled. Figure adapted from (Nelson and Mirabello, 2023).

1.6 Early events in the viral life cycle

1.6.1 HPV entry

Papillomaviruses require infection at multilayered differentiated epithelial sites to enable the full viral life cycle to take place (Doorbar and Griffin, 2019). Viral entry and replication at the cervix will be considered here but many of the underlying features are consistent with infection at other anatomical positions. The cervix consists of distinct epithelial sites: the stratified epithelium at the ectocervix, the columnar epithelium of the endocervix and the transformation zone (Figure 1.6) (Doorbar and

Griffin, 2019; Reich *et al.*, 2017). These areas have different vulnerabilities to infection, with the majority of HPV-induced neoplasms arising from initial infection at the transformation zone (Doorbar and Griffin, 2019). High-risk HPV infection requires entry into basal or reserve (stem-like) epithelial cells (Pyeon *et al.*, 2009; Egawa, 2003). Microabrasions in the stratified epithelium can give virions access to infect the basal cells (Doorbar, 2005). Alternatively, the metaplastic epithelium of the transformation zone represents a replicating layer, which is not protected by a thick layer of non-dividing cells, making infection of these basal or reserve cells easier (Doorbar and Griffin, 2019) (Figure 1.6).

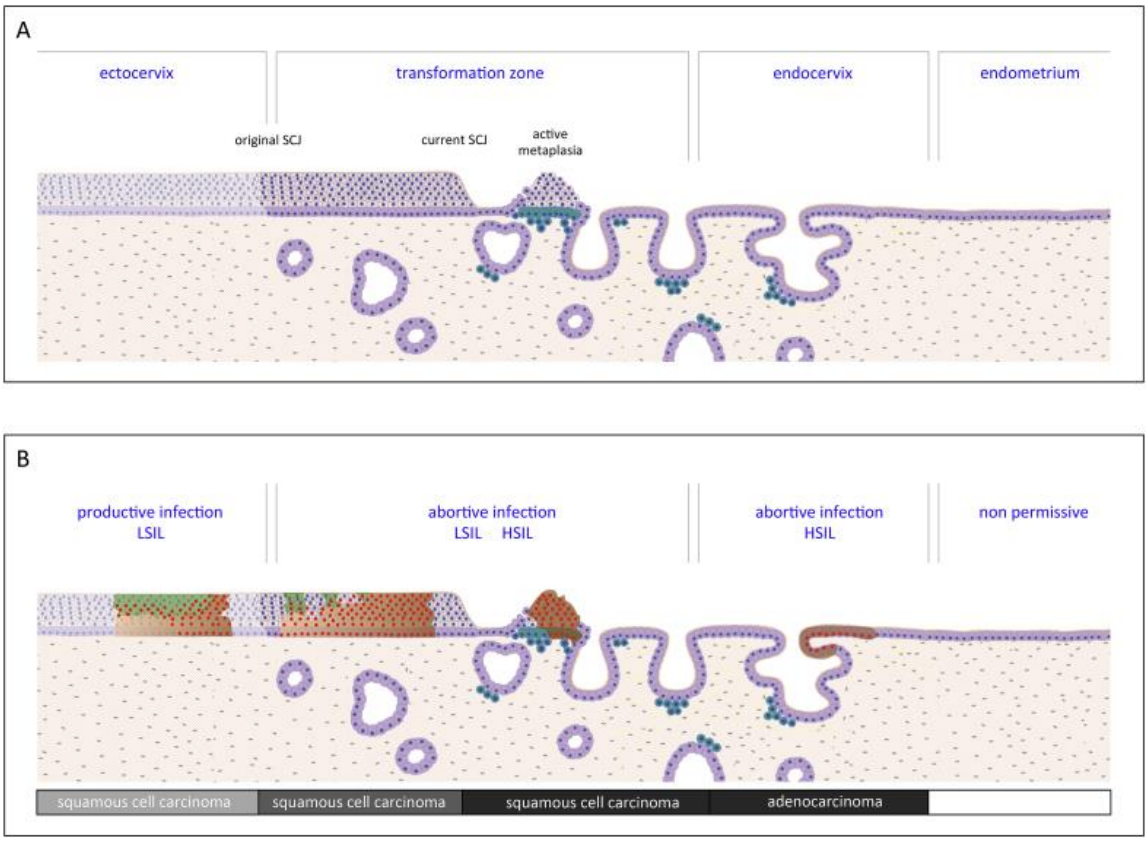

Figure 1.6 HPV infection at different epithelial sites of the cervix and consequences of infection. (A) The cervix has distinct epithelial sites (from left to right): the conventional stratified epithelium at the ectocervix, the transformation zone and the columnar epithelium of the endocervix, which is adjacent to the endometrium. The cells shown in turquoise lying under the basal cells at the transformation zone are the reserve cells that have an important role in metaplasia, resulting in the formation of a new stratified epithelium. (B) HPV infection at different sites results in different outcomes. Infection at the ectocervix is believed to result in productive infection or LSIL whereas other sites are associated with viral life cycle dysregulation and higher potential for malignancy. Figure adapted from (Doorbar and Griffin, 2019).

Once HPV has accessed the basal or stem-like cells, virion entry takes place. The major capsid protein L1 binds to heparan sulphate proteoglycans on the cell surface (Joyce *et al.*, 1999; Cerqueira *et al.*, 2013). This interaction triggers conformational changes in the viral capsid, which results in the exposure of the N-terminus of the minor capsid protein L2 (Selinka *et al.*, 2003; Kines *et al.*, 2009). Proteolytic cleavage of the exposed portion of L2 and interactions with a currently unidentified secondary receptor are necessary for virion internalisation (Richards *et al.*, 2006). Endocytosis of HPV through the plasma membrane uses an actin-dependent mechanism most similar to macropinocytosis (Schelhaas *et al.*, 2012; Spoden *et al.*, 2008; Selinka, Giroglou and Sapp, 2002). The resulting endocytic vesicles undergo acidification, which triggers the disassembly of the viral capsid (DiGiuseppe *et al.*, 2017; Smith *et al.*, 2008). L2 remains associated with the viral DNA and through interactions with the retromer complex, the viral protein/DNA complex is rescued from degradation and trafficked to the trans-Golgi network (Day *et al.*, 2013; Lipovsky *et al.*, 2013; Popa *et al.*, 2015). During mitosis, nuclear envelope breakdown enables transport vesicles containing HPV, which likely bud from the TGN, to access the condensed chromosomes (Aydin *et al.*, 2014; Pyeon *et al.*, 2009). Following cell cycle completion and nuclear envelope reformation, the incoming viral DNA and L2 have been characterised to be associated with Promyelocytic leukaemia (PML) nuclear bodies (NBs) (Day *et al.*, 2004). PML-NBs are targeted by many viruses, likely due to their known functions in innate immunity, cell cycle arrest and apoptosis (Guion and Sapp, 2020). Transcriptional repressors that are associated with PML-NBs such as Sp100 and Daxx, have been shown to restrict the gene expression of several DNA viruses such as adenoviruses (Schreiner *et al.*, 2013), human cytomegalovirus (Kim *et al.*, 2011) and herpes simplex virus 1 (Negorev *et al.*, 2006). In turn, these viruses have evolved effector proteins to induce the reorganisation of PML-NBs and allow for viral transcription and replication (Ryabchenko *et al.*, 2023). It has been postulated that initially, PML-NBs may favour HPV transcription (directed through PML) for the establishment of infection but during persistent infections, they may repress viral transcription (through Sp100) (Day *et al.*, 2004; Stepp, Meyers and McBride, 2013; Habiger *et al.*, 2015).

1.6.2 E1 and E2 play important roles in the early phase of HPV replication

Following nuclear entry, viral replication begins. Initial early transcription within infected basal cells first results in the expression of the viral early proteins, E1 and E2 (Ozbun, 2002). E2 recruits the helicase E1 to the viral origin of replication (Ori) (Sanders and Stenlund, 2000; Sanders and Stenlund, 1998), which in turn assembles components of the host DNA polymerase machinery at the Ori to initiate viral genome replication (Table 1.1) (Chojnacki and Melendy, 2018). There are three different stages of genome replication within the HPV life cycle: establishment, maintenance and amplification. The establishment phase, early in viral infection, amplifies the viral genome copy number to around 50-100 copies per cell (Maglennon, McIntosh and Doorbar, 2011; Stubenrauch and Laimins, 1999). In the maintenance phase, genomes are stably maintained at this number within the basal layers of the epithelium to prevent immune detection, with viral genome replication coincident with cellular DNA replication (Lambert, 1991). Following genome replication, E2 ensures the equal segregation of episomes during mitosis by tethering the viral genome to chromatin (Table 1.1) (Bastien and McBride, 2000; Lehman and Botchan, 1998; Ilves, Kivi and Ustav, 1999). After differentiation of the host cell, the virus genome undergoes a second amplification step, proposed to increase the viral load to several hundreds or thousands per cell for virion production (Hoffmann *et al.*, 2006).

Table 1.1 The functions of the viral proteins from the hrHPV types.

Viral protein	Function
E1	Viral helicase. Interacts with E2 and components of host DNA polymerase machinery to initiate genome replication.
E2	DNA-binding protein which recognises the Ori and recruits E1 to these sites for viral genome replication. Transcriptional regulator. Tethers HPV episomes to host chromatin for equal partitioning of episomes during mitosis.
E4	Interaction with the keratin filaments and the envelope in cornified cells to promote structural instability and aid virion release. Cell cycle arrest.
E5	Regulates cell signalling (EGFR and KGFR) to enable the differentiation-dependent stages of the HPV life cycle. Aids viral immune evasion through the inhibition of MHC class I presentation.

E6	Interaction with E6AP to enable binding and degradation of p53 resulting in inhibition of apoptosis to bypass cellular growth arrest following DNA damage. Inhibition of keratinocyte differentiation and interferon response. Telomerase activation. Degradation of PDZ proteins.
E7	Binding to and degradation of Rb, p107 and p130 enabling unscheduled cell proliferation. Aids viral immune evasion by interfering with the interferon response and inhibition of NF-κB.
E8^E2	Repressor of viral replication and transcription in basal cells. Mediates the switch to late viral events in differentiation.
L1	Major capsid protein.
L2	Minor capsid protein. Mediates viral genome delivery to the nucleus and PML-NBs within the nucleus during virion entry.

1.6.3 HPV gene expression and its regulation

HPV intricately links its gene expression with the differentiation status of the epithelium that it infects (Figure 1.7) (Kirk and Graham, 2024). Alongside its function in viral genome replication (Table 1.1), E2 is also a major regulator of viral transcription. Low concentrations of E2 within undifferentiated cells result in transcriptional activation of the early promoter and production of the early viral proteins E1, E2, E6, E7 and E8^E2 (Figure 1.8) (Steger and Corbach, 1997; Rapp *et al.*, 1997). As the concentration of E2 rises, it acts as a repressor, leading to very low-level expression of the viral oncoproteins (Figure 1.8) (Rapp *et al.*, 1997; Steger and Corbach, 1997; Stubenrauch, Lim and Laimins, 1998). E8^E2 acts synergistically with E2 in undifferentiated cells, and together they repress viral transcription and replication to enable immune evasion (Stubenrauch *et al.*, 2000; Lace *et al.*, 2008b; Zobel, Iftner and Stubenrauch, 2003). E8^E2 has also been proposed to be involved in the switch to productive replication within differentiated cells (Kuehner and Stubenrauch, 2022) (Table 1.1).

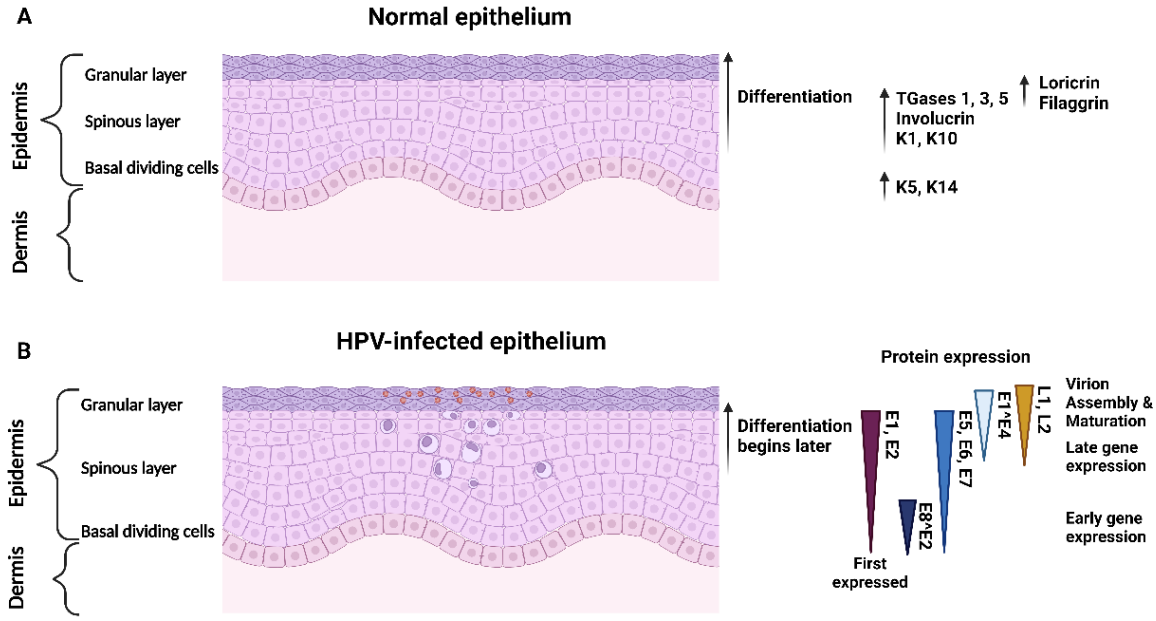

Figure 1.7: HPV viral gene expression is tightly linked to the differentiation status of the epithelium. (A) During differentiation of the epithelium, the transcription of epithelial cells changes. The arrows on the right-hand side indicate the expression of these early and late differentiation markers. (B) Within HPV-infected epithelium, differentiation begins later. The viral proteins are also spatially regulated and their expression within different layers are indicated (coloured triangles) with the stages of the viral life cycle. Figure made in Biorender.com.

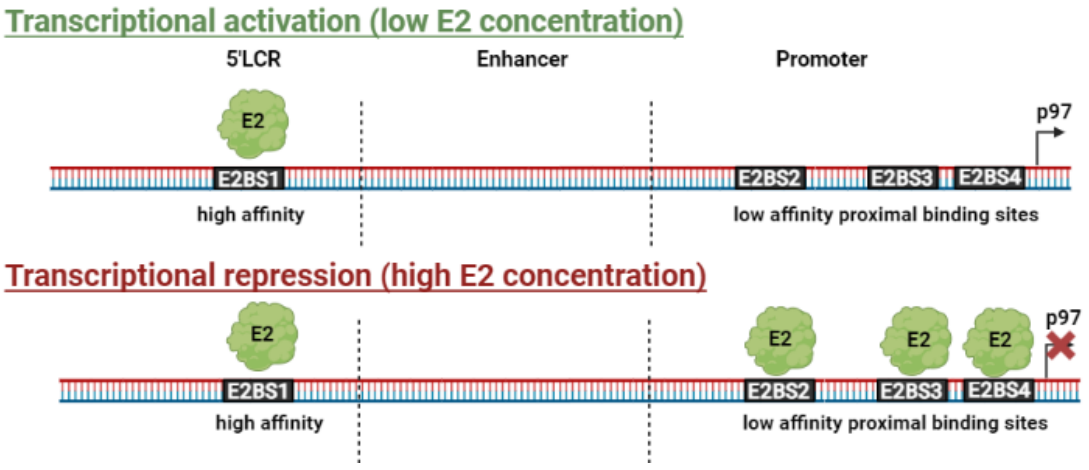

Figure 1.8. The E2 binding sites in the upstream regulatory region (URR) of HPV16. Early in infection, when E2 protein concentrations are low, E2 binds to E2 binding site (E2BS) 1, its most distal binding site from the p97 promoter and the one with the highest affinity. This results in transcriptional activation from p97 and the transcription of the HPV early genes. As these transcripts are translated into proteins and the concentration of E2 increases, E2 begins to bind to the other binding sites, which are proximal to the p97 promoter. Binding at these sites results in transcriptional repression of the HPV early genes. Figure created in Biorender.com.

1.6.4 HPV16 early transcription

Fourteen early HPV16 viral transcripts have been identified that use the early polyadenylation site at 4215 nt (pA_E) (Figure 1.9) (Transcript maps available at PAVE) (Schwartz, 2013; Yu, Majerciak and Zheng, 2022; Graham and Faizo, 2017). Alternative RNA splicing of the early HPV16 pre-mRNAs uses 8 major RNA splicing sites including two 5' splice donor and six 3' splice acceptor sites to produce isoforms of mRNAs for the expression of the seven viral non-structural proteins (E1, E2, E4, E5, E6, E7 and E8^E2) (Figure 1.9) (Graham and Faizo, 2017). Two major splice events are preferred in HPV16 early transcription. The first of these is early in the viral genome between the splice donor at 226 nt to the splice acceptor at 409 nt (SD226^SA409) (McFarlane *et al.*, 2015). Transcripts originating from the minor p14 promoter in HPV16 also use this splice donor and acceptor (species 1, Figure 1.9). This is proposed to result in E1 expression through leaky ribosome scanning (Lace *et al.*, 2008a). In the central part of its genome, HPV16 has one major splice acceptor site at SA3357 (Graham and Faizo, 2017). This was previously observed to be the most commonly used splice site on the HPV16 genome from patient samples (Schmitt *et al.*, 2010). The major transcript originating from the p97 major early promoter uses both of these splice sites between SD226^SA409 and SD880^SA3357 to produce a transcript encoding E6*I, E7, E1^E4, E5 (species 8, Figure 1.9). The remaining six splice acceptor sites (nt 526, 742, 2582 and 2708) allow for the expression of the remaining HPV early genes (Figure 1.9).

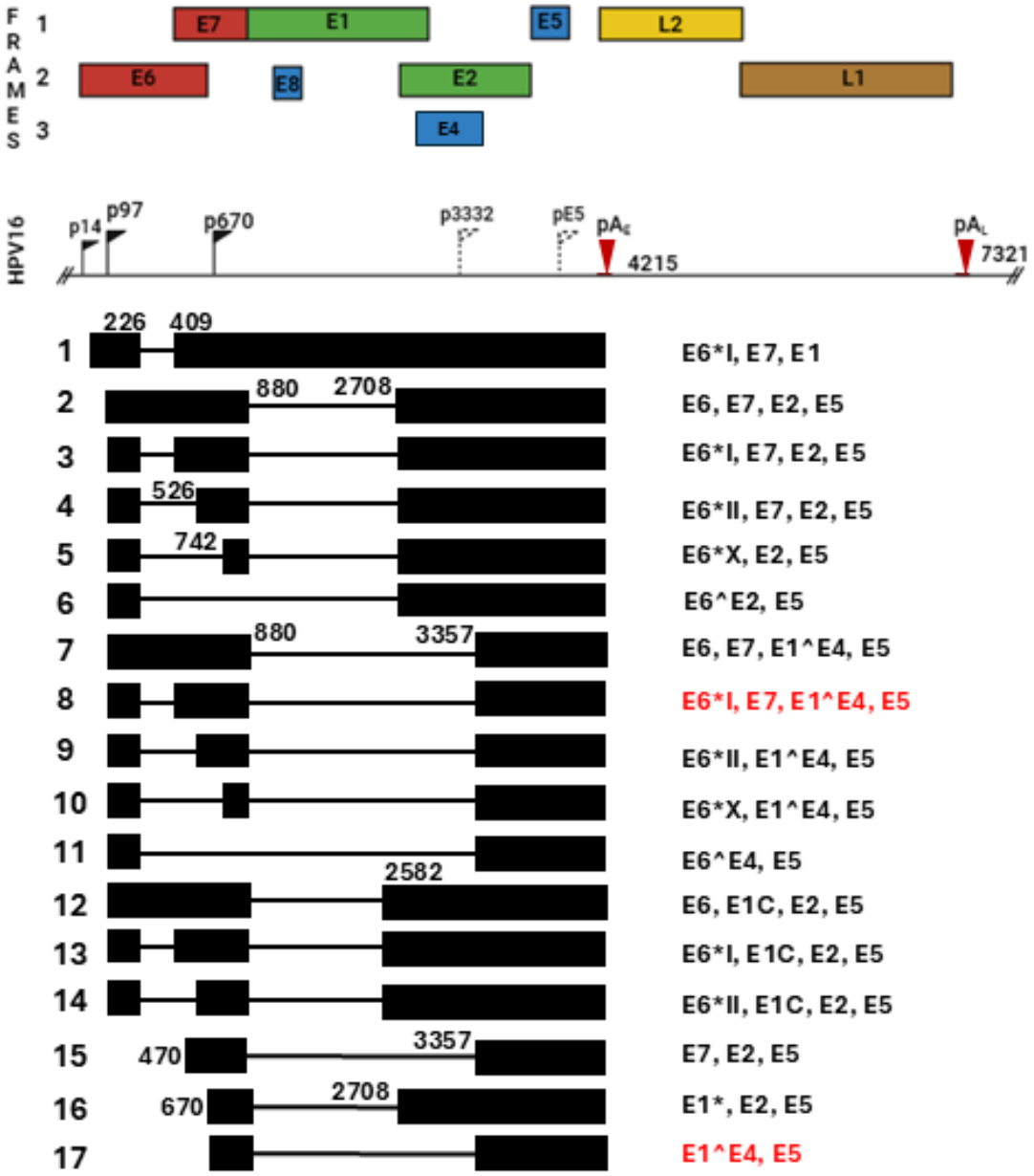

Figure 1.9: Transcript map of HPV16 transcripts that use the early polyadenylation site. The HPV16 genome is shown in a linear form as a black line with the viral promoters (black flags) indicated. Major promoters are larger in size and the putative promoters are shown by a dashed line. The early (pA_E) and late (pA_L) polyadenylation sites are shown with red triangles and the nucleotide position indicated. The diagram is not to scale. Predicted viral ORFs and the coding frame they are in are shown above (coloured boxes). Below the genome, are the mapped viral transcripts that use the early polyadenylation site (species 1-17, numbered on left). Exons are represented by black boxes and introns by black lines. The numbers above each box start/end represent the nucleotide positioning of the splice donor and acceptor site or the promoter used (if not p14 or p97). The coding potential for each transcript is shown on the right. Transcripts in red represent those that are most abundant. Transcript maps used for reference (Milligan *et al.*, 2007; Chen *et al.*, 2014). Figure partially made in biorender.com.

1.6.5 HPV E6 and E7 are essential for the full viral life cycle

In a normal infection, E6 and E7 are expressed at a very low level and are required for the full viral life cycle to take place (Table 1.1). Whilst HPV requires keratinocytes to differentiate for expression of the late viral proteins and virion assembly, this normally results in exit from the cell cycle (Moody, 2017). HPV needs to amplify its genome within the differentiated cells to produce new virions; viral load is limited in the lower layers to prevent immune recognition. Therefore, E6 and E7 expression early in infection modifies cells committing to differentiation to both differentiate and remain within the cell cycle to allow for HPV genome amplification (Moody, 2017). E7 binds to and destabilises Rb and the associated pocket factors p107 and p130 (Berezutskaya *et al.*, 1997; Boyer, Wazer and Band, 1996). This prevents Rb from forming a regulatory complex with E2F and frees E2F to become a transcriptional activator that stimulates S phase entry in cells that would usually undergo terminal differentiation, allowing viral genome replication (Müller *et al.*, 1997; Weintraub, Prater and Dean, 1992). This unscheduled cell proliferation would normally result in apoptosis. To avoid this, the hrHPVs encode E6, which binds to and promotes the degradation of p53 through the formation of a trimeric complex with the cellular ubiquitination enzyme E6-associated protein (Crook, Tidy and Vousden, 1991; Martinez-Zapien *et al.*, 2016). E6 can also inhibit apoptosis through its interactions with FADD, caspase 8 and TNF receptor 1 (Filippova *et al.*, 2002; Filippova, Parkhurst and Duerksen-Hughes, 2004). E6 and E7 additionally aid HPV immune evasion, allowing completion of the viral life cycle without detection (Section 1.9.2).

1.7 Late events in the viral life cycle

Once cells have begun differentiation in the stratified layer, the viral genomes undergo a second round of amplification. This amplification stage is dependent upon the activation of the ATR and ATM DNA damage response pathways (Moody and Laimins, 2009). Normally the activation of these pathways would result in cell cycle arrest for DNA repair to occur but within HPV-infected cells, this regulation is alleviated through the HPV oncoproteins (McKinney, Hussmann and McBride, 2015) (Section 1.6.5).

Transcription at the late promoters is activated by DNA replication and epithelial differentiation (Hummel, Hudson and Laimins, 1992; Ruesch, Stubenrauch and Laimins, 1998; Wang *et al.*, 2017). Viral late gene expression occurs at a similar time to the expression of the late differentiation epithelial markers including involucrin, transglutaminases and loricrin (Figure 1.7) (Kirk and Graham, 2024). This coordination of early and late viral transcription to distinct parts of the epithelium prevents the expression of the highly immunogenic late proteins until the upper layers of the epithelium, an immune-privileged site (Egawa *et al.*, 2015).

1.7.1 HPV16 late gene transcription

Five late HPV16 transcripts originating from the p670 promoter have been discovered. Two of these are polyadenylated at the early site which allows for the expression of E1^E4 (species 17, Figure 1.9) (Chen *et al.*, 2014). The remaining transcripts are polyadenylated at the downstream late polyadenylation site at nt 7321, including those that express the viral capsid proteins L1 and L2 (Figure 1.10). Translation initiation is thought to take place at the first 5' ORF of a transcript and it is proposed that only this initial ORF that will be efficiently translated (Kozak, 1991). Since L1 is always at the 3' end of transcripts, most often with other gene ORFs before it, this represents a problem in producing the major late capsid. However, leaky ribosome scanning (Kozak, 2002) would allow for L1 production (species 19) and a small amount of L1 may also be produced through alternative splicing using the SD880 to SA5639 sites, to produce a transcript with L1 as the most 5' ORF (species 20, Figure 1.10) (Milligan *et al.*, 2007; Johansson and Schwartz, 2013). There are several putative late promoters for HPV16 (transcripts not shown in Figure 1.10). The putative promoter at 1135nt is thought to encode the regulatory protein E8^E2 and use the early polyadenylation site (Straub *et al.*, 2015). The promoter contained within the E4 ORF (p3332) is proposed to encode E5, L2 or L1 (Ozbun and Meyers, 1997) and the promoter within the E5 ORF (pE5) would contain L2 as the first reading frame (Milligan *et al.*, 2007).

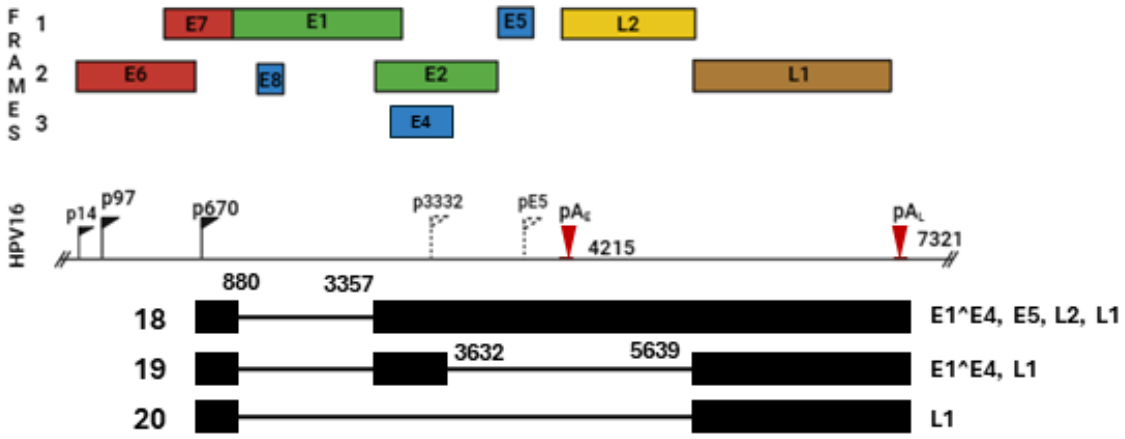

Figure 1.10: Transcript map of HPV16 transcripts that use the late major viral promoter and late viral polyadenylation site. The HPV16 genome is shown in a linear form as a black line with the viral promoters (black flags) indicated. Major promoters are larger in size and putative promoters are shown by a dashed line. The early (pA_E) and late (pA_L) polyadenylation sites are shown with red triangles and the nucleotide position indicated. The diagram is not to scale. Predicted viral ORFs and the coding frame they are in are shown above (coloured boxes). Below the genome, are the mapped viral transcripts that use the late major viral promoter (p670) and the late polyadenylation site (pA_L). Exons are represented by black boxes and introns by black lines. The numbers above each box end/start represent the nucleotide positioning of the splice donor and acceptor site. The coding potential for each transcript is shown on the right. Many other HPV16 transcripts have been identified that use putative promoters within the viral genome. For a full diagram, see PAVE website (https://pave.niaid.nih.gov/). Transcript maps used for reference (Milligan *et al.*, 2007). Figure partially made in biorender.com.

1.7.2 E4 & E5 protein functions

Whilst the E4 and E5 ORFs are contained within the 'early' region of the genome, these proteins are expressed late in the viral life cycle (Doorbar, 2013; Kirk and Graham, 2024). E4 is the most abundantly expressed viral protein, accumulating in the upper, differentiating epithelial layers (Breitburd, Croissant and Orth, 1987; Doorbar *et al.*, 1986; Middleton, 2002). Here, E4 is cross-linked to the cornified envelope by transglutaminase (Bryan and Brown, 2000; Brown *et al.*, 2006) and following cleavage by Calpain, the C-termini can multimerise to form amyloid-like fibres (Table 1.1) (McIntosh *et al.*, 2010). Collectively, this disrupts the cytokeratin network and increases the fragility of cells undergoing desquamation, which has been proposed to facilitate viral egress (Table 1.1) (Bryan and Brown, 2000; Bryan and Brown, 2001; Wang *et al.*, 2004). The E4 C-terminal domain has also been proposed to enable E4

binding to DEAD-box proteins (Doorbar *et al.*, 2000). The functional consequence of this has not been elucidated but DEAD-box proteins regulate gene expression so it is logical that this interaction may regulate the expression of cellular or viral genes (Doorbar *et al.*, 2000; Iost and Dreyfus, 1994). Expression of E4 has also been reported to arrest cells in the G2 phase of the cell cycle, which may produce an environment supportive of viral genome replication, proposed as a 'pseudo-S-phase' (Davy *et al.*, 2002).

HPV E5 regulates cell signalling pathways to enable the differentiation-dependent stages of the HPV life cycle (Table 1.1). Induction of EGFR signalling by E5 is critical for promoting unscheduled DNA synthesis within suprabasal cells (Wasson *et al.*, 2017). Moreover, E5 can suppress the KGFR pathway, which enables the delay in keratinocyte differentiation during the virus life cycle (Belleudi *et al.*, 2011). Additionally, E5 has an important role in immune evasion, as discussed in Section 1.9.

1.7.3 The production of new virions

L1 and L2 are the major and minor papillomavirus capsid proteins (Table 1.1) (Buck, Day and Trus, 2013; Wang and Roden, 2013). Synthesis of L2 precedes L1 expression within the terminally differentiating keratinocytes (Florin *et al.*, 2002a; Florin *et al.*, 2002b). These proteins get translated in the cytoplasm, but early studies established that L1 and L2 predominantly localise to the nucleus, the site of virion assembly (Buck, Day and Trus, 2013). Nuclear import is facilitated by nuclear localisation signals (NLS). L1 contains an NLS within the last seven amino acids of the protein (Zhou *et al.*, 1991) whereas L2 contains two NLSs, one at the N- and C terminus respectively (Sun *et al.*, 1995; Darshan *et al.*, 2004). Five copies of L1 form capsomere structures in the cytoplasm, which are transported into the nucleus through association with Karyopherins (Bird *et al.*, 2008; Nelson, Rose and Moroianu, 2002; Nelson, Rose and Moroianu, 2003; Merle *et al.*, 1999). L2 nuclear transport is also dependent upon the karyopherin import pathway (Darshan *et al.*, 2004; Bordeaux *et al.*, 2006). Within the nucleus, the HPV DNA genome is encapsidated within a structure containing 72 capsomeres of L1 arranged on a $T = 7$ icosahedral lattice (Baker *et al.*, 1991; Goetschius *et al.*, 2021; Trus *et al.*, 1997; Klug and Finch, 1965) with an unknown amount of L2 (Goetschius *et al.*, 2021; Buck *et al.*, 2008). It has been proposed that the

copy number of L2 proteins per capsid may be variable even within a population of virions from one infection or cell preparation, due to previous failures at quantifying the copy number within even high-resolution structures (3.1 Å) (Goetschius *et al.*, 2021). Papillomavirus capsid maturation requires the formation of disulphide bonds (Buck *et al.*, 2005; Conway *et al.*, 2009). Bond formation is dependent upon the redox environment of the cell and desquamation, which is associated with a switch from a reducing to an oxidising environment of cells is a requirement for virion maturation (Conway *et al.*, 2009). Cell egress of HPV virions is poorly understood, but it has been proposed that the shedding of dead squames from the epithelial surface allows for virion release (Graham, 2017).

1.8 Dysregulation of the viral life cycle and its involvement in disease progression

Long-term persistence of infection highly increases the risk of progression to cancer and can often be accompanied by the integration of viral DNA into the host genome (McBride and Warburton, 2017). In persistent infections, HPV gene expression can become dysregulated and expression of the E6 and E7 oncoproteins is greatly increased due to the loss of the repressive function of E2 (Schmitt *et al.*, 2010; Cricca *et al.*, 2009; Chen *et al.*, 2014; Duensing and Münger, 2004). The removal of the G_1 to S phase checkpoint by E6 and E7's inhibition of p53 and Rb (Section 1.6.5) results in increased cell cycling and permits cells containing DNA damage and mutations to pass unchecked. This allows for the accumulation of genomic instability within HPV-infected cells, which can result in malignancy. E6 from hrHPV types can also bind to and activate telomerase, extending the cells' lifetime by bypassing the intrinsic proliferative limit imposed on cells by the length of their telomeres (Oh, Kyo and Laimins, 2001). The E6 C-terminus contains a conserved sequence which encodes a PDZ-binding domain. This domain allows hrHPV E6 to bind to and promote the degradation of PDZ domain-containing proteins such as DLG1 and PTPN13 (Kiyono *et al.*, 1997; Spanos *et al.*, 2008). Loss of these PDZ domain-containing proteins has been shown to contribute to HPV-induced transformation of cells (Spanos *et al.*, 2008). Whilst the low-risk HPV types also encode E6 and E7, these proteins do not target p53

and Rb for degradation (Heck *et al.*, 1992; Crook, Tidy and Vousden, 1991). Moreover, E6 from lrHPV types is unable to activate telomerase and does not contain a PDZ-binding domain, which partly explains why the low-risk HPV types do not cause carcinogenesis (Egawa and Doorbar, 2017).

The late stage of the viral life cycle is typically lost in persistent infections; resulting in an abortive infection where no progeny virions are produced. E1^E4 and L1 expression has previously been observed to be lower in high-grade compared to low-grade lesions (Schmitt *et al.*, 2010; Chen *et al.*, 2014). Changes in methylation may be partly responsible for the decrease in expression of the late viral genes during cancer progression (Schmitt *et al.*, 2010). The papillomavirus genome has hundreds of CpG dinucleotides and an inverse correlation between DNA methylation and HPV genome expression has been demonstrated by several studies (Rösl *et al.*, 1993; Rösl, Dürst and zur Hausen, 1988; Burnett and Sleeman, 1984). HPV16 L1 and L2 gene methylation is lowest in asymptomatic infection, when the transcriptional activity of the virus is high and increases successively with cervical lesion progression to cancer (Sun, Reimers and Burk, 2011; Mirabello *et al.*, 2012; Mirabello *et al.*, 2013; Kalantari *et al.*, 2014). This reduction in expression of the late genes and proteins during cancer progression prevents the full viral life cycle from taking place and instead, infection is considered abortive (Doorbar, 2006).

1.9 HPV and immunity

1.9.1 Epithelial cells as immune sentinels

The epithelium represents the physical barrier between the environment and our body (Proksch, Brandner and Jensen, 2008). Mucosal epithelia are present on all inner body surfaces and are often the entry portal and initial site of establishment for many viral infections, including human papillomavirus (Nestle *et al.*, 2009). To protect against this, epithelial cells contain pattern recognition receptors (PRRs), including Toll-like receptors (TLRs), NOD-like receptors (NLRs) and absent in melanoma-2 (AIM)-like receptors (ALRs), that can recognize pathogen-associated molecular patterns (PAMPs) and activate the NF-kB pathway to produce proinflammatory cytokines and

type I and III interferons (IFNs) for antiviral defence (Moody, 2022). Type I and III IFNs result in JAK/STAT signalling and expression of interferon-stimulated genes (ISGs) that promote pathogen clearance (Lazear, Schoggins and Diamond, 2019). This intrinsic sensing mechanism allows for the early detection of pathogens and the mounting of an immune response to prevent the establishment of infection. ISGs can restrict HPV replication, for example, IFIT1 can bind to the E1 helicase to prevent viral replication (Saikia, Fensterl and Sen, 2010; Terenzi, Saikia and Sen, 2008). The epithelium also contains Langerhans cells (LCs), professional antigen-presenting cells which reside above the basal layer of proliferating keratinocytes (Klagge and Schneider-Schaulies, 1999). This allows LCs to contact HPV antigens, internalise these antigens and activate T-cells (Zhou, Tuong and Frazer, 2019). Natural killer (NK) cells are also involved in the innate immune response against HPV and are important in promoting the regression of lesions (Scott, Nakagawa and Moscicki, 2001; Garzetti *et al.*, 1995).

The pattern of cytokine expression from epithelial cells defines the subsets of CD4+ T cells into a Th1 or Th2-dominated response (Swain, 1995). A dominant proinflammatory cytokine response, including IL-12, TNF-α and IFN-γ, that drives CD4+ Th1 activation is associated with natural HPV clearance and wart regression (Coleman *et al.*, 1994; Scott, Stites and Moscicki, 1999; Dupuy *et al.*, 1997; Kadish *et al.*, 1997; Kim *et al.*, 2012). These Th1 cells can recruit cytotoxic T lymphocytes, which are attributed to the elimination of virus-infected cells and regression (Konya and Dillner, 2001; Nakagawa *et al.*, 2002; Scott, Nakagawa and Moscicki, 2001). Clearance of hrHPV types takes an average of 8-14 months compared to only 5-6 months for the low-risk types (Franco *et al.*, 1999; Giuliano *et al.*, 2002; Brown *et al.*, 2005). In animal models of papillomavirus infection, a similar cellular infiltrate accompanies observations of wart regression (Nicholls *et al.*, 2001; Jain *et al.*, 2006). Moreover, systemic T cell responses can be detected that are directed towards the early E2 and E6 proteins (Jain *et al.*, 2006). These T cell responses and serum-neutralising antibody concentrations peak at periods of wart regression (Ghim *et al.*, 2000; Jain *et al.*, 2006). The developed antibody response is strong and can protect animals against further challenges with even large doses of the virus for the rest of their lives (Ghim *et al.*, 2000). There is evidence that these mechanisms are also important in hrHPV infections with observations of HPV16 E2-specific T cell responses occurring at the

time of CIN clearance (de Jong *et al.*, 2002). The importance of T-lymphocytes to the clearance of HPV infection is evident in cases of infection in HIV-positive individuals. These immune-compromised individuals have a high frequency of recurrence of CIN, viral persistence and incidence of genital warts (Fruchter *et al.*, 1996). Failure to clear or control HPV infection by the immune response results in persistent infection, with an increased likelihood of disease progression (Section 1.4) (Stanley, 2006).

1.9.2 Immune evasion by HPV

Transcriptome studies of undifferentiated keratinocytes containing HPV episomal genomes or E6/E7 oncoproteins show reduced expression of ISGs in comparison to uninfected keratinocytes (Karim *et al.*, 2011; Israr *et al.*, 2018; Kang *et al.*, 2018; Karstensen *et al.*, 2006). This suggests that HPV can evade many of the intrinsic immune sensing mechanisms described above and this evasion is in part mediated through the multifunctional HPV oncoproteins (Scarth *et al.*, 2021). High-risk HPV E6 can interact with IRF3 to prevent the transactivation of IFN-β and downstream ISG induction (Ronco *et al.*, 1998). Moreover, E6 can impair the RIG-I and Jak/STAT signalling pathways which act synergistically with E5 suppression of STAT1 expression (Scott *et al.*, 2020; Scarth *et al.*, 2021). The keratinocyte-specific interferon (IFN-κ) is downregulated by HPV with E5-directed methylation of the promoter and E6-mediated inhibition of transcription, together preventing activation of antiviral ISGs and PRRs (Reiser *et al.*, 2011; Scott *et al.*, 2020). E7 suppresses the cGAS/STING pathway through direct binding to STING and upregulation of the DNA-methyltransferase SUV39H1 (Lau *et al.*, 2015; Cigno *et al.*, 2019). Moreover, E7 can epigenetically silence Toll-like receptor 9 (TLR9) which alongside the effects on cGAS/STING signalling helps to prevent the production of type I interferons (Hasan *et al.*, 2013). The transcription factor nuclear factor-kappa B (NFκB) is activated by cellular stress, inflammation and infection and functions as a central mediator of inflammatory and immune responses (Oeckinghaus and Ghosh, 2009). HPV evades these pathways by E7-mediated inhibition of NFκB activation (Richards *et al.*, 2015). E7 can interact with transcription factors of CCL20 to prevent its transcription and downstream recruitment of LCs (Sperling *et al.*, 2012). HPV can also delay activation of the adaptive immune system. E5 can restrict MHC class I presentation and instead results in its retention in the Golgi (Ashrafi *et al.*, 2006a; Ashrafi *et al.*, 2006b; Gruener *et al.*, 2007; Cortese, Ashrafi and

Campo, 2010; Campo *et al.*, 2010). It can also impede the cell-surface expression of MHC class II and CD1d (Zhang *et al.*, 2003; Miura *et al.*, 2010). Furthermore, E2 can bind to the regulatory region of IL-10 to induce its expression (Bermúdez-Morales *et al.*, 2011). This stimulates T-regulatory cells to create an immune-tolerant environment, distorting the equilibrium of Th1/Th2 towards a Th2 dominant response and enabling viral persistence (Alcocer-Gonzalez *et al.*, 2006; Torres-Poveda *et al.*, 2014).

The niche tropism and life cycle of HPV may have also evolved to promote immune evasion. Vesicular membrane trafficking of HPV during entry shields the viral DNA from recognition by cytosolic PRRs (Section 1.6.1). The endocytic pathway may however expose HPV to endosomal TLR9, which recognises unmethylated CpG motifs in dsDNA viral genomes (Hemmi *et al.*, 2000; Thompson *et al.*, 2011). Papillomaviruses have reduced CpG content in their genomes and can also downregulate TLR9, possibly resembling a co-evolutionary mechanism for delivery of their genomes to the nucleus without recognition (Hasan, 2014; Upadhyay and Vivekanandan, 2015). Moreover, the lack of cytolysis or cytopathic death caused by HPV replication prevents the formation of a 'danger signal' that would alert the immune system to the presence of infection (Stanley, 2006). Instead, virions are produced in cells that are naturally dying through desquamation, presenting an ideal, recognition-free system for progeny production and release.

1.10 Current treatment options and disease burden of HPV infections in the anogenital region

The global burden of pathologies driven by HPV infections is high and continuing to grow. Recent projections have suggested that by 2040, there will be a 32% increase in the number of new cervical cancer cases and a 40.8% increase in the number of deaths compared to 2020 (Table 1.2) (IARC, 2022). It is projected that the number of deaths will increase more rapidly in countries with a low or medium human development index (HDI) (Table 1.2). One key assumption of this model is that the risk of developing or dying from cervical cancer is constant. Increasing vaccination

coverage and screening uptake has the potential to decrease the incidence of cervical cancer; detailed modelling demonstrates that a 90% vaccine coverage and screening uptake would result in cervical cancer elimination worldwide by 2100 (Brisson *et al.*, 2020). However, before then, it is clear that good treatment options are required.

Table 1.2: Global burden of cervical cancer: estimated annual numbers of incident cases and deaths in 2020 and projected to 2040. Taken from (IARC, 2022).

HDI category[a]	Population in 2020		Number of new cases (thousands)		Increase	Number of deaths (thousands)		Increase
	(millions)	(%)	2020	2040	(%)	2020	2040	(%)
Low HDI	494	12.8	82	162	97.3	56	112	99.9
Medium HDI	1136	29.4	183	292	59.6	113	189	66.8
High HDI	1442	37.3	240	297	23.5	129	182	40.6
Very high HDI	791	20.5	99	105	6.1	43	51	18.0
World	3863	100	604	798	32.0	342	481	40.8

Subunit vaccines against HPV, based on the L1 proteins that form viral-like particles, have been demonstrated to be a huge success but are given prophylactically and cannot be used to treat disease (Frazer, 2019). No antivirals for HPV currently exist. Therefore, treatment options target the symptoms and diseases caused by HPV infection such as warts or cancer. Due to cervical screening tests that take place in many countries, the majority of cervical diseases can be caught and the WHO recommends treatment of CIN2+ (Prendeville and Sankaranaryanan, 2017). Current treatment options for these precancerous lesions include local ablative therapies or excisional methods that aim to eradicate the affected tissue and any of the remaining transformation zone (Adams and Mbatani, 2018). Local ablative therapies include thermal coagulation, laser treatment or cryotherapy which aim to destroy cells in the abnormal area. Thermal coagulation involves the application of a probe, heated to around 100 °C, to the lesion (Duncan, 1983). Cryotherapy is a similar protocol, with a probe held in close contact with the transformation zone. Gaseous CO_2 circulates in the probe head, cooling it and freezing the affected tissue, which reaches temperatures of less than -20 °C (Castle *et al.*, 2017; Prendeville and Sankaranaryanan, 2017). Cells in this region die of necrosis due to crystallisation of the intracellular fluid and cell membrane rupture (Prendeville and Sankaranaryanan, 2017). Neither thermal coagulation nor cryotherapy produces smoke, making them safe for virus-positive lesions, but risks include damaging the adjacent epithelium or neighbouring structures (Prendeville and Sankaranaryanan, 2017). Moreover,

individuals cannot have penetrative intercourse for at least a month following treatment and cryotherapy is limited by the requirement for a reliable and inexpensive source of CO_2 (Castle *et al.*, 2017; Maza *et al.*, 2016; Prendeville and Sankaranaryanan, 2017). Lasers can also be used to destroy the transformation zone and since all three therapies ablate the diseased tissue, this cannot be histologically examined afterwards (Prendeville and Sankaranaryanan, 2017). Moreover, whilst ablative therapies are relatively effective (~80 % success rate for each form although reports vary) (Prendeville and Sankaranaryanan, 2017; McCarthy *et al.*, 2016; Higgins *et al.*, 1990) there is a significant associated pain and recurrence rate (Melnikow *et al.*, 2009).

Excisional techniques include hysterectomy, which is mostly reserved for the treatment of cervical cancer, large loop excision of the transformation zone (LLETZ) or cone biopsies. LLETZ involves the removal of the transformation zone using a low-voltage diathermy wire loop. The treatment success is very high, reported at 91- 98% but it typically requires local anaesthesia, patients have bleeding and discharge for 4 weeks following treatment and cannot use tampons or have penetrative sex during this time, similar to cryotherapy (Martin-Hirsch *et al.*, 2013; Prendeville and Sankaranaryanan, 2017). A major disadvantage of this therapy is the risk of subsequent pregnancy-related complications, particularly premature labour (Kyrgiou *et al.*, 2006) and electrosurgical injuries to the bladder, urethra and bowel have been reported (Prendeville and Sankaranaryanan, 2017). Moreover, a recent study found a 12.5% recurrence risk of CIN2+ disease in the 8 years following LLETZ in HPV-positive individuals (Sand, Frederiksen and Kjaer, 2022). Conization is the oldest method of local excision and is still widely used (IARC, 2022). It is typically carried out under general anaesthetic and involves the removal of the entire transformation zone, although often more tissue is removed than necessary, leaving a large cervical defect (Martin-Hirsch *et al.*, 2013). The treatment success rates are similar to LLETZ, reported at 90-94% (Bostofte *et al.*, 1986; Larsson, 1983). However, there are many well-recognized short- and long-term complications, including primary and secondary haemorrhage, cervical stenosis and incompetence and pregnancy-related complications, including mid-trimester pregnancy loss (Kyrgiou *et al.*, 2006; Arbyn *et al.*, 2008).

Anal intraepithelial neoplasms are treated using many of the same methods used for CIN including excision, fulguration with electrocautery (similar to LLETZ) or laser treatments (Siddharthan, Lanciault and Tsikitis, 2019). Topical treatments such as trichloroacetic acid, imiquimod and 5-fluorouracil, which are commonly used for genital warts, can also be used (Megill and Wilkin, 2017).

Overall, excisional methods are effective but require anaesthesia and a trained individual to carry them out. Moreover, they carry with them considerable risks for subsequent complications and risks for future pregnancies (Kyrgiou *et al.*, 2006). Ablative therapies are slightly less effective but can be used as a part of a screen-and-treat approach in many low-and middle-income countries (Dey *et al.*, 2002). However, unlike excisional techniques, ablation of the transformation zone prevents the opportunity for histopathological examination and therefore is not recommended when the suspicion of malignancy is high (IARC, 2022). Therefore, there remains a gap in the field for better treatment options for HPV-infected cervical precancerous lesions.

1.11 Heat as a therapy

Hyperthermia is defined as an abnormally high body temperature, typically above 40 ^{o}C. Whilst hyperthermia is now a well-documented anti-cancer treatment, its use can be traced throughout history and backdated as far back as 1600 B.C in the world's oldest surgical text, the Edwin Smith Surgical papyrus (~1600 B.C.) (Moore, 2011), which documents a patient with a tumour in the breast treated with heat in the form of red-hot irons (Breasted, 1930). Early Greek (Hippocrates 400 B.C.) and Roman (Galen 200 A.D.) translations also show records of heat treatments (Storm, 1983). Fast forward in time, reports of tumour regression in patients with a fever due to ongoing infection led to the implementation of fever-induced treatment with Coley's toxin to control tumours at the end of the 19th century (Storm, 1983). Fever was induced for several days at temperatures of around 40 °C (Storm, 1983). With the technological developments in the present day, more reproducible, well-controlled and high-quality hyperthermia treatments can be produced (Trefná *et al.*, 2017; Crezee *et al.*, 2016).

Multiple options are available to deliver the energy required to result in hyperthermia including electromagnetic radiation, ultrasound, and nanotechnologies (Trefná *et al.*, 2017; Crezee *et al.*, 2016; Crezee, Franken and Oei, 2021).

Hyperthermia is commonly used alongside radiotherapy and chemotherapy in anti-cancer treatments with three basic categories: local, regional or whole-body (Elming *et al.*, 2019; Mantso *et al.*, 2016; Franckena, 2012). Local hyperthermia involves applying heat to a solid tumour. Temperatures can be as high as 80 °C when the purpose is to completely ablate the tumour however, more commonly temperatures in the range of 40-45 °C are applied (Toraya-Brown and Fiering, 2014). This results in cell death at the site of treatment, without causing injury to adjoining tissue and allows for several physiological effects that sensitise tissue to anti-cancer therapies. These include inhibition of the DNA repair pathways, allowing sensitisation to radiotherapy, improved vascularisation, which helps overcome the areas of hypoxia attributed to radiation resistance, and activation of immune responses (Toraya-Brown and Fiering, 2014). Regional hyperthermia involves treating an entire limb or peritoneal cavity and whole-body hyperthermia is most commonly used for cases of metastatic cancer which have spread throughout the body and typically involves heating to fever-range temperatures (39-41 °C) (Wust *et al.*, 2002). Local hyperthermia has been used in the treatment of cervical pre-cancerous lesions and cancers. Treatment of low-grade, hrHPV-positive lesions at 44 °C can increase the rate of clearance in comparison to no intervention (Yang *et al.*, 2021; Bulkmans *et al.*, 2007). Moreover, using hyperthermia alongside radiotherapy treatment for cervical cancer patients increased the response rate, pelvic control and overall survival rates (Franckena *et al.*, 2008; van der Zee *et al.*, 2000; Lutgens *et al.*, 2010).Heating improves anti-tumour immunity through increased expression of surface molecules on heated tumour cells (including MICA and MHC I), exosome release of tumour antigens to antigen-presenting cells (APCs) and direct effects on immune cell activity following heating (Ito *et al.*, 2003; Ostberg *et al.*, 2007; Chen *et al.*, 2011; Mace *et al.*, 2012; Zheng *et al.*, 2003; Basu and Srivastava, 2003). Moreover, the increased perfusion allows for better immune trafficking to tumour sites (Meyer *et al.*, 2000; Song *et al.*, 1997; Kong, Braun and Dewhirst, 2001). Accumulating evidence also indicates an additional role of the heat shock proteins in inducing immunity, as they can become powerful immunogens when complexed with antigenic

peptides (Binder and Srivastava, 2005; Suto and Srivastava, 1995). Several studies have observed tumour peptides chaperoned by heat-shock proteins in cancer (Tamura *et al.*, 1997; Udono and Srivastava, 1993), and in infected cells, complexes of heat-shock proteins with pathogen-derived peptides are common (Srivastava, 2002). This additional role of heat shock proteins has the potential to be used therapeutically, with mammals immunised with HSP-peptide complexes shown to elicit a potent CD8+ and CD4+ T-cell response against the chaperoned peptides (Suzue *et al.*, 1997). This method has even been extended to HPV16 E7, which when complexed with HSP70, resulted in high E7-specific T-cell mediated immune responses in vaccinated mice (Cheng *et al.*, 2001). Tiny amounts of the peptide, in the femtomole range, are required to result in immunogenicity if chaperoned by heat shock proteins (Nieland *et al.*, 1996). This powerful immunogenicity is in part due to the CD91 receptor on APCs which allows for the internalisation of the HSP-peptide complex and processing for presentation by MHC class I and II for CD8+ and CD4+ activation respectively (Figure 1.11) (Hu *et al.*, 2022). This induces antigen-specific adaptive immunity, but innate immunity can also be triggered by these HSP-peptide complexes interacting with CD91 and other receptors, resulting in dendritic cell maturation and secretion of pro-inflammatory cytokines (Basu *et al.*, 2000). Innate immunity may also be triggered by heat shock through activation of the non-canonical heat shock proteins. For example, HSF1 regulates the expression of IL-8 (CXCL8), a pro-inflammatory cytokine which has been observed to initiate neutrophil recruitment in the lung following hyperthermia (Singh *et al.*, 2008; Tulapurkar *et al.*, 2012). Other inflammatory chemokines that recruit NK cells, T cells and monocytes (CXCL9, CXCL10, CXCL11 and CXCL12) have been shown to contain HSF1-binding sites (Hasday, Thompson and Singh, 2014), suggesting that following heat shock, HSF1 may promote immunity through several pathways.

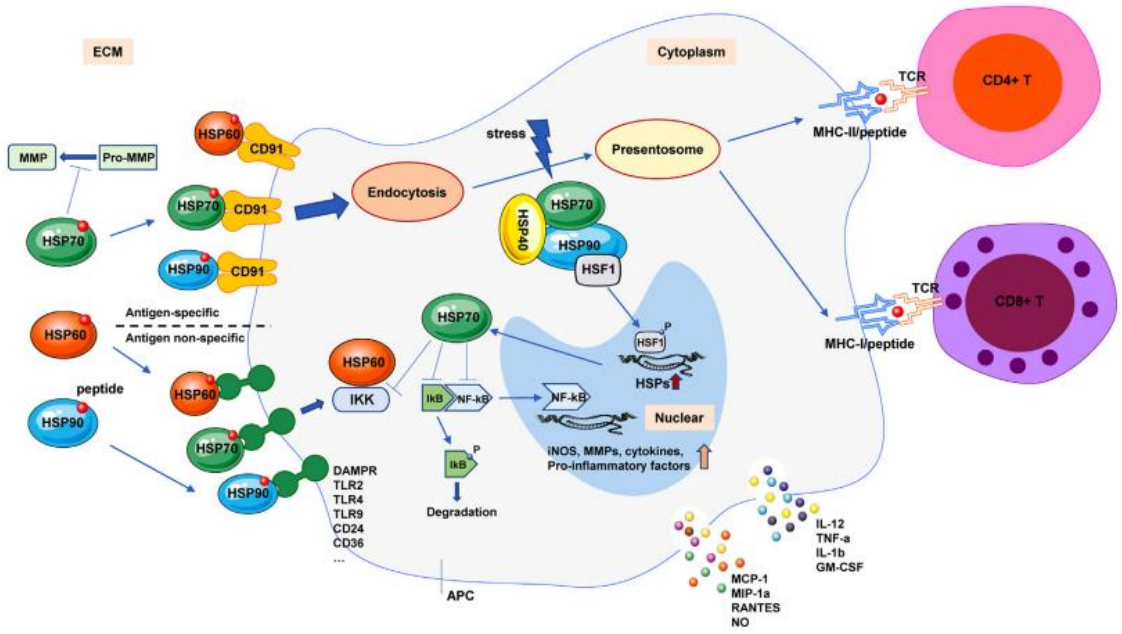

Figure 1.11. The interaction between heat shock proteins and APCs stimulates innate and adaptive immunity. Heat shock proteins can bind to APCs through CD91 (orange receptors) and other APC receptors (green receptors) to stimulate adaptive and innate immunity respectively. Internalisation of heat shock proteins with their chaperoned peptides through endocytosis can result in MHC class I and II presentation of the peptides to CD8+ and CD4+ T cells (upper pathway). Interaction of HSP-peptide complexes with other APC receptors results in the secretion of pro-inflammatory cytokines and innate immune activation (lower pathway). Adapted from Hu *et al.*, 2022.

1.12 Microwave radiation as a form of delivering hyperthermia

1.12.1 Current microwave treatments

Microwaves are a form of electromagnetic radiation with wavelengths between 1 meter to one millimetre (Marion, 1981). They are a non-ionising form of radiation, due to their low frequency and therefore do not carry the risk of inducing strand breaks in DNA (Borrego-Soto, Ortiz-López and Rojas-Martínez, 2015). Microwave radiation generates heat internally within materials, including cells and tissues, by penetrating and propagating through tissues and generating an internal electric field within the material (Mishra and Sharma, 2016). This electric field induces translational motions

of free-of-bound charges such as electrons or ions (Mishra and Sharma, 2016). It can also cause the rotation of charged complexes such as water, which is a dipolar molecule, to attempt to align with the microwave field (Brace, 2009; Mishra and Sharma, 2016). Inertial, elastic and frictional forces resist these induced motions and the resulting energy loss results in volumetric heating.

Thermal ablation by radio- and microwaves, types of electromagnetic radiation, is becoming a popular method for early-stage cancer treatment (Breen and Lencioni, 2015). Microwaves offer excellent heating uniformity, larger ablation volumes and shorter ablation times compared to radiofrequency ablation (RFA) (Yu *et al.*, 2020; Breen and Lencioni, 2015; Wang *et al.*, 2021). This has led to the use of microwave ablation for liver (Wang *et al.*, 2021), breast (Zhou *et al.*, 2012; Zhou *et al.*, 2014; Liu *et al.*, 2022) and lung cancer (Wei-Chun *et al.*, 2016; Moussa *et al.*, 2019). Since these are internal organs, percutaneous microwave application is required, using a probe that passes through the skin to reach the tumour. In one meta-analysis, microwaves were observed to offer better tumour control and disease-free survival compared to RFA (Facciorusso *et al.*, 2020). Moreover, microwave treatment could induce immune activation. This was initially observed in mouse models of breast cancer that showed activation of macrophages and NK cells following microwave treatment (Yu *et al.*, 2020). NK cell activation was proposed to inhibit metastatic progression (Yu *et al.*, 2020). In patients, microwave ablation activated T lymphocyte expansion and resulted in a T-cell polarisation shift to Th1 (Zhou *et al.*, 2021). Immune activation by microwave treatment makes this therapy attractive for cancer treatment and signifies its potential use for infected lesions.

1.12.2 Microwave-delivered hyperthermia using the Swift® device

The Swift® is a CE-marked hand-held medical device which allows for the targeted delivery of microwaves through a 6.7 mm contact site, developed by Emblation Ltd. The application of microwaves through the Swift® is different compared to the delivery method used in the previously mentioned studies for breast, lung and liver cancer where a probe was delivered percutaneously. Instead, a flat-headed probe is used which allows the treatment of lesions at the surface of the skin. The Swift® is approved for use in podiatry and dermatology clinics for the treatment of plantar warts (verrucas)

and common warts. Previously, treatment options for plantar warts involved the use of cryotherapy, laser and radiofrequency devices but these methods had a low efficacy and induced discomfort through tissue destruction (Kwok, Holland and Gibbs, 2011; Veitch, Kravvas and Al-Niaimi, 2017). Microwave treatment of plantar warts resulted in the shrinkage and clearance of lesions without significant inflammation, tissue damage or scarring (Bristow *et al.*, 2017). Moreover, the resolution rate of microwave treatment (75.9%) was much greater than cryotherapy (33%). Of the resolving lesions, 94% had cleared following 3 treatments, limiting the amount of time patients need to attend clinics. Microwave treatment had a low pain score and this decreased significantly as the treatment plan proceeded (Bristow *et al.*, 2017). Moreover, *in vitro* work suggested that microwave treatment could induce an anti-viral response with enhanced IL-6 secretion, increased expression of surface cell activation markers and enhanced cross-presentation of HPV antigens from primed monocyte-derived dendritic cells (moDCs) to CD8+ lymphocytes (Bristow *et al.*, 2017). However, this work used HPV-negative keratinocyte cell lines so it is unclear if this can be extended to cases of HPV infection, given the immune evasion mechanisms employed by the virus (Section 1.9.2).

Subsequently, a UK clinical trial showed that microwave therapy was a safe and effective treatment option for actinic keratoses (AK), common precancerous skin lesions often with a β-HPV aetiology (Jackson *et al.*, 2020). Actinic keratoses are precursors to cutaneous squamous cell carcinoma (cSCC) (Hufbauer and Akgül, 2017). Whilst the individual risk of progression to cSCC is low, 65% of cSCCs on the head and neck arise from AK (Marks, Rennie and Selwood, 1988; Hufbauer and Akgül, 2017). Currently, available AK treatments can significantly reduce the risk of cSCC development but require dedicated application over weeks and result in inflammation (de Berker *et al.*, 2017; Jackson *et al.*, 2020). Therefore, a lesion-directed treatment, that can be delivered in primary care, may be effective in reducing the cSCC burden (Jackson *et al.*, 2020).

Given the current lack of good treatment options for HPV-infected anogenital lesions (Section 1.10), we aim to determine if the Swift® device could be extended to treat these lesions. Hyperthermia has many proven benefits as a therapy, including immune

activation (Section 1.11) (Toraya-Brown and Fiering, 2014) and microwaves offer an attractive option to deliver this hyperthermia due to the linearity, excellent heating uniformity, and short ablation times of radiation. Due to the location of these anogenital lesions on the surface of the mucosal epithelium, the probe head applicator of the Swift® will allow for the precise delivery of microwaves at these sites.

We have previously published work that reveals the molecular effects of microwave treatment on HPV-infected epithelial tissues *in vitro* (Conley et al., 2023). Our study focussed on models of cervical cancer, using 3D organotypic raft cultures of SiHa, transformed cervical cells that contain two integrated copies of HPV16 (Friedl *et al.*, 1970). Microwave treatment resulted in cell ablation, precisely at the treatment site (Conley *et al.*, 2023). Additionally, the tumorigenic phenotype of these cells was reversed; cell proliferation was decreased alongside an increase in apoptosis and autophagy. The expression of the viral oncoproteins E6 and E7 was decreased, with a corresponding upregulation in the downstream target proteins p53 and Rb (Conley *et al.*, 2023). Microwave treatment resulted in a cell stress response, with clear formation of cytoplasmic stress granules and HSP70 upregulation, indicating translational stress and heat shock respectively. We extended our analysis into an earlier model of disease using normal immortalised keratinocytes (NIKS) stably transfected with the HPV16 genome (NIKS16) (Flores *et al.*, 1999; Wechsler *et al.*, 2012). Growth of these cells in organotypic raft cultures allows for keratinocyte differentiation and the reconstruction of the full viral life cycle (Meyers and Laimins, 1994). Microwave treatment decreased NIKS16 cell proliferation and increased the differentiated compartment of these tissues, through increased transglutaminase and keratin 10 (Conley *et al.*, 2023). Microwave treatment may be most applicable for the treatment of anogenital pre-cancers. Therefore, further understanding of how treatment affects non-transformed cells and the productive viral life cycle as a model for earlier disease is required.

1.13 Aims

The present gaps in knowledge that this thesis aims to address are as follows:

Aim 1: Investigate how microwave treatment affects the transcriptional landscape of keratinocytes and if it can induce innate immunity.

- Optimise microwave treatment for *in vitro* 3D epithelial raft cultures.
- Determine if microwave treatment can induce a hyperthermic response.
- Investigate the impact of microwave-delivered hyperthermia on the transcriptional landscape of keratinocytes.
- Determine if microwave treatment can induce an innate immune response.

Aim 2: Analyse the effects of microwave treatment on HPV16 gene expression and replication.

- Investigate how microwave treatment impacts HPV gene expression from the early and late promoters.
- Determine if these transcriptional changes are taking place at sites proximal or distal to the site of microwave treatment.
- Assess whether any transcriptional changes are translated to the protein level.
- Investigate changes in viral genome replication following microwave treatment.

Aim 3: Investigate the late life cycle stages of HPV within *in vitro* models of disease, including production and localisation of the major capsid protein and virion assembly, and determine if this is impacted by microwave treatment.

- Characterise HPV16 L1 expression and spatial localisation within differentiated keratinocytes.
- Determine if virion production can be observed within *in vitro* differentiated keratinocytes.
- Analyse how microwave treatment impacts L1 expression and localisation.

Chapter 2 Materials and Methods

2.1 Materials

2.1.1 Cell lines

The following cell lines were used in this study.

Table 2.1: Details of the cell lines used in this study. The respective media and supplements used for growing each cell line in 2D are summarised.

Cell type	Description	Medium composition
3T3 J-2	Mouse embryonic fibroblast cell line used as feeder layer for growth of keratinocytes	'3T3 medium' Dulbecco's Modified Eagle Medium (DMEM) (Gibco, Cat # 31966-021) supplemented with 10% donor calf serum (Gibco, Cat #), 2 mM L-Glutamine (Gibco, Cat #25030-024) and 1% (v/v) penicillin-streptomycin (Gibco, Cat #15140-122).
SiHa	HPV-16-positive transformed cervical cancer cells containing two host-integrated copies of HPV-16 (Friedl *et al.*, 1970)	'HeLa medium' DMEM supplemented with 10% foetal bovine serum (FBS) (Gibco, Cat #10290-106), 2 mM L-Glutamine and 1% (v/v) penicillin-streptomycin.
HaCaT	Human spontaneously immortalized HPV-negative keratinocytes (Boukamp *et al.*, 1988)	
NIKS16	Normal immortalised keratinocytes stably transfected with the HPV16 genome (Flores *et al.*, 1999)	'E medium' 3:1 ratio of DMEM: F12 medium (Gibco Renfrew, UK, ref no 21765-029) supplemented with 10% FBS, 2 mM L-Glutamine, 1% (v/v) penicillin-streptomycin, 180 µM adenine, 5 µg/ml transferrin (Sigma-Aldrich, T1147), 5 µg/ml insulin (Sigma-Aldrich 16624-50MG), 0.4 mg/ml hydrocortisone (Sigma-Aldrich, H0888) and 0.1 nM cholera toxin. Media was supplemented with 0.2 ng/ml epidermal growth factor (EGF) (Sigma-Aldrich, GF144) the day after plating.
W12E	HPV-16 positive keratinocytes derived from a CIN-grade lesion (Stanley *et al.*, 1989)	'W12 medium' DMEM supplemented with 10% FBS, 2 mM L-Glutamine, 1% (v/v) penicillin-streptomycin, 0.4 mg/ml hydrocortisone and 0.1 nM cholera toxin. Media was supplemented with 0.2 ng/ml epidermal growth factor (EGF) the day after plating.

2.1.2 Antibodies

Primary antibodies used in immunofluorescence (IF), immunohistochemistry (IHC) and flow cytometry experiments are summarised in Table 2.2.

Table 2.2: Information on the primary antibodies used in this investigation.

Antibody	Application	Species	Dilution	Manufacturer	Reference Number
HPV16 L1	IF	Mouse	1:500	Abcam	ab69
p53	IHC	Mouse	1:3000	Abcam	ab1101
Rb	IHC	Mouse	1:1600	Cell Signalling Technology	9309
CD14	Flow Cytometry	Mouse	1:20 (5 µl per million cells in 100 µl)	BioLegend	367103
CD40	Flow Cytometry	Mouse	1:20 (5 µl per million cells in 100 µl)	BioLegend	334307
CD80	Flow Cytometry	Mouse	1:20 (5 µl per million cells in 100 µl)	BioLegend	305207
CD86	Flow Cytometry	Mouse	1:20 (5 µl per million cells in 100 µl)	BioLegend	374205

2.1.3 Primers and probes

Primers and probes used for the amplification and detection of gene products in reverse transcription-quantitative polymerase chain reaction (RT-qPCR) are shown in Table 2.3. All probes were FAM-labelled except GAPDH which was HEX-labelled.

Table 2.3: Sequences for each of the primer/probe sets used in this study. All primer/probe sets were designed using PrimerQuest (Integrated DNA Technologies) and purchased from Eurogentec. The nucleotide positions of the HPV primers and probes on the HPV16 genome are indicated. For primers developed in house, the efficiency of each set is shown in the appendix (work performed by Andrew Stevenson).

Gene	Forward Primer	Reverse Primer	Probe	Reference
E4	5'-CACACCACTAAGTTGTTG-3' (nt 3508 – 3525)	5'-CTATGGGTGTAGTGTTAC-3' (nt 3619 – 3602)	5'-CTCAGTGGACAGTGCTCCAATCCTCACTGC-3' (nt 3534 – 3563)	(Veerapraditsin, 2004)
E4^L1	5'-CACACCACTAAGTTGTTG-3' (nt 3508 – 3525)	5'-CAAAGAGACATCTTTTAAATGT-3' (cross-junctional splice site 5647-5637: 3630- 3621)	5'-CTCAGTGGACAGTGCTCCAATCCTCACTGC-3' (nt 3534 – 3563)	(Klymenko *et al.*, 2016)
E6E7	5'-CAATGTTTCAGGACCCACAG-3' (nt 102 – 121)	5'-CTGTTGCTTGCAGTACACACATTC-3' (nt 211 – 188)	5'-CCACAGTTATGCACAGAGCTGC-3' (nt 140 – 161)	(McFarlane *et al.*, 2015)
L1	5'-CAACGAGCACAGGGCCAC-3' (nt 6576– 6593)	5'-TACTGAAGTAGATATGGCAGCAC-3' (nt 6692 – 6670)	5'-CCAACTATTTGTTACTGTTGTTGATACTACACGCAG-3' (nt 6617 – 6652)	(Chambers *et al.*, 2013)
GAPDH	5'-GAAGGTGAAGGTCGGAGT-3'	5'-GAAGATGGTGATGGGATTTC-3'	5'-CAAGCTTCCCGTTCTCAGCC-3'	(Klymenko *et al.*, 2017)
B-actin	5'-AGCGCGGCTACAGCTTCA-3'	5'-CGTAGCACAGCTTCTCCTTAATGTC-3'	5'-ATTTCCCGCTCGGCCGTGGT-3'	(Klymenko *et al.*, 2017)
HSP70	5'-AGGCCAACAAGATCACCATC-3'	5'-GTCCTCCGCTTTGTACTTCTC-3'	5'-ATGCGCTCGATCTCCTCCTTGC-3'	Developed in house
TNF-α	5'-AGAGGGAGAGAAGCAACTACA-3'	5'-GGGTCAGTATGTGAGAGGAAGA-3'	5'-AAACAACCCTCAGACGCCACATCC-3'	Developed in house

IL-6	5'-CCTAGAGTACCTCCAGAACAGA-3'	5'-CAGGAACTGGATCAGGACTTT-3'	5'-AGTGAGGAACAAGCCAGAGCTGTG-3'	Developed in house
IL-1β	5'-TCTGTACCTGTCCTGCGTGTTGAA-3'	5'-TGCTTGAGAGGTGCTGATGTACCA-3'	5'-CAAGCTGGAATTTGAGTCTGCCCAGT-3'	(Klymenko *et al.*, 2017)
KRT10	5'-GCTGACCTGGAGATGCAAAT-3'	5'-AGCATCTTTGCGGTTTTGTT-3'	5'-TGTGTCCACTGGTGATGTGAATGTGG-3'	(Klymenko *et al.*, 2017)
TGT	5'-CGGTTGGATGGTACTCACTTAC-3'	5'-GGGAAATAGAGTCTGCCCTTATC-3'	5'-AGGCCTCTTCCTGTCAGCCTATCT-3'	Developed in house

2.1.4 Kits

Kits used in this study are summarised in Table 2.4.

Table 2.4: Kits used in this study.

Kit	Manufacturer	Reference Number
RNeasy	Qiagen	74104
Maxima First Strand cDNA Synthesis	ThermoFisher Scientific	K1641
Human High Sensitivity Cytokine A Premixed Magnetic Luminex Performance Assay	Biotechne	FCSTM09
QIAamp DNA extraction kit	Qiagen	51304
MojoSort Human CD14+ Monocytes Isolation kit	BioLegend	480047

2.2 Methods

2.2.1 Cell culture

J2 3T3 fibroblasts, HaCaT cells, and SiHa cells were cultured in a humidified incubator at 37 ^{o}C and 5 % CO2. Cells were detached from plates using 0.05 % trypsin-EDTA (Gibco Renfrew, UK, ref no 25300-054) and passaged three times a week at either 1:5 or 1:10 dilution depending on growth rate. 3T3 cells were only maintained in culture for up to 2 weeks to prevent transformation and ensure their effectiveness as feeder cells.

2.2.1.1 Cell culture of HPV-positive W12E and NIKS16 cells

HPV-positive W12E and NIKS16 keratinocytes cannot be conventionally passaged, as this can cause loss of the episomal copies of HPV16 within these cell lines, and instead must be grown each time from frozen stocks to a maximum passage number of 15-17. In addition, the cells are required to be grown on feeder layers to mimic the dermis. 3T3 fibroblast cells were treated with Mitomycin C (50µg per 10cm plate) (Sigma Aldrich, M050) and incubated for 2 hours at 37 ^{o}C to arrest proliferation. These cells were then detached from plates using 0.05 % trypsin-EDTA and pelleted at 1,000 x g for 5 minutes. Then, $7.5x10^{6}$ 3T3 cells were resuspended with $1x10^{6}$ keratinocytes into W12 or E medium (for W12E or NIKS16 cells respectively, Table 2.1). The mixture of 3T3 and keratinocytes was plated equally onto five 10 cm dishes. The following day, cells were supplemented with 0.2 ng/ml epidermal growth factor (EGF). The medium was changed every other day and cells were grown for up to 7 days to prevent the cells from beginning to differentiate. On day 7, the media was removed, cells were washed with PBS, and trypsin was incubated on the cells for 5 minutes. This protocol benefits from the strong attachment of keratinocytes to the culture plate as a 5-minute incubation in trypsin is sufficient to remove the 3T3 fibroblast cells but the keratinocytes remain attached. The plates were washed 3 times with PBS to remove all of the 3T3 cells and then trypsin was added for a subsequent 15-minute incubation. This removes the keratinocytes, which were then pelleted at 1,000 x g for 5 minutes. Cells were resuspended and either seeded onto collagen matrices to form 3D organotypic raft cultures or were frozen to produce aliquots of the next passage. For analysis of the late HPV life cycle stages within keratinocytes grown in 2D, cells were

grown to 10 or 15-day time points to allow for differentiation of the cells, with the media changed every second day.

2.2.1.2 Preparation of Cell Stocks

Cells were removed from culture vessels using trypsin as described, counted with a haemocytometer and centrifuged at 1,000 x g for 5 minutes. The supernatant was removed and the pellet resuspended in the appropriate growth media + 10 % (v/v) DMSO (Sigma-Aldrich, D1435) to give a concentration of 1 x 10^6 cells/ml. Cells were stored in 1 ml aliquots at -80 °C overnight before being transferred for long-term storage within a liquid nitrogen tank.

2.2.1.3 3D organotypic raft culture

3D culture of HPV-positive and negative keratinocytes was performed as previously described (Meyers *et al.*, 1992). A dermal equivalent was prepared which consists of a collagen-fibroblast matrix. Cells of interest were then overlaid onto this dermal equivalent and grown at the air-liquid interface (Figure 2.1). Whilst preparing the collagen-fibroblast matrices, solutions must be kept cold to prevent the collagen from solidifying, so solutions were prepared in a 'pre-chilled' Duran bottle. J2 3T3 fibroblast cells were dissociated using 0.05% trypsin/EDTA and then centrifuged to pellet the cells for 5 minutes at 1,000 x g. One confluent 10 cm dish of 3T3 cells was used to prepare 12 full-sized (14 mm diameter) or 24 'mini' organotypic rafts (7 mm diameter). During the centrifugation, 17 ml of collagen isolated from rat tail tendons was added to a pre-chilled 100 ml Duran bottle. 10 ml of filter-sterilised 1:1000 acetic acid was added with 3 ml 10x MEM (Gibco Renfrew, UK, ref no 11430-030). The pH was adjusted to 7.4 (indicated by an orange/pink colour) using 0.5 N NaOH as recommended (Roth-Carter *et al.*, 2022). The 3T3 cells were resuspended in 3 mL FBS and added to the collagen mixture and then 2.5 ml of the resulting mixture was added to each well of a 6-well plate (for the growth of 'full-sized' 14 mm diameter rafts) or 1.25 ml to each well of a 12-well plate (for the growth of 'mini' 7mm diameter rafts). The collagen was allowed to polymerise for 20 minutes at 37 ^{o}C in a cell culture incubator. Following this, 2 or 1 ml of '3T3 media' (Table 2.1) was added to each well of a 6- or 12-well plate respectively and the collagen detached from the side of the dish using a 20 µl filter tip. The collagen matrices were allowed to contract to the desired size of the well of a 24-

well or 48-well plate for 'full-sized' and 'mini' rafts respectively over 7 days in a 37 ^{o}C incubator (Figure 2.1). The media was changed every second day.

3D organotypic raft cultures were produced by overlaying the collagen-fibroblast dermal equivalent with cells of interest (Figure 2.1). Cells grown in 3D included HaCaT, SiHa, NIKS16 and W12E (Table 2.1). Following contraction of the collagen, the cells of interest were seeded on top and incubated in media for 24-72 hours. The exact number of cells and the length of incubation in media or at the air-liquid interface varied between the cell lines and the optimised values are shown (Table 2.5). Rafts were transferred to metal grids and E medium added such that it was just in contact with the bottom of the grid, with no media covering the collagen-fibroblast matrices. Rafts were then grown at the air-liquid interface for 12-14 days with the media changed every second day (E medium supplemented with EGF (0.2 ng/ml) (Figure 2.1).

Table 2.5: Organotypic raft culture preparation details for each cell line. The number of cells to seed on top of 'mini' or 'full-sized' rafts for each cell line is denoted in the table alongside the time left in media before raising to the air-liquid interface (ALI).

Cell line	Number of cells seeded on mini raft	Number of cells seeded on full-sized raft	Hours incubated in media before raising to ALI	Days grown at the ALI
HaCaT	5x10^5	1x10^6	48 hours	13 days
SiHa	2.5x10^5	5x10^5	72 hours	12 days
NIKS16	2x10^5	4x10^5	24 hours	14 days
W12E	2x10^5	4x10^5	24 hours	14 days

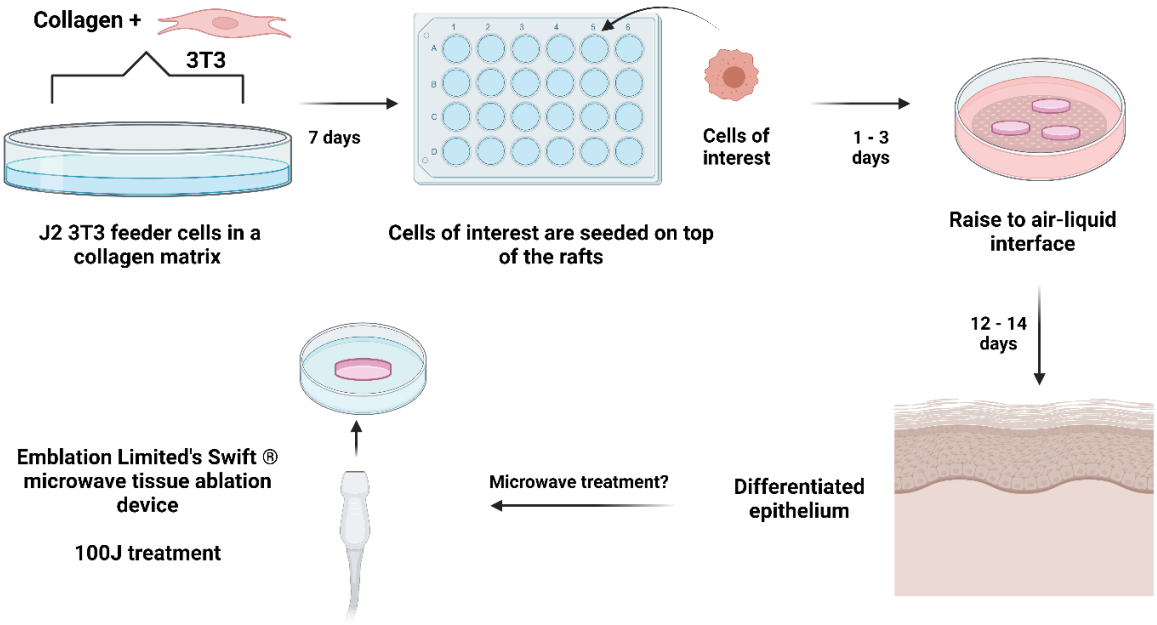

Figure 2.1 Diagrammatic workflow of organotypic 3D raft culture. 3T3 fibroblasts were seeded in a collagen matrix to provide a "feeder layer" representing a dermal equivalent. The collagen matrices were incubated for up to 7 days to allow for contraction and overlaid with the cells of interest (Table 2.5). 24 to 72 hours later, depending on the cell line (Table 2.5), the rafts were transferred onto metal grids and grown at the air-liquid interface (ALI). The media in the dish was changed every other day and on days 12 to 14 (Table 2.5) the rafts were microwave- or mock-treated.

2.2.1.4 Microwave treatment of 3D organotypic rafts

3D organotypic raft cultures were microwave or mock-treated by transferring the tissue to the lid of a dry 5 cm dish that had been pre-incubated at 37 °C, with the cell side facing down. The dish was closed, and the microwave probe was positioned underneath the plastic such that the microwaves would first travel through the plastic lid and then into the top of the tissue containing the cells, before going through the collagen matrix. Microwaves were delivered at a power of 10 W for a 10 s duration (unless otherwise stated). Mock-treated tissues underwent the same procedure but without the microwave treatment to account for any cell loss caused by placing tissues cell-side down on the culture dish. Tissues were either immediately fixed (to produce a 0 H time point) or returned to the air-liquid interface in the original orientation (with cells facing up) at 37 °C for up to 72 hours and then fixed. Samples for RNA extraction were frozen in 700 µl QIAzol Lysis reagent (Qiagen ref no 79306) and stored at -70 °C. Samples for H&E, IF, RNAScope and EM were fixed in 10 % Neutral

buffered formalin (NBF) (Sigma, F-1635) for 16 hours, followed by a wash in PBS and then storage in PBS.

2.2.2 Temperature measurements of organotypic raft cultures

A temperature probe (NOMAD-Touch by Neoptix, Canada) was used to measure the temperature of rafts undergoing microwave treatment at different energies. The probe was positioned such that it was in contact with the surface of the tissue facing the microwave probe. Readings were taken every second during the treatment (10 s) and continued for 20 s after treatment. Three biological replicates were included. A subsequent experiment used two probes, one directly under the site of treatment and another at a site in the tissue distant from that of treatment (Figure 2.2).

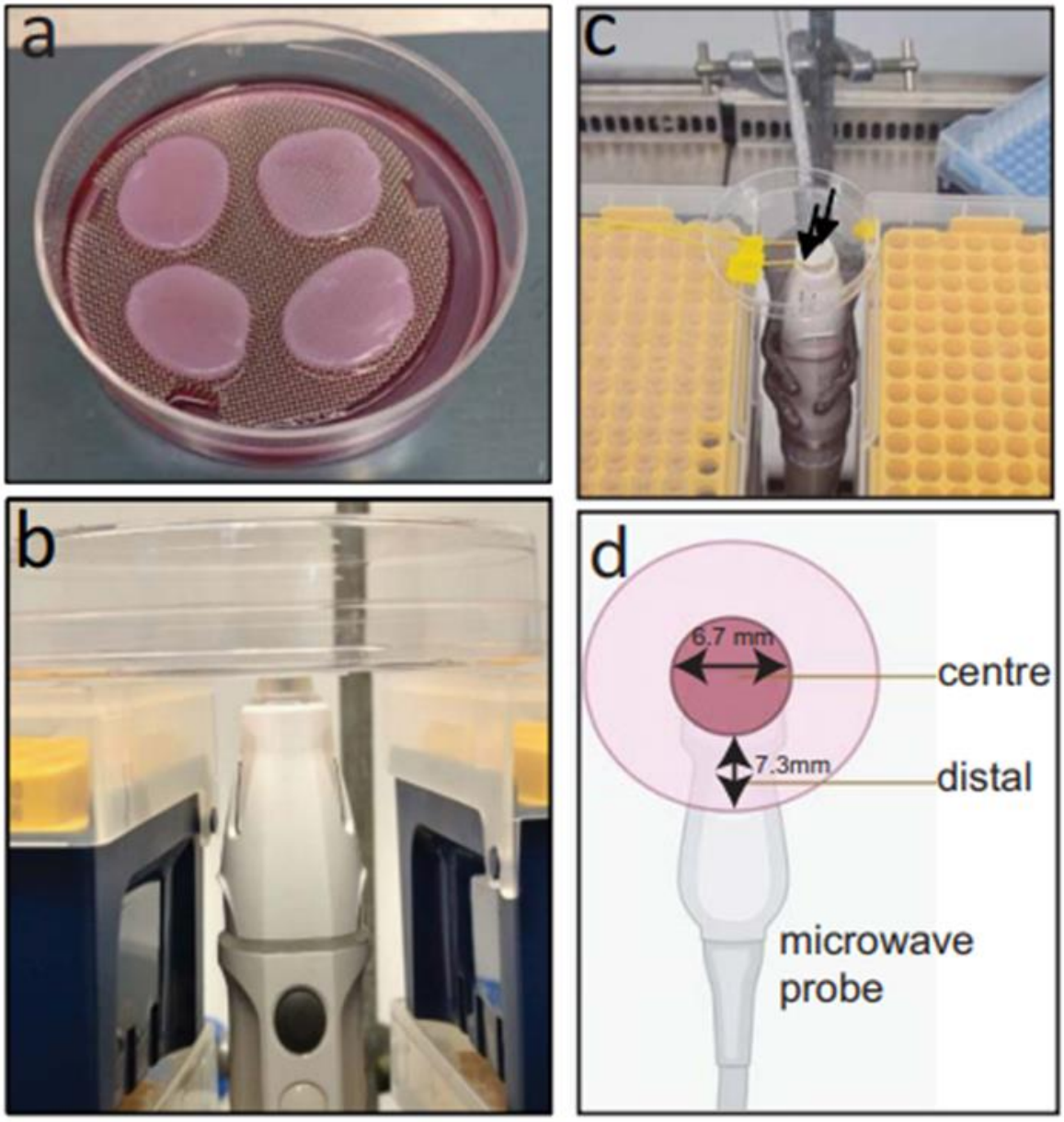

Figure 2.2: Experimental set-up for microwave treatment of 3D organotypic raft cultures and temperature measurement. (A) 'Full-sized', 14 mm diameter SiHa tissue growing on a metal grid at the air-liquid interface. (B) Tissues were inverted onto the lid of a pre-heated tissue culture dish with the top surface of the raft in contact with the plastic and directly above the microwave probe. (C) A top view of the experimental set-up, this time showing the yellow temperature probes that were used. One probe was positioned directly under the centre of the raft, above the microwave probe and another was at a distant site from treatment as shown in the cartoon (D). Figure adapted from Conley *et al.,* 2023.

2.2.3 RNA extraction

Samples of HaCaT, SiHa, NIKS16 and W12E rafts that had been frozen in QIAzol were thawed on ice and vortexed to remove cells from the collagen matrix. The supernatant containing the cells was transferred into a clean tube (Eppendorf), leaving the collagen matrix. Cells were homogenised with a subsequent vortex. 200 µl of chloroform (VWR, 0757) was added, the sample vortexed and then incubated for 3 minutes at 25 ^{o}C. Samples were centrifuged at 12,000 x g for 15 minutes at 4 ^{o}C. The upper aqueous phase was transferred to a clean LoBind 1.5 ml tube (Eppendorf, 022431021) and 230 µl of 100% ethanol (RNAse free) added. The sample was transferred to an RNAeasy column (Qiagen, 74104). Total RNA was prepared using the RNeasy kit (Qiagen, 74104) in accordance with the manufacturer's protocol. RNA was eluted using 80 µl of RNAse-free water (Qiagen, 129112) incubated on the membrane for 1 minute followed by centrifuging at 12,000 x g for 30 seconds at room temperature. Eluates were transferred and the concentration of the RNA was determined using a Nanodrop One/One Microvolume UV-Vis Spectrophotometer (Thermofisher).

2.2.4 cDNA synthesis

cDNA was synthesised from total RNA (500 ng) using the Maxima First Strand cDNA Synthesis Kit (Table 2.4) for RT-qPCR with dsDNase as per the manufacturer's instructions. Samples were diluted to 100 µl and stored at -20 ^{o}C.

2.2.5 Real-time quantitative PCR

Primers for HPV16, epithelial differentiation and heat shock genes were designed using PrimerQuest (Table 2.3). The housekeeping gene β-actin was included in RT-qPCR analysis to use as a reference for relative quantification. RT-qPCR was performed using a 7500 Real Time PCR System (Thermofisher). For each RT-qPCR reaction (total volume of 20 µl), 10 µl of Takyon ROX Probe 2X MasterMix dTTP blue (Eurogentec, UF-RPMT-B0701), 4 µl of Primer Probe Mix (final concentrations 900 nM and 100 nM for primers and probes respectively) and 1 µl of water were used. 5 µl of cDNA was added. The following reaction conditions were used: 50 ^{o}C for 2 minutes, 95 ^{o}C for 3 minutes followed by 40 cycles of 95 ^{o}C for 10 seconds followed by 60 ^{o}C for 1 minute. Each sample was run in triplicate. Data produced in each qPCR reaction was

analysed on the 7500 Real-Time SDS Software (Thermofisher). The threshold line for C_T determination was assigned automatically or manually and was always within the exponential phase. Relative quantification of genes of interest was done using the Livak method ($2^{-\Delta\Delta CT}$) (Livak and Schmittgen, 2001). The output generated the expression ratio of genes of interest in treated compared to untreated rafts using β-actin as a reference. Four biological and three technical replicates were tested per condition unless otherwise specified and statistical analysis was carried out using a Kruskal Wallis test (Statistics Kingdom), a non-parametric alternative to the One-Way ANOVA, to determine significance.

2.2.6 Droplet digital PCR

Droplet digital PCR (ddPCR) allows the partitioning of individual samples into 20,000 nanolitre-sized droplets. This enables the measurement of thousands of independent amplification events within a single sample. Absolute quantification can be carried out without the need for standard curves. Droplet digital PCR was used to determine the average HPV16 viral load per cell in W12E rafts with and without microwave treatment using copy number variant (CNV) analysis. ddPCR assays were set up as duplexes with the cellular RPP30 control probe primer set and custom-designed HPV16 L1-specific primers and probes as previously described (Stevenson *et al.*, 2020). For L1, the reporter dye was FAM and the dark quencher BHQ1 (IDT). Human RPP30 was used as an endogenous control for every ddPCR reaction as a copy number reference with the reporter dye HEX (Bio-Rad, 10031243). Each reaction run contained a negative control.

Each ddPCR reaction (total volume of 25 µl) contained 11 µl of 2x ddPCR SuperMix for Probes (no dUTP) (Bio-Rad, 186-3023), 0.7 µl of the RPP30 endogenous control assay (Bio-Rad, 10031243), HPV16 L1 Primer Probe mix (300 nM final concentration), 1.25 µl of restriction digest mix (4 U of the enzymes *Eco*RI and *Hind*III in 1x NEB buffer) and 2 µl of template DNA (10-100 ng). Reactions were prepared in a semi-skirted 96-well plate (Eppendorf). In-reaction restriction digest of DNA, using the restriction enzymes *Eco*RI and *Hind*III, helped the partitioning of DNA into droplets and was confirmed to not cut within the viral or control target sequences. Reactions (21 µl) were mixed with 70 µl Droplet Generation Oil on DG8 cartridges in the QX200 droplet generator (Bio-Rad) to generate droplets. The plate was then sealed with a pierce-able foil heat seal

(Bio-Rad). Subsequently, PCR was performed with the reaction conditions: 95 °C for 10 minutes followed by 40 cycles of 94 °C for 30 seconds and 60 °C for 1 minute followed by a final extension at 98 °C for 10 minutes. Samples were incubated at 12 °C for a minimum of 4 hours to allow for maximum yield recovery of droplets (Rowlands *et al.*, 2019). Droplets were analysed on a QX200 Droplet Reader (Bio-Rad). The data was analysed using the QuantaSoft analysis software (Bio-rad) to assign droplets as positive/negative and determine the copy number of viral genomes per cell in comparison to RPP30. Each diploid human cell contains 2 copies of the RPP30 gene per cell which allows quantification. Statistical analysis was performed using an unpaired Student's t-test to determine any significant differences in the means between mock or treated conditions at each time point.

2.2.7 RNAScope

A 2.5 LS Duplex RNAScope assay was carried out using target HPV16 E6/E7 (ACD-Bio, 311528-C2) and L1 (ACD-Bio, 315608) probes on the Leica Biosystems' BOND RX Research Advanced Staining System. Sections (4 µm) of formalin-fixed paraffin-embedded (FFPE) raft tissues were placed onto a Superfrost plus slide, heat treated at 60 °C for 2 hours and loaded onto the Leica Autostainer. Positive controls using the human PPIB (ACD-Bio, 488978) and pol UBC (ACD-Bio, 312028) probes were performed and a negative control was carried out using dapB. Slides were imaged on an Aperio Versa 8 slide scanner. Images were imported into HALO and each raft was annotated as a separate layer. The HALO® Nuclear Segmentation AI module was used to segment nuclei within tissues. The HALO® ISH module was used to quantify E6/E7 and L1 staining within tissues. The RGB profile of each probe was characterised by selecting an area that contained a single staining dot of E6/E7 (0.135, 0.26, 0.357) and L1 stain (0.208, 0.267, 0.208). The ISH module parameters were optimised to enable identification of true positive staining with minimal cross-reactivity between the two stains using the 'real-time tuning' window. The contrast threshold (0.179), spot segmentation aggressiveness (0.95), spot size (0, 20) and E6/E7 size (2.1) were adjusted for E6/E7 analysis accordingly. For L1, the following parameters were used: contrast threshold (0.225), spot segmentation aggressiveness (0.95), spot size (0, 20), L1 size (2.1). The boundaries for treated-proximal-distal zones were set using the

previously determined lengths (Conley *et al.*, 2023) and these areas were annotated using the drawing tool.

2.2.8 Immunohistochemistry

Sections (2.5 µm) of FFPE tissues were subject to heat-induced antigen retrieval using sodium citrate buffer pH6 (Rb) or EDTA buffer pH9 (p53). Sections were then stained with the appropriate antibodies (Veterinary Pathology Laboratory, University of Glasgow). Haematoxylin and eosin (H&E) staining of 2.5 µm samples was also carried out (Veterinary Pathology Laboratory, University of Glasgow).

2.2.9 Confocal immunofluorescence microscopy

Coverslips of 2D cell cultures of W12E cells with 3T3 fibroblast cells were fixed with 4% paraformaldehyde (PFA) for 20 minutes. The PFA was removed and the coverslips washed with phosphate buffered saline (PBS). Cells were then acetone permeabilised (neat) for 1 minute followed by 3 x 5-minute washes in PBS. Cells were blocked in PBS 10% (v/v) donkey serum (Sigma, D9663) for 1 hour at room temperature followed by a PBS wash. The CamVir1 HPV16 L1 primary antibody (Table 2.2) was diluted in PBS 5% (v/v) donkey serum (1:500) and incubated on the coverslips at 4 ^{o}C overnight. The antibody was removed, and five PBS washes were carried out. The secondary AlexaFluor488 Donkey α-mouse antibody (Life Technologies, A21202) (1:1000) was diluted in PBS 5% (v/v) donkey serum and incubated on the coverslip for an hour at room temperature. Coverslips were washed in PBS 5 times and a final deionised water wash was carried out before mounting coverslips on a slide with ProLong Gold Antifade reagent with DAPI (ThermoFisher Scientific, P36935). Slides were imaged on a Zeiss LSM880 laser scanning microscope using ZEN3.2 software.

2.2.10 Corelative light and electron microscopy (CLEM)

An indirect CLEM approach was undertaken for W12E cells grown in 2D or 3D as described (Hanson *et al.*, 2010). W12E cells were grown in 2D to 15 days as detailed in Section 2.2.1 on a gridded 35mm dish (kindly provided by Mattek, P35G-1.5-14-C-Grid). To analyse cells on the top surface of raft tissues, rafts were inverted at days 10-16 onto gridded glass-bottomed 35mm dishes (Mattek) and incubated on the glass for

1 minute. This enabled the top cell layers from the tissue to adhere to the glass surface. Cells were fixed in PFA (4%) for 20 minutes and permeabilized with Triton (0.1%) (BDH, 30632) for 5 minutes. Subsequently, three 5-minute PBS washes were performed and the samples were blocked in PBS 10% (v/v) donkey serum. The remainder of IF staining was carried out as above for L1 except no DAPI was added. Instead, after incubation with the secondary antibody, cells were washed 5 times in PBS and then incubated for 5 minutes in Hoescht (abcam, ab139483) (1:1000). Cells were washed three times in PBS to remove the Hoescht and then left in PBS for imaging. Mattek dishes were imaged on a Zeiss LSM880 laser scanning microscope, using 405 nm, 488 nm and transmitted light for identification of where on the grid cells of interest were. Airyscan imaging was carried out to enable enhanced resolution and full thickness z-stacks were taken of the nuclei of cells.

Following confocal microscopy, cells were fixed in glutaraldehyde (2.5%) (Sigma, G5882) at 4 ºC overnight. They were then stained and processed for EM. Cells were washed twice with PBS and then stained with osmium tetroxide (1%) (Sigma, 208868) for 1 hour. Osmium tetroxide was removed, and the cells washed twice with PBS and then 3 times with water. Cells were then negatively stained for 30 minutes with uranyl acetate (2%). Cells were washed twice with water and then dehydrated by passing through a graded alcohol series (30% - 100%) followed by a second change into 100% ethanol. The alcohol was replaced with Epon 100 resin (TAAB Laboratories, AGR1141). Prior to solidification, an open-ended BEEM® embedding capsule (Agar Scientific, AGG360) was placed onto the dish surrounding the cells of interest, using the grid markers as a guide. A small layer of resin was added to the tube (1 cm) and polymerised in a vacuum oven at 65 °C for 48 hours. Once solidified, the capsule was topped up with more resin and placed back in the oven for a subsequent 48 hours.

The BEEM® capsule was detached from the glass-bottomed dish by placing the dish on a heat block at 60 ºC for 3 minutes 30 seconds (Hanson *et al.*, 2010). In some cases, the glass coverslip came away with the resin face. To remove the glass, sequential dips of the face into and out of liquid nitrogen for 2 s, followed by gently applying force to the glass with tweezers enabled separation. It was evident that cells had transferred to the face of the resin even when imaging on a low-powered microscope and the grid

lines could be visualised. The block was trimmed using a double-edged razor blade to isolate the area of interest and then the face was polished with a glass knife. A Diatome diamond trimming knife was used to cut 120 nm sections using a LEICA EM UC6 microtome set to a speed of 1.6 mm/s. Samples were transferred to continuous carbon-coated grids and images acquired on a JEOL 1400 flash microscope.

2.2.11 Negative staining and resin embedding of tissue sections for transmission electron microscopy (TEM)

W12E organotypic raft cultures fixed in 10% NBF were sectioned to create 1 mm^3 blocks. These sections were fixed in glutaraldehyde (2.5%) (Sigma, G5882) at 4 ^oC overnight. Tissue sections were washed twice with PBS and then stained with osmium tetroxide (1%) (Sigma, 208868) for 2 hours. The osmium tetroxide was removed, and the tissue sections were washed twice with PBS and then 3 times with water, incubating the tissue in the washing reagent for 5 minutes each time. Tissues were then negatively stained for 1 hour with uranyl acetate (2%). Tissues were washed twice with 5-minute incubations in water and then dehydrated by passing through a graded alcohol series (30% - 100%) followed by a second change into 100% ethanol. Each percentage of alcohol was incubated on the tissues for at least 2 hours and at 70% ethanol, an overnight incubation at 4 °C was carried out. The alcohol was replaced with Epon 100 resin (TAAB Laboratories, AGR1141). The resin was removed and the tissue section positioned at the top of an embedding mould (Agar Scientific). The mould was filled with resin and polymerised in a vacuum oven set to 65 °C for 48 hours. The mould was allowed to cool to room temperature and the embedded sample was removed. The block was trimmed using a double-edged razor blade to isolate the area of interest and then the face was polished with a glass knife. A Diatome diamond trimming knife was used to cut 120 nm sections using a LEICA EM UC6 microtome set to a speed of 1.6 mm/s. Samples were transferred to continuous carbon-coated grids and images were acquired on a JEOL 1400 flash microscope.

2.2.12 Luminex assays

Human High Sensitivity Cytokine A Premixed Magnetic Luminex Performance Assays (Table 2.4) were used to determine how microwave treatment altered the concentration of cytokines secreted into the media from HPV-negative and HPV-

positive rafts. Following mock or microwave treatment, HaCaT, NIKS16 and W12E rafts were transferred to 12 mm transwells (Corning, CLS3462-48EA). The media was collected from different replicates at 1, 8 and 16-hour time points post-treatment. Media samples were centrifuged to remove debris, and the supernatant aliquoted and frozen. Samples were analysed in duplicate using a Human High Sensitivity Cytokine A Premixed kit (Biotechne) (Table 2.4), following the manufacturer's instructions. The mean fluorescent intensity (MFI) of each cytokine was analysed using a Luminex 100/200 (The Cellular Analysis Facility, University of Glasgow). A five-parameter logistic (5-PL) curve fit was applied using the included standards and the cytokine concentration in each sample was calculated. Three biological replicates and two technical replicates were analysed per experimental condition and an unpaired t-test was used to determine significant differences between mock and treated cytokine concentrations at the same time point.

2.2.13 Monocyte isolation, differentiation to moDC and exposure to microwave-treated media

2.2.13.1 Isolation of monocytes from PBMCs

Frozen peripheral blood mononuclear cells (PBMCs) were removed from liquid nitrogen storage. To maximise recovery of monocytes, exposure to room temperature was minimised during thawing. Vials were stored on dry ice whilst transporting from liquid nitrogen. In a biosafety cabinet, the cap was turned a quarter turn to relieve pressure and then retightened. PBMCs were then thawed in a 37 ^{o}C water bath with gentle swirling of the vial. When a small amount of ice remained, the vials were removed and transported into the biosafety cabinet. The following steps were carried out quickly to maximise yield. The cell volume was transferred to a 50 ml falcon tube, the vial was washed with 1 ml complete media composed of RPMI-1640 with 1% L-Glutamine (Gibco, 11875093), 10% FBS (Gibco, 10290-106) and 1% Pen-Strep (Gibco, Cat #15140-122). This wash was added to the cells dropwise with gentle swirling. The cells were washed with 15 mL complete media and pelleted by centrifuging at 300 x g for 10 minutes at room temperature. The supernatant was removed so that a small amount of media remained and 100 µg of DNase I was incubated with the cells for 10 minutes to prevent cell clumping. A subsequent wash with 15 ml of complete media was followed by centrifuging at 300 x g for 10 minutes.

Monocytes were isolated using the MojoSort Human CD14+ Monocytes Isolation Kit (BioLegend, 480047). The supernatant was removed from the previous spin and PBMCs were resuspended in MojoSort Buffer (BioLegend, 480017) at a concentration of 1 x 10^8 cells/ml. Monocytes were isolated in accordance with the manufacturer's protocol such that the magnetically labelled fraction of cells was discarded and the untouched monocytes retained. Samples of magnetically labelled and unlabelled cells were reserved for CD14+ antibody staining to determine the specificity of separation. The cell number of unlabelled cells was determined and the cell suspension was centrifuged for 10 minutes at 300 x g. A wash was carried out using 10 ml of complete media.

2.2.13.2 Differentiation of monocytes into moDC

The cell pellet was resuspended and cells were seeded at a concentration of 1.5 x 10^6 cells per well of a 6-well plate in complete media supplemented with 100 ng/ml GM-CSF (Thermofisher, 300-03) and 20 ng/ml IL-4 (Thermofisher, 200-04) for differentiation of monocytes. Cells were cultured in a humidified incubator at 37 ^{o}C and 5 % CO2. On day 3, the plate was spun down at 300 x g for 5 minutes. The media was collected from each well and centrifuged at 300 x g for 10 minutes. The media was replaced in each well using 1 mL of complete media with IL-4 and GM-CSF to prevent the attached cells from drying out. Cell pellets were retained from the centrifuge step, resuspended in 2 mL per well and returned to the well of the plate. On day 6, plates were spun at 300 x g for 5 minutes. The media was removed to a 50 ml falcon tube. The cells were detached by incubating cells in 1 ml Accutase™ (Stempro™, A1110501) per well for 10 minutes. Detached cells were added to the 50 ml falcon tube. Wells were washed three times with 2 ml complete media which was added to the 50 ml falcon tube followed by centrifuging at 300 x g for 10 minutes. Cells were resuspended and exposed to media from microwave-treated or mock-treated 3D W12E organotypic raft cultures for 24 hours.

2.2.13.3 moDC flow cytometry

Following treatment, moDCs were collected using the previously described protocol for Accutase detachment (Section 2.2.13.2). The resulting cell pellet was resuspended in 100 µl PBS 10% (v/v) goat serum (Sigma, G9023) and incubated at 4 ^{o}C in the dark

for 30 minutes to block Fc receptors and prevent unspecific antibody binding. Cells were washed two times with PBS containing 1% BSA and pelleted between each wash at 350 x g for 5 minutes. Phycoerythrin-conjugated antibodies to CD14 (BioLegend, 367103), CD40 (BioLegend, 334307), CD80 (BioLegend, 305207) and CD86 (BioLegend, 374205) were incubated with the moDC at 4 ^{o}C in the dark for 20 minutes. Cells were washed twice using PBS containing 1% BSA with cells pelleted between each wash at 350 x g for 5 minutes. Cells were then fixed in PBS containing 1% PFA for 20 minutes at 4 ^{o}C in the dark. Samples were loaded onto a round-bottomed 96-well plate (Costar 2795) in triplicates such that there were 2x10^5 cells per well for analysis using the Guava Easycyte. Samples were analysed for fluorescence using the blue laser and yellow filter (YEL-B parameter, Guava Easycyte), The Incyte software was used to determine the percentage of positive cells (CD14+ analysis) or mean fluorescence intensity (CD40, CD80, CD86 analysis). Dead cells were removed from the analysis and only cell singlets were analysed using the Incyte software.

2.2.14 Illumina TruSeq Next Generational Sequencing

2.2.14.1 RNA extraction and library preparation for RNA Sequencing

Total RNA was prepared from 3D tissues using the RNeasy kit with on-column DNase treatment (Qiagen, 79254) according to the manufacturer's instructions. RNA concentration was initially determined using a Nanodrop One/One Microvolume UV-Vis Spectrophotometer (Thermofisher). The integrity of the RNA was assessed using an Aglient 2100 Bioanalyzer. All samples had an RNA integrity number (RIN) > 8.5. Prior to library preparation, 0.15 ng of SIRV spike-ins (SIRV-Set 2, Lexogen) were added to each sample to represent 1% of the total mRNA reads. These were used for normalisation during the analysis to account for differences in efficiency during the library preparation. Libraries were prepared using the Illumina TruSeq Stranded mRNA Library Prep (Illumina, #20020595) with 500 ng of total RNA and sequenced on an Illumina NextSeq 2000 using paired-end sequencing with reads of 100 bp. RNA-Seq reads were quality assessed using FastQC. RNA-Seq reads were aligned to the Homo sapiens genome (GRCh38.110) downloaded via Ensembl using Hisat2 (Kim *et al.*, 2015). After the alignment, FeatureCount (Liao, Smyth and Shi, 2014) was used to count reads mapping to genes annotation files. The Human papillomavirus type 16 reference genome was downloaded via NCBI (K02718.1). Both the Lexogen Spike-In RNA Variant

Controls (SIRVs) and the External RNA Controls Consortium (ERCC) spike-ins were added to the sample before library preparation.

We performed differential expression analysis on sample groups mock 4-hour vs 4-hour treated and mock 16-hour vs 16-hour treated respectively using the R package DESeq2 (Love *et al.*, 2014). DESeq2 estimates variance-mean dependence in count data from high-throughput sequencing data and tests for differential expression based on a model using the negative binomial distribution (work performed by Quan Gu using the DESeq2 pipeline referenced in Meehan *et al.*, 2023). The ERCC spike-in sets were used for normalisation of gene expression value.

2.2.14.2 Functional analysis of differentially expressed genes

Gene set enrichment analysis, protein-protein interaction networks and transcription factor target gene set enrichment analyses were performed using Metascape (Zhou *et al.*, 2019). An R script was used to produce the volcano plots using ggplot2 and heatmaps were created using the pheatmap package. The R script used is available: https://github.com/annak2-tech/Microwave_transcriptome_pipeline/tree/main. The Viridis colour scheme was used in heatmaps to enable accurate interpretation of scientific data for individuals with colour vision deficiency (Nuñez, Anderton and Renslow, 2018). Circos allowed the visualisation of correlations between features shared between groups or their annotations (Krzywinski *et al.*, 2009).

Chapter 3 An investigation into how microwave treatment affects the transcriptional landscape of the cell and if it can induce innate immunity

3.1 Introduction

3.1.1 The cell transcriptome following hyperthermia

Hyperthermia is a well-documented adjunct to cancer therapy, commonly used in combination with chemo- and radiotherapy (Cheng *et al.*, 2019) (Section 1.11). When exposed to hyperthermic temperatures, cells invoke a heat shock response to prevent proteolysis and other forms of cell damage. Cells respond by rapidly altering the cellular transcriptional landscape to result in the production of heat shock proteins (HSPs), cytoprotective proteins which are rapidly induced upon stress (Santoro, 2000). The main role of these HSPs is to maintain the appropriate folding of proteins within cells to protect them against proteolysis (Hartl, Bracher and Hayer-Hartl, 2011; Lang *et al.*, 2022). The classification of heat shock proteins is based on their molecular weight (kDa's) and compartmentalisation within the cell. There are several transcription factors induced by heat shock but HSF1 plays a major role in altering the transcriptional landscape upon stress (Gomez-Pastor, Burchfiel and Thiele, 2018). HSF1 is normally bound as an inert monomer in a complex with HSP70 and other chaperones which represses its DNA-binding and transcriptional transactivation activity (Abravaya *et al.*, 1992; Zou *et al.*, 1998; Guo *et al.*, 2001) (Figure 3.1). Upon heat shock, these chaperones are sequestered by damaged cellular proteins, thus releasing HSF1. This allows for the translocation of HSF1 to the nucleus where sumoylation and phosphorylation changes activate the transcription factor (Voellmy, 1996). HSF1 forms homotrimers which then bind to and activate transcription from genes containing heat shock elements (HSEs), series of pentameric units arranged as inverted adjacent arrays of 5'-nGAAn'3' (Amin, Ananthan and Voellmy, 1988). HSF1's targets include the canonical heat shock proteins, which prevent protein misfolding and, once levels have increased enough, act to regulate this response by binding back to HSF1 to repress its transcriptional transactivation (Figure 3.1) (Sivéry, Courtade and Thommen, 2016). Alongside these canonical heat shock proteins, many other genes get induced following heat stress, with some that do not contain HSEs or show

evidence of HSF1 binding, revealing the complexity of this response (Trinklein *et al.*, 2004; Mahat *et al.*, 2016).

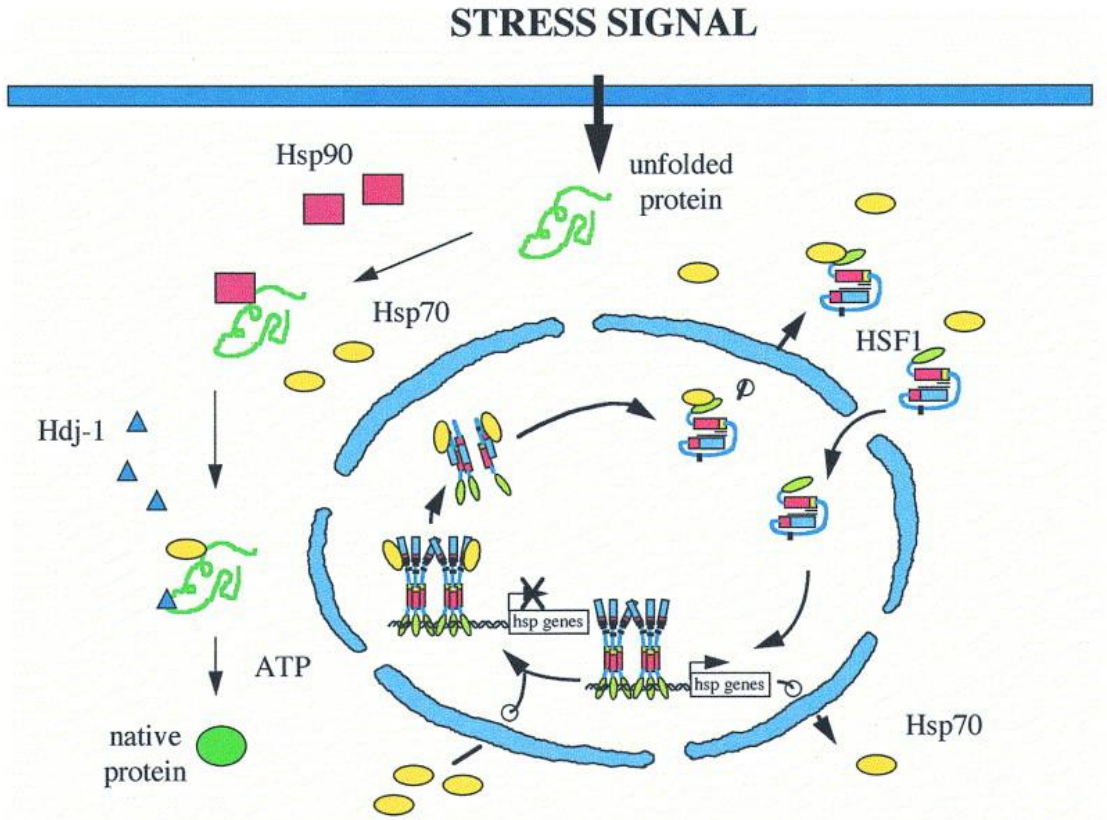

Figure 3.1: Regulation of the heat shock response by HSF1. Within unstressed cells, HSF1 is present as an inert monomer in the cytoplasm, bound to HSP70 and other chaperones. Following stress and the appearance of non-native proteins, the chaperones (HSP70, HSP90 and Hdj1) bind to these misfolded proteins to prevent proteolysis. HSP70 also has ATPase activity and ATP binding allows conformational changes for stable substrate binding. The diversion of chaperones to non-native proteins releases HSF1 monomers which translocate to the nucleus. Here HSF1 oligomerizes to a trimeric state, becomes inducibly phosphorylated and binds to and activates transcription from HSE elements, upstream of *hsp* genes. This results in the synthesis of heat shock proteins. As the concentrations of heat shock proteins rise in the cell, the chaperones localise to the nucleus and bind to HSF1, repressing *hsp* gene transcription and leading to the dissociation of the HSF1 trimers and refolding of HSF1 to its inert monomeric state. Adapted from (Santoro, 2000).

Several meta-analyses have sought to identify common transcriptome alterations in cells following hyperthermia (Scutigliani *et al.*, 2022; Yonezawa and Bono, 2023; Richter, Haslbeck and Buchner, 2010). Many of these meta-analyses focus on or have a high proportion of studies that come from cancer cell lines due to the interest in using hyperthermia as an adjunct to radio- and chemotherapy (Section 1.11). Due to the dysregulation of many genes within cancer cells, this weighting is important to

consider alongside the results. Scutigliani and colleagues conducted an extensive meta-analysis of cancer cells subjected to hyperthermia (Scutigliani *et al.*, 2022). Whilst many previously observed pathways could be identified within these datasets including protein folding, cell cycle, mitosis and cell death, no 'universal' heat stress response could be identified within cells. The most commonly overexpressed gene was *CRYAB*, with many heat shock genes including *HSPA6* commonly overexpressed, and KRAS and TNF-α signalling were commonly upregulated (Scutigliani *et al.*, 2022). Yonezawa and colleagues analysed a larger number of datasets from human and mice cell lines and tissues following hyperthermia (Yonezawa and Bono, 2023). The authors produced an 'HN score' for each transcript, defined as the difference between the number of experiments with downregulated expression of the transcript and the number of experiments with upregulated expression (Bono and Hirota, 2020). This data set was then used as their 'differentially expressed' gene set and input for subsequent analysis. Within human data sets, *HSPA6* had the highest 'HN score': upregulated across most studies (Yonezawa and Bono, 2023) (Supplementary Figure 3.1). Gene ontology analysis revealed the highest upregulated pathway to be protein folding. Other upregulated pathways included 'response to steroid hormone' and 'NGF-stimulated transcription' (Supplementary Figure 3.1). Comparing genes induced in mouse and human datasets following hyperthermia, the enriched pathways included 'response to heat' and 'response to topologically incorrect protein'. This second term included molecular chaperones and cofactors with the largest representation from heat shock 70 kDa proteins (HSPA), DNAJ (HSP40) heat shock proteins and small heat shock proteins (HSPB), with these genes shared between humans and mice. This study also identified several immediate early genes (IEGs), which are known to be rapidly expressed in response to stimuli, whose expression was induced by heat stress. This included *FOS, FOSB* and *JUN* which encode the transcription factor AP-1 as well as *EGR1*, *EGR2*, and *ARC*. Transcription factor mapping revealed the importance of HSF1 and SRF, which may regulate genes induced early in heat shock in an HSF1-independent manner.

3.1.2 Previous work in this area

No previous studies have profiled how microwave-delivered hyperthermia changes the transcriptional landscape to our knowledge at the time of writing. The most

common treatment condition in the meta-analyses described above was 42 °C for 60 minutes, delivered through conduction heating using a water bath (Scutigliani *et al.*, 2022; Yonezawa and Bono, 2023). This heats cells from the outside in and delivers heat to all cells universally. Microwave treatment for plantar warts typically lasts 10 seconds (Bristow *et al.*, 2017) and results in dielectric hysteresis to a defined tissue area and heating from the inside out. Different heating methods can result in differing biological responses (Yang *et al.*, 2016; Whitney, Carswell and Rylander, 2013) which alongside cell type was proposed to be responsible for differences between studies in the meta-analyses described above (Yonezawa and Bono, 2023; Scutigliani *et al.*, 2022). Therefore, it is important to investigate how microwave-delivered hyperthermia affects transcription in our keratinocyte models.

Accumulating evidence indicates the role of heat shock in inducing immunity. The heat shock proteins themselves play a role in this, forming complexes with peptides and becoming powerful immunogens that can stimulate antigen-presenting cells to induce an innate and adaptive immune response (Section 1.11). Hyperthermia can also result in increased expression of surface molecules involved in immunity as well as exosome release that may help transfer antigens to APCs (Section 1.11). Moreover, some non-canonical heat shock proteins, such as IL-8 are upregulated by HSF1 and have roles in innate immunity (Singh *et al.*, 2008). HPV employs many strategies to regulate immunity to prevent the detection and clearance of infection (Moody, 2022) (Section 1.9.2) so it is important to determine if microwave-delivered hyperthermia can alleviate this immune repression.

Local hyperthermia has previously been demonstrated to promote migration and maturation of Langerhans cells *ex vivo* in samples of condyloma acuminatum, anogenital warts caused by HPV (Li *et al.*, 2009). Greater effects were observed at higher temperatures (45 °C). Bristow and colleagues proposed that hyperthermia delivered by the Swift® microwave device may induce anti-HPV immunity (Bristow *et al.*, 2017). The authors showed that exposure to media from microwave-treated keratinocytes could induce moDC activation. Moreover, these activated moDCs exhibited enhanced cross-presentation of HPV antigens to HPV-specific CD8+ T cells (Bristow *et al.*, 2017). Epithelial cells are key immune sentinels (Section 1.9.1) and the

microwave-treated keratinocytes in this study produced IL-6 in response to treatment and showed increased expression of cell surface activation markers (HLA-DR, CD40 and CD80) (Bristow *et al.*, 2017). This study was carried out in a monolayer of HaCaT cells (Boukamp *et al.*, 1988), human spontaneously immortalised HPV-negative keratinocytes, which limits the extensions of these findings to HPV-infected lesions as the immunoregulatory functions of the HPV oncoproteins cannot be accounted for (Section 1.9.2). This includes the interference with the interferon signalling pathways by E5, E6 and E7, E7 mediated inhibition of NFκB activation and E5's inhibition of MHC class I proteins which are involved in antigen presentation to cytotoxic T cells (Section 1.9.2) (Scarth *et al.*, 2021). Therefore, it is unclear if the anti-HPV immunity discovered here would occur in infected cells.

To model different disease stages of HPV16 infection, the cell lines SiHa, NIKS16 and W12E were used. SiHa cells are cervical cancer cells which contain two host-integrated copies of HPV16, at locus 13q21, with a break-point in the E2 coding region (Xu *et al.*, 2021; Adler, Erickson and Bobrow, 1997; Baker, 1987; El Awady *et al.*, 1987). As HPV16 is integrated in these cells, they represent cancer formation where viral gene expression is deregulated and the control over E6 and E7 expression is lost. This infection is no longer productive due to disruption of the E2 and E4 ORFs by integration which prevents viral replication and late gene expression. NIKS16 are normal, spontaneously immortalised keratinocytes which have been stably transfected with HPV16 genomes (Flores *et al.*, 1999). When cultured at a low passage, these cells can maintain episomal HPV16 genomes and upon raft culture, form a stratified epithelium that supports the productive stage of the viral life cycle and resembles a low-grade squamous intraepithelial lesion (LSIL) (Flores *et al.*, 1999; Wechsler *et al.*, 2012). W12E cells are a subclone of the W12 human cervical keratinocyte cell line derived from a low-grade cervical lesion that contains episomal copies of HPV16 (Stanley *et al.*, 1989). Upon differentiation, W12E cells support the production of the late HPV16 mRNAs and proteins (Milligan *et al.*, 2007). W12E cells originate directly from natural *in vivo* HPV infections of the cervix and therefore provide a more clinically relevant early disease model over NIKS cells which are derived from neonatal foreskin and stably transfected with HPV16 (Allen-Hoffmann *et al.*, 2000). HaCaT cells were also

included in the analysis to compare the heat shock and immune responses in an HPV-negative model.

Aims of the study

- Determine a suitable energy for microwave treatment of *in vitro* 3D epithelial raft cultures.
- Confirm a hyperthermic response within cells that have been microwave-treated.
- Investigate the impact of microwave-delivered hyperthermia on the transcriptional landscape of keratinocytes.
- Determine if microwave treatment can induce an innate immune response.

3.2 Optimising the energy required for microwave treatment of 3D organotypic raft cultures

To optimise the treatment energy in 3D organotypic raft cultures, we determined the temperature increase in tissues following microwave treatments at a range of power levels (5W, 10W and 15W up to 30 seconds of treatment). SiHa 3D organotypic raft cultures were grown at the air-liquid interface and then inverted onto the lid of a plastic cell culture dish preheated to 37 °C. The microwave probe was positioned underneath the plastic such that the microwaves would first travel through the plastic lid and then into the top of the tissue containing the cells before going through the collagen matrix (Figure 3.2A, B). This method best resembles how the device would be used *in vivo* whereby the cells at the top of the epithelium would be in contact with the microwave probe, covered with a disposable plastic cap, without compromising the sterility of tissue cultures. Previous studies have demonstrated a considerable loss of microwave energy when applying the Swift® device through the plastic of a cell culture dish (Bristow *et al.*, 2017) so it was important to determine the optimal energy to deliver the target temperature within our model system.

All power levels tested produced a temperature increase in the SiHa tissues analysed (Figure 3.2C, D, E). Treatment at 5W for 10 s raised the temperature of rafts, although

this did not exceed 40 °C (Figure 3.2C). Extending the length of treatment at 5 W to 30 s could not raise the temperature above 45 °C (data not shown). Treatment at 15 W raised the temperature dramatically, as seen by the gradient of the line, to above 70 °C (Figure 3.2D). This caused gross disturbance to the tissue, even away from the site of treatment, seen visually by the eye during treatment and was considered too large of an increase in temperature for future use. Treatment at 10W for 10 s raised the temperature of rafts to 45 – 48 °C with no further significant increase in temperature after this time and no gross change to the tissue morphology outside of the site of treatment (Figure 3.2E). This energy was used for all subsequent work.

Extending this analysis to include two temperature probes allowed us to investigate the precision of microwave treatment. Probes were positioned to record temperature rises in sites directly below the microwave probe contact site (defined as the treated area) and in the tissue at sites further away from the probe contact site (defined as the distal site) (Figure 3.2B). Large temperature increases were only evident at the 'treated' site of the tissue where temperatures above 45° C were reached (Figure 3.2F). Within the distal sites, temperatures only reached 32 °C highlighting the spatial precision and linearity of the temperature rise caused by the microwave treatment.

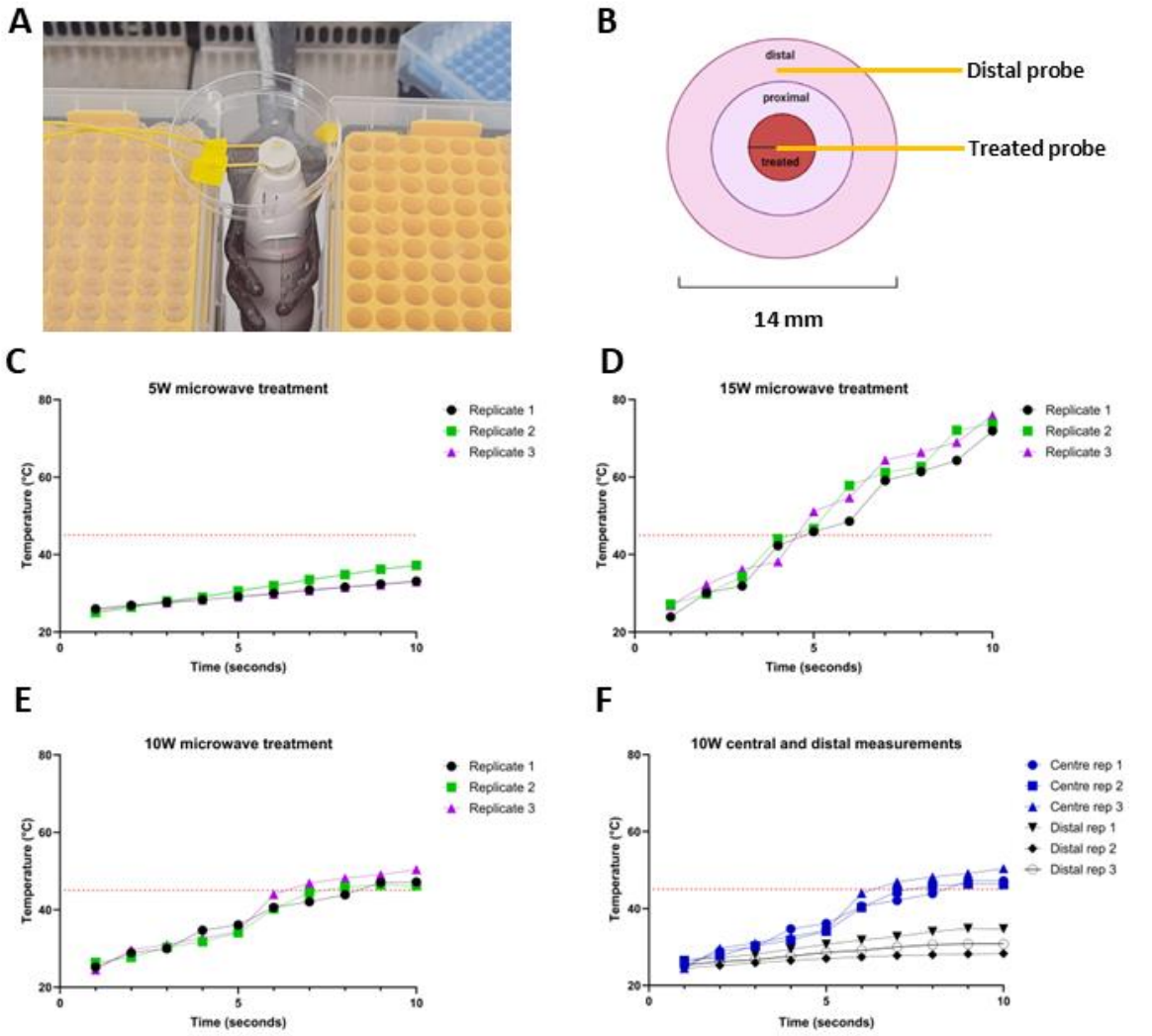

Figure 3.2: Optimisation of the thermal dose delivered to 3D organotypic raft cultures. (A) The reaction set-up for temperature measurements within raft tissues. 'NOMAD-Touch' optical thermometers (Neoptrix) were positioned such that one probe was directly under the 5 mm Swift® microwave probe contact site on the raft and a second positioned at a site distant from the site of treatment, with the probe positioning shown diagrammatically in (B). (C-E) Temperature increases recorded at the treated site of 14 mm SiHa rafts following microwave treatment for 10 s at 5 W (C), 15W (D) and 10 W (E). A horizontal red dotted line indicates 45 ^{o}C, the target temperature to ensure consistency with temperatures reached in the skin during clinical application of the device. (F) The temperature increases from probes at the central treated (blue) and distal sites to treatment (black) are shown. Three individual rafts were used for each treatment condition.

3.3 Definition of areas within a microwave-treated raft

Microwave treatment results in immediate damage to the tissue at the site of treatment. This area is obvious when analysing a cross-section of a raft, often associated with a loss of cells in this area or cells that have detached from the collagen matrix and each other, with large morphological changes evident (Figure 3.3A, B red line). The collagen matrix can also be seen to contract at the treated site (Figure 3.3A, C red line). In the neighbouring tissue to the treatment site, tissue integrity is disturbed with cell-to-cell adhesion often lost (Figure 3.3A, B). This area is defined as the 'proximal' tissue. Further away from the site of treatment, the tissue appears similar to mock-treated tissue and is undisturbed (Figure 3.3A). This area is defined as the 'distal' tissue. These terms will be used throughout the rest of this thesis to describe these areas.

Previous work has determined the size of each area over time (Conley *et al.*, 2023). Within 'full-sized' 14 mm tissues, the average treated area was 2.2 mm, which increased in size over time to around 3 mm. The disrupted 'proximal' region had an average width of 3.4 mm (cumulative over both sides of the treated site) which increased to a maximum of 5.5 mm. These sites are shown labelled on a 'full-sized' 3D W12E tissue (Figure 3.3A). For subsequent experiments, we sought to produce 'mini' 3D organotypic rafts with a diameter of 7 mm in which the majority of the cells had been exposed to microwave treatment. In these tissues, the largest area is the 'treated' site, with some 'proximal' region on either side (Figure 3.3C). Whilst every effort is made to treat rafts in the centre, sometimes there is a larger proximal side on one side of the tissue (Figure 3.3C).

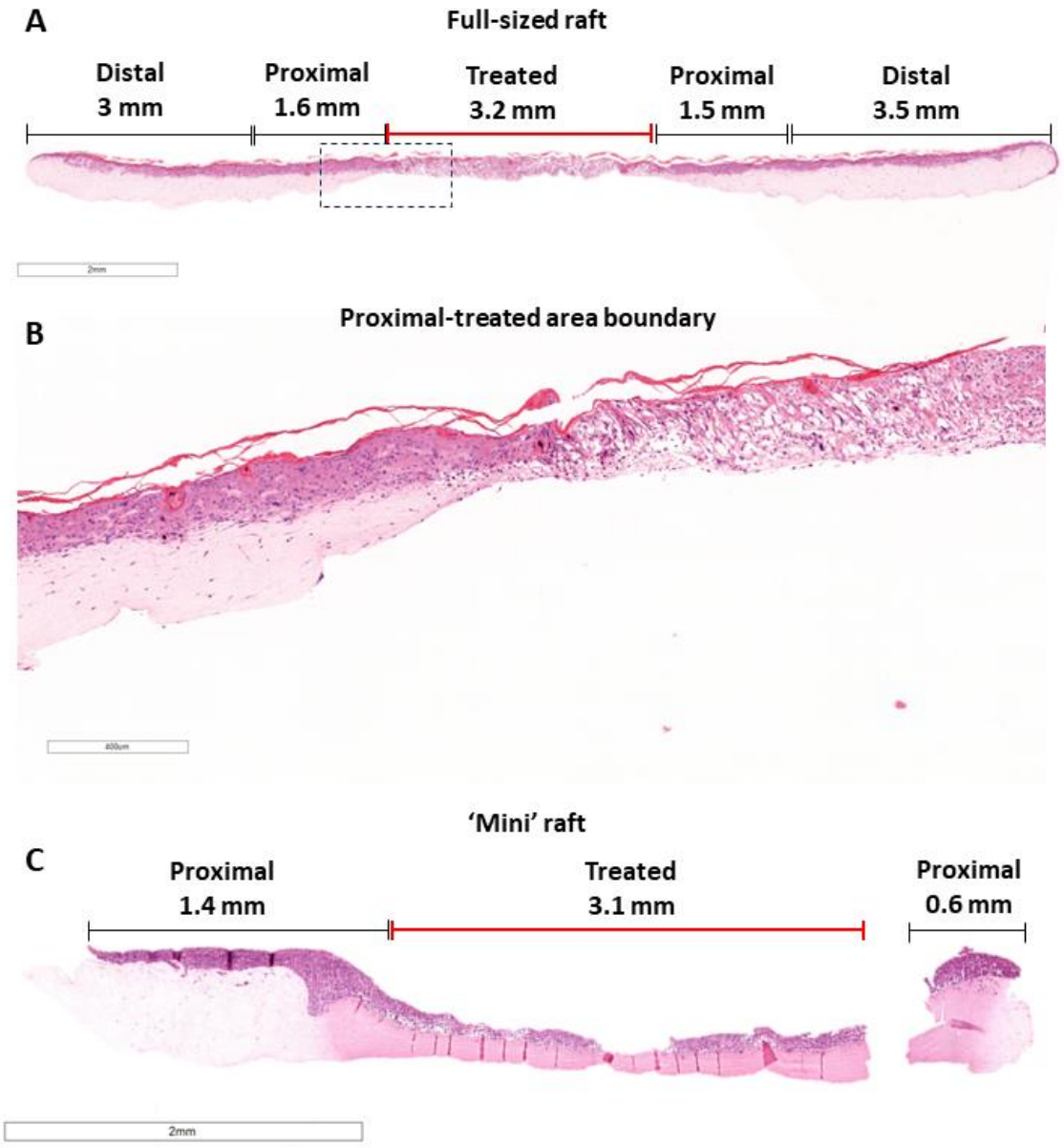

Figure 3.3: The defined areas within microwave-treated 3D tissues. Annotated 'full-sized' and 'mini' rafts show our defined tissue regions following treatment. (A) A 'full-sized' 14 mm W12E tissue that has been microwave treated. Bars show the lengths of the 'treated', 'proximal' and 'distal' areas. The area within the black dashed box containing the treated-proximal boundary is shown at a higher magnification in (B). (C) A 'mini' 7 mm SiHa tissue that has been microwave-treated. In comparison to the full-sized tissue, the treated area makes up the majority of the tissue. Some 'proximal' regions can be seen on either side of the treated zone. Due to dehydration during raft processing, the total raft diameters do not add up to 14 mm and 7 mm for full-sized and mini rafts respectively. Processing can also result in the breaking of rafts as seen in (C). Scale bars = 2 mm (A & C) and 400 μm (B).

3.4 Microwave treatment results in the induction of HSP70 and a heat shock response

Induction of heat shock requires temperature increases over 4 ^{o}C from baseline (Feder and Hofmann, 1999; Ray, 1999), which we observed within microwave-treated tissues at our chosen treatment energy. Still, we aimed to verify the induction of a heat shock response by analysing the expression of heat shock proteins following treatment. Microwave treatment has previously been demonstrated to cause induction of the heat shock proteins HSP90, HSP72 and HSP27 within human skeletal muscles (Ogura et al., 2007 Br J Sports Med). We analysed the transcriptional expression of the heat shock protein HSP70 within microwave-treated 'mini' tissues which contain only the treated and proximal zones. Microwave treatment consistently resulted in the rapid upregulation of HSP70 transcription in both HPV-negative (HaCaT) and HPV-positive (NIKS16 and W12E) tissues (Figure 3.4).

The increase in HSP70 transcripts peaked at 4H for NIKS16 and W12E tissues with an average fold change of 22 and 36 times that of untreated tissues fixed at the same time point (Figure 3.4A, B) ($p<0.001$). There was a statistically significant increase in HSP70 transcripts at 4H, 8H and 16H post-treatment in NIKS16 and W12E tissues (Figure 3.4A, B). This increase was transient and in NIKS16 tissues, HSP70 expression had fallen to comparable levels to mock-treated tissues by 72 hours post-treatment, demonstrating the self-regulatory nature of this pathway (Figure 3.4A). Within HPV-negative HaCaT tissues, an increase in HSP70 transcription was observed at 4- and 8 hours post-treatment, however, this was not significant (Figure 3.4C). This response declined sooner in HPV-negative tissues, with levels of HSP70 similar to mock-treated tissues by 16 hours post-treatment. This suggests that microwave treatment induces an HSP70-driven heat shock response to a greater extent in HPV-positive tissues and this effect is sustained for longer compared to HPV-negative tissues.

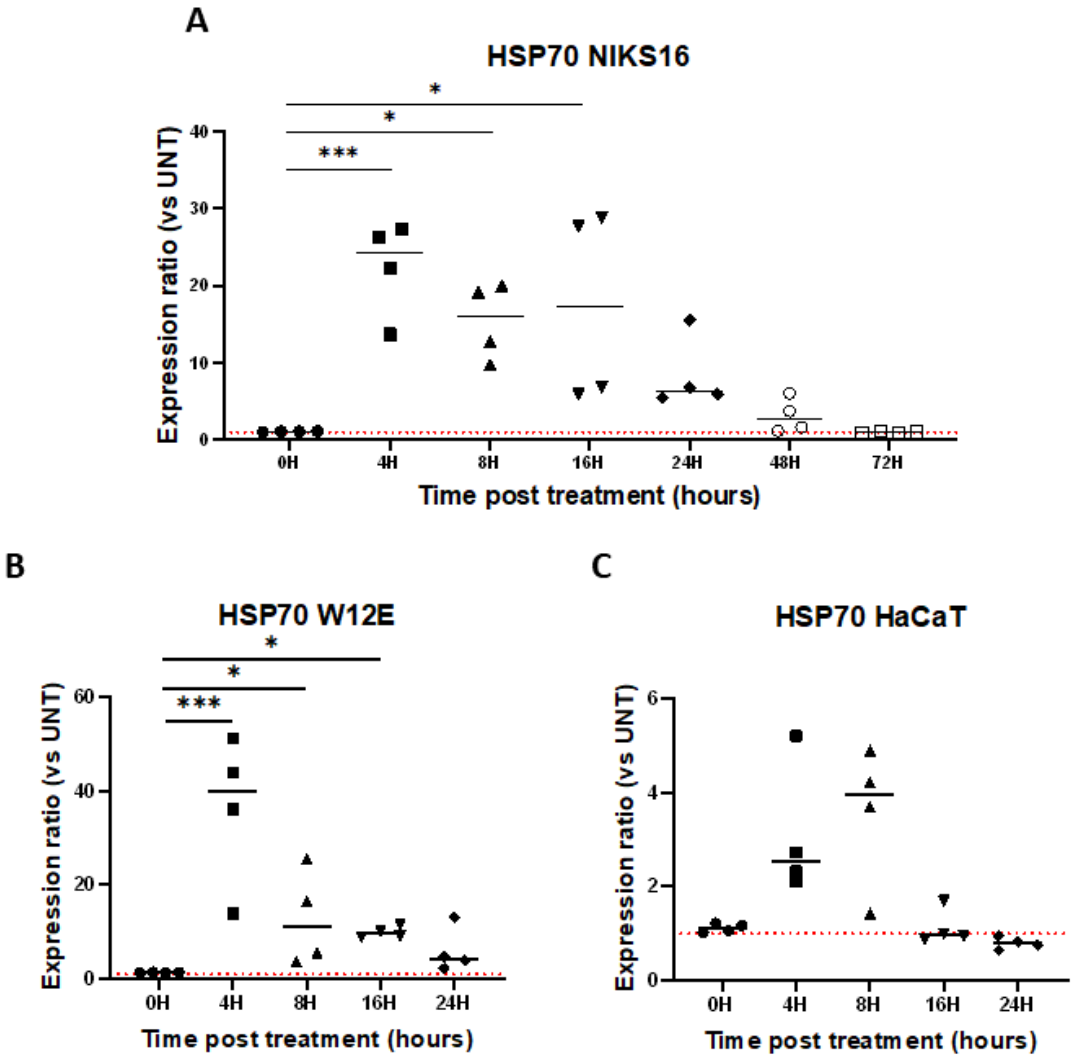

Figure 3.4: Microwave treatment induces HSP70 gene expression within tissues. RT-qPCR analysis of HSP70 mRNA in microwave-treated NIKS16 (A), W12E (B) and HaCaT (C) tissues. Total RNA was extracted from tissues and used for RT-qPCR. Delta Ct changes were calculated relative to the housekeeping gene Beta-actin and expression ratios of treated to mock tissues were determined using $2^{-\Delta\Delta CT}$. The median expression ratio is displayed (black line) for each time point post-treatment and each point represents one biological replicate (n=4). The red dashed line indicates an expression ratio with no change between the mock and treated tissues (y=1). Each biological replicate represents an average of three technical replicates. A Kruskal-Wallis test was used to determine if there was a statistical difference between groups. * Indicates $p< 0.05$, ** indicates $p< 0.01$ and *** indicates $p< 0.001$.

3.5 Transcriptomic analysis of NIKS16 3D organotypic rafts following microwave treatment

3.5.1 RNA Sequencing reveals a rapid transcriptional response to microwave-delivered hyperthermia in keratinocytes

RNA Sequencing was performed using RNA prepared from mock or microwave-treated NIKS16 3D organotypic raft cultures at 4- and 16 hours post-treatment. Biological replicates within each sample group clustered together and variance between the treated and mock conditions can be visualised (Figure 3.5). Treated samples at each time point were compared to mock samples at the same time point for differential gene analysis. Differentially expressed genes included in the analysis were defined by those with an adjusted p-value < 0.05 and a log2 Fold Change < -1 or >1 in comparison to mock-treated samples. At 4 hours post-treatment, there were 59 differentially expressed genes with 56 significantly upregulated and 3 significantly downregulated (Figure 3.6A) with a range of 5-fold downregulated to 794-fold upregulated. In contrast, there were 150 differentially expressed genes at 16 hours compared to mock-treated tissues (Figure 3.6C). All of these were upregulated with a range of a 2.3-fold to 208-fold change in expression in comparison to mock-treated tissues. Of the genes upregulated at 4 hours, 54% overlapped with genes upregulated at 16 hours post-treatment (Figure 3.6E). This implies a rapid transcriptional response to microwave-delivered hyperthermia which is transient for some genes, whilst others remain or become upregulated at later time points post-treatment. Many genes had a high fold change in expression, but this change was not significant (Figure 3.6A, C grey dots). These genes typically had a low expression which limits the power to define significance (Figure 3.7A, B). Increasing the sequencing depth or including more samples may have resulted in more significant genes at both time points (Figure 3.7A, B). Variability between samples may also account for the reasonably small number of significantly changed genes (Figure 3.6B, D). In particular, treated samples at 16 hours showed a high degree of variability (Figure 3.5), with one sample showing increased expression of almost every upregulated gene in comparison to the other treated samples (Figure 3.6D). Among genes expressed at high levels in this sample is *CXCL8*, the non-canonical heat shock protein involved in innate immunity and induced by

HSF1 following heat shock (Singh *et al.*, 2008; Tulapurkar *et al.*, 2012). This gene was also significantly upregulated at 4 hours.

Across the top 10 most significantly upregulated genes at 4 and 16 hours (based on adjusted p-value), nine are shared between both time points post-treatment (Table 3.1). These genes include heat shock proteins (*HSPA6, HSPA1A, HSPA1B and HSPA7*), immediate early genes (*ARC*), chaperones (*CLU*), GTP-binding proteins (*GEM* and *RASD1*) and the transcriptional co-regulator (*ANKRD1*) which functions alongside AP-1. Extracellular stimuli such as UV radiation, oxidative stress and cytokines are known to stimulate AP-1 expression and promote its binding to the TPA-responsive element (TRE) of target genes which have roles in cell growth, inflammatory responses and repair (Eferl and Wagner, 2003; Shaulian *et al.*, 2000; Angel and Karin, 1991). The expression of these nine shared genes had decreased slightly by 16 hours post-treatment but remained upregulated in comparison to mock-treated tissues (Table 3.1). Alongside *ARC*, multiple other immediate early genes were induced following microwave treatment, including *EGR1* and *FOS*. This is similar to transcriptomes which have been generated from cells exposed to hyperthermic temperatures by other delivery methods (Yonezawa and Bono, 2023).

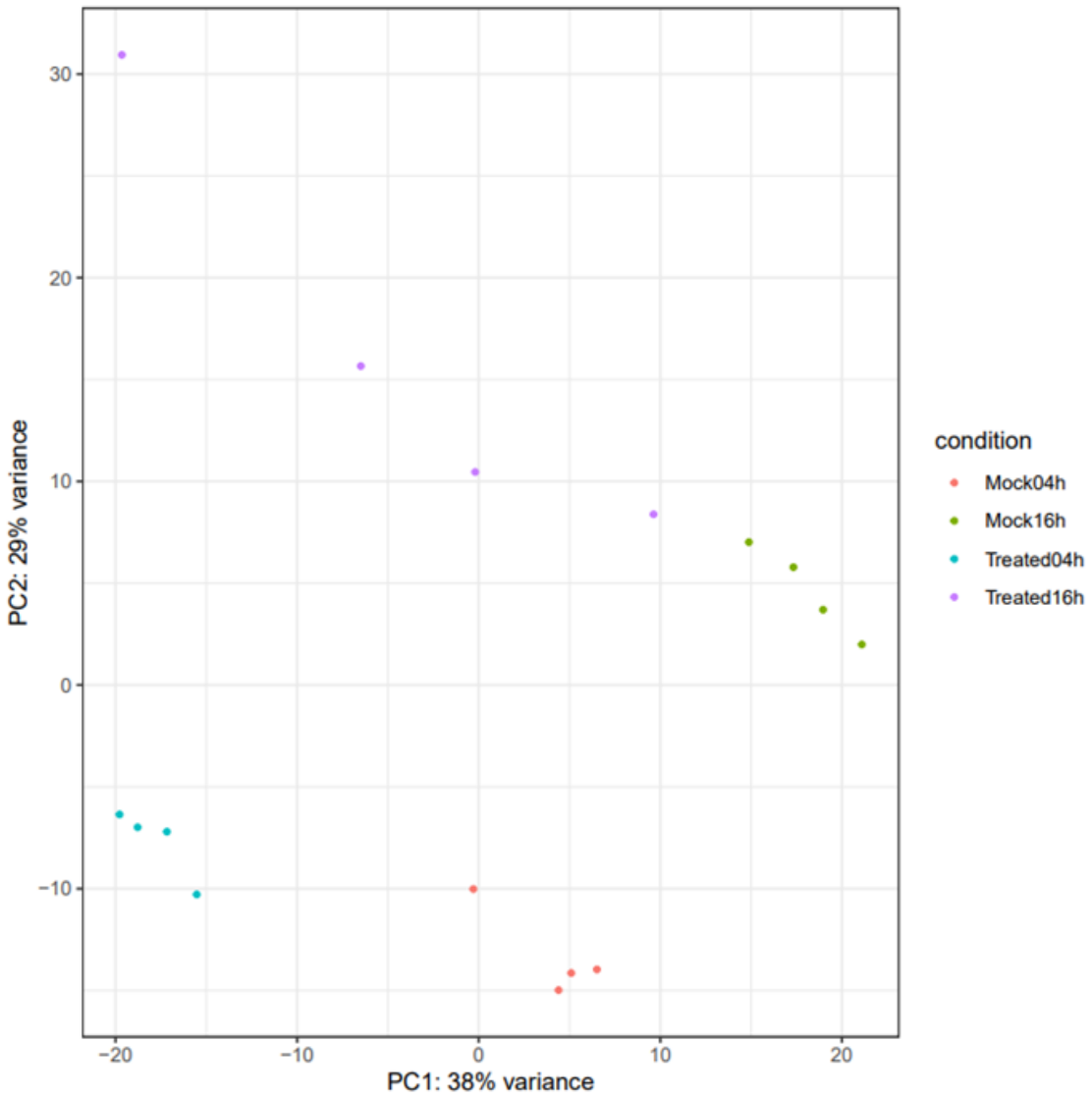

Figure 3.5: The variance between mock and treated sample groups. A PCA plot showing the variance between 4 and 16-hour mock and treated samples. Each dot represents a biological replicate and sample types are colour-coded (see key on right).

Table 3.1: Genes shared between the top 10 differentially expressed genes at 4- and 16-hours post microwave treatment. Gene names are displayed in order of significance with their log2 Fold Change at 4- and 16-hours post-treatment.

Gene	Log_2 Fold change at 4 hours	Log_2 Fold change at 16 hours
HSPA6	8.1	7
ARC	5.7	5.6
HSPA1A	3.9	2.9
HSPA7	9.6	7.7
HSPA1B	3.5	3.0
CLU	3.3	3.4
ANKRD1	6.9	6.4
GEM	4.3	3.7
RASD1	5.4	5.0

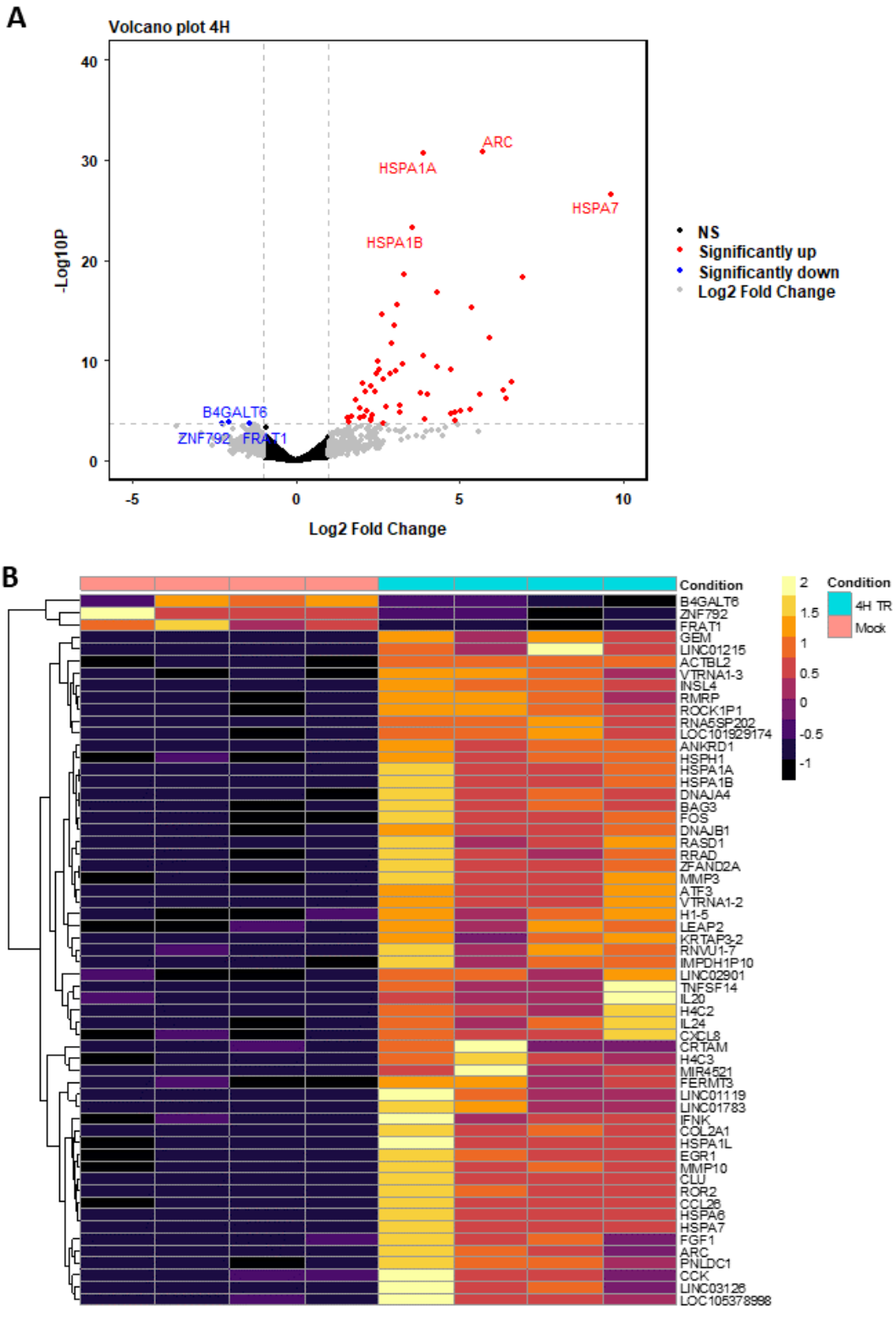
A
Volcano plot 4H
-Log10P
Log2 Fold Change
ARC
HSPA1A
HSPA7
HSPA1B
B4GALT6
ZNF792
FRAT1
NS
Significantly up
Significantly down
Log2 Fold Change
B
Condition
4H TR
Mock
B4GALT6
ZNF792
FRAT1
GEM
LINC01215
ACTBL2
VTRNA1-3
INSL4
RMRP
ROCK1P1
RNA5SP202
LOC101929174
ANKRD1
HSPH1
HSPA1A
HSPA1B
DNAJA4
BAG3
FOS
DNAJB1
RASD1
RRAD
ZFAND2A
MMP3
ATF3
VTRNA1-2
H1-5
LEAP2
KRTAP3-2
RNVU1-7
IMPDH1P10
LINC02901
TNFSF14
IL20
H4C2
IL24
CXCL8
CRTAM
H4C3
MIR4521
FERMT3
LINC01119
LINC01783
IFNK
COL2A1
HSPA1L
EGR1
MMP10
CLU
ROR2
COL26
HSPA8
HSPA7
FGF1
ARC
PNLDC1
CCK
LINC03126
LOC105378998

C

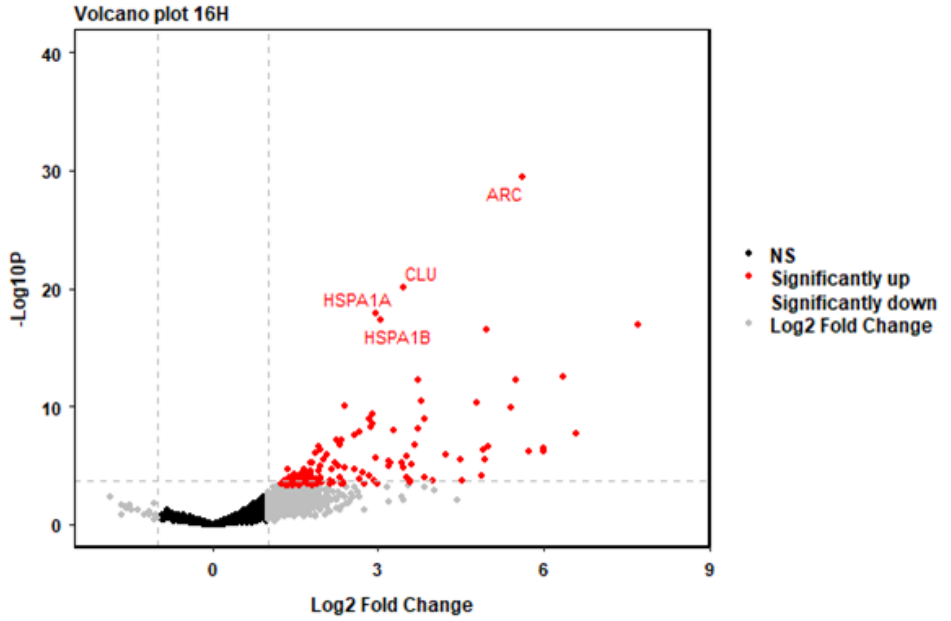
Volcano plot 16H
-Log10P
40
30
20
10
0
0
3
6
9
Log2 Fold Change
ARC
CLU
HSPA1A
HSPA1B
NS
Significantly up
Significantly down
Log2 Fold Change

D

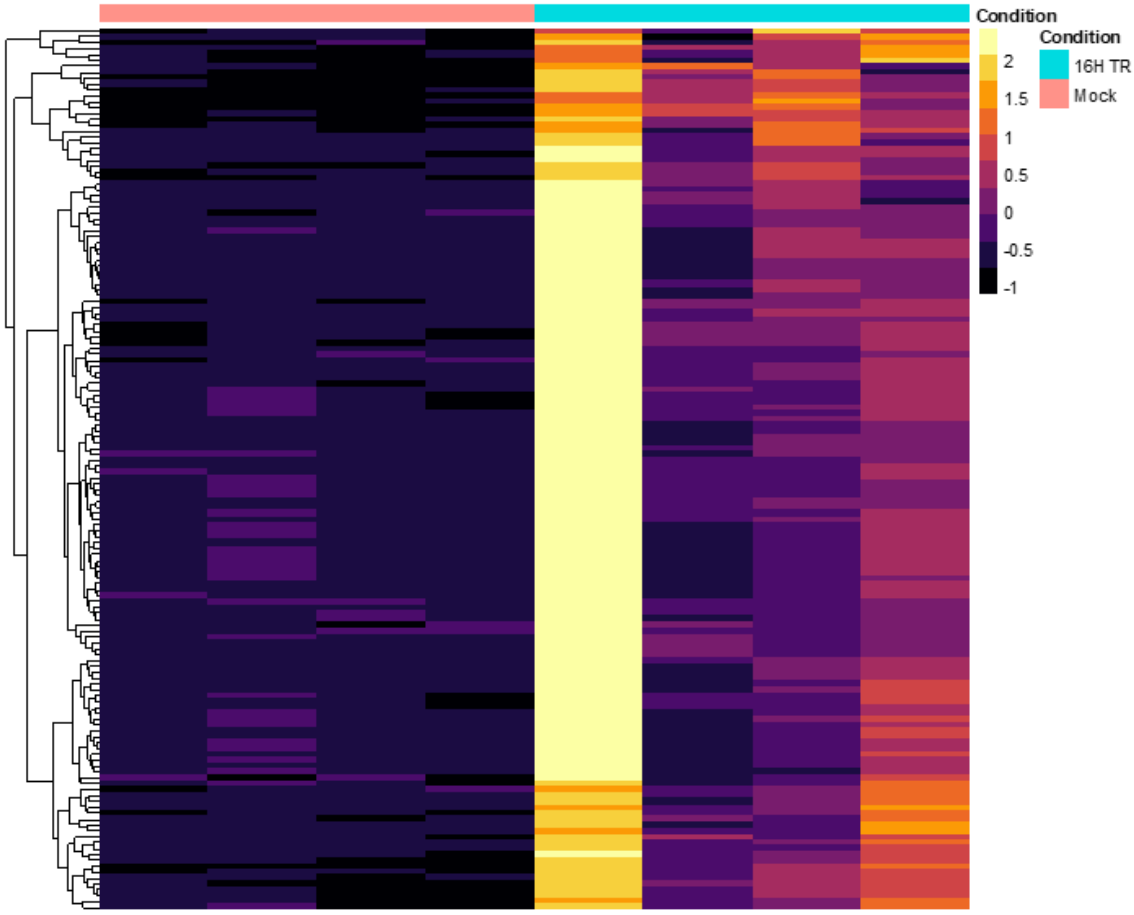
Condition
Condition
16H TR
Mock
2
1.5
1
0.5
0
-0.5
-1

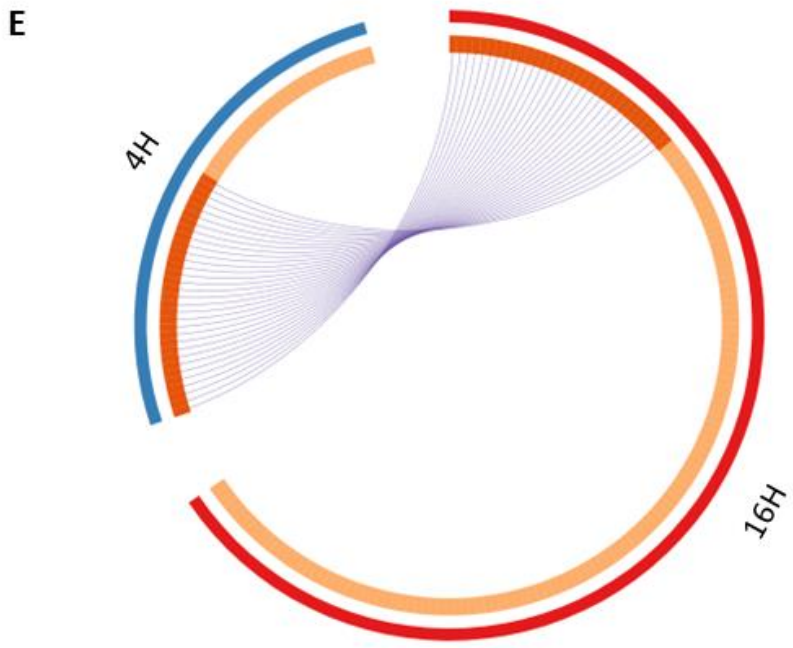

Figure 3.6: Microwave treatment of NIKS16 3D organotypic rafts leads to transcriptomic changes. Volcano plots showing the Log2 fold change and p-value of genes from NIKS16 treated rafts at 4 hours (A) and 16 hours (C) in comparison to mock-treated tissues at the same time point. Each dot represents one gene. Genes that have a Log2 fold change within the range of -1 to 1 are plotted in black. Any genes with a Log2 fold-change < -1 or >1 but with an adjusted p-value> 0.05 are plotted in grey. Differentially expressed genes (DEGs) that have an adjusted p-value < 0.05 and Log2FoldChange <-1 or >1 are shown in red (for upregulated DEGs) or blue (for downregulated DEGs). A y-axis limit of 40 was used to allow visualisation of the spread of the data however this removed one point corresponding to *HSPA6* in both the 4-hour and 16-hour graphs. (B & D) Clustered heatmaps for all differentially expressed genes at 4 hours (B) and 16 hours (D) in microwave-treated NIKS16 tissues. Each column represents 1 of 4 replicates per condition. The heatmap for 4 hours includes the gene names of DEGs. (E) Circos plot of the overlapping upregulated genes at 4 hours and 16 hours. The outside arc represents the identity of each gene list: 4 hours (blue) and 16 hours (red). The inside arc represents each gene member as a tile on the arc. Genes coloured dark orange are shared between 4 and 16 hours and light orange genes are unique to each time point. Purple lines link the same genes shared by each group.

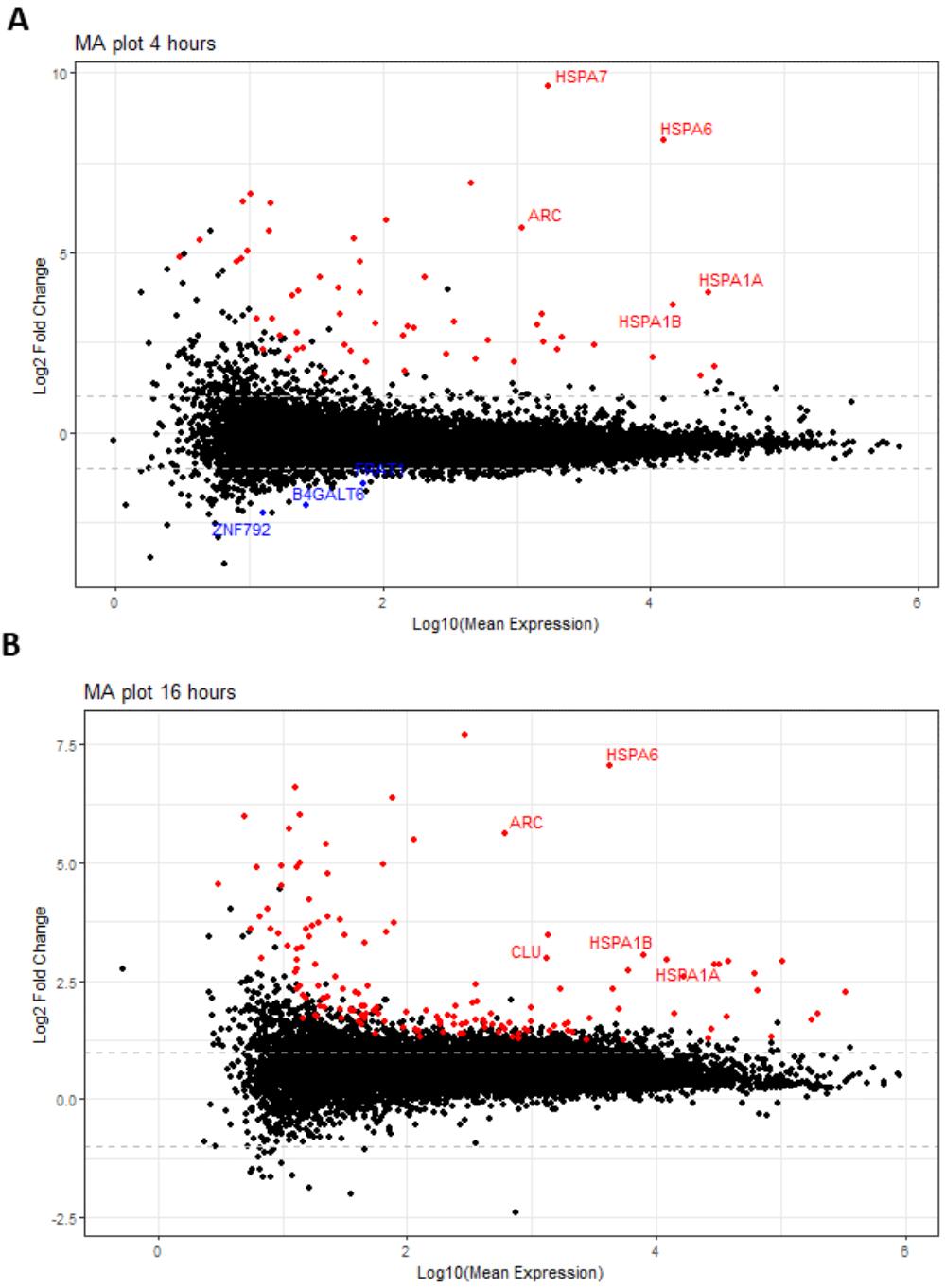

Figure 3.7: The differential expression compared to mean expression values of genes across each data set. MA plots showing the Log2 fold change and mean expression of genes at 4 (A) and 16 hours (B). Each dot represents one gene. Genes that were significantly upregulated are shown as red dots and those significantly downregulated as blue dots. Labels indicate the top 5 differentially up or downregulated genes.

3.5.2 Microwave treatment results in upregulation of genes involved in protein folding and innate immunity.

To interpret the biological consequences of the transcriptome changes caused by microwave treatment, gene set enrichment analysis (GSEA) was carried out on the differentially expressed genes at 4 and 16 hours using Metascape (Zhou *et al.*, 2019). In the upregulated gene group at 4 hours, 'chaperone cofactor-dependent protein refolding' (GO:0051085) was the most significantly enriched term (Figure 3.8A). The genes included in this term included the heat shock 70kDa proteins (*HSPA1A, HSPA1B, HSPA1L, HSPA6, HSPA7, HSPH1*) and DNAJ heat shock proteins (*DNAJB1*) (Figure 3.8A). This is consistent with findings from the meta-analysis on heat stress described above (Section 3.1) where following GSEA, protein refolding was determined to be the most significantly enriched term for both human and mice studies (Yonezawa and Bono, 2023). Metascape accounts for redundancy between terms by clustering similar pathways from GSEA into a representative group (Zhou *et al.*, 2019). The term within the cluster with the highest significance is then displayed within the bar graph. The second most significantly enriched term is 'Overview of proinflammatory and profibrotic mediators' but this cluster of redundant terms includes many immune pathways. 'NGF-stimulated transcription' was also in the top 5 significantly enriched terms. Again, Metascape attempts to account for redundancy by clustering similar terms and included in this cluster are response pathways to interleukin-1 and tumour necrosis factor, indicating innate immune activation following microwave treatment (Figure 3.8A). There were only three significantly downregulated genes at 4 hours post-treatment and these did not result in any significantly enriched pathways when submitted for analysis.

At 16 hours post-treatment, GSEA of the upregulated genes reveals several shared pathways with those upregulated at 4 hours (Figure 3.8B, C). Protein folding pathways were still significantly enriched. Only four genes were present within 'chaperone cofactor-dependent protein refolding' (GO:0051085), compared to the seven at 4 hours post-treatment, but all four are shared with those included at 4 hours. Innate immune pathways were still enriched at 16 hours with 'cellular response to cytokine stimulus' and 'Cytokine signalling in the immune system' in the top 6 terms (Figure 3.8B). Treated cells appeared to show an energy requirement at later time points due

to ‘oxidative phosphorylation’ (GO:006119) being the most significantly enriched term at 16 hours (Figure 3.8B). Many mitochondrial metabolism pathways are included within this redundant cluster. This pathway appears to only be switched on at later time points following microwave treatment since it is not enriched at 4 hours. Another upregulated pathway at later time points is ‘Formation of the cornified envelope’ (R-HAS-6809371) (Figure 3.8B). Included in this pathway are the keratins (*KRT37*, *KRT75*), late cornified envelope proteins (*LCE3D*, *LCE3A*, *LCE3C*, *LCE6A*) and corneodesmosomes (*CDSN*).

Immune genes upregulated by microwave treatment at 4 hours included the interleukins (*IL20*, *IL24*), the keratinocyte-specific interferon (*IFNK*), TNF superfamily members (*TNFSF14*) and chemokine ligands (*CCL26*) (Figure 3.9A, Table 3.2). The non-canonical heat shock protein and innate immune gene *CXCL8* was also upregulated. Heat shock proteins are also implicated in these pathways due to their importance in immune activation (Hu *et al.*, 2022) (Figure 3.9A). Some genes involved in immunity had increased in expression by 16 hours, including *IL1R2*, *CRTAM*, *CLCF1*, *TNFRSF18*, *CCL24, ITGAX* and *IL18BP,* whilst others showed a slight decrease or no change in expression (Figure 3.9B, Table 3.2).

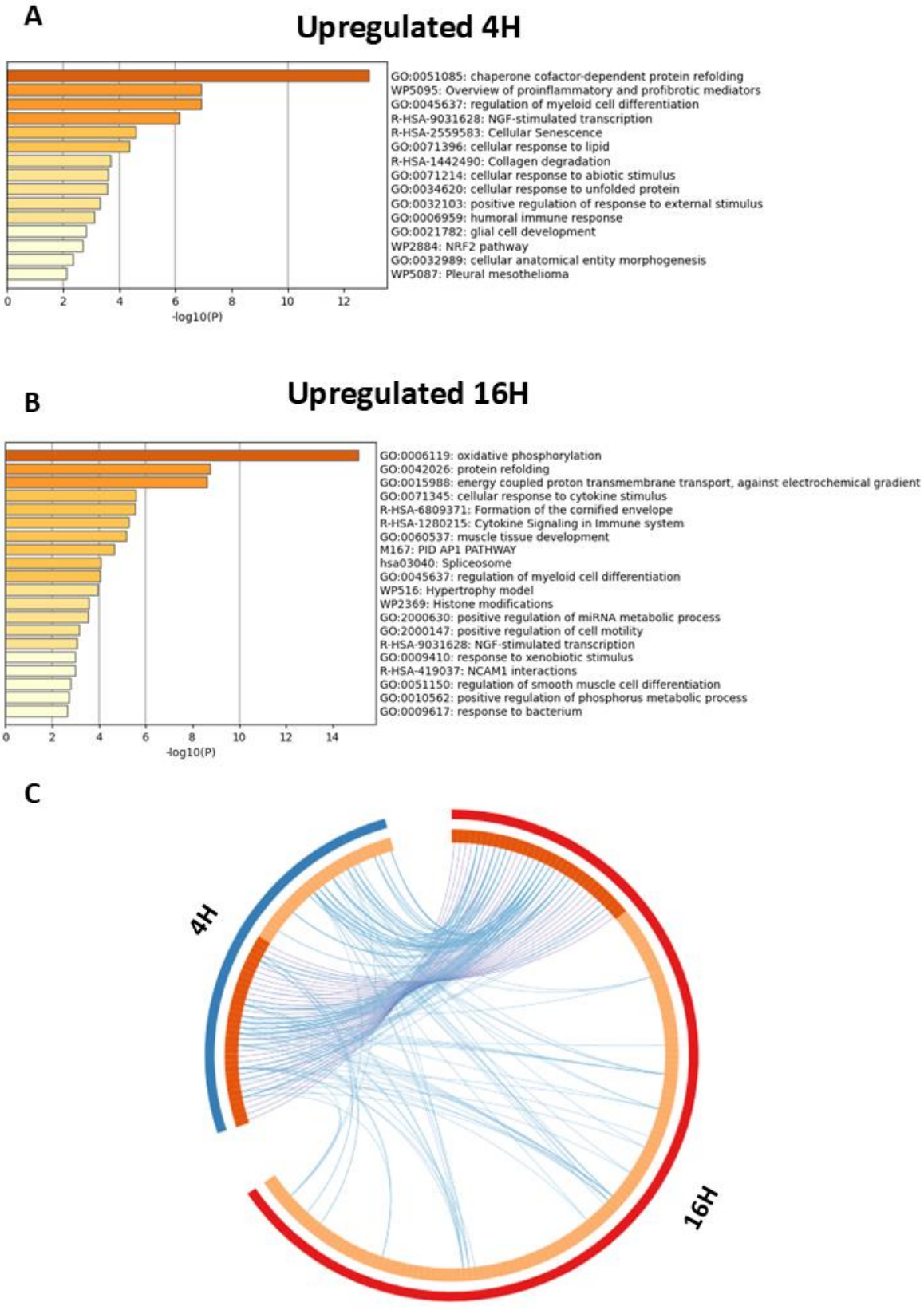

Figure 3.8: Pathway analysis of genes upregulated by microwave treatment at 4 and 16 hours. The top 20 pathways enriched following Metascape analysis of the significantly upregulated genes at 4 hours (A) and 16H post-treatment (B). The significant terms were hierarchically clustered and a 0.3 kappa score was applied to cast similar pathways into term clusters. The term within each cluster with the highest

significance is displayed as the output on the graph. Darker orange colours represent pathways that are predicted to be enriched with more confidence than lighter colours. (C) Circos plot of the overlapping upregulated genes at 4 hours and 16 hours. The outside arc represents the identity of each gene list: 4 hours (blue) and 16 hours (red). The inside arc represents each gene member as a tile on the arc. Genes coloured dark orange are shared between 4 and 16 hours and light orange genes are unique to each time point. Purple lines link the same genes shared by each group. Blue lines link the genes that fall under the same statistically significant ontology term following Metascape analysis. Figures made using Metascape (Zhou *et al.*, 2019).

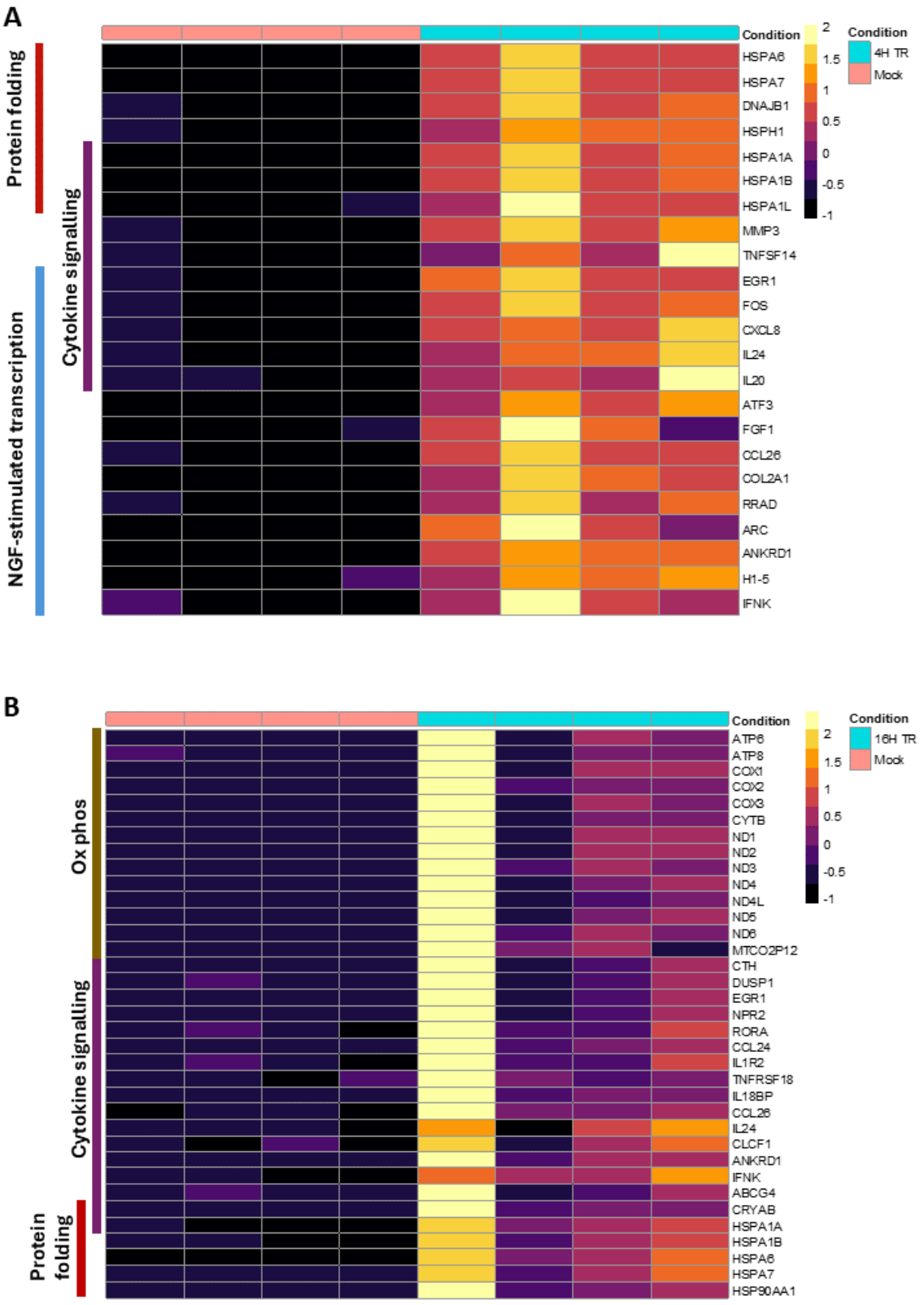

Figure 3.9: Pathway analysis reveals upregulation of cytokine signalling, protein folding and oxidative phosphorylation following microwave treatment. (A, B) Heatmaps of differentially expressed genes involved in pathways upregulated at 4 hours (A) and 16 hours (B) post-treatment. Coloured bars on the left represent the pathways that the genes are involved in, protein folding (red bar), cytokine signalling (purple bar), NGF-stimulated transcription (blue bar) and oxidative phosphorylation (gold bar). The pathway within the redundant Metascape cluster with the highest significance was chosen for data visualisation.

Table 3.2: Changes in expression of immune genes following treatment. The log2 fold change of immune genes at 4 and 16 hours post microwave treatment. Fold changes in green and black represent significantly upregulated and non-significant changes at that time point respectively.

Gene name	4H Log2 Fold Change	16H Log2 Fold Change
CCL26	3.9	3.3
IL24	3	1.8
TNFSF14	2.9	1.6
IL20	2.8	1.2
CRTAM	2.7	3.6
IFNK	2.4	1.8
LEAP2	2.1	1
CXCL8	1.9	0.8
IL1R2	0.9	1.8
CLCF1	0.8	1.7
TNFRSF18	0.2	2.1
CCL24	0.2	1.5
ITGAX	0	1.8
IL18BP	-0.1	1.9

3.5.3 Predicted protein interactions of the up- and downregulated genes following microwave treatment

Predicted protein-protein interaction (PPI) networks provide a detailed analysis of the interconnectivity of upregulated genes (Zhou *et al.*, 2019). Genes upregulated at 4 hours have a small but tightly connected protein interaction network (Figure 3.10A). A cluster of genes encoding chaperones involved in protein folding was visualised using the Molecular Complex Detection (MCODE) algorithm which extracts protein complexes within the network and then annotates these for their putative biological roles (Figure 3.10A, red cluster). This cluster involves the heat shock proteins and co-chaperones which were annotated in the 'Regulation of HSF1-mediated heat shock response' pathway (Figure 3.10A). The genes upregulated at 16 hours have a larger network of protein interactions. Three clusters of proteins were predicted from the MCODE algorithm. One cluster contained genes involved in the electron transport chain and oxidative phosphorylation (Figure 3.10B, red cluster). This suggests that

there is an energy requirement for cells undergoing microwave-driven hyperthermia. A second cluster includes genes involved in protein folding (Figure 3.10B, blue cluster) and a third includes genes involved in keratinocyte differentiation (Figure 3.10B, green cluster), annotated in the 'Formation of the cornified envelope' pathway. This corresponds with our previous observations of increased differentiation following microwave treatment (Conley *et al.*, 2023).

Enrichment analysis was performed to infer transcription factor-target regulatory interactions using TRRUST (Han *et al.*, 2015). At 4 hours, genes regulated by FOS, a subunit of AP-1, were the most enriched (Figure 3.11A). Another AP-1 subunit, JUN, is also predicted to control the upregulation of several genes at 4 hours. Genes upregulated by NFKB1 were observed to be enriched at both 4 and 16 hours. NFKB1 is a subunit of NF-kB and another of its subunits, RELA, was also enriched (Figure 3.11A). NF-kB can be induced by stress, inflammatory cytokines and infection (Baeuerle and Henkel, 1994; Hayden, West and Ghosh, 2006). It functions as a central mediator of inflammatory and immune responses with downstream target genes involved in apoptosis, proliferation and the immune response (Oeckinghaus and Ghosh, 2009). Other strongly induced genes include targets of HSF1, STAT3, STAT6 and TP53, which is normally targeted by high-risk HPV's E6 for degradation (Figure 3.11A). The enriched regulatory interactors upregulated at 16 hours are very similar to those at 4 hours with TP53, NFKB1, RELA, STAT3 and JUN all inferred by TRRUST to be enriched (Figure 3.11B).

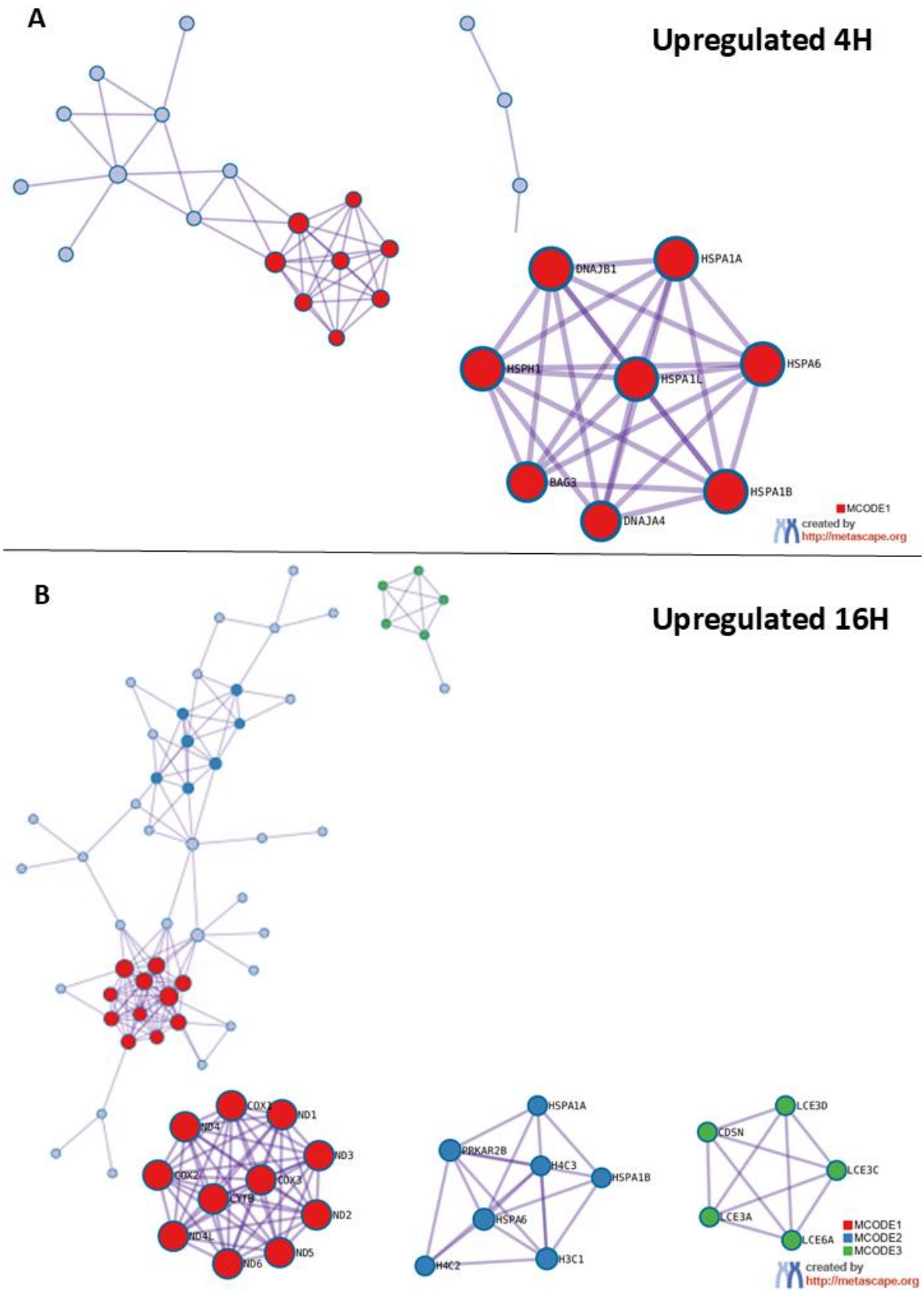

Figure 3.10: The predicted protein interaction network of genes upregulated by microwave treatment. Predicted protein-protein interaction (PPI) networks for genes significantly upregulated at 4 hours (A) and 16 hours (B) post microwave treatment. The MCODE algorithm identifies areas where proteins are densely connected (red, blue and green-coloured clusters) and GO enrichment was applied to each cluster of proteins to extract biological meanings. Figures made using Metascape (Zhou *et al.*, 2019).

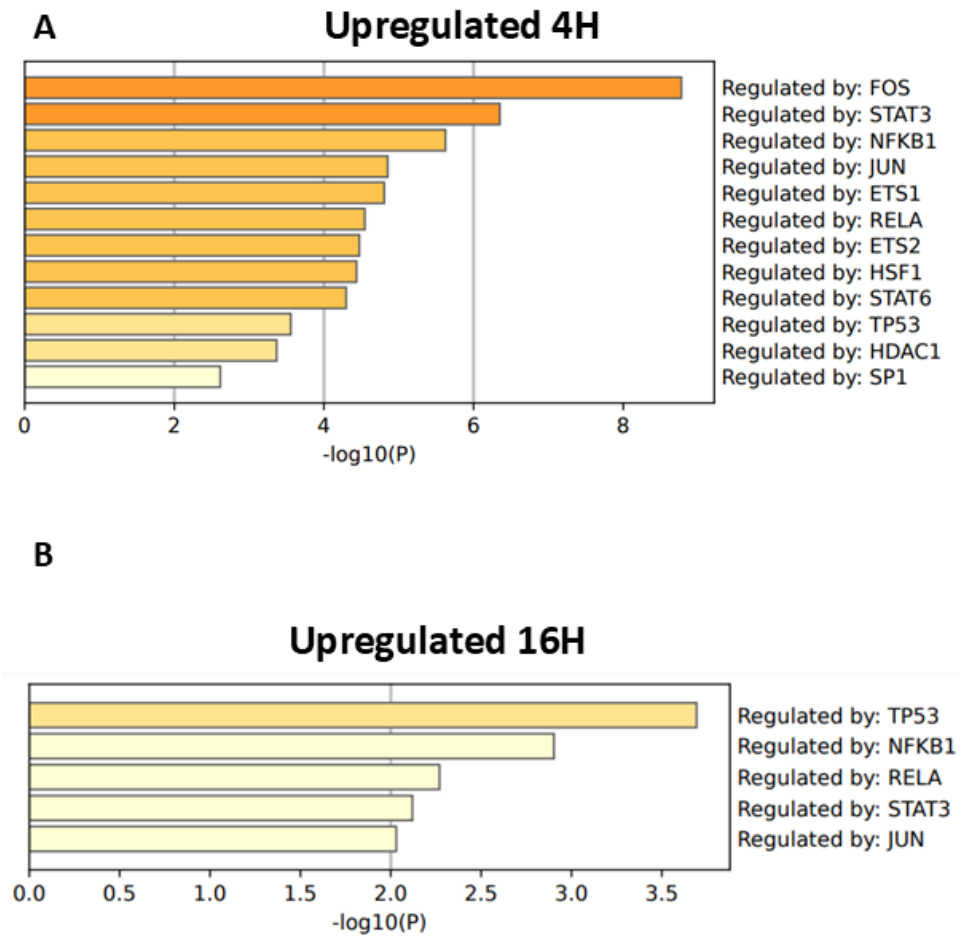

Figure 3.11: Transcription factors predicted to regulate the transcription of upregulated genes following microwave treatment. The output from transcription factor-target regulatory interactions (TRRUST) enrichment for genes upregulated at 4 hours (A) and 16 hours (B) post microwave treatment. Figures made using Metascape (Zhou *et al.*, 2019).

3.6 Investigating the change in expression of the epithelial differentiation markers transglutaminase and keratin 10 following microwave treatment

RNA Sequencing pathway analysis revealed an increase in the transcription of keratinocyte differentiation genes in NIKS16 rafts following microwave treatment (R-HSA-6809371, Figure 3.8B). We therefore wished to validate these changes using RT-qPCR. Initially, we investigated keratin 10 and transglutaminase transcription following microwave treatment. Keratin 10 is a more general differentiation marker, expressed by non-basal cells in the stratified epithelium whilst transglutaminase is expressed during the late stages of differentiation due to its importance in cornification, which takes place in the upper layers of the epithelium (Moll, Divo and Langbein, 2008; Chermnykh, Alpeeva and Vorotelyak, 2020). There was a decrease in keratin 10 following microwave treatment but an increase in transglutaminase (Figure 3.12A, B). The decrease in keratin 10 was observed at 16 and 72 hours post-treatment although this was non-significant; at other time points, levels were similar to mock-treated tissue. Whilst transglutaminase expression was shown to increase up to 48 hours post-treatment, none of these increases were statistically significant compared to the 0H time point (Figure 3.12A). This is possibly due to the large variation between replicates and the 0H time point having increased transglutaminase expression relative to mock-treated tissue.

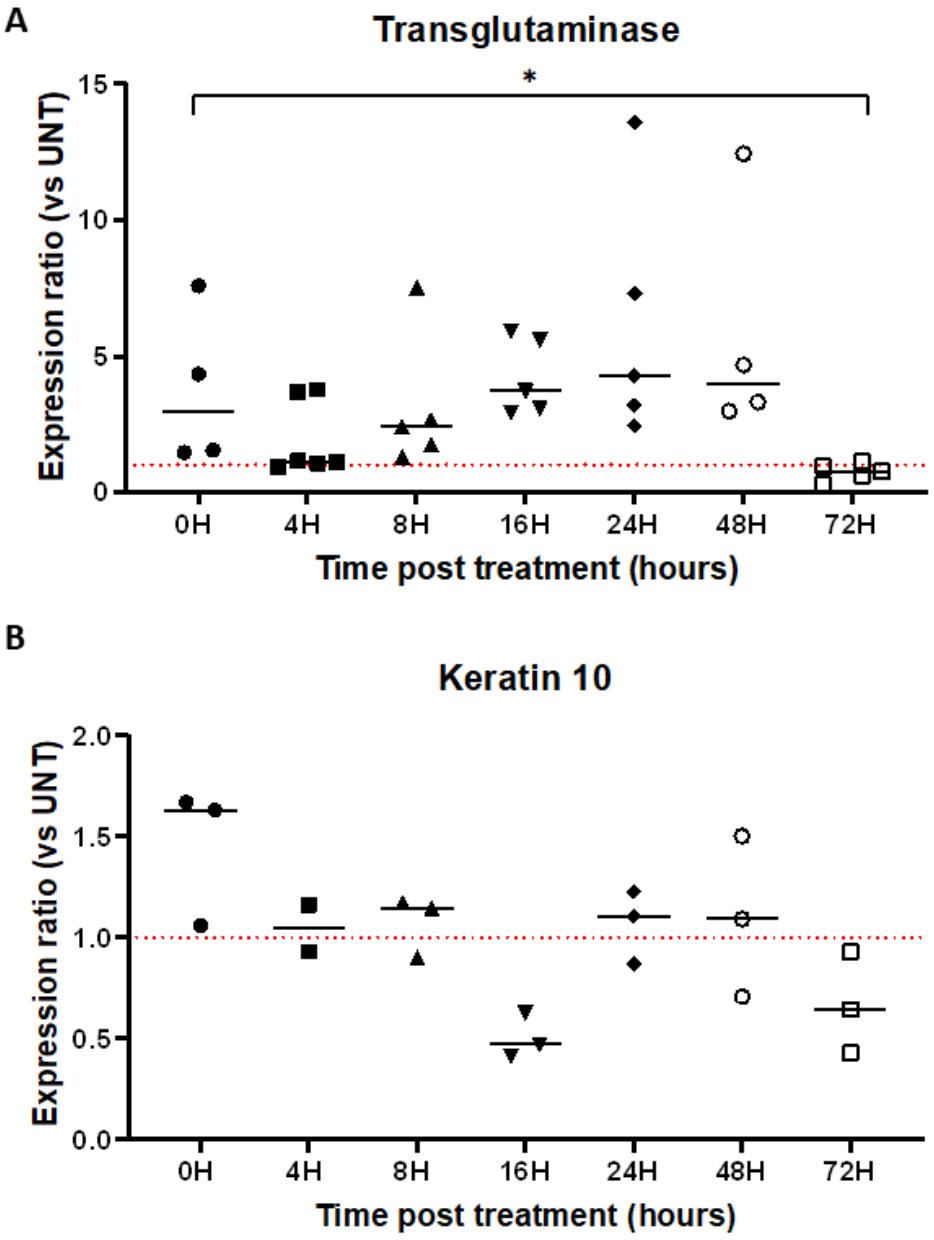

Figure 3.12: Microwave treatment enhances the gene expression of the differentiation marker transglutaminase but not keratin 10. Expression ratio of epithelial differentiation genes transglutaminase (A) and keratin 10 (B) in NIKS16 mini rafts 0 – 72 hours following treatment. Delta Ct changes were calculated relative to the housekeeping gene Beta-actin and expression ratios of treated to mock tissues were determined using $2^{-\Delta\Delta CT}$. The median expression ratio is displayed (black line) for each time point post-treatment and each point represents one biological replicate (n=5 and n=3 for A and B respectively). The red dashed line indicates an expression ratio with no change between the mock and treated tissues (y=1). Each biological replicate represents an average of three technical replicates. A Kruskal-Wallis test was used to determine if there was a statistical difference between groups. * Indicates $p < 0.05$.

3.7 Microwave treatment induces an innate immune response

3.7.1 The mRNA expression of the pro-inflammatory cytokines TNF-α, IL-6 and IL-1β increases following microwave treatment

Innate immune pathways were observed to be enriched from our RNA Sequencing analysis of microwave-treated tissues. Previous work using the Swift® microwave device has demonstrated increased expression of the cytokines IL-1β, TNF-α and IL-6 in treated 2D HaCaT cultures (Bristow *et al.*, 2017). We wished to follow up these observations by investigating changes in cytokine expression in a 3D model system, which better represents the *in vivo* environment in which the device would be used. Moreover, we aimed to address how HPV16 positivity would influence the induction of innate immunity since the virus regulates the immune response in a complex fashion (Section 1.9.2). We analysed the mRNA expression of IL-1β, TNF-α and IL-6 following microwave treatment, using RT-qPCR in HPV-negative (HaCaT) and HPV16-positive (NIKS16 and W12E) tissues. All three tissue types showed a transient increase in these innate immune markers (Figure 3.13).

In HaCaT tissues, IL-6 increased to a greater extent following microwave treatment than either IL-1β or TNF-α (Figure 3.13). IL-6 expression peaked at 4 hours and by 16 hours, had decreased to similar levels to mock-treated tissues. This IL-6 dominant response had previously been observed in 2D HaCaT cells (Bristow *et al.*, 2017). In comparison, the expression of IL-1β and TNF-α did not increase much above mock-treated tissues following treatment (Figure 3.13). A small significant increase in IL-1β was observed 16 hours post-treatment but this was small in magnitude (~1.5x) and expression had decreased to levels below that of untreated tissues by 24 hours (Figure 3.13). A small rise in TNF-α was also observed up to 8 hours post-treatment, although this was not significant, and expression had fallen below mock-treated tissues by 16 hours (Figure 3.13).

In NIKS16 tissues, IL-6 also showed the largest fold change in expression following microwave treatment (Figure 3.13). This was significant at 8 and 16 hours ($p<0.05$) and continued rising to 24 hours, where it peaked, at ~ 6.5 x that of mock-treated levels (Figure 3.13) ($p<0.05$). Moreover, IL-1β expression was significantly increased at 4 and

24 hours post-treatment ($p<0.01$) (Figure 3.13). TNF-α also increased significantly following microwave treatment in NIKS16 tissues, with a peak in expression at the same time as IL-6, at 24 hours post-treatment ($p<0.05$) (Figure 3.13).

Similarly to NIKS16 and HaCaT, W12E tissues showed an IL-6 dominant response, with a peak in expression at 4 hours post-treatment, where treated tissues had an 18-fold higher expression compared to mock-treated tissues ($p<0.001$) (Figure 3.13). IL-6 levels remained above that of mock-treated tissues up to 24 hours post-treatment (Figure 3.13). There was also a significant increase in IL-1β and TNF-α following treatment. TNF- α and IL-1β expression peaked at 4 and 16 hours respectively but remained elevated above mock-treated tissues up to 24 hours post-treatment (Figure 3.13).

Our analysis reveals an increase in IL-6, IL-1β and TNF-α transcription following microwave treatment in HPV-positive tissues. The observed increase in expression is longer-lasting in the HPV-positive compared to HPV-negative tissues analysed, with expression remaining elevated in comparison to mock-treated tissues up to 24 hours post-treatment. Of the cytokines analysed, IL-6 had the largest fold change in expression relative to mock-treated tissues across all cell lines.

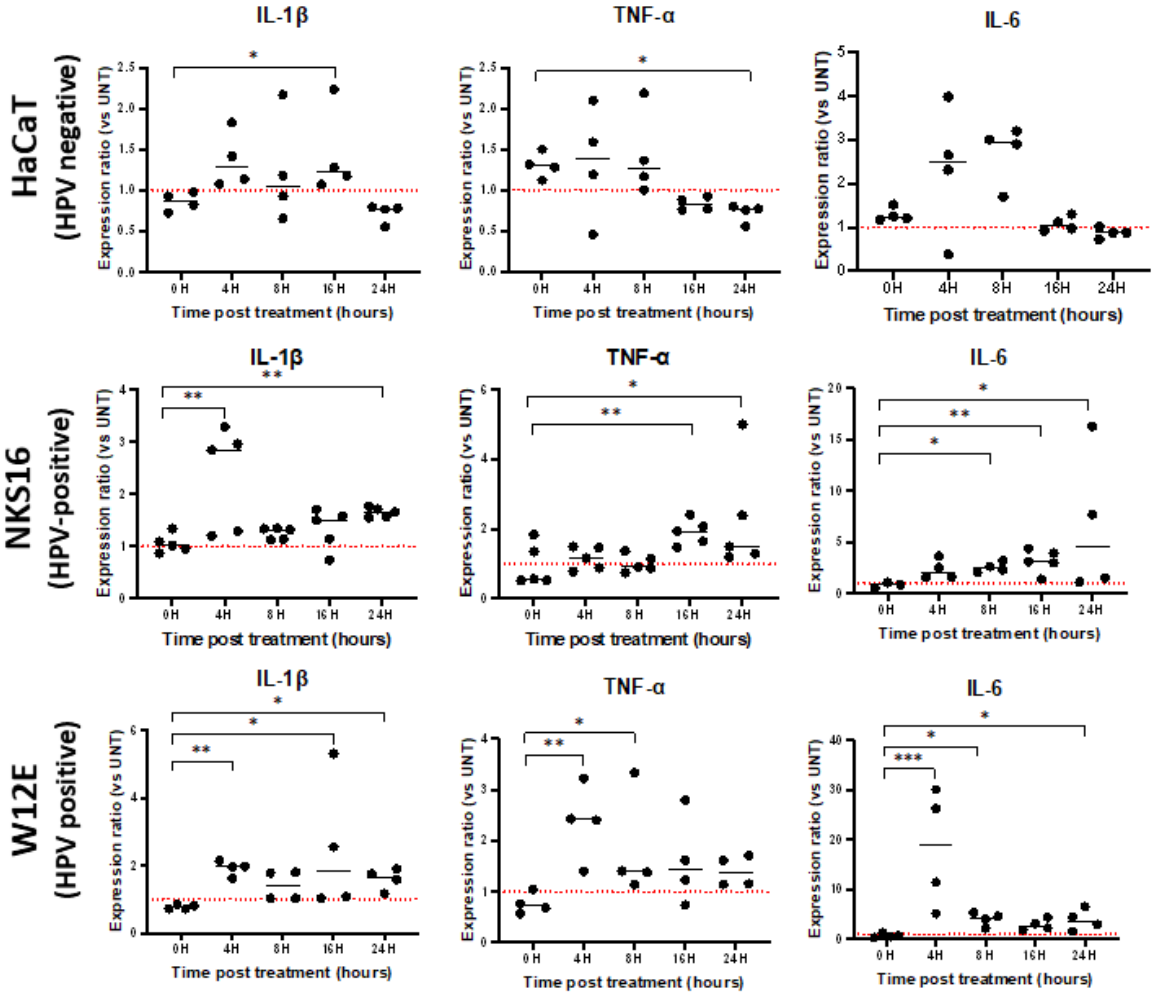

Figure 3.13: Microwave treatment stimulates the transcription of several innate immune markers in HPV-negative and HPV-positive tissues. RT-qPCR analysis of IL-1β (left column), TNF-α (middle column) and IL-6 (right column) in HaCaT (first row), NIKS16 (middle row) and W12E (lower row) tissues. Delta Ct changes were calculated relative to the housekeeping gene Beta-actin and expression ratios of treated to mock tissues were determined using $2^{-\Delta\Delta CT}$. The median expression ratio is displayed (black line) for each time point post-treatment and each point represents one biological replicate (n=4 for HaCaT and W12E, n=5 for NIKS16, some NIKS16 biological replicates had IL-6 C_T values too low for detection and were removed from the analysis). The red dashed line indicates an expression ratio with no change between the mock and treated tissues (y=1). Each biological replicate represents an average of three technical replicates. A Kruskal-Wallis test, a non-parametric alternative to the One Way ANOVA was used to determine if there was a statistical difference between groups. * Indicates $p< 0.05$, ** indicates $p< 0.01$ and *** indicates $p<0.001$.

3.7.2 Microwave treatment increases the concentration of cytokines secreted into the media from HPV-negative and HPV-positive tissues following microwave treatment

Given the increase in transcription of cytokines in HPV-negative and HPV-positive tissues following microwave treatment, a subsequent analysis was conducted to investigate if this could be observed downstream at the protein level. A Luminex® Human High Sensitivity Cytokine assay was used to determine if the concentration of twelve cytokines, including IL-1β, IL-6 and TNFα, changed following microwave treatment. Analysis of cytokines secreted from HaCaT, W12E and NIKS16 mini rafts into the surrounding media was conducted at 1-, 8- and 16 hours post-treatment. Cytokine concentrations increased for both untreated and treated tissues over time, possibly as cytokines accumulated in the media alongside media evaporation (Figure 3.14, Figure 3.15, Figure 3.16). Thus, the cytokine concentration in the media of treated tissues was compared to mock-treated tissues at the same time point post-mock or microwave treatment.

Within HPV-16 negative tissues, an IL-6 dominant response was observed, similar to observations by RT-qPCR. At 8 hours post-treatment, microwave-treated tissues had almost 5 times the concentration of IL-6 compared to mock-treated tissues (Figure 3.14A) ($p<0.01$). At 16 hours, the concentration was still raised in treated tissues compared to untreated, although this was non-significant. There was also a significant increase in IL-1β and GM-CSF in the media from treated HaCaT tissues at 8 hours (Figure 3.14A). Increased TNF-α, IL-10, IL-4, IFN-γ, and IL12-p70 were also observed at this time point, although this was not significant (Figure 3.14A). By 16 hours post-treatment, all cytokines in treated HaCaT tissues, except IL-6, had decreased to concentrations below that of mock-treated tissues (Figure 3.14A). This decrease was significant for TNF-α, IL-10, IL-4, IFN-γ, IL-2 and GM-CSF. The angiogenic factor vascular endothelial growth factor (VEGF) was decreased at both 8- and 16 hours post-treatment (Figure 3.14A). The concentration of IL-8 and IL-5 could not be confidently calculated, due to the Mean Fluorescence Intensity (MFI) reading falling outside the standard curve (above for IL-8 and below for IL-5). It has been proposed that it is still acceptable to use the fluorescent values for differential analysis and for assigning statistical significance to treatment effects (Breen, Tan and Khan, 2016). There was a

small increase in IL-8 at 1 hour post-treatment, but this effect was lost quickly, with levels similar between mock and treated samples at 8 hours and by 16 hours, treated samples had less IL-8 (Figure 3.14B). IL-5 was upregulated at 8 hours, but this was lost at 16 hours (Figure 3.14B).

Within the media of NIKS16 tissues, seven of the twelve cytokines analysed had concentrations which could be determined using the five-parameter logistic curve plotted from standard samples (Figure 3.15A). Of these, the concentrations of all except VEGF were increased following microwave treatment when compared to mock-treated samples at the same time point (Figure 3.15A). This increase was statistically significant for all six increased cytokines at 8 hours post-treatment ($p<0.05$). This includes IL-8, TNF-α, IL-4, GM-CSF, IL-1β and IL-10, in descending order of concentration. At 16 hours post-treatment, the concentration of these cytokines was still higher in the media of treated tissues compared to mock-treated tissues at the same time point, although this was only significant for IL-4 ($p<0.05$) (Figure 3.15A). A similar observation to HaCaT tissues was made for VEGF in NIKS16 tissues, where the concentration of VEGF was decreased in the media from treated rafts relative to mock-treated rafts across all time points (Figure 3.15A). Using the approach described above for MFI readings that fall outside of the standard curve, we determined that all remaining cytokines analysed (IL-2, IL-6, IFN-ɣ, IL-5, IL-12 p700) had increased expression following microwave treatment when compared to mock-treated samples at the same time point for 8- and 16-hours post-treatment (Figure 3.15B). This increase was statistically significant at 8 hours post-treatment for all of the aforementioned cytokines ($p<0.05$) (Figure 3.15B).

In W12E tissues, ten of the twelve cytokines analysed had MFI readings which fell within the standard curve to allow for concentration measurements (Figure 3.16A). Of these, 6 were significantly upregulated following treatment (IL-6, TNF-α, GM-CSF, IL-1β, IFN-γ and IL-10) (Figure 3.16A). A rapid rise in the pro-inflammatory cytokine TNF-α was evident following treatment, with a significant rise in concentration at 1-, 8- and 16 hours post-treatment (Figure 3.16A). The profile of TNF-α activation was very different to that of IL-6, where no evident increase was observed until 16 hours, when treated rafts had an average concentration that was 3.25x more than mock (Figure

3.16A). The profiles of the other cytokines corresponded well to those observed for NIKS16 with a larger increase in cytokine concentration in the media of treated rafts at 8 hours compared to mock but with concentrations remaining elevated in the media from treated tissues at 16 hours post-treatment (Figure 3.16A). In both HPV-positive tissues, a significant increase in IL-6, TNF-α, GM-CSF, IL-1β, IFN-γ and IL-10 was observed following treatment (Figure 3.15, Figure 3.16).

All tissues showed an increase in the secretion of several cytokines into the media following microwave treatment. IL-8 had the highest concentration in the media of all cell types analysed. Moreover, all tissues shared significant increases in the pro-inflammatory cytokines IL-6, GM-CSF and IL-1β. In HPV-negative tissues, the response appeared short-lived, with many cytokines decreasing in concentration at 16 hours to below that of mock-treated tissues. This effect was not observed in HPV-positive tissues; cytokines were still raised in the media of treated tissues compared to mock-treated tissues at 16 hours, suggesting a longer-lasting effect within infected tissues. The expression of the angiogenic factor VEGF was decreased for all tissues following treatment.

A

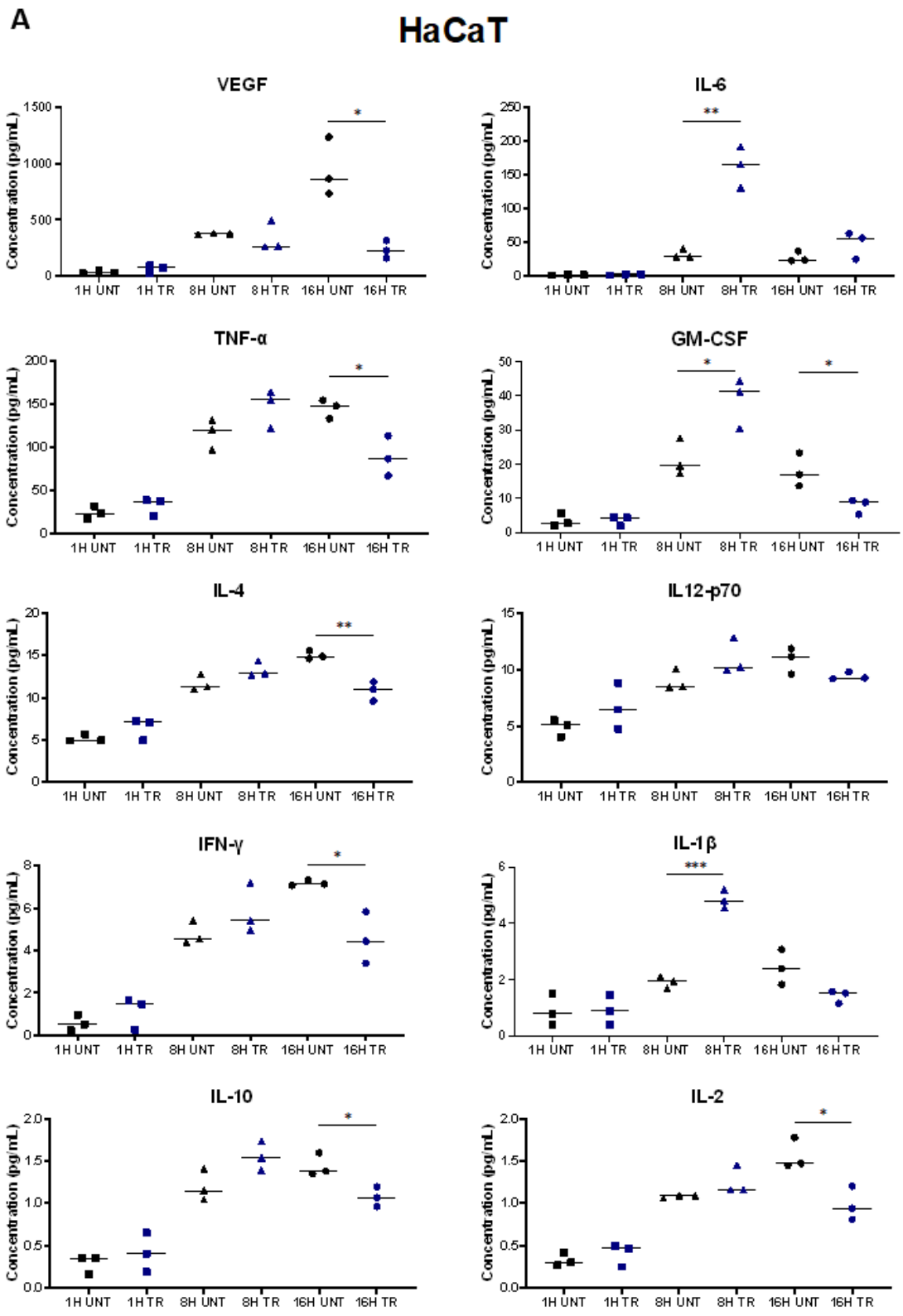
HaCaT
VEGF
IL-6
TNF-α
GM-CSF
IL-4
IL12-p70
IFN-γ
IL-1β
IL-10
IL-2
Concentration (pg/mL)
1H UNT
1H TR
8H UNT
8H TR
16H UNT
16H TR

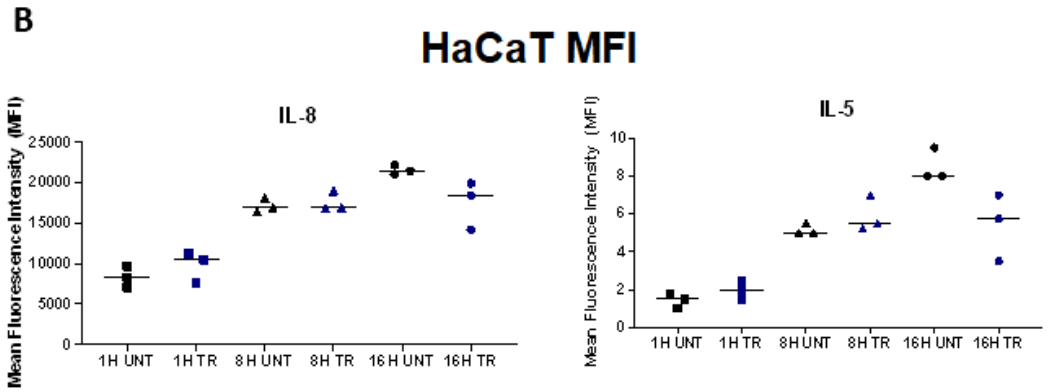

Figure 3.14: Cytokines secreted from HaCaT tissues following microwave treatment. (A) Luminex analysis of cytokine concentrations (pg/ml) secreted from 'mini' HaCaT tissues at 1H, 8H or 16H following mock or microwave treatment. (B) The Mean Fluorescence Intensity (MFI) is plotted for any cytokines where the signal fell outside the standard curve and the concentration could not be accurately calculated. Each dot represents one biological replicate (n=3) and each biological replicate was run in duplicate. An unpaired t-test was used to determine if there was a statistical difference in the means between mock and microwave-treated samples at the same time point. * Indicates $p< 0.05$, ** indicates $p< 0.01$ and *** indicates $p< 0.001$

A

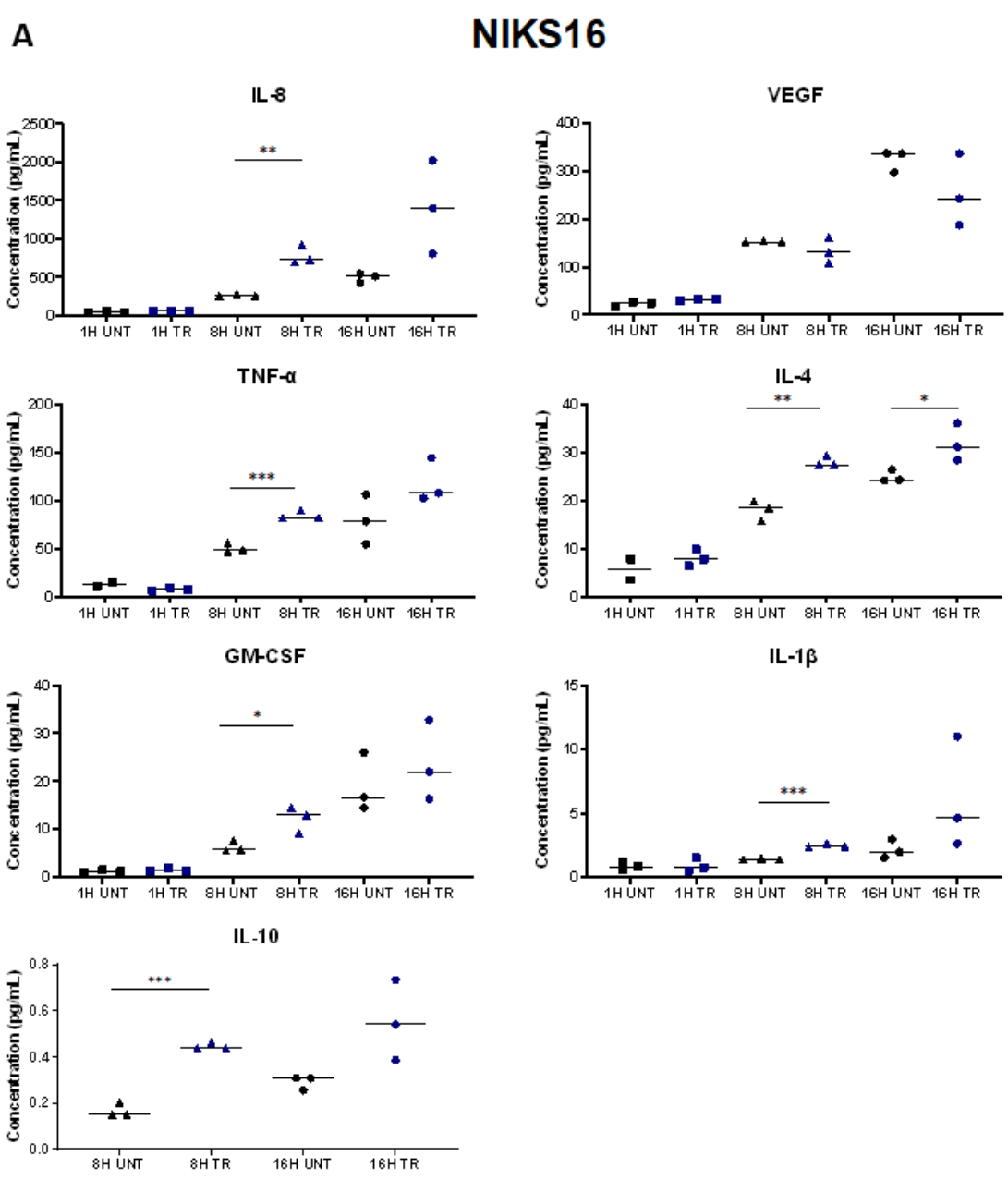
NIKS16
IL-8
VEGF
TNF-α
IL-4
GM-CSF
IL-1β
IL-10
Concentration (pg/mL)
1H UNT
1H TR
8H UNT
8H TR
16H UNT
16H TR

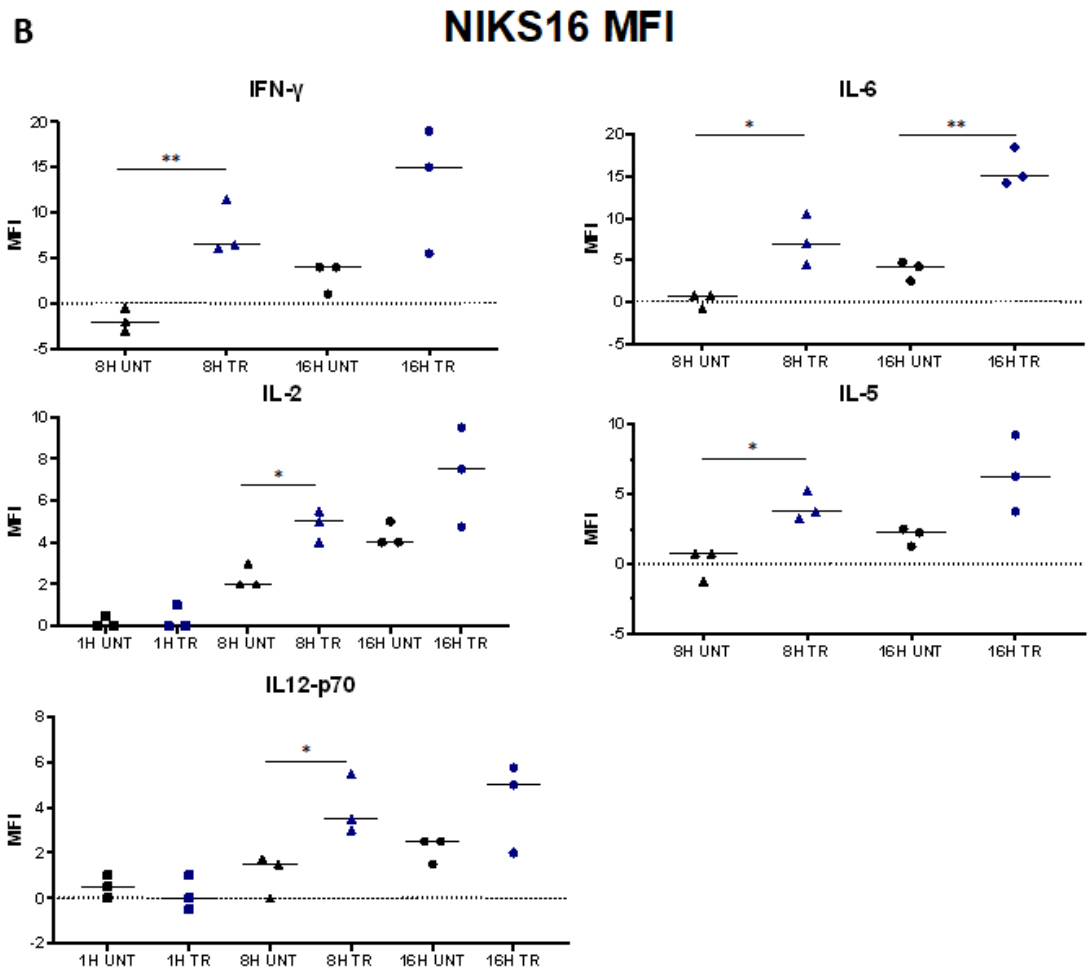

Figure 3.15: Cytokines secreted from NIKS16 tissues following microwave treatment. (A) Luminex analysis of cytokine concentrations (pg/ml) secreted from 'mini' NIKS16 tissues at 1H, 8H or 16H following mock or microwave treatment. (B) The Mean Fluorescence Intensity (MFI) is plotted for any cytokines where the signal fell outside the standard curve and the concentration could not be accurately calculated. Each dot represents one biological replicate (n=3) and each biological replicate was run in duplicate. An unpaired t-test was used to determine if there was a statistical difference in the means between mock and microwave-treated samples at the same time point. * Indicates $p< 0.05$, ** indicates $p< 0.01$ and *** indicates $p< 0.001$

W12E

A

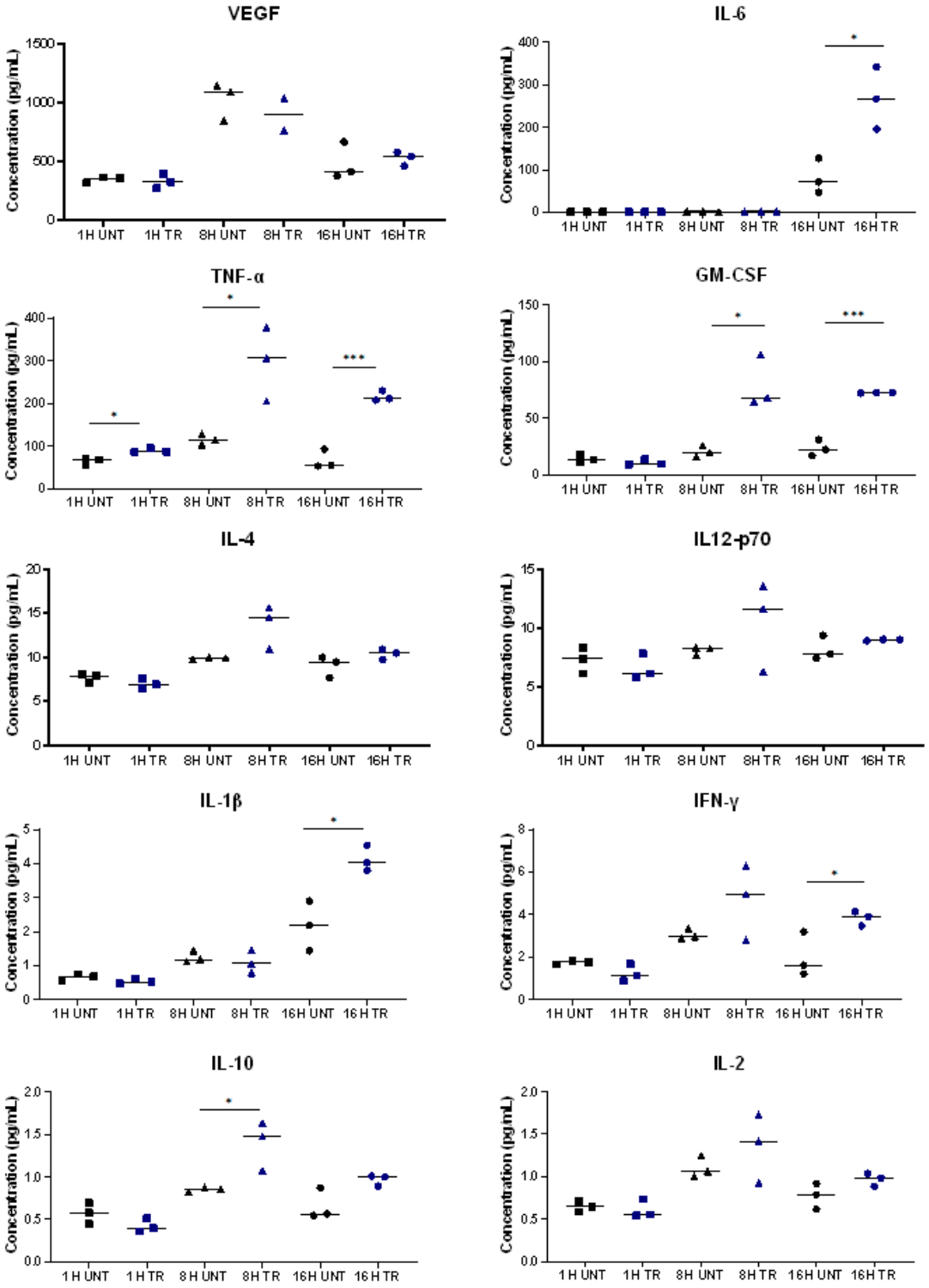
VEGF
IL-6
TNF-α
GM-CSF
IL-4
IL12-p70
IL-1β
IFN-γ
IL-10
IL-2
Concentration (pg/mL)
1H UNT
1H TR
8H UNT
8H TR
16H UNT
16H TR

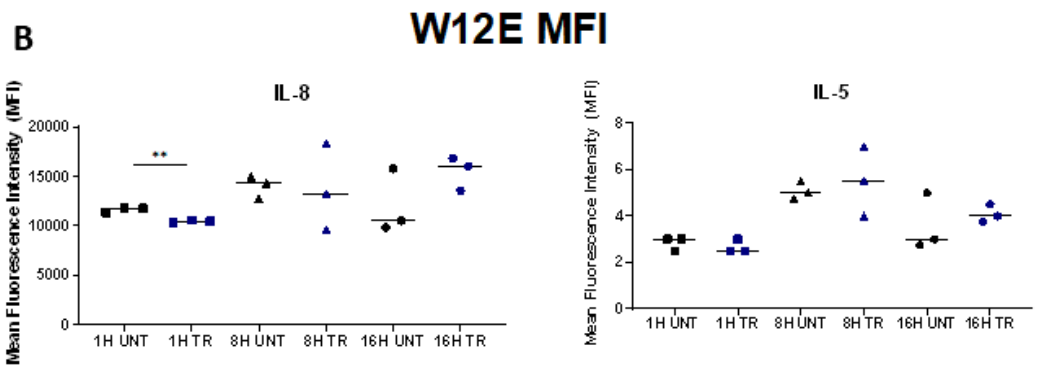

Figure 3.16: Cytokines secreted from W12E tissues following microwave treatment. (A) Luminex analysis of cytokine concentrations (pg/ml) secreted from 'mini' W12E tissues at 1H, 8H or 16H following mock or microwave treatment. (B) The Mean Fluorescence Intensity (MFI) is plotted for any cytokines where the signal fell outside the standard curve and the concentration could not be accurately calculated. Each dot represents one biological replicate (n=3) and each biological replicate was run in duplicate. An unpaired t-test was used to determine if there was a statistical difference in the means between mock and microwave-treated samples at the same time point. * Indicates $p < 0.05$, ** indicates $p < 0.01$.

3.8 An investigation into the activation of dendritic cells by media from mock- or microwave-treated keratinocytes

We wished to investigate if our observations of an increase in innate immunity in keratinocytes following microwave treatment could induce adaptive immunity. Dendritic cells are the most powerful APC and act as messengers between innate and adaptive immunity (Zanna *et al.*, 2021). The media from microwave-treated keratinocytes grown in 2D has previously been observed to induce moDC activation (Bristow *et al.*, 2017). We exposed moDCs to media from mock or microwave-treated keratinocyte raft cultures for 24 hours and then analysed CD40, CD80 and CD86 expression. Media from microwave-treated keratinocytes resulted in moDC activation with enhanced expression of CD40 and CD80 (Figure 3.17). The media from microwave-treated keratinocyte tissues also increased CD86 expression in comparison to moDCs grown in complete media. However, the media from mock-treated tissues increased CD86 expression to a greater extent in comparison to media from microwave-treated tissues (Figure 3.17).

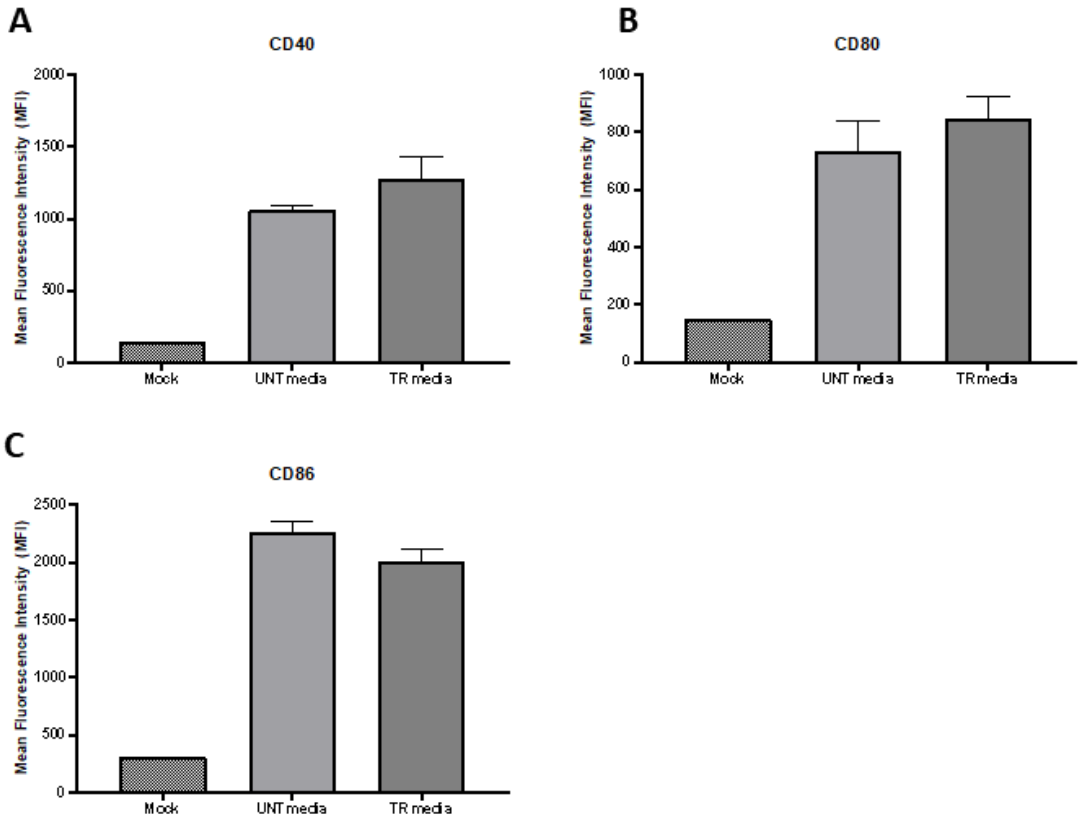

Figure 3.17: Activation of dendritic cells with the media from mock or microwave-treated keratinocytes. Flow cytometric analysis of CD40 (A), CD80 (B) and CD86 (C) expression on viable monocyte-derived dendritic cells (moDCs) exposed to media from mock (UNT media) or microwave-treated (TR media) W12E tissue samples, or moDCs kept in complete media (mock). W12E organotypic raft cultures were mock or microwave-treated and rested in culture on transwells for 16 hours. The media was collected and transferred to moDCs. MoDCs were incubated in the media for 24 hours before harvesting for analysis. Data representative of the treatment of moDCs with media from three biological replicates of W12E tissues which were analysed by flow cytometry in triplicate.

3.9 Discussion

We optimised the thermal dose delivered through the Swift® microwave device to 3D organotypic raft cultures. This ensured temperature increases were consistent with that applied *in vivo,* with our chosen treatment energy of 100 J resulting in heating to 45 – 48 °C (Bristow *et al.*, 2017). This energy dose is within the range of that used within the clinic, with routine energies of 80 – 100 J per treated lesion (personal communications with Emblation Ltd.). A rapid and transient temperature increase was recorded within the raft tissue. Increases to fever temperatures were spatially localised directly under the probe contact site and we confirmed that these large temperature increases (8 – 11 ^{o}C) did not spread out into the distal areas of the tissue, as expected due to the linearity of microwaves. Heating to 4 ^{o}C over basal temperatures has been shown to produce a heat shock response in mammals (Feder and Hofmann, 1999; Ray, 1999). HSP70 plays a key role in this response, binding to and stabilising proteins against denaturation or aggregation (Mayer and Bukau, 2005). Our analysis by RT-qPCR revealed a rapid induction of HSP70 following microwave treatment which peaked at 4 hours in both HPV-positive and HPV-negative tissues. This peak was much greater in magnitude within HPV-positive tissues compared to HPV-negative. Moreover, whilst this increase was transient in all tissues, it was lost earlier in HPV-negative tissues. The short-lived nature of the response demonstrates the self-limiting cycle of heat shock; as HSP70 levels rise within cells, they bind back to HSF1, preventing its transcriptional activity (Santoro, 2000). This increase was observed in tissues that contain only the treated and proximal areas. Since we observe cell death at the site of treatment, we suggest that this transcriptional response is taking place within the proximal tissue. Some evidence for this comes from our previously published work where IHC staining revealed the majority of HSP70 upregulation within the proximal tissue. Only low levels of HSP70 were detected in areas distal to microwave treatment, confirming the linearity of microwave treatment and demonstrating a localised heat shock response (Conley *et al.*, 2023).

RNA Sequencing analysis provided further evidence for hyperthermia taking place within microwave-treated NIKS16 tissues, with many HSF1-driven genes peaking in expression at 4 hours and remaining upregulated 16 hours post-treatment. This trend followed that observed by RT-qPCR for HSP70 mRNA. One limitation of this analysis is

the high degree of variation observed in transcriptomes at 16 hours post-treatment. This limits the confidence in the results of the downstream analysis from this sample group but the trends will be discussed.

The transcriptional landscape of microwave-treated keratinocytes corresponded well with previous transcriptomic studies that delivered hyperthermia with other methods (Yonezawa and Bono, 2023; Scutigliani *et al.*, 2022). This suggests that although microwave-driven temperature changes have a shorter duration than a lot of the studies included within the meta-analysis and the mechanism of heating is different, the overarching cellular response is similar. Therefore, the temperature reached within cells undergoing hyperthermia may be the most important factor that determines the cellular response rather than the method of heating. Protein folding was predicted to be the most upregulated and second most upregulated term at 4 and 16 hours respectively from our GSEA, with many chaperones upregulated in expression that bind to misfolded proteins following heat stress (Lang *et al.*, 2022). This term was also the most upregulated in a meta-analysis of human and mouse transcriptomes following hyperthermia (Yonezawa and Bono, 2023). There was a large degree of overlap between the upregulated genes at 4 and 16 hours, representing conserved pathways upregulated in response to heat shock. Moreover, some pathways appeared to respond later, with oxidative phosphorylation and keratinocyte differentiation pathways only enriched at 16 hours. Very few genes were significantly downregulated following microwave treatment, with only three at 4 hours and none at 16 hours post-treatment. We propose that the downregulation of genes following microwave-delivered hyperthermia may therefore be more random with no clear molecular functions or pathways targeted, in stark contrast to those upregulated. Previous studies on hyperthermia have identified a greater number of significantly downregulated genes, however, they have had few shared pathways or protein interactions (Yonezawa and Bono, 2023). Post-transcriptional pathways such as ubiquitination may therefore be more important to downregulate the expression of proteins following heat shock. This may explain why we observed fewer genes significantly decreased at the transcriptional level.

Innate immunity was stimulated by microwave treatment in HPV-negative and HPV-positive tissues. Pathway analysis of differentially expressed genes from NIKS16 tissues revealed cytokine signalling and other innate immune pathways to be enriched and many upregulated genes were determined to be regulated by NF-κB, a principal component of immune signalling. Following its induction, NF-κB drives the expression of pro-inflammatory genes, including cytokines and chemokines, and regulates the activation and differentiation of T cells (Liu *et al.*, 2017). Subunits of NF-κB have previously been observed to be negatively regulated by HPV infection (Klymenko *et al.*, 2017) so it appears this HPV-mediated regulation of immunity is overcome by microwave-delivered hyperthermia. HPV16 E6 has previously been shown to repress IFN-κ transcription through promoter methylation (Rincon-Orozco *et al.*, 2009). Again, this negative regulation by HPV appears to be overcome by microwave treatment with a 5- and 3.5-fold increase in IFN-κ at 4 hours and 16 hours respectively following treatment. Alongside NF-κB, the AP-1 transcription factor subunits were predicted to be upregulated in activity following microwave treatment. These represent two major transcription factors induced by stress which regulate diverse cellular responses including inflammation and immunity (Duman, Adams and Simen, 2005; Karin, Liu and Zandi, 1997).

Following observations of increased transcription of innate immune genes post-microwave treatment by RNASeq, we sought to verify these findings at the transcriptional level and determine if downstream cytokine concentrations could also be increased. The mRNA expression of TNFα, IL-1β and IL-6 in HaCaT, NIKS16 and W12E tissues increased following microwave treatment. This correlated with an increase in the cytokine concentration of these and other cytokines secreted from microwave-treated rafts. We hypothesise that the increase in cytokine concentration secreted from mock-treated tissues is due to the accumulation of cytokines in the media (as media was changed at the time of mock/treatment) and due to evaporation of the media at later time points causing the concentration to increase. Nevertheless, the concentration of many cytokines secreted from treated rafts was significantly greater than from mock-treated tissues. Immune activation was short-lived in HPV-negative tissues, with mRNA and protein levels returning to mock-treated tissue levels at 16 hours. Within HPV-negative HaCaT tissues, an IL-6 dominant response was

observed, concordant with previous reports of immune activation following microwave treatment in 2D HaCaT cells (Bristow *et al.*, 2017). IL-6 had the highest fold change in mRNA of the three cytokines analysed in HPV-positive tissues but when analysing cytokine concentrations, GM-CSF and IL-1β were observed to increase the most in W12E and NIKS16 tissues respectively. The response in HPV-positive tissues had a longer duration, with many cytokines still increased in concentration compared to mock-treated tissues by 16 hours post-treatment. It is unclear whether HPV's negative regulation on immunity is lost following hyperthermia or if the upregulation of immune pathways by hyperthermia overcomes this regulation. Either way, the increased duration of the response in HPV-positive tissues could represent a system in which once immunity is activated, it is positively reinforced by the detection of viral infection. One limitation of our analysis is the use of HaCaT as an HPV-negative control. NIKS cells would represent a more biologically meaningful HPV-negative control as they have an isogenic background to NIKS16, which would allow a direct comparison of the effect of HPV-positivity (Flores *et al.*, 1999). Difficulties in growing NIKS in 3D cultures prevented including these cells as an HPV-negative control for this study.

There is a dynamic and ever-shifting balance between pro- and anti-inflammatory cytokines in cells that mediates and modulates inflammation (Cicchese *et al.*, 2018). Therefore, it is not unusual that we observed an increase in many pro-inflammatory cytokines (including IL-8, IL-6, IL-1β, TNF-α, GM-CSF, IFN-ɣ) and anti-inflammatory cytokines (including IL-4 and IL-10) following microwave treatment. This has previously been observed in cases of hyperthermia (Heled, Fleischmann and Epstein, 2013). Pro-inflammatory cytokines induced following mild hyperthermia within tumours have been demonstrated to enhance T-cell trafficking (Newton *et al.*, 2018). We observed an upregulation of several Th1 cytokines (including IL-1β, IL-8, IL-2, TNF-α, IFN-ɣ) following microwave treatment. These cytokines are normally downregulated by HPV infection to enable virus persistence (Moody, 2022). In particular, IL-8, which was the cytokine secreted at the highest concentration from microwave-treated tissues, recruits leukocytes to sites of inflammation (Taub *et al.*, 1996). The recruitment of and differentiation of leukocytes into a Th1 response by the actions of these cytokines may enable viral clearance (Konya and Dillner, 2001). This has

important implications for the recurrence of HPV-driven disease following microwave treatment if treatment does not clear the entirety of the viral infection. This could occur from cases of multi-focal disease or through infection remaining in the stem-like reserve cells below the basal layer of the epithelium, proposed to be common sites of recurrence (Reich and Regauer, 2023). An immune response induced by microwave treatment in the neighbouring area to treatment may therefore act to clear any remaining viral infection to prevent persistent forms of recurrence.

To determine if the innate immune response triggered by microwave treatment could protect against disease recurrence, we attempted to analyse if it could be relayed downstream to stimulate adaptive immunity. Dendritic cells act as messengers between the innate and adaptive immune system. Initial experiments indicate that moDCs can be activated by microwave-treated media from W12E tissues with increased expression of CD40 and CD80, which agrees with previous reports (Bristow *et al.*, 2017). This may enable enhanced cross-presentation of HPV proteins to CD8+ T cells as previously observed (Bristow *et al.*, 2017). This has the potential to be aided *in vivo* by heat shock proteins, which are upregulated following microwave treatment and can chaperone viral proteins for cross-presentation via APCs to CD4+ and CD8+ T cells (Hu *et al.*, 2022). Limitations of our analysis include one PBMC donor and one-time point investigated following microwave treatment. The media from mock-treated W12E tissues also activated moDCs. We propose that HPV positivity in mock-treated tissues may be responsible for this greater activation in comparison to previous studies that used HPV-negative cells (Bristow *et al.*, 2017). Additional studies are required to confirm an increase in cross-presentation to CD8+ T cells in cases of HPV infection following microwave treatment.

RNA sequencing revealed an upregulation of keratinocyte differentiation at later time points following microwave treatment. Subsequent RT-qPCRs for the differentiation markers keratin 10 and transglutaminase revealed an increase in transglutaminase expression but not keratin 10 following microwave-delivered hyperthermia (Eckert *et al.*, 2005; Michel *et al.*, 1992; Fuchs and Green, 1980). The increase in transglutaminase, which is more tightly confined to the upper layers of the epithelium than keratin 10 suggests that microwave treatment drives an increase in the terminal

stages of differentiation within the epithelium (Moll, Divo and Langbein, 2008; Chermnykh, Alpeeva and Vorotelyak, 2020). Previous studies have revealed that differentiation of HPV-infected epithelial cells results in increased expression of innate immune genes (Moody, 2022). Therefore, hyperthermia may drive innate immune activation both directly and indirectly. This change in the keratinocyte transcriptome towards a more differentiated phenotype may result in changes to HPV viral gene expression, which is tightly linked to epithelial cell differentiation (Section 1.7).

Overall, microwave treatment resulted in hyperthermia within 3D organotypic raft cultures. The transcriptional landscape of cells exposed to microwave-delivered hyperthermia had increased expression of genes involved in protein folding, mitochondrial metabolism and innate immunity which agrees well with published hyperthermia transcriptomes. A heat shock response was observed in keratinocytes following microwave treatment alongside an increase in differentiation and innate immunity. These changes to the host cell may alter the dynamics of human papillomavirus infection, which is the topic for the next two chapters.

3.10 Supplementary figures:

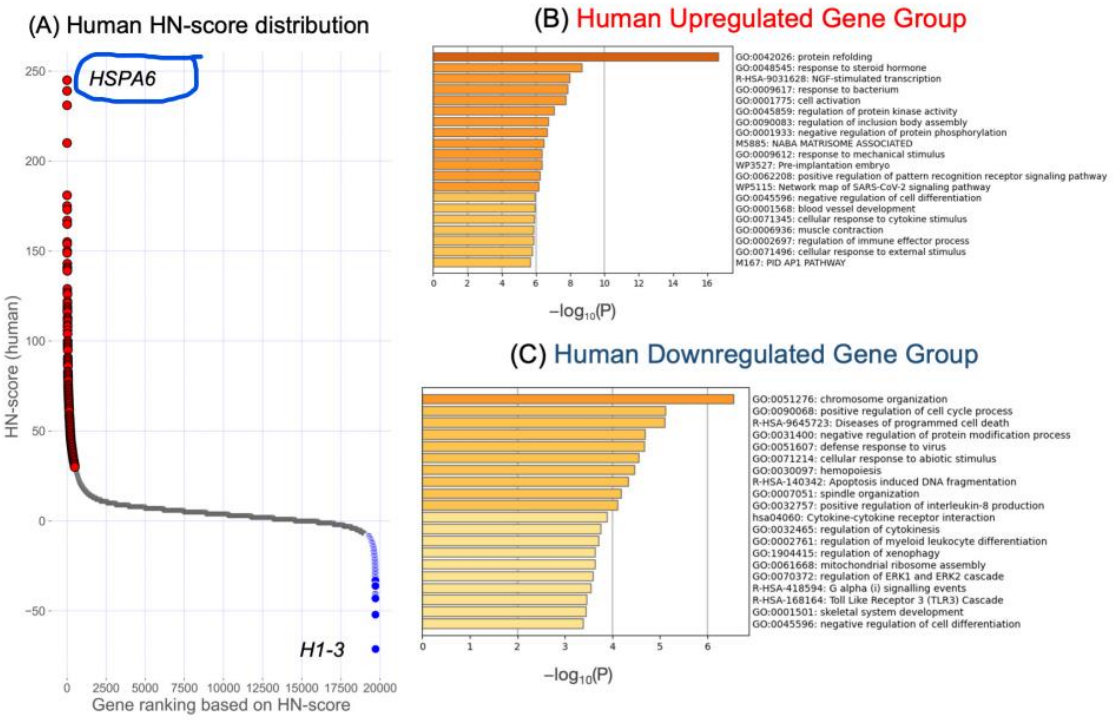

Supplementary Figure 3.1: The results of a meta-analysis of hyperthermia in human cell lines. (A) Scatter plots of HN-scores for all genes included in the meta-analysis. The HN score was determined by calculating the number of times a gene was upregulated across all studies within the meta-analysis minus the number of times a gene was downregulated. Red and blue dots represent the top 500 up- and downregulated genes based on HN-score. Annotations reveal the genes with the highest or lowest HN score. (B & C) Results of gene set enrichment analysis of upregulated genes (B) and downregulated genes (C) in humans. Adapted from Yonezawa et al., 2022.

Chapter 4 An investigation into the effects of microwave treatment on HPV16 gene expression and replication

4.1 Introduction

Papillomaviruses employ multiple strategies to encode the proteins required for the viral life cycle from their compact genome (Section 1.5). HPV16 uses early and late promoters and polyadenylation sites, and complex splicing for the production of the viral proteins (Section 1.5). The expression of the HPV proteins is also spatially coordinated with the differentiation status of the epithelium (Section 1.6, Section 1.7). This spatial coordination enables viral genome amplification and production of the late immunogenic viral proteins to be restricted to the upper epithelial layers, an immune-privileged site, thus preventing immune detection (Stanley, 2012; Westrich, Warren and Pyeon, 2017). There is limited existing work on how hyperthermia may impact HPV transcription and replication. Yang and colleagues have previously demonstrated clearance of hrHPV in individuals with low-grade disease when delivering localised hyperthermia at the cervix (Yang *et al.*, 2021). A temperature of 44 °C delivered for 30 minutes each day for three consecutive days followed by two additional 30-minute treatments resulted in an ~85% clearance rate of detectable hrHPV within 3 months. Oei and colleagues observed E6 degradation and loss of the E6-p53 complex formation within cancer cell lines treated at 42 °C for 1 hour (Oei *et al.*, 2015a). This resulted in an increase in p53 levels and downstream activation of p53-dependent apoptosis and G2 arrest. This study used SiHa and HeLa cells grown in 2D, *in-vivo* tumours of SiHa on the hind legs of athymic mice and *ex-vivo* cervical carcinoma biopsies. Hyperthermia was delivered by submerging cells or the tumour-bearing legs of mice in a water bath (Oei *et al.*, 2015a). Neither of these studies investigated viral gene expression changes following hyperthermia (Yang *et al.*, 2021; Oei *et al.*, 2015a). Since we have observed changes to the keratinocyte transcriptome following microwave-induced hyperthermia (Chapter 3), there may also be relevant changes to viral transcription. Moreover, observations of reduced E6 expression following microwave treatment were in models of cervical cancer, containing integrated copies of HPV16 (Oei *et al.*, 2015a), which prevents a full examination of the viral transcripts and proteins. Therefore, extending these findings to a model of an

earlier disease stage (CIN) that contains episomal copies of HPV16 is important. Episomal HPV genomes may be under different epigenetic control compared to integrated copies and may therefore respond differently to hyperthermia. Finally, conductive heating using a water bath involves heating from the outside in and is applied universally to all cells. Microwave treatment results in dielectric hysteresis to a defined tissue area and heats from the inside out (Section 1.12). It is important to consider any differences this causes to viral replication and consider any effects on the neighbouring tissue of the treatment site, which has implications for disease recurrence in a clinical setting.

To model the impact of microwave treatment on the transcription and replication of HPV16 in different disease stages, we used SiHa, transformed cervical cells containing integrated copies of HPV16, and NIKS16 and W12E, keratinocytes that contain episomal HPV16 genomes that support the productive viral life cycle when grown in 3D and thus represent an earlier disease stage (Section 3.1 for an in-depth introduction). These cell lines were used to investigate the following aims:

- Investigate how microwave treatment impacts HPV gene expression from the early and late promoters.
- Determine where these transcriptional changes are taking place around the site of microwave treatment.
- Assess whether any transcriptional changes are translated to the protein level.
- Investigate changes in viral genome replication following microwave treatment.

4.2 Microwave treatment reduces HPV16 oncoprotein expression in a cervical carcinoma cell line

The hrHPV oncoproteins E6 and E7 act to drive tumour progression through their repressive effects on p53 and Rb respectively (Section 1.6.5). It was important, therefore, to determine if the expression of these oncoproteins was altered following microwave treatment in models of cervical cancer. Initially, total RNA was harvested

from SiHa 'full-sized' rafts (14 mm diameter) and analysed by RT-qPCR. However, distinguishing the effect of treatment on these tissues was difficult as most cells had not been exposed to microwave treatment due to the 6.7 mm contact site of the Swift® microwave probe head (data not shown). We instead used 'mini' 3D organotypic rafts with a diameter of 7 mm, such that the majority of the cells were exposed to microwave treatment (classed as 'treated') or were neighbouring cells (classed as 'proximal') (Section 3.3, Figure 3.3). The level of E6/E7 bicistronic mRNAs within these tissues did not change significantly up to 48 hours following treatment but at 72 hours post-treatment, E6/E7 expression was significantly downregulated ($p<0.05$) (Figure 4.1).

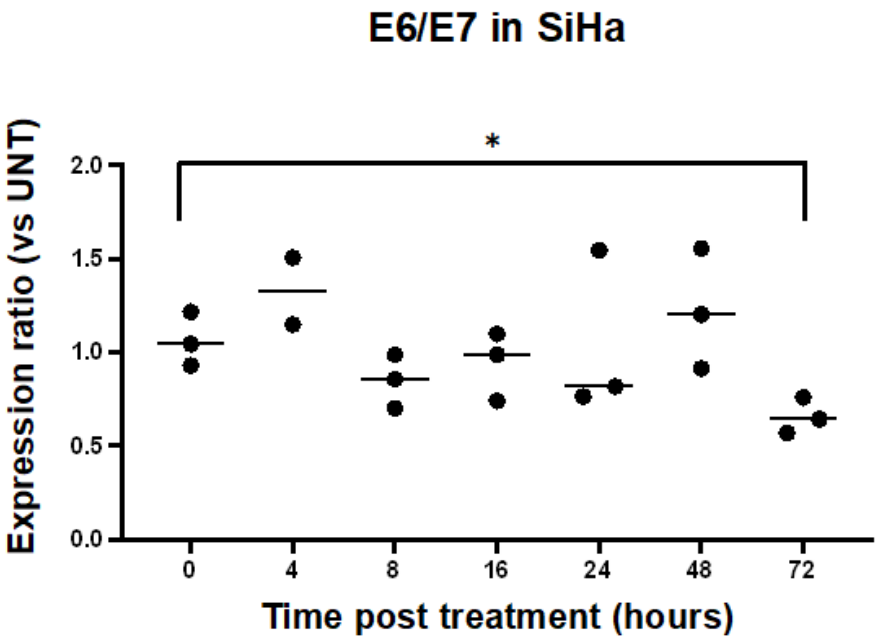

Figure 4.1: Microwave treatment in a model of cervical cancer. Total RNA from 7 mm diameter SiHa tissues was extracted and RT-qPCR was carried out to determine the expression of E6/E7 encoding transcripts. Delta Ct changes were calculated relative to the housekeeping gene Beta-actin and expression ratios of treated to untreated tissues were determined using $2^{-\Delta\Delta CT}$. The median expression ratio for each time point post-treatment is displayed (black line) and each point represents one biological replicate at each time point (n=3). Each biological replicate represents an average of three technical replicates. A Kruskal-Wallis test, which is a non-parametric alternative to the One-way ANOVA, was used to determine if there was a statistical difference between groups. * Indicates $p< 0.05$.

4.3 Microwave treatment of a 3D model of cervical precancerous disease transiently increases HPV16 viral transcription followed by a decrease.

Subsequently, we aimed to investigate how the transcription of HPV16 genes was affected in models of CIN, which is more likely to represent the disease stage where microwave treatment will be used. The expression of early (E6/E7 and E4 containing) viral transcripts was analysed within 'mini' NIKS16 and W12E organotypic rafts. E6 and E7 expression increases and becomes deregulated during disease progression, thus making it important to analyse following microwave treatment (Schiffman *et al.*, 2007) (Section 1.8). Although E4 is a late protein, E4 primers will detect any transcripts with the coding potential for E1^E4 and due to the abundance of early transcripts, the majority of the signal will be derived from viral early genes (Chen *et al.*, 2014) (Figure 1.9). A small increase in the expression of E6/E7 and E4 containing HPV16 mRNA species was observed following microwave treatment in NIKS16 rafts (Figure 4.2A, B, Table 4.1). At 16 hours post-treatment, the expression ratio of both E6/E7 and E4 containing transcripts was ~2 times greater in treated rafts compared to mock-treated rafts (2X and 2.5X respectively), which was statistically significant ($p<0.01$)(Figure 4.2A, B, Table 4.1). This increase in expression of the early transcripts was transient and at 72 hours post-treatment, it had fallen to levels below mock-treated tissues (Figure 4.2A, B, Table 4.1).

To determine changes in late viral gene expression following microwave treatment, we focused on the expression of the transcripts containing the E4^L1 splice product and the L1 ORF. The primer set for E4^L1 detects E4-containing late viral transcripts of HPV16 that use the splice donor site at 3632 and the splice acceptor at 5637 (Transcript 19, Figure 1.10) (Milligan *et al.*, 2007) whilst the primer set for L1 detects all late transcripts of HPV16 (Figure 1.10). An increase in the expression of E4^L1- and L1-containing late HPV16 transcripts following microwave treatment was observed (Figure 4.2C, D). At 16 hours post-treatment, the expression of E4^L1 and L1 containing transcripts was ~3 times and ~8.5 times greater in microwave-treated samples than in mock-treated tissue respectively, which was statistically significant ($p<0.05$, $p<0.01$) (Table 4.1). The increase in E4^L1 expression was temporary and was followed by a substantial although non-significant decrease in expression, to levels

even below those of mock-treated tissue at 72 hours post-treatment (~0.3x) (Figure 4.2C, Table 4.1). Whilst the expression ratio of L1 also decreased over time, at 72 hours post-treatment, the expression in treated NIKS16 tissues was still above that of mock-treated tissue (~1.5 fold change), although this was not statistically significant (Figure 4.2D, Table 4.1).

We repeated our analysis of early and late viral transcription following microwave treatment in W12E tissues from 0 to 24 hours post-treatment (Figure 4.3). The observed trend for the viral early genes was similar to that in NIKS16 with a small transient rise (Figure 4.3A, B). However, unlike in NIKS16 tissues, this increase was not significant for any time point analysed in W12E tissues (Figure 4.3A, B, Table 4.2). The fold change in expression was also lower within W12E tissues compared to NIKS16 with the greatest average fold change in both E6/E7 and E4 at 1.5 times that of mock tissues (Table 4.2). In agreement with our results in NIKS16, the late viral transcripts showed a larger fold change in expression compared to early transcripts (Figure 4.3C, D). At 8 hours post-treatment, the expression of E4^L1 and L1 containing transcripts was ~3.5 and ~3 times greater than mock-treated tissue respectively which was statistically significant ($p<0.05$) (Table 4.2). Whilst E4^L1 and L1 levels remained high in NIKS16 tissues until 48 hours post-treatment, the expression of these transcripts within W12E tissues was approaching that of untreated tissues by 24 hours post-treatment (Figure 4.3C, D, Table 4.2).

The data indicate that the expression of HPV16 early and late transcripts in 3D models of cervical precancerous disease transiently increases following microwave treatment before falling to levels of or below that of untreated tissues at later time points. The increase in expression was greater in magnitude for the viral late transcripts.

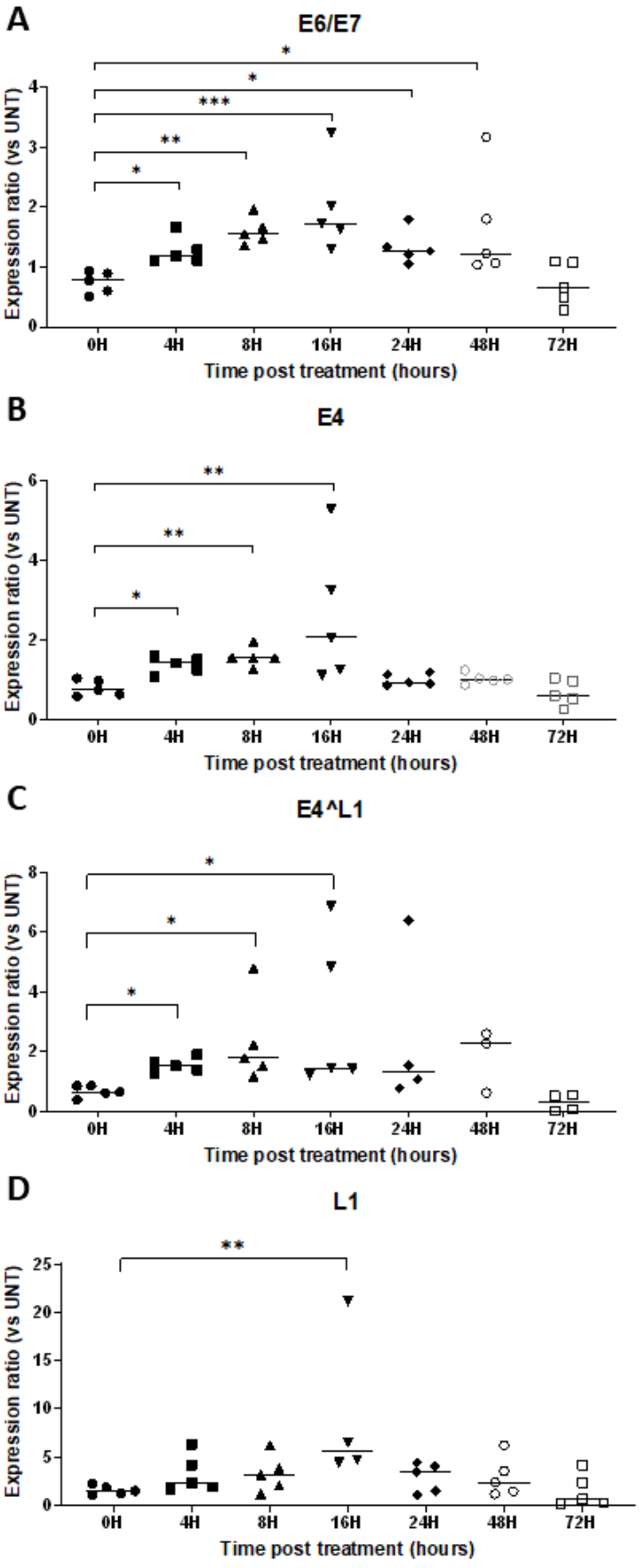

Figure 4.2: HPV16 gene expression in NIKS16 'mini' rafts at 0 – 72 hours following treatment. (A-B) HPV16 early gene expression following microwave treatment was

analysed by RT-qPCR to compare the expression of E6/E7 bicistronic transcripts and E4 containing transcripts in microwave-treated rafts compared to mock-treated. (C-D) HPV16 late gene expression following microwave treatment was analysed by RT-qPCR to compare the expression of spliced E4^L1 containing transcripts and L1 containing transcripts in microwave-treated rafts compared to mock-treated. (A-D) Delta Ct changes were calculated relative to the housekeeping gene Beta-actin and expression ratios of treated to mock tissues were determined using $2^{-\Delta\Delta CT}$. The median expression ratio is displayed (black line) for each time point post-treatment and each point represents one biological replicate (n=5, except E4^L1 24H (n=4), 48H (n=3) and 72H (n=4) where missing samples had < 2 technical replicates with detectable transcripts and L1 16H where one outlier was removed (n=4)). Each biological replicate represents an average of three technical replicates. A Kruskal-Wallis test was used to determine if there was a statistical difference between groups. * Indicates p< 0.05, ** indicates p< 0.01 and *** indicates p< 0.001.

Table 4.1: Average change in expression of the HPV16 transcripts analysed in NIKS16 tissues following microwave treatment. The table shows the mean fold change (FC) and standard deviation (SD) for each gene from Figure 4.3 at different time points post-treatment (H.P.T = hours post-treatment). The p-value results from Kruskal-Wallis statistical testing are shown to 2 significant figures (black, green and red text indicates non-significant, p<0.05, and p<0.01 respectively).

E6/E7

H.P.T	Mean FC	SD	p value
0	0.74	0.18	N/A
4	1.27	0.23	0.045
8	1.60	0.23	0.0015
16	1.99	0.75	0.00034
24	1.33	0.28	0.031
48	1.66	0.90	0.021
72	0.72	0.36	0.88

E4

H.p.t	Mean FC	SD	P value
0	0.79	0.20	N/A
4	1.36	0.21	0.011
8	1.57	0.24	0.0018
16	2.58	1.73	0.0016
24	1.00	0.15	0.46
48	1.02	0.13	0.37
72	0.67	0.33	0.78

E4^L1

H.P.T	Mean FC	SD	p value
0	0.67	0.20	N/A
4	1.54	0.24	0.044
8	2.30	0.14	0.012
16	3.16	2.56	0.014
24	2.44	2.65	0.096
48	1.83	1.06	0.062
72	0.29	0.29	0.45

L1

H.P.T	Mean FC	SD	p value
0	1.54	0.49	N/A
4	3.25	1.97	0.12
8	3.24	1.93	0.18
16	9.18	8.05	0.0023
24	2.85	1.54	0.25
48	2.91	2.05	0.25
72	1.47	1.74	0.92

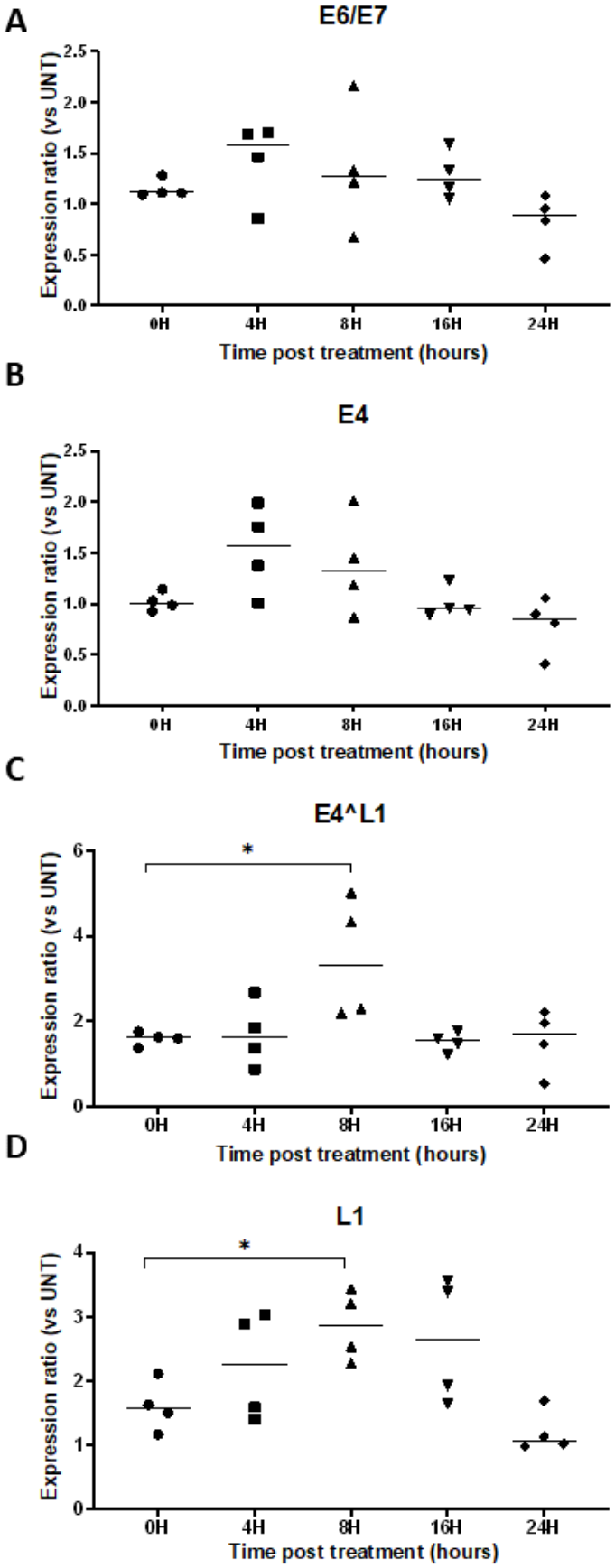

Figure 4.3: HPV16 gene expression in W12E 'mini' rafts at 0 – 24 hours following treatment. (A-B) HPV16 early gene expression following microwave treatment was analysed by RT-qPCR to compare the expression of E6/E7 bicistronic transcripts and

E4 containing transcripts in microwave-treated rafts compared to mock-treated. (C-D) HPV16 late gene expression following microwave treatment was analysed by RT-qPCR to compare the expression of spliced E4^L1 containing transcripts and L1 containing transcripts in microwave-treated W12E rafts compared to mock-treated. (A-D) Delta Ct changes were calculated relative to the housekeeping gene Beta-actin and expression ratios of treated to untreated tissues were determined using $2^{-\Delta\Delta CT}$. The median expression ratio is displayed (black line) and each point represents one biological replicate at each time point (n=4). Each biological replicate represents an average of three technical replicates. A Kruskal-Wallis test was used to determine if there was a statistical difference between groups. * Indicates $p < 0.05$.

Table 4.2: Average change in expression of the HPV16 transcripts analysed in W12E tissues following microwave treatment. The table shows the mean fold change (FC) and standard deviation (SD) for each gene from Figure 4.4 at different time points post-treatment (H.P.T = hours post-treatment). The p-value results from Kruskal-Wallis statistical testing are shown to 2 significant figures (black text indicates non-significant, green indicates $p<0.05$).

E6/E7

H.P.T	Mean FC	SD	p value
0	1.15	0.09	N/A
4	1.43	0.40	0.31
8	1.35	0.61	0.59
16	1.28	0.23	0.63
24	0.83	0.27	0.15

E4

H.P.T	Mean FC	SD	p value
0	1.02	0.09	N/A
4	1.53	0.43	0.15
8	1.38	0.48	0.37
16	1.00	0.15	0.77
24	0.79	0.28	0.26

E4^L1

H.P.T	Mean FC	SD	p value
0	1.59	0.16	N/A
4	1.69	0.76	0.77
8	3.46	1.43	0.023
16	1.52	0.23	0.90
24	1.55	0.74	0.81

L1

H.P.T	Mean FC	SD	p value
0	1.60	0.39	N/A
4	2.23	0.86	0.44
8	2.87	0.55	0.049
16	2.63	0.99	0.094
24	1.20	0.33	0.40

4.4 Employing RNAScope as an In Situ Hybridisation (ISH) approach to determine how the expression of the viral transcripts is spatially altered following microwave treatment.

4.4.1 Training and optimisation of the HALO® ISH module for RNAScope analysis

We aimed to determine the spatial localisation of changes to viral transcript expression relative to the site of treatment. We performed dual RNAScope, an RNA in situ hybridisation (ISH) technique that allows the visualisation of mRNAs within tissue sections, with probes specific for E6/E7 and L1 transcripts (Wang *et al.*, 2012). In SiHa tissues, only E6/E7 staining (brown) was visualised, as expected due to the integration of the viral genome preventing the expression of the late viral transcripts (Figure 4.4A). We employed HALO®, a digital pathology image analysis platform, to quantify the RNAScope staining. Modification of the HALO® ISH module allowed accurate identification of E6/E7. The contrast threshold was adjusted using the 'Real Time tuning window' so that only E6/E7 staining was detected; the green dots in the middle row of Figure 4.4A. Nuclei were segmented using the HALO® Nuclear Segmentation AI module to enable transcript quantification within the cell nucleus or cytoplasm (Figure 4.4A, bottom row). Cells could be scored based on the number of transcripts they contained (Table 4.3). In some cases, the E6/E7 stain appeared as larger dots (Figure 4.5). This might result from two transcripts being in close proximity and due to the amplification step in RNAScope, chromogen binding may end up being concentrated into one spot. To address these areas, we set the maximum 'spot size' within the HALO® ISH program to the size of the smaller, individual mRNA dots. Any particles larger than this were then segmented into multiple spots, with the same diameter as individual mRNA dots, and then scored as multiple mRNAs. Since this method introduces a degree of variability, we cannot be accurate on the number of transcripts per cell and therefore, the expression relative to mock-treated tissues was used for analysis.

In NIKS16 tissues, both E6/E7 staining (brown) and L1 staining (pink) were observed (Figure 4.4B, top row). We modified the parameters of the HALO ISH module to enable detection of each stain with minimal crosstalk between the stains. This helped to

prevent any false positivity that derived from the detection of E6/E7 staining in the L1 channel (Figure 4.4B, middle row). The overlaid result shows cells of different colours depending on the presence of one or both stains at different concentrations. (Figure 4.4B, lower row). The software mistakenly identified the cornified cells in NIKS16 and W12E tissues (light brown) as the chromogen for E6/E7 (brown) (data not shown). Therefore, this layer was excluded from analysis for all tissues.

In NIKS16 tissues, E6/E7 staining was restricted to the lower layers of the raft (Figure 4.4B), demonstrating the spatial regulation of the viral early genes to the basal and suprabasal cells of the tissue. L1 staining was sparse in comparison to E6/E7 staining with only a few cells within the tissue positive for L1 and these cells contained few L1 transcripts. The restriction of E6/E7 staining and the rarity of L1 staining left many cells within the mid-layers unstained (Figure 4.4B). The majority of L1 staining was observed within the upper layers of NIKS16 rafts. Rarely, L1 was observed within the basal cells but in these locations, it was always within the nucleus. These basal transcripts probably represent pre-mRNA L1 transcripts that lack a polyA tail, previously observed to be present within undifferentiated cells (Milligan *et al.*, 2007). Throughout the entire tissue, nuclear L1 staining was predominant (63% average +/- 2%). In contrast to the tight regulation of E6/E7 transcripts to the lower layers of NIKS16 rafts, E6/E7 transcripts were ubiquitously distributed throughout the tissue in SiHa rafts, signifying the loss of early gene spatial regulation following the transformation of these cells (Figure 4.4A). Transcripts were evenly distributed between the nucleus and cytoplasm with 55% of transcripts in the cytoplasm on average and 45% in the nucleus.

Table 4.3: Cell scoring using HALO®. Cells were scored in categories 0 – 4 depending on the detected number of transcripts per cell.

Scored phenotype	Number of transcripts detected in cell
0+	0
1+	1 < x < 4
2+	4 < x < 10
3+	10 < x < 16
4+	> 16

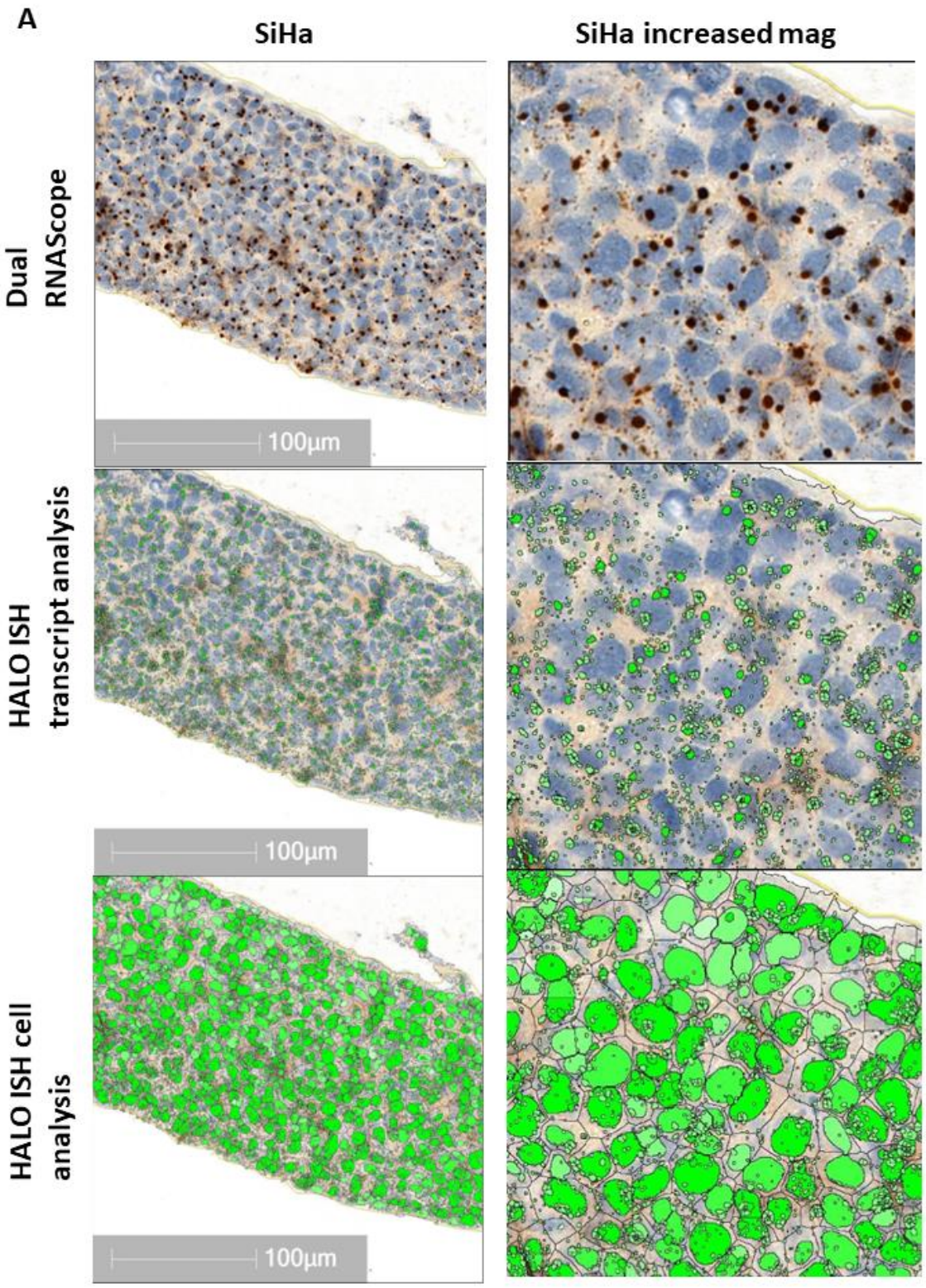
A
SiHa
SiHa increased mag
Dual RNAScope
HALO ISH transcript analysis
HALO ISH cell analysis
100µm
100µm
100µm

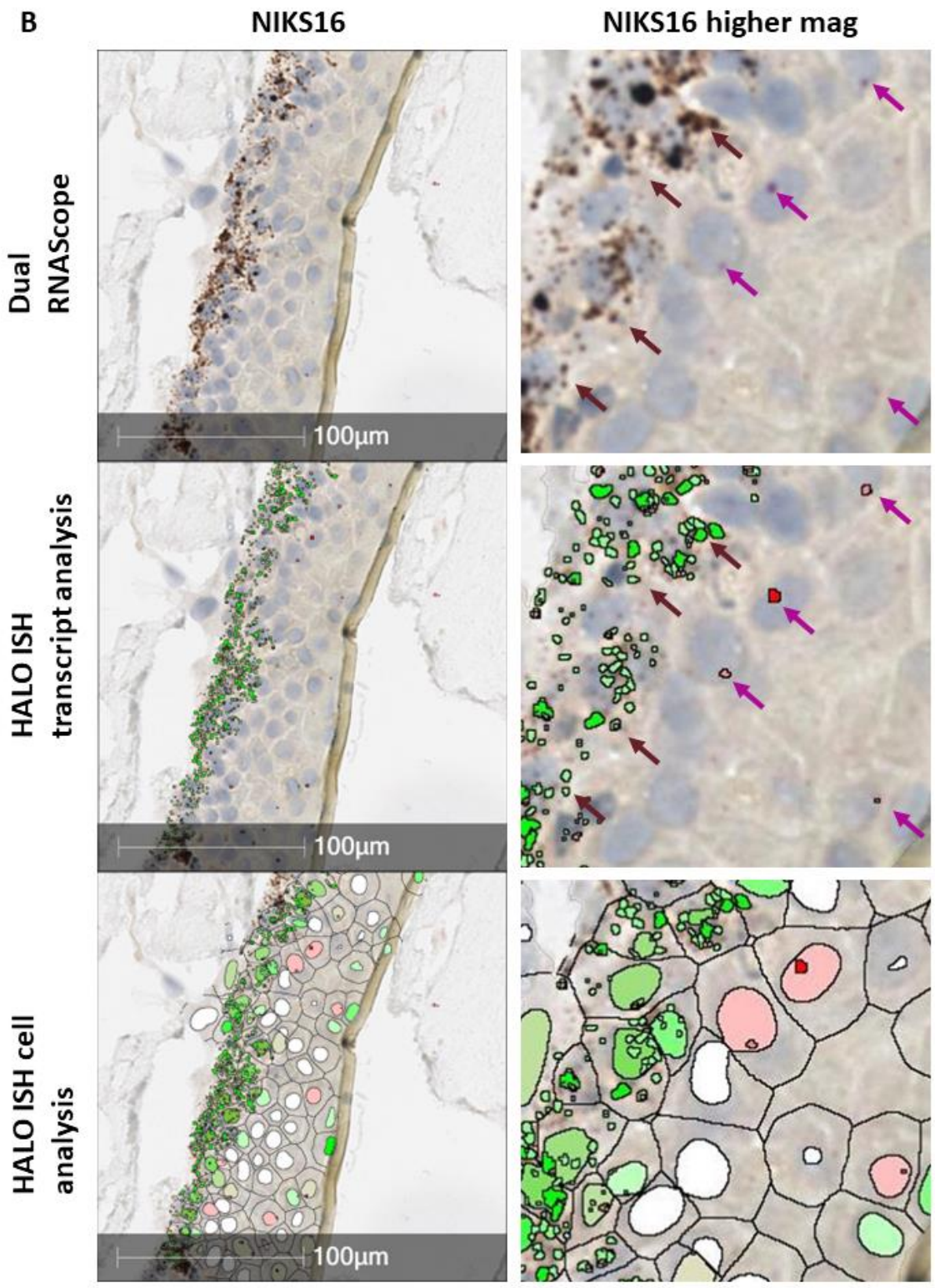

Figure 4.4: Optimisation of the HALO ISH module for RNAScope analysis. (A & B) Dual RNAScope for E6/E7 (brown) and L1 (pink) mRNAs in SiHa (A) and NIKS16 (B) tissues. The right panel provides zoomed-in images of the left panel to allow for identification of the staining and in NIKS16 tissues, brown and purple arrows indicate E6/E7 and L1 staining respectively. The top row shows scanned tissues following staining. The second row includes an overlay showing transcripts identified by our

optimised HALO ISH module with green dots representing detected E6/E7 mRNAs and pink representing L1 mRNA. The bottom row shows the overlaid analysis including cell identification. Cells are coloured based on the detection of one or both stains at different concentrations. White cells had no detectable transcripts, green had only E6/E7 transcripts and pink L1. Brown cells were positive for both E6/E7 and L1 staining. Different shades of each colour indicate the relative concentration of transcripts per cell (with darker colours indicating more detected transcripts).

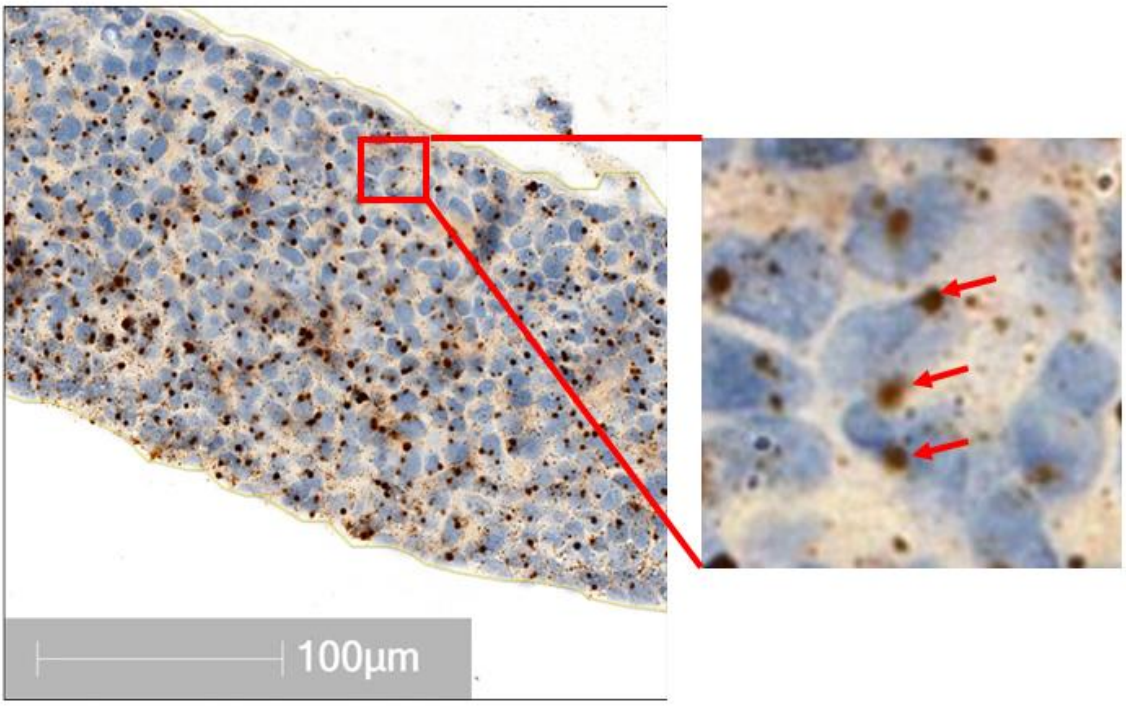

Figure 4.5: The variation in spot size by RNAScope. SiHa mock-treated tissue with E6/E7 mRNAs stained brown. Some chromogen staining is present as small dots, which are likely individual mRNA molecules whilst others appear as larger dots (red arrows). This was also observed within NIKS16 tissues for E6/E7 staining but not L1.

4.4.2 RNAScope reveals a spatially localised decrease in E6/E7 expression within treated SiHa rafts.

We used 'full-sized' 14 mm diameter tissues for RNAScope since we could identify the treated, proximal and distal areas by examination of the tissue structures and previously determined lengths of each area (Section 3.3) (Conley *et al.*, 2023). This allowed the inclusion of sites distant from the site of treatment in our analysis, which were not present within our RT-qPCR analysis of mini rafts that only included the treated and proximal areas. E6/E7 RNA expression across entire SiHa tissues decreased slightly following treatment at 16 and 48 hours post-treatment (Figure 4.6A, B). Subsequently, tissues were annotated to differentiate transcript expression in the treated, proximal and distal areas of the raft. E6/E7 expression was reduced within the treated areas at all time points post-treatment compared to the proximal and distal zones (Figure 4.6D). Moreover, later time points showed a reduction in expression of E6/E7 in the proximal and distal zones in comparison to the same areas 0 hours post-treatment (Figure 4.6D). The statistical power for determining these results' significance is limited by only two biological replicates. Some thinning of the tissue within the proximal zone is evident at later time points which is commonly observed due to tissue disruption taking place at these sites (Figure 4.6A) (Conley *et al.*, 2023). Cells were scored based on the concentration of E6/E7 staining in each cell (Table 4.3). At 16 and 48 hours post-treatment, the percentage of cells containing no, or less than four E6/E7 transcripts (categories 0+ and 1+ respectively) had increased in comparison to mock-treated tissues (Figure 4.6C, Table 4.3). Overall, RNAScope revealed a small decrease in E6/E7 RNA in SiHa rafts 16 and 48 hours post microwave treatment. This decrease appears to be in a spatially localised manner, with fewer transcripts in cells at the treated and proximal relative to distal sites.

A

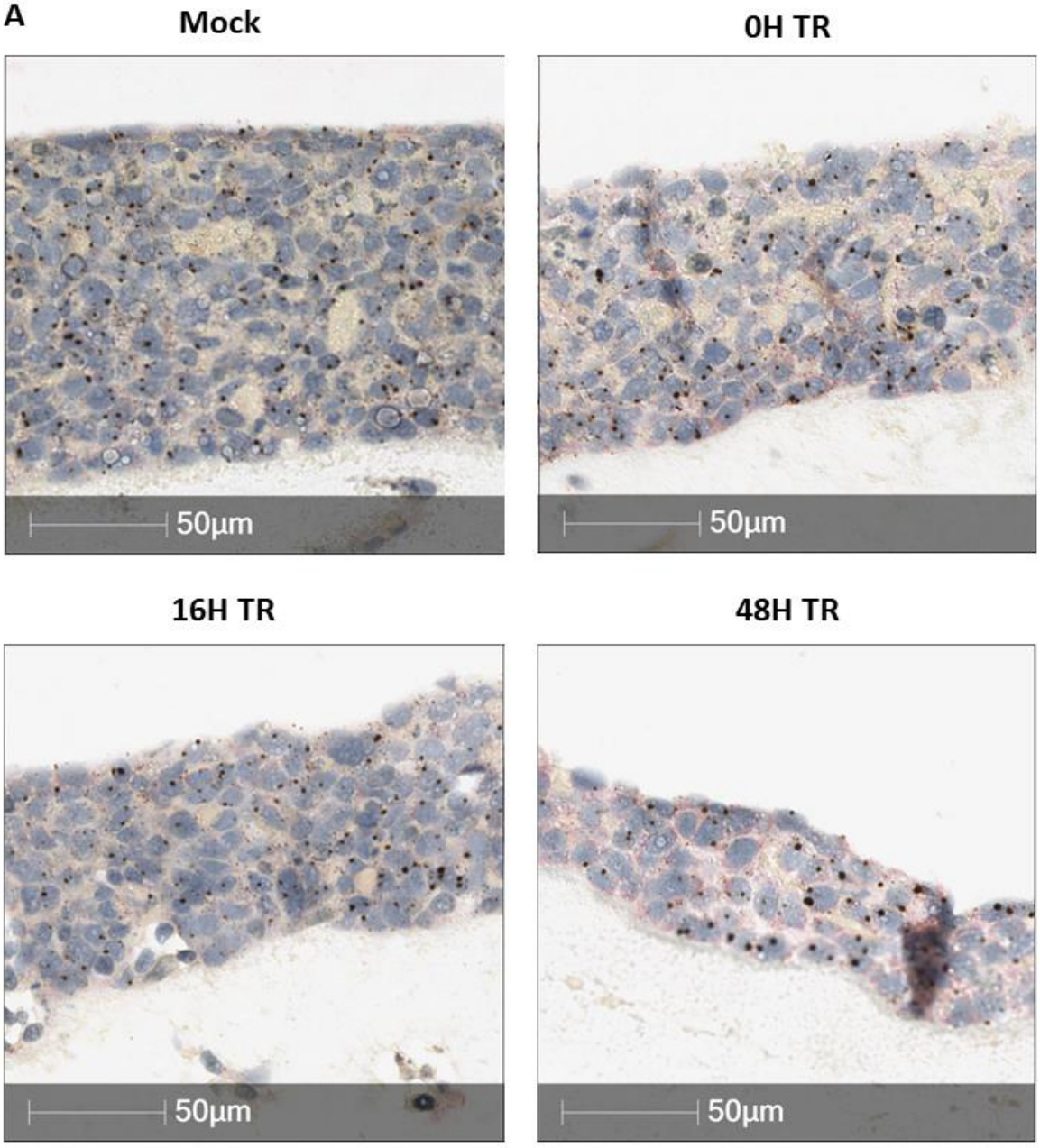

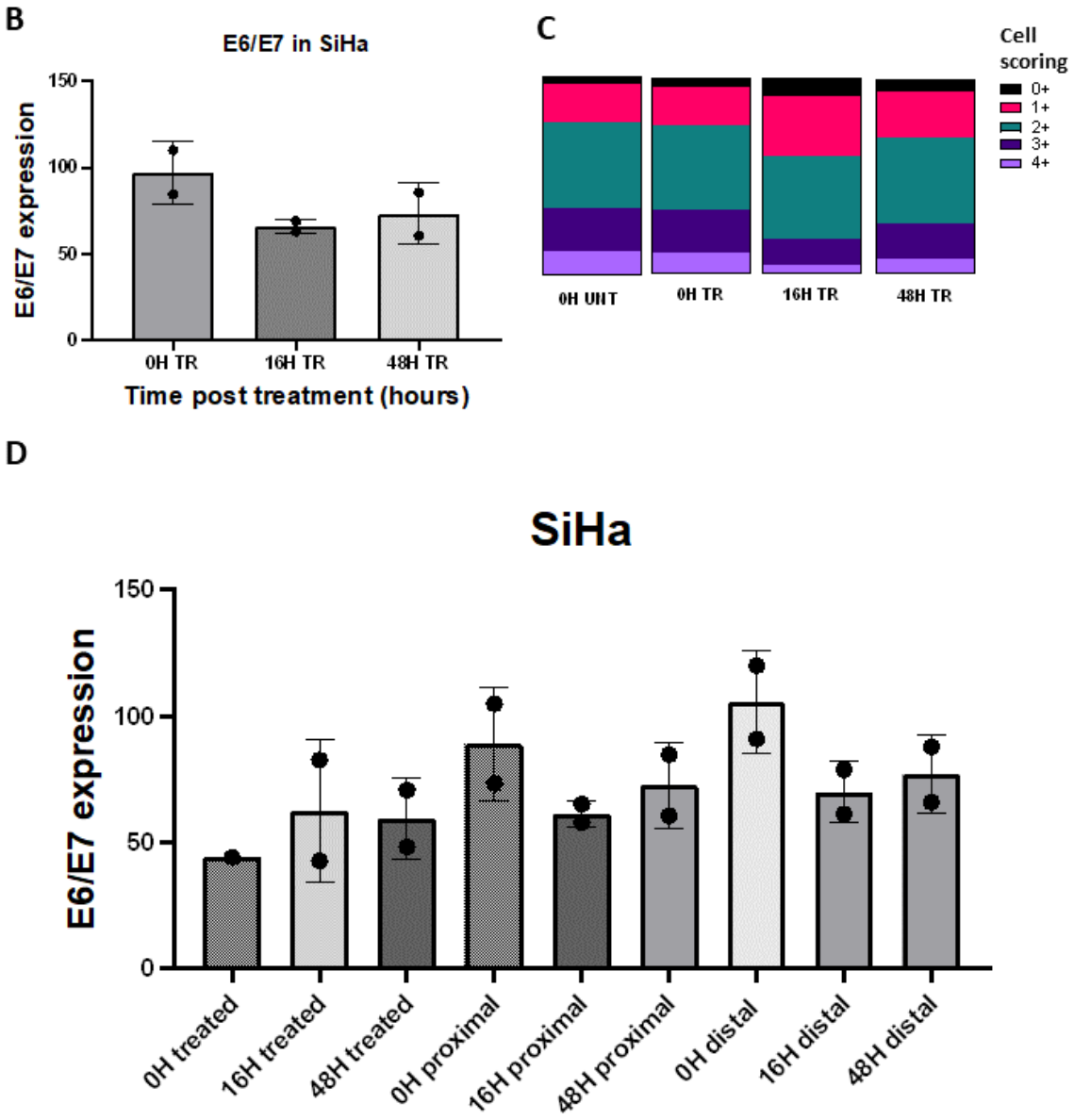

Figure 4.6: Dual RNAScope of E6/E7 and L1 transcripts in SiHa 3D rafts. (A) RNAScope stained tissues showing positivity for E6/E7 (brown staining). Mock-treated tissue is shown in the top left panel compared to the proximal areas of rafts 0, 16 and 48 hours post-treatment. Some thinning of the tissue and disruption is evident at the late time points, likely due to cell death taking place. (B) Images were quantified using HALO to determine E6/E7 expression and this is expressed relative to mock-treated tissues. E6/E7 expression across the total treated raft at 0H, 16H and 48H post-treatment. The mean expression from two biological replicates, relative to mock-treated tissues is plotted with SD bars. (C) Using the relative staining per cell, cells can be assigned a score based on the concentration of transcripts they contain (from 0 to 4) (Table 4.3). Distribution of cells in each of these categories following mock/microwave treatment at different time points. The black area represents cells with no transcripts and colours associate with increasing concentrations of E6/E7 staining (pink, teal, dark purple, light purple in ascending order) (colour-blind friendly colour scheme). (D) Annotations of each area (treated/proximal/distal) within treated rafts were defined by length from previously published results. Relative E6/E7 expression compared to mock-treated tissue is shown per area for 0, 16 and 48 hours following treatment. (B-D) Data from 2 biological replicates.

4.4.3 RNAScope reveals the spatial localisation of the transient rise and subsequent decrease in E6/E7 mRNAs following microwave treatment in models of an earlier disease stage.

We extended the RNAScope analysis to determine where changes in the gene expression of the viral transcripts took place relative to the treatment site, in models of an earlier disease stage, using NIKS16 and W12E rafts. The total E6/E7 expression within rafts was observed to rise slightly at 16 hours and then decrease at 48 hours post-treatment in both cell lines (Figure 4.7C, E). This is similar to our observations by RT-qPCR (Figure 4.2, Figure 4.3). At later time points (16 and 48 hours), E6/E7 expression was reduced within the treated and proximal areas of NIKS16 tissues compared to the distal sites (Figure 4.7D). Following treatment, fewer NIKS16 cells across the entire raft had high concentrations of E6/E7 mRNA, and more cells were negative for E6/E7 mRNAs (Figure 4.7G). Overall, microwave treatment reduces the expression of E6/E7 transcripts in NIKS16 tissues in a spatially localised manner over time.

Within the treated areas of W12E tissues, E6/E7 expression was reduced at 16 and 48 hours post-treatment, with very few visible transcripts remaining (Figure 4.8A, B). In the neighbouring 'proximal' zones, there was a small increase in staining at 16 hours followed by a statistically significant decrease at 48 hours ($p<0.05$) (Figure 4.8C, D). We propose that this increase at 16 hours in the proximal zone may represent the transient increase in E6/E7 transcripts detected by RT-qPCR (Figure 4.3). In distal sites to treatment, there was no significant change at 0 and 16 hours post-treatment but by 48 hours post-treatment, E6/E7 transcripts were significantly reduced ($p<0.05$) (Figure 4.8E, F). The increased E6/E7 expression at 16 hours can be visualised by the distribution of cells in the cell scoring categories at this time point, with more positive cells (Figure 4.7H). The number of cells positive for E6/E7 was reduced by 48 hours in W12E and very few cells were scored within the most concentrated categories, indicating a total decrease in transcription at later time points (Figure 4.7H). We observed less E6/E7 staining in both mock and treated W12E tissues compared to the corresponding NIKS16 tissues (Figure 4.7, Figure 4.8).

We also wished to investigate the spatial localisation of changes in expression of the late viral genes following treatment. Dual RNAScope assays allowed the detection of L1 transcripts within tissues alongside E6/E7 mRNAs (Figure 4.7A, B pink dots annotated by purple arrows). However, due to running two individual RNAScope experiments, we only have L1 data for two NIKS16 biological replicates due to a reagent failure on the second experiment (preventing analysis of a third NIKS16 biological replicate and W12E tissues). Previously stained positive controls and the first two NIKS16 biological replicates also showed no staining at the time of the second run, confirming that it was a problem with the reagent rather than no expression of the viral transcripts within these tissues (data not shown). This limits the statistical power of the analysis, but the trends will be discussed. L1 expression within entire NIKS16 treated rafts showed a small increase at 16 hours post-treatment, followed by a decrease at 48 hours (Figure 4.9A). This trend in expression is similar to our observations by RT-qPCR, which showed a transient increase in L1 transcripts that peaked at 16 hours and then decreased at later time points (Figure 4.2). Most treated NIKS16 rafts showed a reduction in L1 expression in the treated compared to the proximal and distal areas, however, there was variability between replicates (Figure 4.9B). At 16 hours, the increase in L1 expression could be detected within the proximal (replicate 1) or distal areas (replicate 2) to treatment (Figure 4.9B).

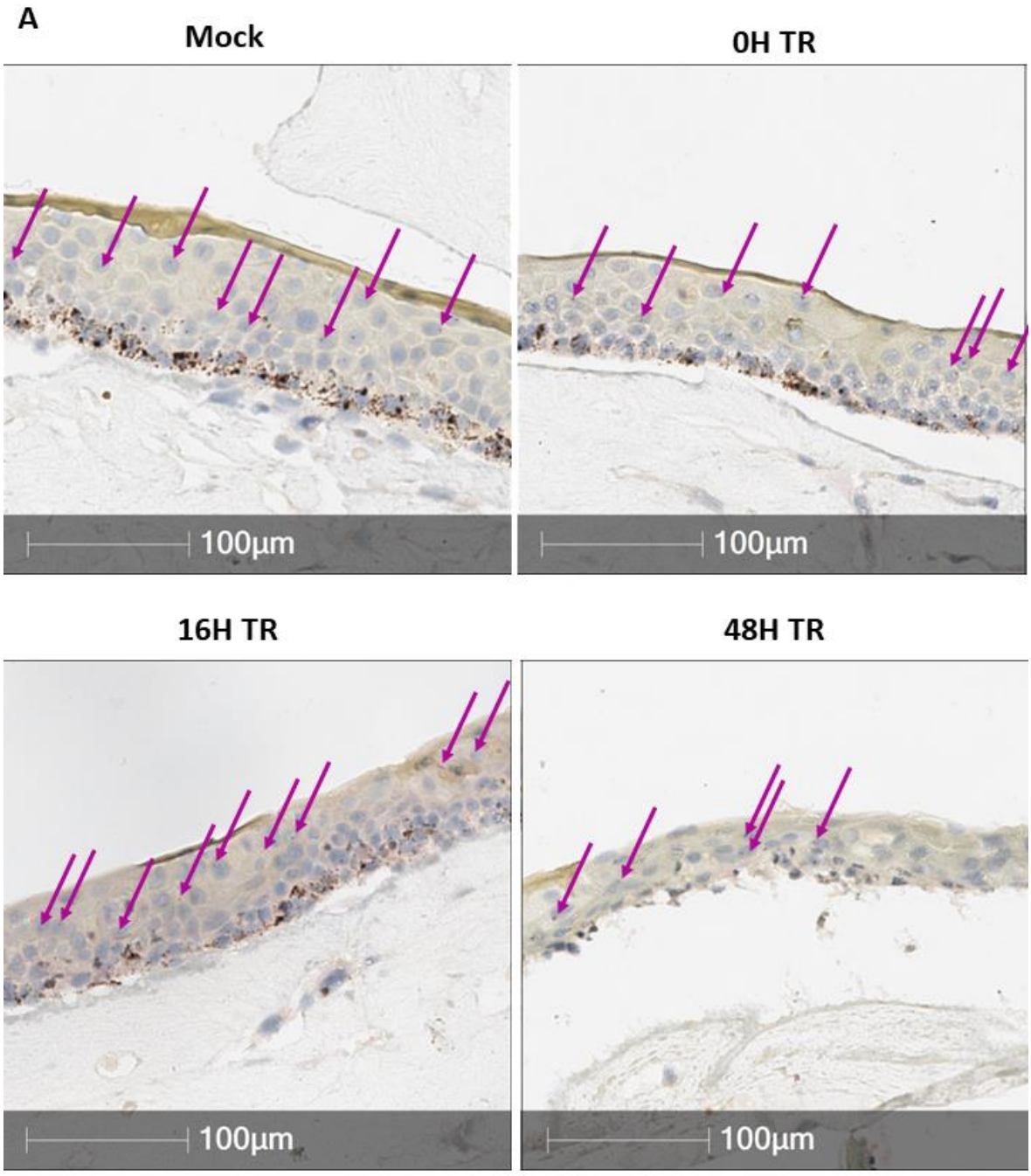
A
Mock
0H TR
100μm
100μm
16H TR
48H TR
100μm
100μm

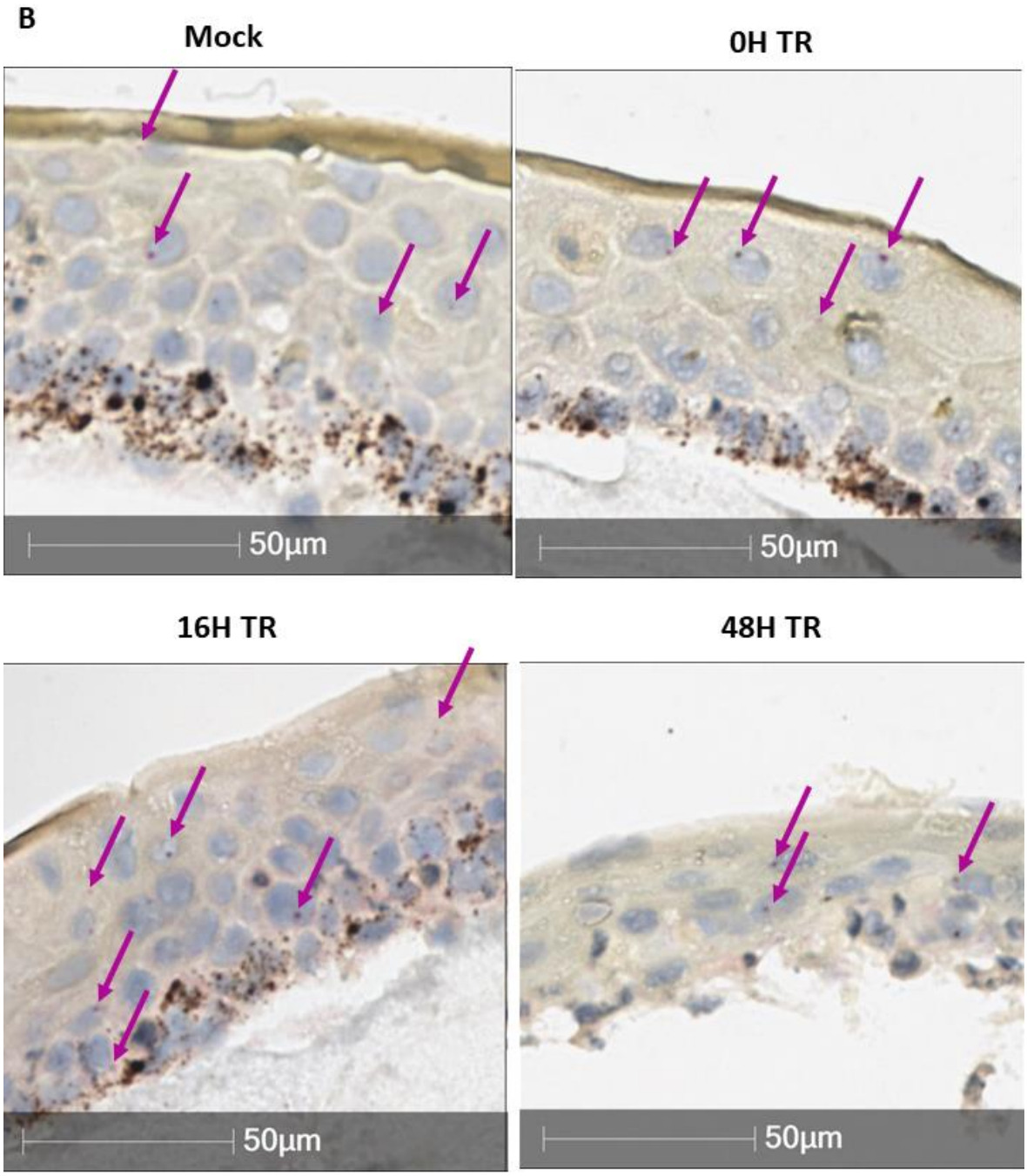
B
Mock
0H TR
50µm
50µm
16H TR
48H TR
50µm
50µm

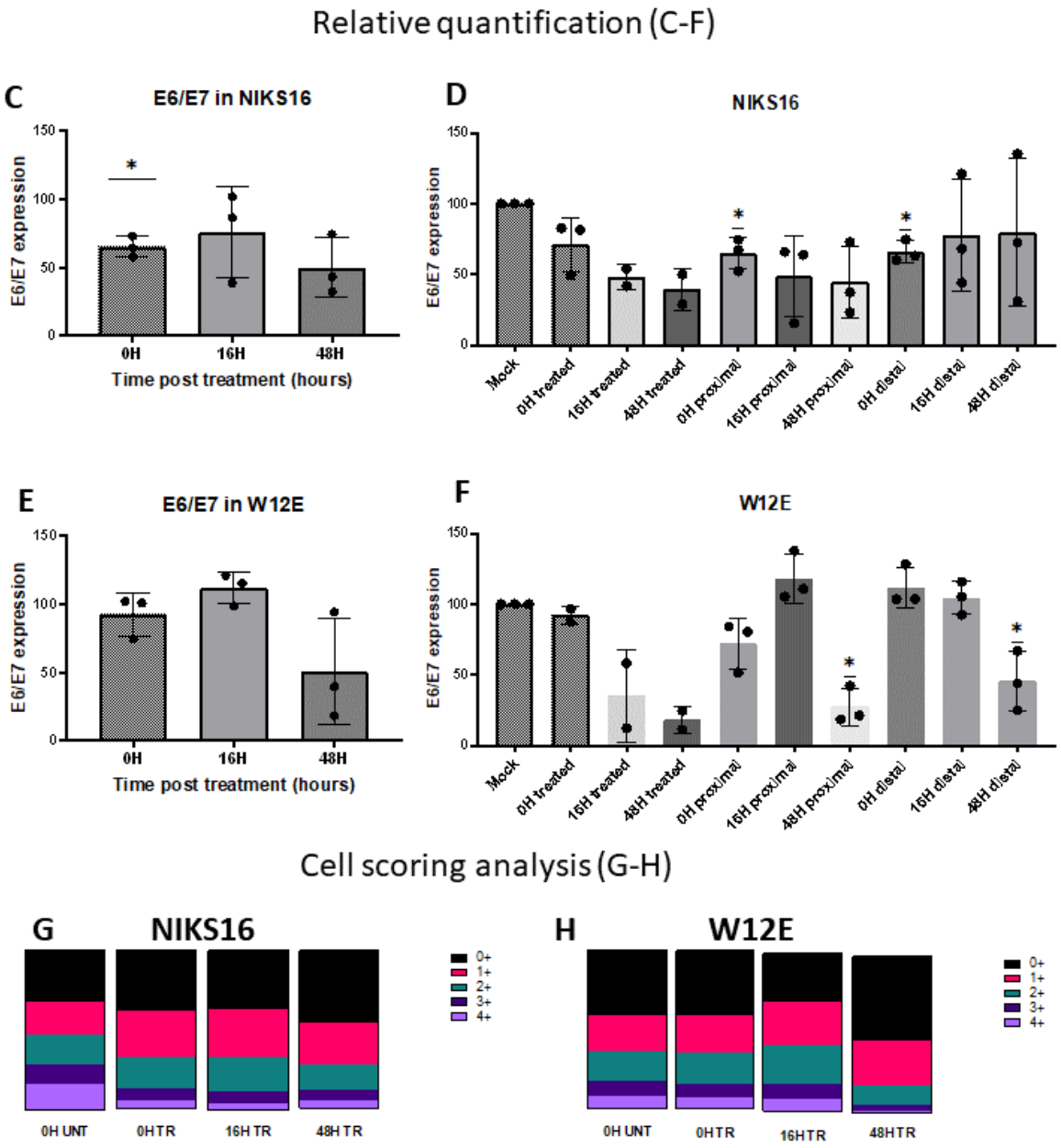

Figure 4.7: RNAScope analysis of E6/E7 (brown) and L1 (red) transcripts in NIKS16 and W12E 3D rafts. (A) Dual RNAscope staining of E6/E7 (brown) and L1 (pink) in NIKS16 tissues. Mock-treated tissue is shown in the top left panel compared to the proximal areas of rafts 0, 16 and 48 hours post-treatment. Dark pink arrows indicate L1 staining in the images as it is difficult to distinguish by eye at this magnification. Zoomed-in sections of each panel are included in (B) to enable identification of spots. (C-F) Relative E6/E7 expression in tissues following microwave treatment as a percentage relative to mock-treated tissue. E6/E7 expression across entire NIKS16 (C) and W12E (E) tissues. (D &F) Each area (treated/proximal/distal) within treated rafts was defined by length from previously published results (Conley *et al.*, 2023). Relative E6/E7 expression in each area for 0, 16 and 48 hours following treatment. Each point represents a biological replicate (n=3). For some treated areas, only 2 points are displayed as the treated area was lost in these tissues during processing. A one-sample t-test was used to determine if the mean of each group was significantly different from mock-treated tissues using a hypothetical mean of 100. * indicates p

<0.05. (G & H). Using the relative staining per cell, cells can be assigned a score based on the concentration of transcripts they contain (from 0 to 4) (Table 4.3). Distribution of cells in each of these categories following mock/microwave treatment at different time points. The black area represents cells with no detectable E6/E7 transcripts and the remaining colours associate with increasing concentrations of E6/E7 staining (pink, teal, dark purple, light purple in ascending order) (colour-blind friendly colour scheme).

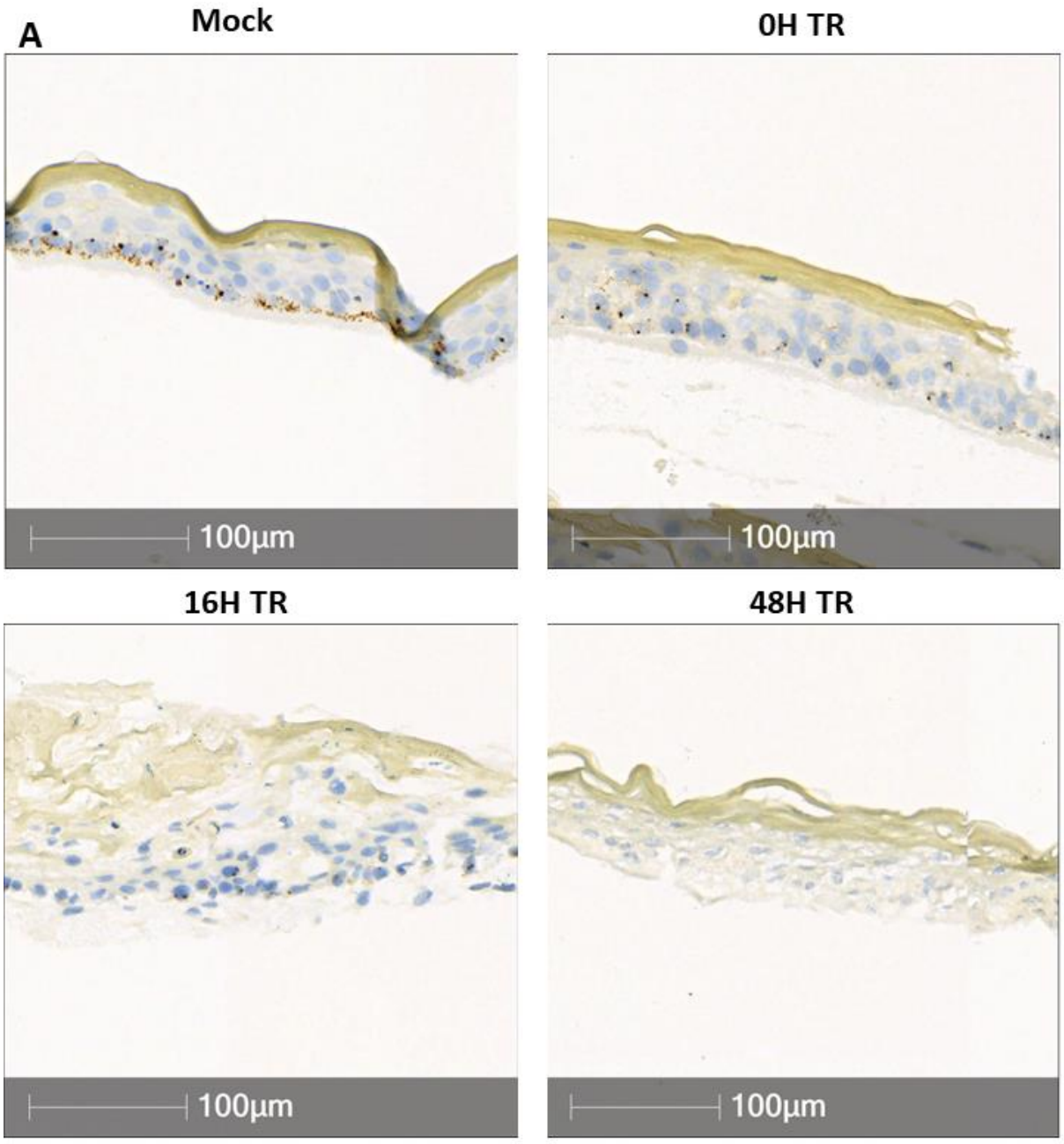
A
Mock
0H TR
16H TR
48H TR
100µm
100µm
100µm
100µm

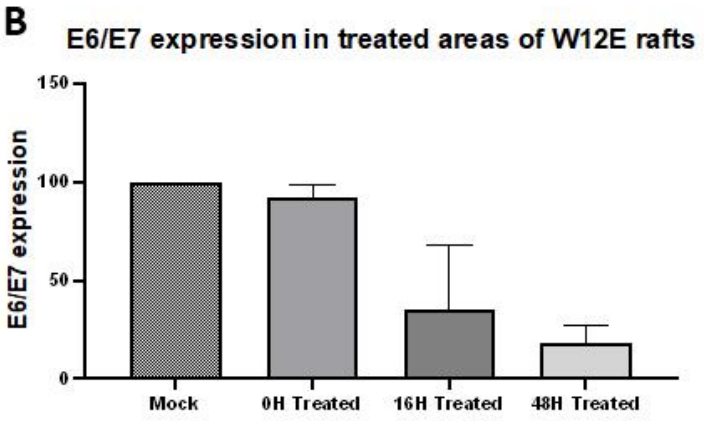
B
E6/E7 expression in treated areas of W12E rafts
E6/E7 expression
150
100
50
0
Mock
0H Treated
16H Treated
48H Treated

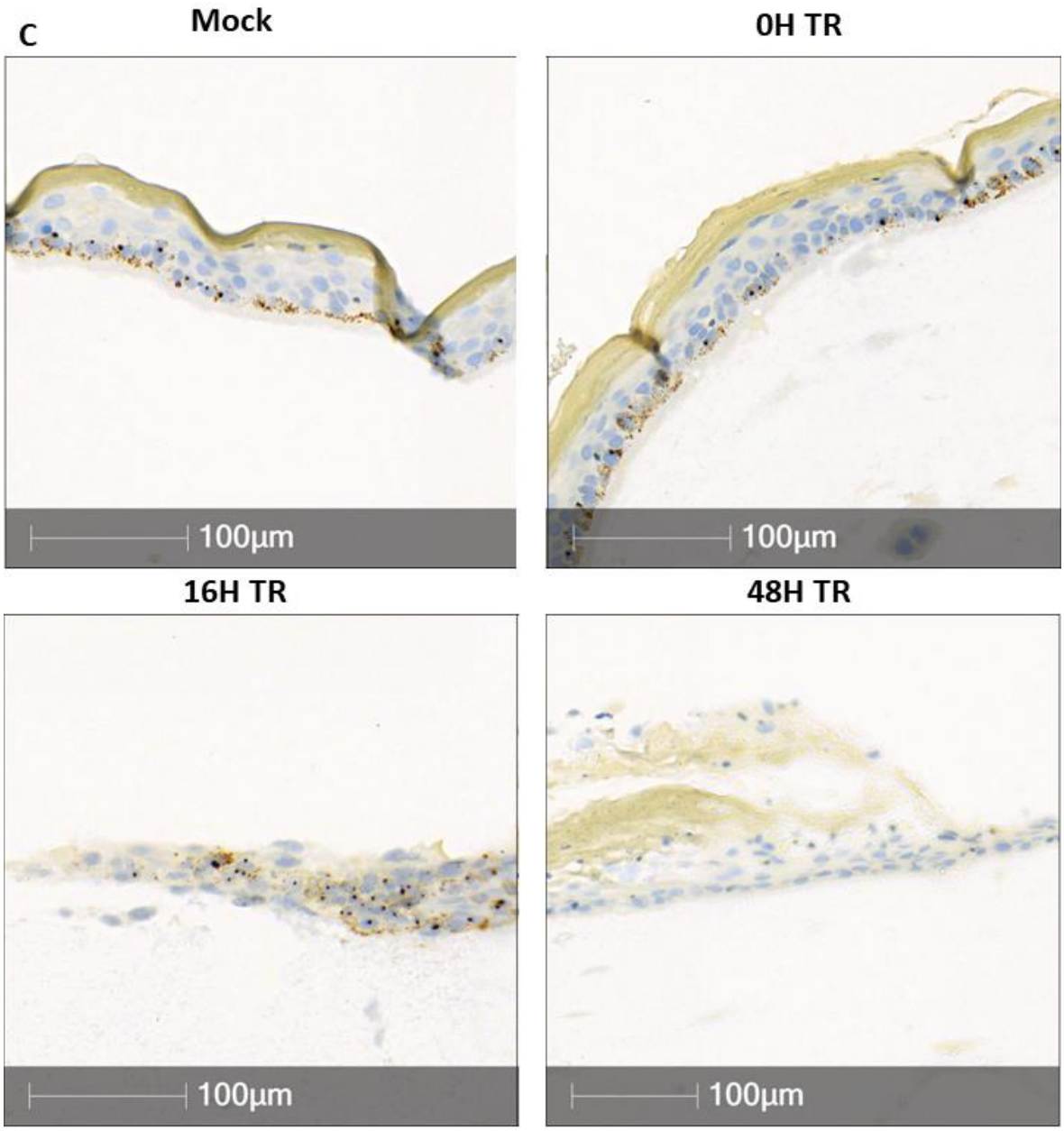
C
Mock
0H TR
16H TR
48H TR
100µm
100µm
100µm
100µm

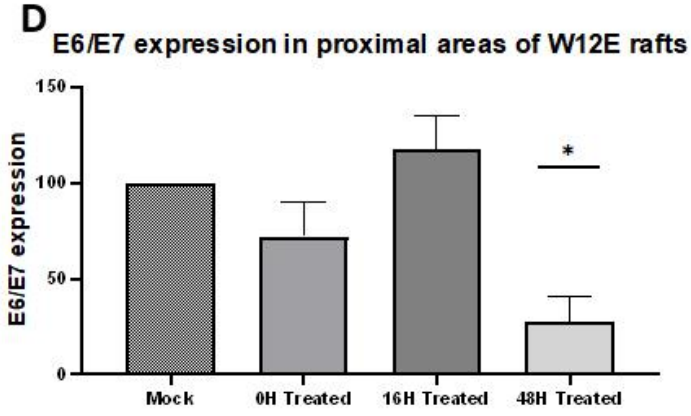
D
E6/E7 expression in proximal areas of W12E rafts
E6/E7 expression
150
100
50
0
*
Mock
0H Treated
16H Treated
48H Treated

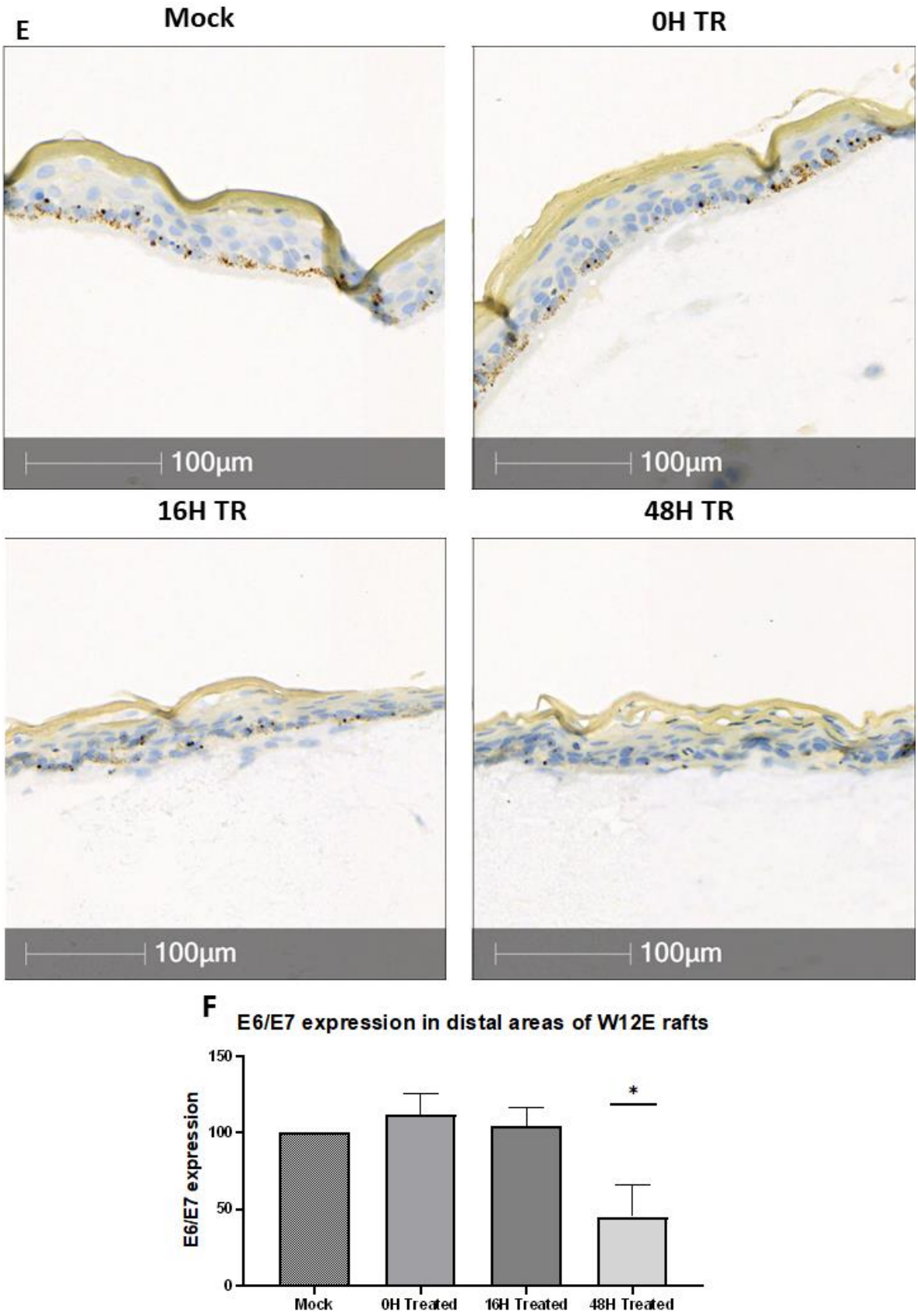

Figure 4.8: Spatial analysis of E6/E7 mRNA by RNAScope in treated, proximal and distal areas of treated W12E tissues. (A & B) RNAScope staining of E6/E7 mRNA (brown dots) within treated areas of W12E tissues following microwave treatment in comparison to mock-treated tissue with HALO quantification (B). (C & D) RNAScope staining of E6/E7 mRNA within proximal areas of W12E tissues following microwave treatment in comparison to mock-treated tissue with HALO quantification (D). (E & F)

RNAScope staining of E6/E7 mRNA within distal areas of W12E tissues following microwave treatment in comparison to mock-treated tissue with HALO quantification (F). Images are representative of 3 biological replicates. Bar graphs plot the mean results of E6/E7 expression across the biological replicates with SD. A one-sample t-test was used to determine if the mean of each group was significantly different from mock-treated tissues using a hypothetical mean of 100. * indicates $p < 0.05$.

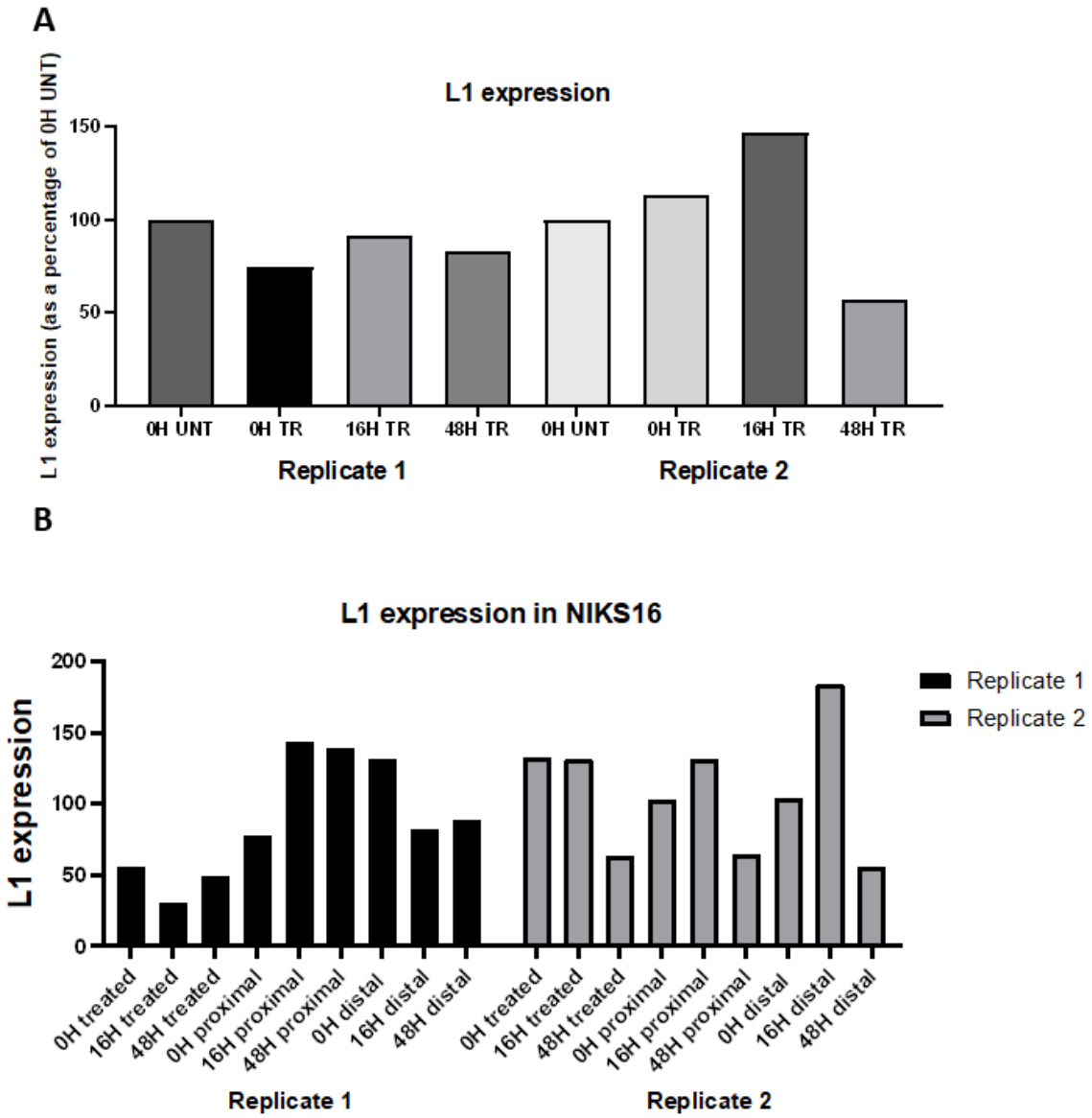

Figure 4.9: RNAScope analysis of L1 transcripts in NIKS16 3D rafts. (A) Quantified L1 mRNA levels as determined by HALO quantification as a percentage relative to mock-treated tissue in NIKS16 rafts. (B) L1 expression within treated, proximal and distal areas of NIKS16 tissues (areas defined by length). Data from two biological replicates are displayed.

4.5 Determining if the rise in transcription of the HPV16 oncoproteins following microwave treatment is translated through analysis of the downstream targets of E6 and E7, p53 and Retinoblastoma (Rb)

Due to the lack of good antibodies against the HPV16 oncoproteins, we indirectly analysed their expression following microwave treatment by investigating the change in expression of the proteins regulated by E6 and E7: p53 and Rb. IHC analysis showed relatively few cells expressing Rb in mock W12E tissues (Figure 4.10A). Rb expression was restricted to the mid-layers of the raft (Figure 4.10A), similar to previous observations of suprabasal positivity in CIN (Del Nonno *et al.*, 2011; Li *et al.*, 2004). Following microwave treatment, there was a small, non-significant increase in cells positive for Rb in the proximal tissue at 48 hours post-treatment (Figure 4.10B, C). More cells stained positive for p53 than Rb in both mock and treated tissues. The majority of this staining was within the suprabasal and upper layers of mock-treated W12E tissues (Figure 4.11A). Following microwave treatment, p53 levels increased within the proximal and distal areas up to 16 hours (Figure 4.11A, B, C) ($p<0.001$). At this time point, almost all cells appeared positive for p53, with even some positivity within the basal cells observed (Figure 4.11A). By 48 hours the number of cells positive for p53 had decreased slightly, however, tissues still contained more p53 than at 0 hours post-treatment (Figure 4.11A). Altogether these results suggest that microwave treatment increases the expression of p53 and to a lesser extent, Rb. Whilst an indirect form of analysis, this may indicate that there is no increase in functional E6 and E7 proteins following microwave treatment, which would target p53 and Rb for degradation and result in a decrease in the expression of these proteins.

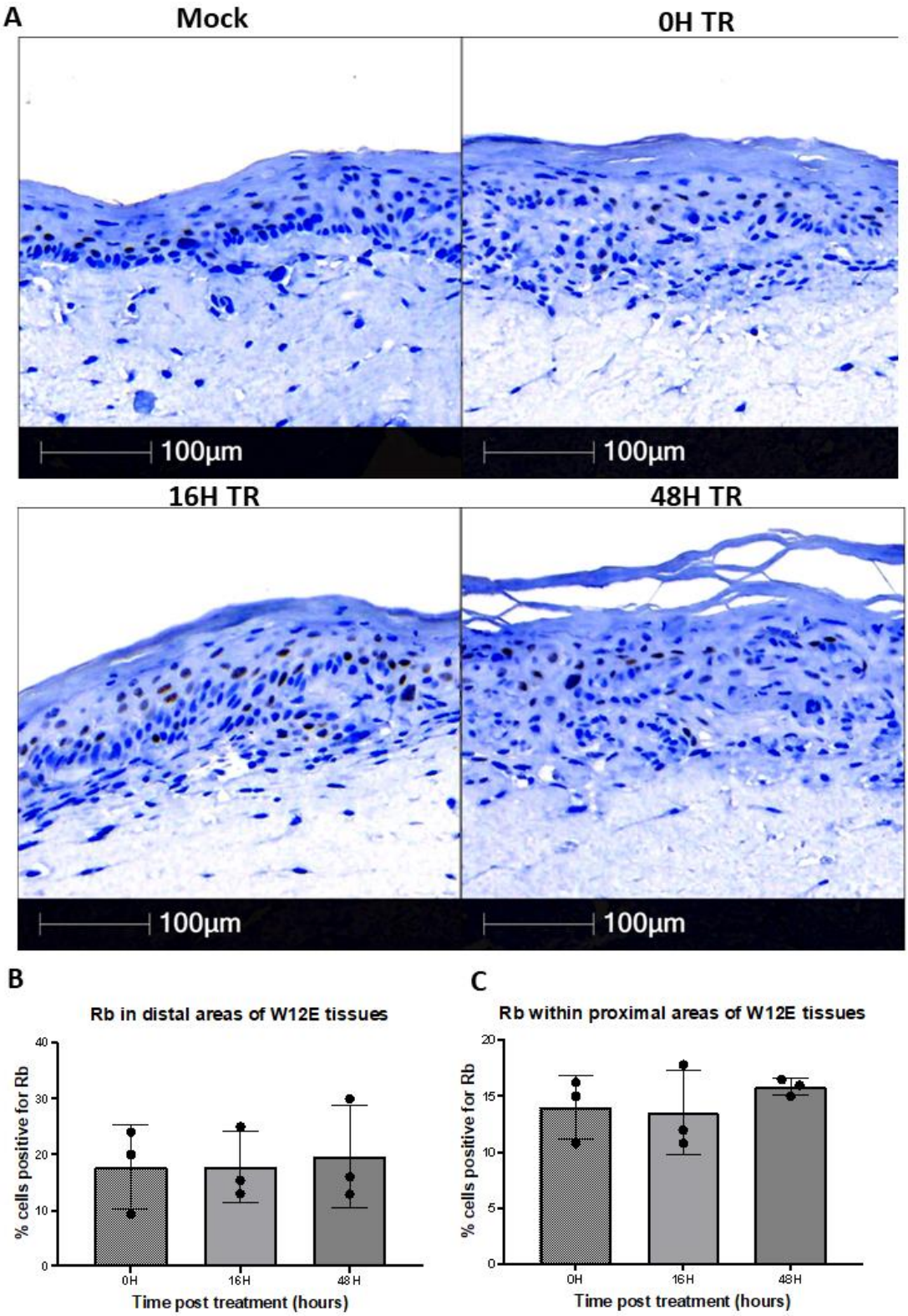

Figure 4.10: Rb IHC staining in mock and treated W12E tissues. (A) W12E tissues stained by IHC for Rb protein (positive cells are stained black). Mock-treated tissues (top left) compared to tissues at 0, 16 and 48 hours post-treatment. The number of positive cells is indicated in the distal (B) and proximal (C) areas of W12E tissues at 0, 16 and 48 hours post-treatment. The mean across three biological replicates is displayed with SD.

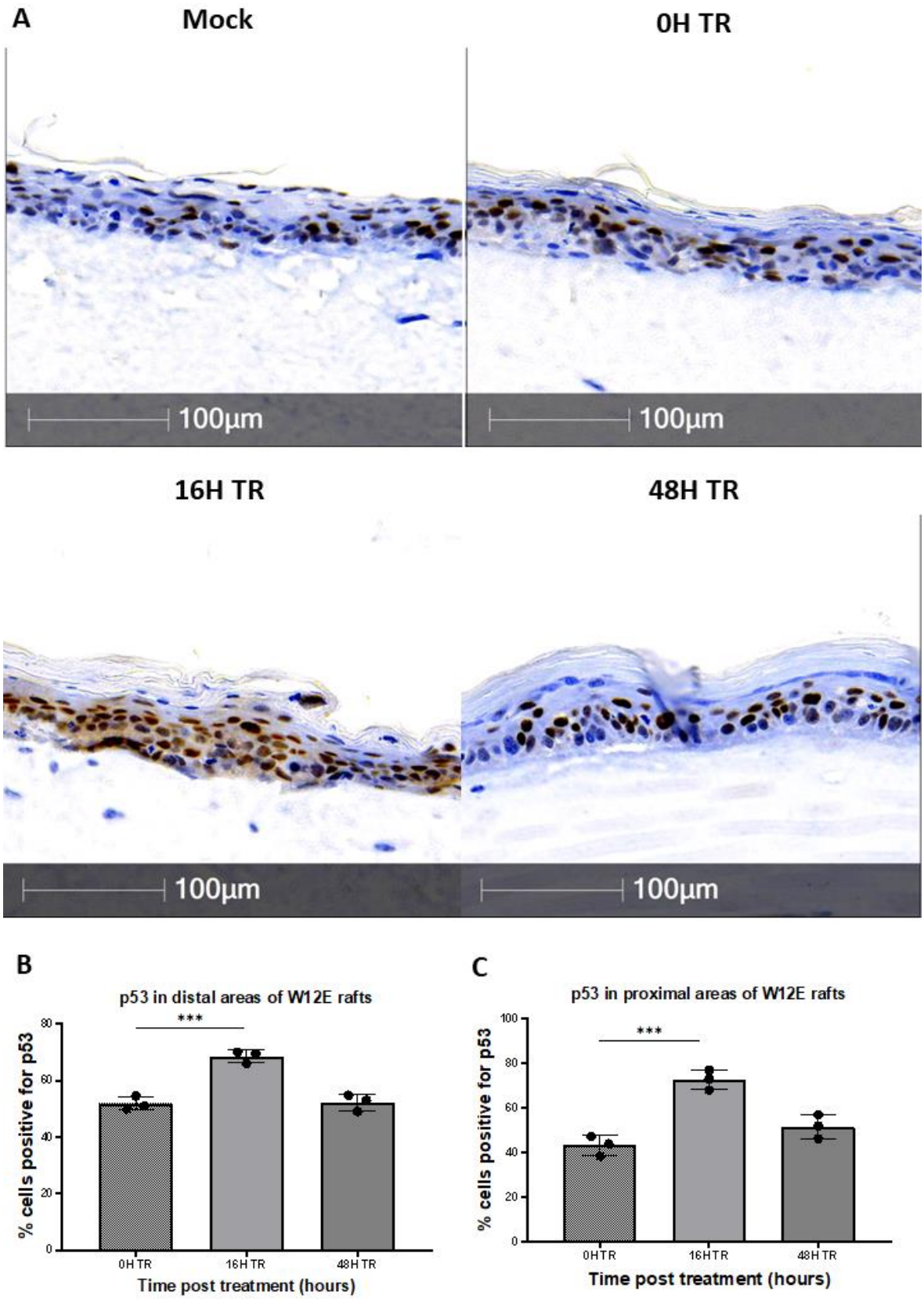

Figure 4.11: p53 staining in mock and treated W12E tissues. (A) W12E tissues stained by IHC for p53 protein (positive cells are stained black). Mock-treated tissues (top left) compared to tissues at 0, 16 and 48 hours post-treatment. The number of positive cells is indicated in the distal (B) and proximal (C) areas of W12E tissues at 0, 16 and 48 hours post-treatment. The mean across three biological replicates is displayed with SD. p-values were determined using a One-Way ANOVA and Tukey HSD test. *** indicates $p<0.001$.

4.6 The number of genome copies per cell decreases in microwave-treated tissues

We aimed to determine if microwave treatment could impact other aspects of the viral life cycle alongside transcription. For a productive viral life cycle, genome replication is essential to create new virions. We investigated if microwave treatment could impact viral replication through droplet digital PCR which enables absolute quantification of viral load without standard curves. We used human RPP30 as a reference for our copy number variance analysis as each human cell should contain 2 copies of this gene. The viral load was significantly reduced per cell following microwave treatment (Figure 4.12A). This effect was observed as early as 4 hours post-treatment and was sustained until 24 hours post-treatment (Figure 4.12B). Over time, the viral load in mock-treated tissues increased and whilst this was also evident for treated tissues, the mean viral load was still reduced in comparison to mock-treated tissue fixed at the same time. (Figure 4.12B). One tissue within the mock-treated group at 24 hours appears as an outlier with a much greater viral load than any other tissue (~130 copies per cell) (Figure 4.12B). This value was retained as it is likely a biological effect, i.e. this tissue has more viral amplification, rather than experimental error.

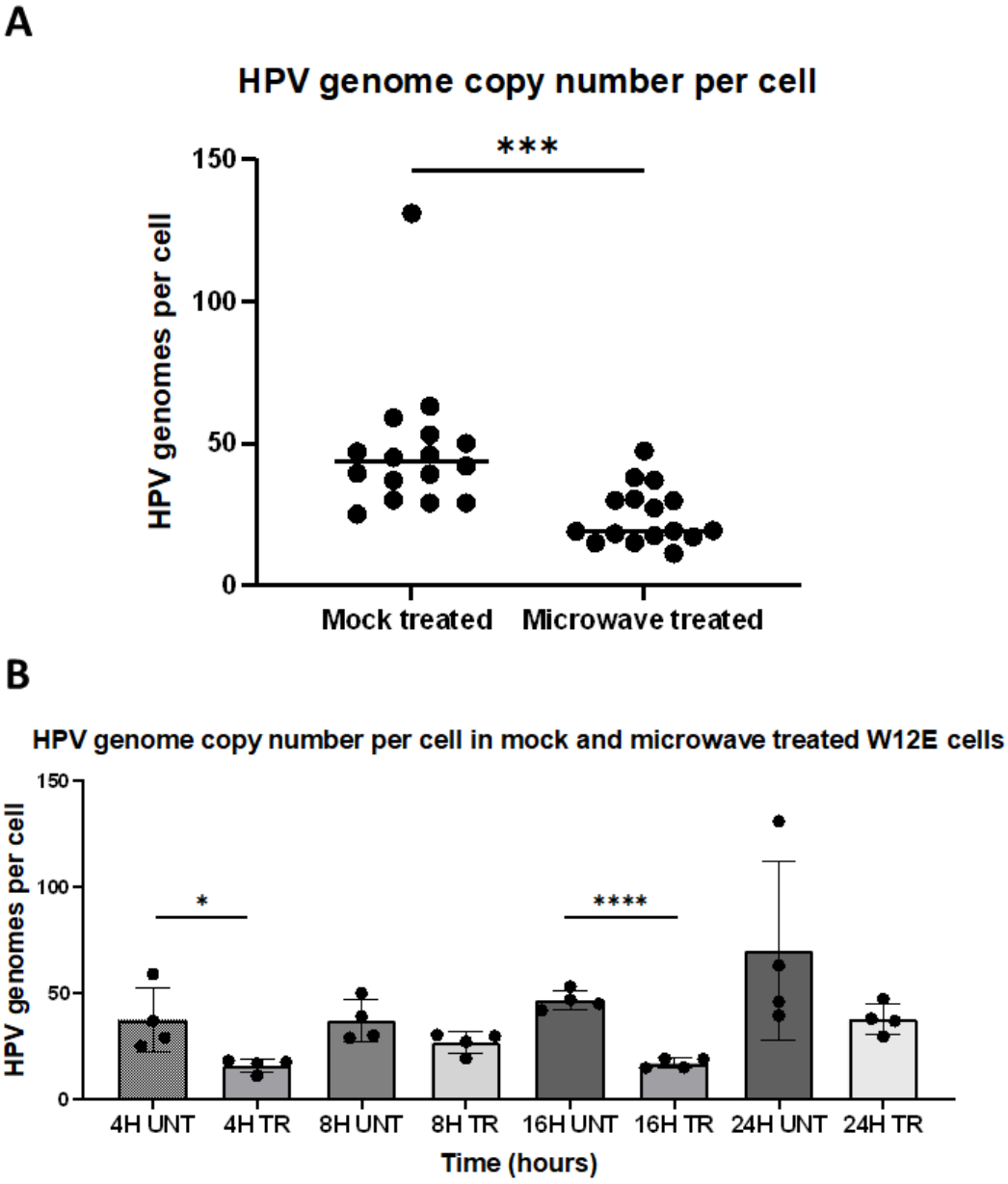

Figure 4.12: Viral load per cell in W12E tissues following microwave treatment. DNA was extracted from mock and microwave-treated W12E tissues. Droplet digital PCR was performed to determine the number of HPV16 genomes per cell using the human gene RPP30 as a reference (with 2 copies per cell). (A) Grouped analysis of mock and microwave-treated tissues. Each point represents one biological replicate. Black lines represent the median of each group. (B) Genome copy number per cell values separated by time following mock or microwave treatment. The mean and SD are displayed with each point representing one biological replicate. An unpaired t-test was performed to determine any significant differences in the means between mock or treated conditions at each time point. * Indicates $p< 0.05$, ** indicates $p< 0.01$, *** indicates $p< 0.001$ and **** indicates $p<0.0001$.

4.7 Discussion

We analysed the effect of microwave treatment on several aspects of the HPV life cycle including transcription, translation and genome replication. Within a model of cervical cancer, using the SiHa cell line, microwave-treated 3D tissues exhibited no change in the expression of E6 and E7 mRNAs until 72 hours post-treatment, when a significant decrease was observed by RT-qPCR. RNAScope allowed us to investigate where this change in expression was happening in the context of the tissue. Transcripts encoding the oncoproteins E6 and E7 were decreased in a spatially localised manner, in the treated compared to proximal and distal sites at 16 and 48 hours in response to microwave treatment. Our previously published work identified that E6 and E7 protein levels also decrease following microwave treatment in SiHa tissues in the treated and proximal areas relative to distal sites (Conley *et al.*, 2023). We reported a correlative upregulation of p53 and Rb, the target proteins of the viral oncoproteins, and a reduction in proliferation, which suggests a reversal of the E6/E7-driven tumorigenic phenotype of these cells (Conley *et al.*, 2023). This result is similar to that seen by another group that induced hyperthermia at 42 ^{o}C for one hour in cervical cancer cell lines and observed upregulated p53 and its activity (Oei *et al.*, 2015a). We predict that the greater reduction at the protein rather than mRNA level of E6/E7 is due to the inhibition of translation due to heat-shock-induced cell stress, as previously demonstrated (Conley *et al.*, 2023).

We observed a slightly different response when extending this analysis to models of earlier disease stages using NIKS16 and W12E tissues. The expression of the early and late HPV16 transcripts was transiently increased, with a peak at 8-16 hours, following microwave treatment, with late viral transcripts upregulated to a greater extent. At later time points, transcripts then decreased to levels below that or similar to mock-treated tissue levels. W12E tissues showed less E6/E7 staining by RNAScope compared to NIKS16. Moreover, there was no significant upregulation in E6/E7 expression following microwave treatment in W12E tissues by RT-qPCR or RNAScope. This suggests that the expression of the oncoproteins is more tightly regulated in these tissues, thus resembling an earlier stage of disease. W12E cells additionally provide a more relevant model for cervical precancerous disease as they were derived from a CIN lesion (Stanley *et al.*, 1989). Therefore, the changes to HPV gene expression in

these cells may be more translatable to the application of microwave treatment *in vivo*.

The transient increase in viral gene expression observed in NIKS16 and W12E tissues may be due to an increase in the differentiation phenotype of cells in response to microwave treatment. Pathway analysis of differentially expressed genes following microwave treatment in NIKS16 tissues revealed an increase in keratinocyte differentiation (Section 3.5.2) and previous work has revealed an increase in involucrin and keratin 10 protein expression following treatment (Conley *et al.*, 2023). The late stage of HPV gene expression is tightly linked to keratinocyte differentiation, through E2-mediated inhibition of the early promoter and activation of the late promoter with the cellular LAP isoform of the terminal differentiation transcriptional factor C/EBPβ (Gunasekharan, Haché and Laimins, 2012). The HPV regulatory protein E8^E2, which restricts viral replication and transcription in undifferentiated cells, has also been proposed to be involved in the switch to productive HPV replication within differentiated cells (Kuehner and Stubenrauch, 2022). Therefore, an increase in differentiation following microwave treatment may result in increased production of late gene transcripts (Chow, 1987; Hummel, Hudson and Laimins, 1992; Bedell *et al.*, 1991; Gunasekharan, Haché and Laimins, 2012). Transcription factors that drive differentiation-dependent cellular genes may be upregulated in activity or level following hyperthermia which may also drive viral gene expression. For example, some transcription factors such as Kruppel-like factor 4 (KLF4) regulate the expression of differentiation-dependent cellular genes (Sen *et al.*, 2012; Kalabusheva *et al.*, 2023) and can activate late viral gene expression (Gunasekharan *et al.*, 2016). Increasing evidence shows that the viral early genes also increase in expression following differentiation. Since the viral episome associates with histones to form nucleosomes, it is subject to epigenetic modification. There have recently been several elegant studies demonstrating CTCF-YY1-driven chromatin looping within the HPV genome, between the URR and E2 ORF, which results in epigenetic repression of the viral oncogenes (Paris *et al.*, 2015; Pentland *et al.*, 2018). Following differentiation, the downregulation of YY1 removes this epigenetic silencing and drives the expression of the viral early genes (Pentland *et al.*, 2018; Ferguson *et al.*, 2021). A combination of epigenetic and transcription factor changes that result in a more differentiated cellular

phenotype following microwave treatment may result in our observation of increased viral early and late gene expression. Moreover, this may explain the difference between SiHa, NIKS16 and W12E tissues. Since SiHa cells have lost the ability to differentiate following transformation, these mechanisms would not enhance the expression of the oncogenes in these cells.

At later time points post-treatment, the transcription of the viral genes decreased to levels similar to or below that of untreated tissues. This decrease occurred earlier for W12E (observed at 24 hours) compared to NIKS16 tissues (72 hours) for RNA derived from tissues containing the treated and proximal zones. When we interrogated the spatial localisation of these changes using RNAScope, we observed a decrease in E6/E7 expression within the treated areas from 16 hours post-treatment, likely due to cell death in this area. Subsequently, a decrease in expression was observed within the proximal areas (of both NIKS16 and W12E tissues) and distal areas (of W12E tissues) at 48 hours, suggesting cell-to-cell communication from the treated area conveys this response radially across the tissue. We propose that the induction of innate immunity following microwave treatment may inhibit viral transcription at later time points (Chapter 3). Exposure to interferon has previously been reported to reduce the transcription of the viral oncoproteins (De Marco and Marcante, 1993). Additionally, the cell stress response upregulated by hyperthermia may result in transcriptional inhibition at later time points (Mahat *et al.*, 2016; Vihervaara *et al.*, 2017).

Will the observed changes in transcription be translated into protein?

It is unclear if the transcripts we have analysed through RT-qPCR are stable mRNAs which will be translated. HPV transcripts associate with several RNA-binding proteins following transcription that influence mRNA stability and translation (Graham, 2024). We have limited methods to analyse E6/E7 protein levels following treatment due to the poor quality of the antibodies against these species. However, analysing their downstream targets, p53 and Rb can help determine their activity and levels. We observed a significant increase in p53 following microwave treatment and a small, non-significant increase in Rb. Heat shock-induced cellular stress is likely responsible for the greater upregulation of p53, which results in its phosphorylation and tetramer

formation in the nucleus (Jentsch *et al.*, 2020; Matsumoto *et al.*, 1997). In support of this, our RNA Sequencing analysis predicted an increase in the transcriptional activity of p53 following microwave treatment, with many genes regulated by p53 upregulated in expression (Section 3.5.3). Reduced expression of the HPV oncoproteins would add to the increase in p53 levels and may be responsible for the small rise in Rb staining observed following microwave treatment. Heat shock may result in a reduction of E6 and E7 through translational stress, which we previously observed following microwave treatment (Conley *et al.*, 2023). However, our indirect analysis method is a major limitation, and quantitative proteomics would be required to determine how E6 and E7 protein levels were affected by microwave treatment with confidence.

Viral load is decreased following microwave treatment

We observed a significant decrease in viral replication following microwave treatment. This response was fast-acting with a significant reduction in the viral load from 4 hours post-treatment. Within mock-treated tissues, the viral load continued to rise throughout the experiment as cells became more differentiated and viral amplification took place. There was some increase in the viral load over time in treated tissues, but it was always below that of untreated cells at the same time point, suggesting impaired replication of the viral genome. Heat shock can inhibit replicative DNA synthesis through arrested or decelerated progression of replication forks and the movement of nucleolin into the nucleoplasm to target RPA (Velichko *et al.*, 2012; Wang *et al.*, 2001). DNA replication remained inhibited following heat shock for up to 8 hours (Wang *et al.*, 2001). Since HPV requires host cell DNA replication machinery to replicate its genome, this inhibition may also impact viral genome replication. Hyperthermia can also temporarily inhibit the DNA damage response (DDR) via homologous recombination pathways and decreased activity of the DNA-dependent protein kinase (DNA-PK) (Ihara *et al.*, 2014; Oei *et al.*, 2015b). DDR pathways are important for viral genome amplification, so their inhibition following microwave treatment may account for the reduction in viral genomes seen in treated tissues. Moreover, innate immunity has previously been observed to inhibit viral genome replication. IFN-β treatment of HPV31- and HPV16-positive keratinocytes resulted in a loss of viral episomes (Herdman *et al.*, 2006; Chang *et al.*, 2002). Moreover, the interferon-stimulated gene (ISG), IFIT1 can bind to and inhibit the E1 helicase in HPV11 and 18 (Hong, Mehta and

Laimins, 2011; Saikia, Fensterl and Sen, 2010; Terenzi, Saikia and Sen, 2008). If this mechanism extends to HPV16, our observed increase in interferons upon microwave treatment (Section 3.7) could drive IFIT1 expression and thus inhibit viral replication.

Limitations to our transcriptional analysis involve the clustering of staining seen by RNAScope that prevents accurate determination of transcript numbers per cell. Relative changes are sufficient to address our aims, but subsequent work could make use of smFISH a non-amplifying technology which should only result in single-stained mRNA molecules (Femino *et al.*, 1998). It would also be important to repeat the L1 RNAScope analysis in both NIKS16 and W12E tissues with a new probe since a reagent failure limited our analysis to two NIKS16 biological replicates. Although the trend for L1 expression by RNAScope was similar to that observed by RT-qPCR for NIKS16 tissues, variability between the replicates made it difficult to draw firm conclusions. Budget constraints for this expensive technology limited the purchase of a new probe and repetition of the L1 analysis. The viral load observed in W12E tissues by ddPCR analysis is quite low, as during amplification in differentiated cells, the viral load is proposed to increase to several hundreds or thousands per cell (Hoffmann *et al.*, 2006). Previous work has shown that few cells within the top layers of raft cultures stain positive for viral episomes, indicating the rare occurrence of the productive phase of the viral life cycle in this model system (Bedard *et al.*, 2023). Additionally, if productive amplification is rare, the resulting high viral load may be difficult to detect when analysing the average copy number throughout a raft culture. The proportion of cells in the terminally differentiating layers is much lower than those in the basal and suprabasal layers and the low viral load in these basal and suprabasal cells may conceal any cells undergoing productive amplification.

Overall, microwave treatment impairs human papillomavirus replication. Viral genome replication is inhibited and viral transcription is decreased, at later time points post-treatment. The decrease in transcription is greatest in the treated area but this extends into neighbouring tissue and even distal sites from treatment at later time points post-treatment. Analysis of the late stage of the virus life cycle following microwave treatment is carried out in the next chapter (Chapter 5).

Chapter 5 Investigating the spatial localisation of the HPV late protein, L1 and virions and how their expression is affected by microwave treatment

5.1 Introduction

The viral lifecycle and pathogenicity of HPV are intricately linked to the localisation and functions of the viral proteins within host cells. Viral late proteins, including the major capsid protein L1, are produced within the differentiated cells of the epithelium (Ozbun and Meyers, 1998; Doorbar *et al.*, 1997; Florin *et al.*, 2002a). Following translation in the cytoplasm, L1 is transported to the nucleus in association with Karyopherins (Bird *et al.*, 2008; Nelson, Rose and Moroianu, 2002; Nelson, Rose and Moroianu, 2003; Merle *et al.*, 1999)(Bird *et al.*, 2008; Cerqueira and Schiller, 2017). Here, virion assembly takes place (Section 1.7.3). Unlike many viruses, it is very difficult to produce large quantities of papillomavirus virions *in vitro*. This is partly due to the requirement for epithelial cell differentiation for expression of the late capsid proteins and virion assembly (Pyeon *et al.*, 2005). Therefore, detailed structural models of HPV have been produced using virus-like particles (VLPs), quasiviruses or pseudovirions (PsVs). VLPs are composed of the major capsid protein (L1) alone or in combination with L2 (Kirnbauer, 1992). Pseudoviruses and quasiviruses contain the major and minor capsid proteins and dsDNA (papillomavirus genome for quasiviruses and plasmid DNA as a mock genome for pseudoviriuses) (Buck *et al.*, 2005; Christensen, 2005). Papillomaviruses are also quite inefficient at packaging genomic information. For example, Phage P2 has similar-sized icosahedral capsids to PVs (60 nm) but can package linear 33 kb dsDNA, compared to the 8 kb PV genomes which are packaged (Christie and Calendar, 2016). Moreover, no packaging sequence has been identified for PVs and it appears that the length of dsDNA is the limiting factor. PVs can pack completely unrelated dsDNA into capsids so long as the size of 8 kb is not exceeded (Cardone *et al.*, 2014; Buck *et al.*, 2004; Stauffer *et al.*, 1998).

Limited work has been carried out on the localisation of the late HPV proteins within differentiated cells and how virion assembly takes place, partly due to difficulties in replicating HPV production *in vitro*. The current understanding of L1 and L2 localisation within differentiated cells is based on the following studies. Transfection of plasmids

expressing HPV16 L1 into cervical cancer cell lines resulted in diffuse nuclear staining with nucleolar exclusion (Siddiqa *et al.*, 2015) (Figure 5.1A). L1 was also observed to interact with HPV16 E2 and prevent E2's nucleolar localisation (Siddiqa *et al.*, 2015), normally seen as foci staining that colocalises with nucleolar markers (Prescott *et al.*, 2014). This diffuse nuclear L1 staining was also observed in studies demonstrating the nuclear import of the HPV16 L1 capsomeres (Nelson, Rose and Moroianu, 2002) (Figure 5.1B). Results from Day and colleagues also showed diffuse bovine papillomavirus (BPV) L1 staining when introducing this protein alone, expressed from recombinant Semiliki Forest Virus (SFV) into fibroblast cells (Day *et al.*, 1998). However, these authors showed that when L1 and L2 were introduced together, L2 could recruit L1 to tightly stained nuclear dots that colocalise with promyelocytic leukaemia nuclear bodies (PML-NBs) (also known as ND10) (Day *et al.*, 1998) (Figure 5.1D). Viral genomes localise to PML-NBs through E2 during cellular differentiation so this may represent a conserved site of virion assembly (Day *et al.*, 1998). Moreover, PML-NBs are a common target during replication of other DNA viruses including herpes viruses and SV40 (Kieback and Müller, 2006). Other groups have also observed foci of HPV33 L1 when co-expressed with L2 using recombinant vaccinia viruses (Figure 5.1C) (Schafer, Florin and Sapp, 2002). These studies used viral vectors due to the limitations of transient transfection assays of the papillomavirus structural genes resulting in poor expression, even when under the control of strong promoters. However, development of codon-optimised HPV16 L1 and L2 allowed for transfection assays that produce sufficient quantities of the papillomavirus structural proteins to be used (Kieback and Müller, 2006). Within this system, the dot-like expression pattern of L1 and L2 in PML-NBs was observed to be a rare phenomenon and the majority of L1 and L2 staining was homogenously distributed throughout the nucleus when stably expressed (Kieback and Müller, 2006). The authors demonstrated that foci staining was directly correlated to protein concentration (4% of cells showing PML-NB localisation at low concentrations to 13% at higher concentrations) and the presence of a virus vector (capable of increasing the observation of PML-NB localisation from 13 to 50%) (Kieback and Müller, 2006). An anti-viral response mechanism generated against the viral vector used to deliver the papillomavirus L1 and L2 may therefore be responsible for the increased PML-NB localisation since it is known that type I interferons can alter PML-NB composition (Regad and Chelbi-Alix, 2001). Overall,

HPV16 L2 could recruit L1 to PML-NBs but most cells showed diffuse distribution of both proteins throughout the nucleus.

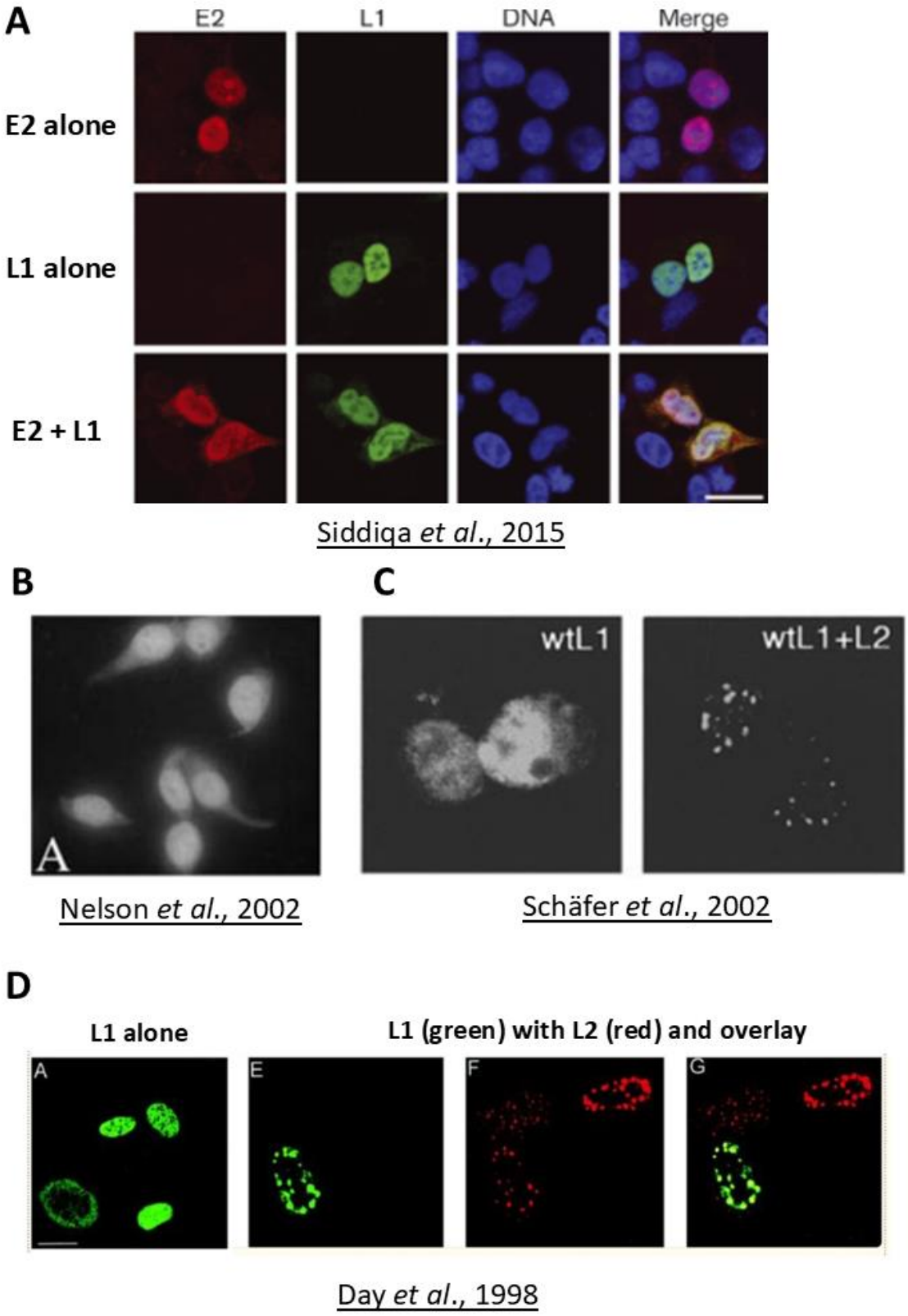

Figure 5.1: Previous studies of L1 nuclear localisation when introduced via transfection or viral vector assays. Adapted figures from several studies which introduced L1, L2 and E2 proteins via several techniques. (A) HPV16 E2 and L1 were

transfected independently or together into C33a cells. (B) L1 staining of cells following HPV16 L1 capsomere transport into HeLa cells. (C) HPV33 L1 alone or with L2 was introduced into HEK293 cells using recombinant vaccinia virus. (D) BPV L1 alone or with L2 was introduced into BPHE-1 cells (hamster fibroblast cells) using recombinant SFV. The staining patterns observed are shown. (Figures adapted from (Siddiqa *et al.*, 2015; Nelson, Rose and Moroianu, 2002; Schafer, Florin and Sapp, 2002; Day *et al.*, 1998).

Additionally, studies have analysed L1 staining within differentiated cells that stably maintain the entire viral genome, which may more accurately resemble natural infection and model how the other viral proteins affect late protein localisation. In differentiated, 2D W12E cells the majority of L1 staining is cytoplasmic with almost all cells positive (Milligan *et al.*, 2007). When extended to organotypic raft cultures, the majority of L1 staining is in the nuclei in the uppermost layers of tissues (Ferguson *et al.*, 2021; Song *et al.*, 2010). Some cells at the very top of rafts show more dispersed staining, which may also represent L1 within the cytoplasm as these cells flatten and enucleation takes place (Laganà *et al.*, 2024; Wechsler *et al.*, 2012; Matsui and Amagai, 2015). In productive lesions, HPV16 L1 is predominantly nuclear in the mid and upper layers of the epithelium (Middleton *et al.*, 2003). Interestingly, the amount of L1 staining within differentiated cells varies amongst the HPV type and the cell line or model used. L1 expression from HPV31 in CIN612 9E organotypic rafts is a rare observation (Song *et al.*, 2010) but almost half of cells containing HPV18 in the upper layers of organotypic rafts have L1 positivity (Laganà *et al.*, 2024) and almost all HPV16 positive W12E cells show L1 expression when differentiated in 2D (Milligan *et al.*, 2007).

Overall, our current understanding of the localisation of the HPV late capsid proteins is limited. Although providing information on protein localisation, none of these studies serve as good models for natural infection or contain the entire HPV genome. Therefore, cell differentiation, other viral proteins and/or the viral genome may play additional roles in the localisation of the capsid proteins. Previous reports of L1 localisation within models that contain HPV episomes provide limited resolution due to the challenges of immunofluorescent labelling within tissue sections. Therefore, patterns within the nucleus of diffuse or foci staining are difficult to discern. To overcome these challenges and obtain high-resolution images of capsid protein localisation, this chapter aims to:

- Characterise HPV16 L1 expression and spatial localisation within differentiated W12E cells, which serve as a good model for natural infection and contain the entire viral genome.
- Determine if L1 staining correlates to the production of virions within differentiated W12E cells.
- Analyse how microwave treatment impacts L1 expression and localisation.

5.2 The expression and localisation of the HPV major capsid protein L1 within undifferentiated and differentiated W12E cells grown in 2D

We aimed to characterise the production and localisation of the major capsid protein L1 within epithelial cells as they differentiate. Initially, we used W12E cells grown in 2D on a 3T3 fibroblast layer, fixed cells from day 4 to day 15 and stained for L1 (Figure 5.2). W12E cells grown in 2D are known to begin differentiating at day 7 (Milligan *et al.*, 2007; Veerapraditsin, 2004). There was a small amount of cytoplasmic L1 within undifferentiated cells at day 4, as previously observed (Figure 5.2) (Milligan *et al.*, 2007). Following W12E cell differentiation, the expression of L1 increased (Figure 5.2, day 8 - 15). Staining was exclusively cytoplasmic in all cells fixed up to and including day 10 (Figure 5.2). After 15 days of growth, the majority of staining was still cytoplasmic but it now appeared filamentous, with parallel lines of staining across the cell (Figure 5.2). Moreover, condensates of brightly stained spots were visible around the cell periphery (Figure 5.2). We collected z-stacks to visualise how L1 staining changed throughout the thickness of W12E cells fixed at day 15. Slices through the nucleus revealed most cells to have exclusively cytoplasmic L1 although a few showed diffuse nuclear L1 staining (Figure 5.3A). Within these cells, L1 was excluded from the nucleoli (seen as holes in the DAPI stain) (Figure 5.3A, white dashed ovals outline the nucleoli). When moving to planes just above or below the nucleus of the same cells, punctate spots of L1 staining could be observed (Figure 5.3B, red-boxed cell). These may be capsomeres of L1 that are being imported into the nucleus or may represent HPV nuclear assembly sites depending on their positioning inside or on the periphery of the nucleus.

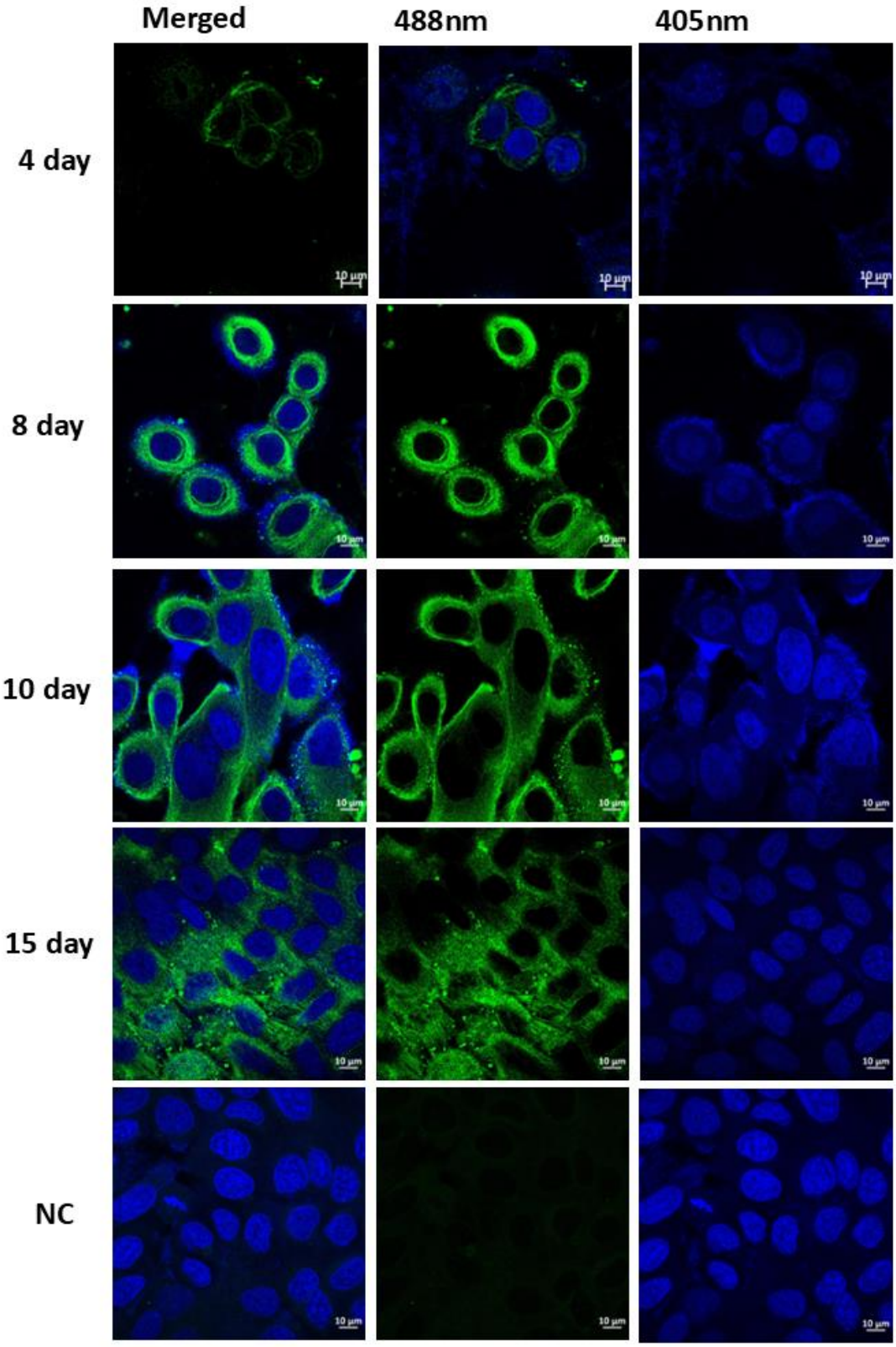

Figure 5.2: HPV16 L1 staining of W12E cells grown in 2D. Immunofluorescent staining of L1 (green, 488 nm) and cell nuclei (blue, 405 nm) in W12E cells. Cells were grown for up to 15 days on a 3T3 fibroblast layer. Cells were fixed at days 4 to 15 of growth to show L1 expression and localisation in undifferentiated cells (before day 7) and differentiated cells (after day 7). A no-primary negative control sample was imaged and processed identically. The merged 488nm (L1) and 405nm (DAPI, nuclear stain) channels are shown as well as individually. Results are representative of three individual experiments. Scale bars = 10 μm.

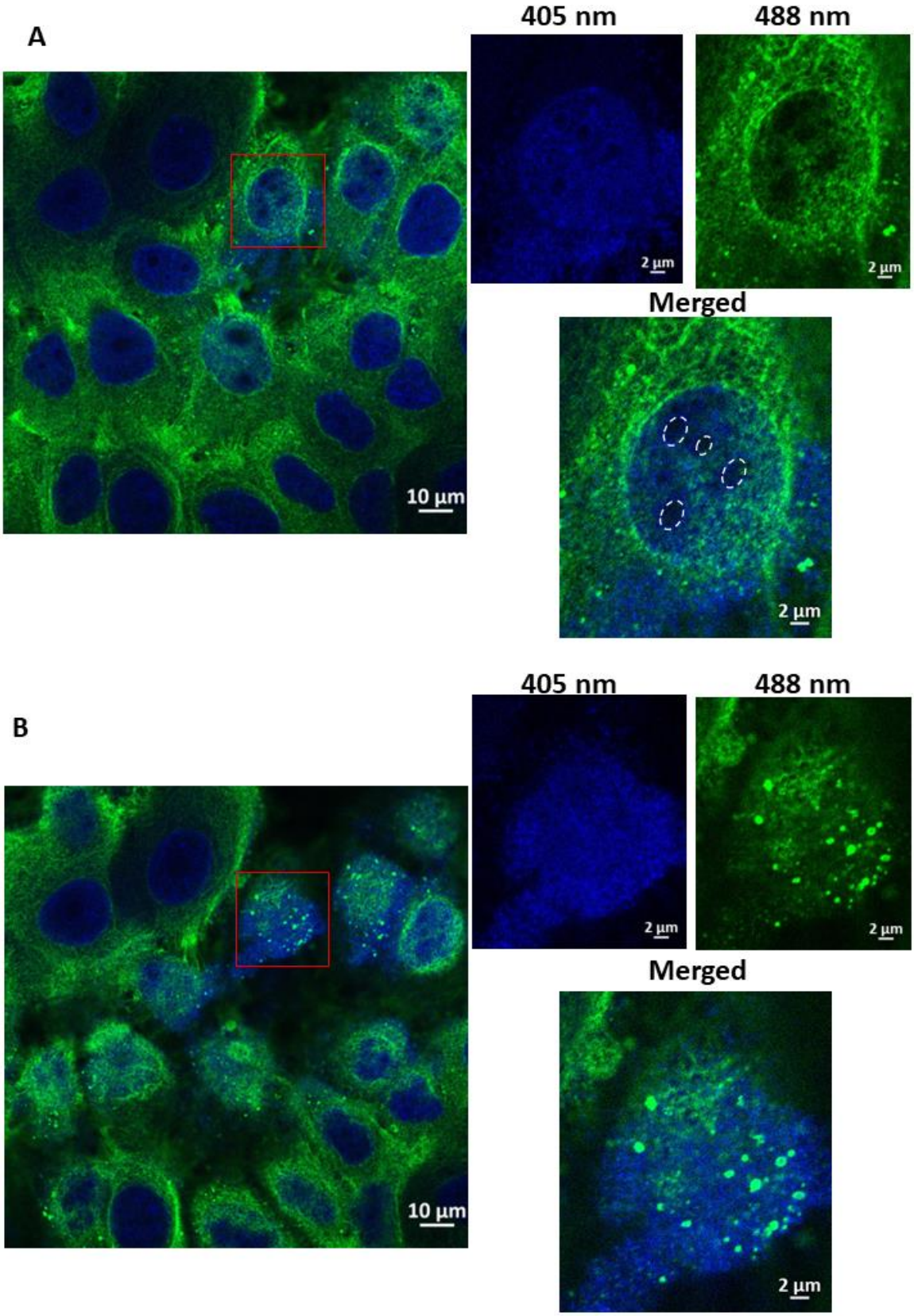

Figure 5.3: L1 localisation throughout differentiated 2D W12E cells. Immunofluorescent staining of L1 (green, 488 nm) and cell nuclei (blue, 405 nm) in 15-day W12E cells. A z-stack was performed with images taken every 0.57 µm for a total of 10 images. Images collected in the plane of the nucleus (A) and in line with the top of the nucleus (B) for the same cells are shown. The cell enclosed by the red box is shown at different z heights enlarged on the right-hand side. Results are representative

of three individual experiments. Scale bars = 10 μm and 2 μm for the full-sized and zoomed, single cell images respectively.

5.3 Ultrastructural imaging of differentiated W12E cells grown in 2D to determine if virion assembly takes place

We subsequently used a correlative light and electron microscopy (CLEM) approach to determine if we could gain additional insights into the location of these brightly stained spots of L1. CLEM is a powerful technique that allows the identification of molecules of interest within cells by fluorescent labelling and light microscopy (LM) followed by high-resolution imaging of these features by electron microscopy (EM) (de Boer, Hoogenboom and Giepmans, 2015). The resulting overlay of the images adds resolution and cellular context to light microscopy observations whilst the fluorescent signal enables target identification in the EM images. We aimed to use CLEM to determine if the fluorescently labelled clusters of L1 visualised by confocal microscopy were inside or outside the nucleus and thus identify if these were HPV replication factories or capsomeres being transported into the nucleus. Cells were grown for 15 days on gridded glass-bottomed dishes (Figure 5.4A, B), fixed, antibody labelled for L1 and imaged by confocal microscopy. Immunofluorescence data was collected for cells of interest and the location of the cells could be determined on the grid using differential interference contrast (DIC) (Figure 5.4C). Cells were subsequently negatively stained, and resin embedded. Following detachment of the resin from the glass coverslip, the resin face retains an imprint of the grid such that cells can be relocated (as described in (Hanson *et al.*, 2010)) (Figure 5.4D). The face of the resin block was then trimmed and cut as thin resin sections to isolate cells of interest and subsequently, imaged and analysed by EM.

Cells visualised by confocal microscopy showed a similar L1 staining pattern to that previously observed (Figure 5.5A). Following resin embedding, the grid and cells could be visualized as they had been effectively transferred into the face of the resin (Figure 5.5B). A face was cut into the resin, around the region of interest that had been imaged by confocal microscopy and thin sections were taken from this area. When imaged by EM, these cells had intact nuclear membranes but the cellular membranes were disrupted (Figure 5.5C, D). This could have been due to dehydration during processing.

Limited conclusions can be made about the cell structures due to the disintegration of the cell membranes and no virions could be visualised within the W12E cells differentiated in 2D. Due to the lack of cellular membranes, it is possible that if L1 clusters seen by IF were putative L1 capsomeres awaiting nuclear import, these structures may have been disrupted following cell membrane breakdown. The breakdown of cellular membranes also made it difficult to identify cells to produce an overlay of the LM and EM images. Overall, our analysis of L1 staining within 2D W12E cells revealed an increase in the production of the major late capsid protein within differentiated cells, in line with previous reports (Milligan *et al.*, 2007). The majority of this staining was cytoplasmic and although brightly stained spots could be visualized just above the nucleus of cells grown to 15 days, these did not correspond to observable virions by EM analysis.

It is probable that cells cultured in 2D may not differentiate enough to represent the terminally differentiated cells of the epithelium where HPV assembly takes place and 3D models may instead be required to mimic this fully. Therefore, our subsequent CLEM analysis made use of 3D models of W12E cells to maximise the chance of visualizing HPV assembly.

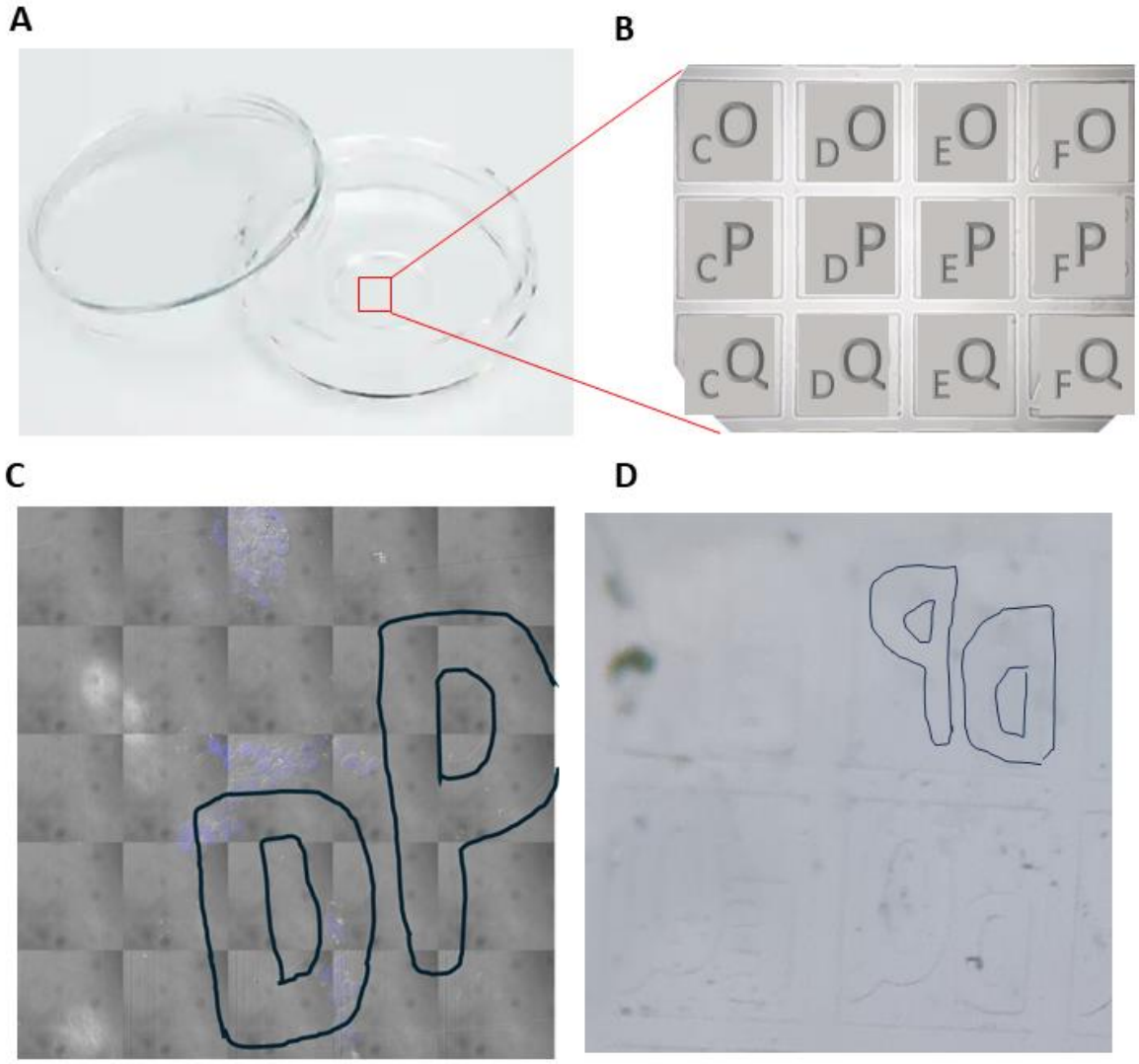

Figure 5.4: Method for indirect CLEM analysis of W12E cells. (A) W12E cells were grown for 15 days on gridded, glass-bottomed 35 mm dishes (Mattek). (B) The gridded coverslips at the base of the dish have a unique alphanumeric pattern within each square to enable location of cells. (C) Cells imaged by confocal microscopy can be located on the grid using the DIC channel. This is overlaid with DAPI staining from the 405 nm channel to confirm the presence of cells. The grid markings are outlined here to enable easier identification. (D) The cells were then negatively stained and embedded into resin. Once the polymerised resin surface is detached from the surface of the glass dish, it retains an imprint of the grid on the surface. This allowed relocation of the cells that had been imaged by confocal microscopy and resin sections could be cut from this area for an indirect CLEM approach.

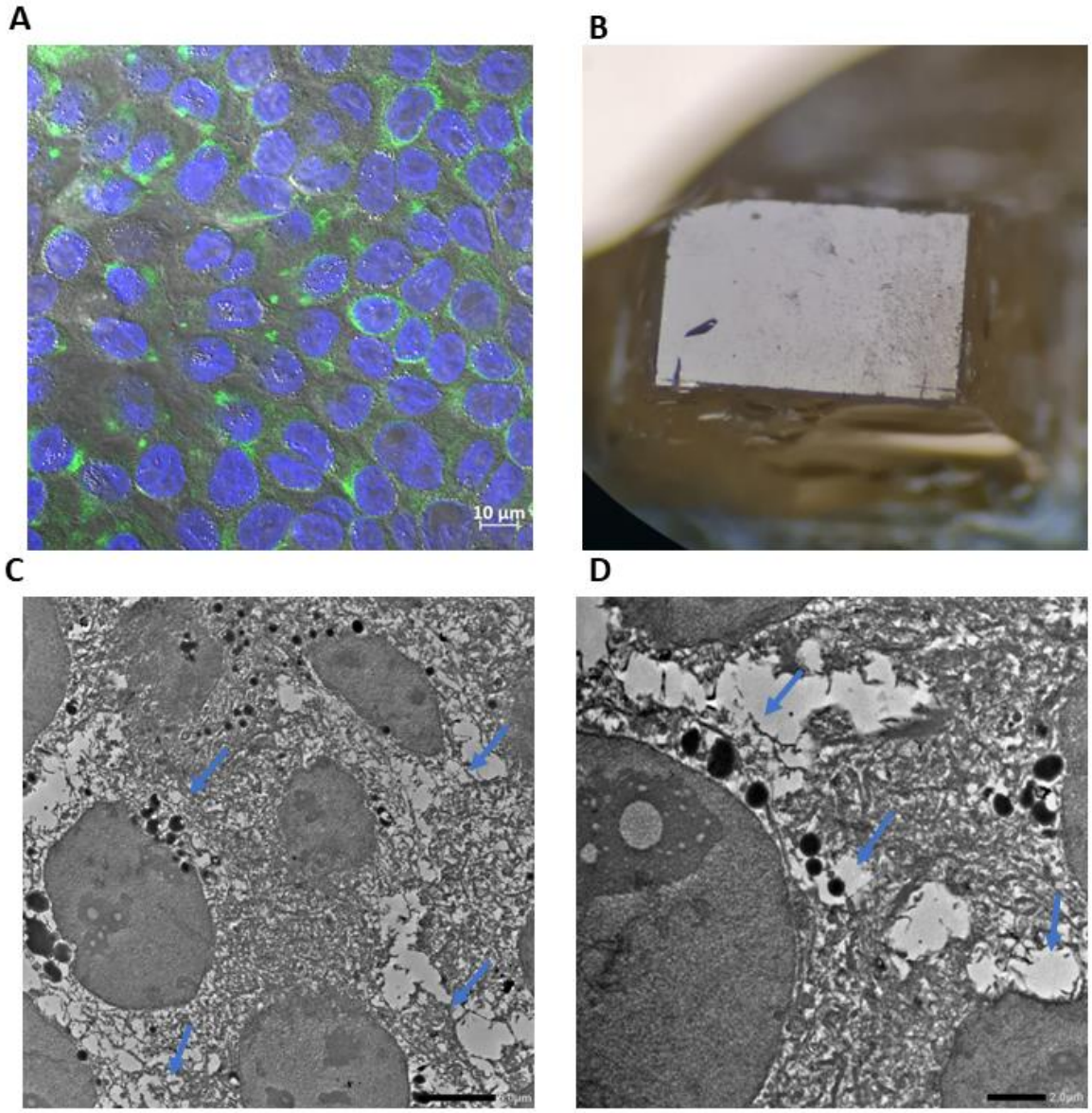

Figure 5.5: Indirect CLEM analysis of W12E cells differentiated in 2D. (A) Immunofluorescent staining of L1 (green, 488 nm) and cell nuclei (blue, 405 nm) in W12E cells grown to 15 days on gridded, glass-bottomed 35 mm dishes (Mattek). (B) The grid of the Mattek dish was imprinted in the resin surface and allowed relocation of the cells that had been imaged by confocal microscopy. The resin was trimmed to create a surface isolating the cells of interest and sections taken from this. (C, D) Resin sections containing W12E cells grown to 15 days in 2D were imaged by EM. Blue arrows indicate the loss of the cell membrane. Scale bars = 10 µm, 5 µm and 2 µm in (A), (C) and (D) respectively.

5.4 Expression and localisation of the HPV major capsid protein L1 within differentiated W12E cells from 3D organotypic raft cultures

To better resemble the epithelial environment that is known to be important for human papillomavirus virion assembly (Pyeon *et al.*, 2005), we extended our analysis of L1 cellular localisation to 3D organotypic raft cultures. Immunofluorescence in tissue sections often results in a lot of autofluorescence and limited resolution, which would make it difficult to identify staining patterns within nuclei. Moreover, tissue sections (2.5 µm) do not allow for the entire thickness of the cell to be visualised. To overcome this and enable spatial analysis of L1 expression within the differentiated cells of 3D tissues to a high resolution, we developed a technique to study the cells within the top layer of W12E organotypic rafts for CLEM analysis. W12E rafts were inverted onto a pre-heated gridded glass-bottomed dish. The cells at the top of the raft attached to the glass such that once the tissue was removed, a layer of cells remained on the glass, which represented the upper, most differentiated layer of the W12E raft. These cells were then fixed and processed for immunofluorescence. This overcame the size constraint of tissue sections (2.5 µm) and enabled entire cells to be stained and imaged to high resolution.

Almost all cells that were derived from the most differentiated layers of W12E tissues stained positive for L1. Specifically, three L1 staining phenotypes could be observed (Figure 5.6A, B). Cells showed either no nuclear L1 staining (phenotype A), diffuse L1 nuclear staining, which was absent from the nucleoli and areas of dense nuclear material (phenotype B) or tightly condensed spots (foci) of L1 staining (phenotype C). Phenotype A most closely resembles the majority of L1 staining seen in differentiated W12E cells grown in 2D (Figure 5.3, Figure 5.6B). However, the minority of cells differentiated in 2D that showed nuclear staining best resembles phenotype B, with diffuse nuclear staining (Figure 5.3, Figure 5.6B). All phenotypes showed speckled L1 staining at the nuclear periphery (Figure 5.6A, B). We propose that this may be the translation of L1 taking place at the polysomes, which tightly associate with the ER at the nuclear boundary (Duan *et al.*, 2020). In cells with the staining pattern C, the L1 foci never colocalised with DAPI, with holes in the DAPI staining at these sites (Figure 5.6B). These DNA-free spaces could represent nucleoli or the high concentration of

HPV proteins in these areas excluding DNA. The staining patterns of each phenotype did not vary throughout the cell, as demonstrated by z-stacks that traversed the full width of the cell (Supplementary Figure 5.1).

To determine if cells progressed between these observed phenotypes over time, we quantified the number of cells demonstrating each staining phenotype on days 10, 14, and 16 of organotypic raft growth (Figure 5.6C). At day 10, most cells had either no nuclear staining (A) (43%) or diffuse nuclear staining (B) (56%), with very few cells showing discrete L1 staining spots (C) (Figure 5.6C). At day 14, the number of cells with no nuclear staining had decreased and 72% had diffuse nuclear staining (Figure 5.6C). Therefore, cells may progress from phenotype A to B as L1 is transported into the nucleus (Buck, Day and Trus, 2013). The number of cells with L1 foci increased over time to a maximum at day 16, although this was still a rare observation, with 12% of cells showing this phenotype (Figure 5.6C). The observed proportion of cells with foci staining patterns is similar to previous reports (Kieback and Müller, 2006). The increase in cells with foci staining (phenotype C) correlated with a decrease in cells with diffuse nuclear staining (phenotype B) at day 16. Therefore, we propose that staining phenotype B may be a precursor to C. Strengthening this hypothesis are observations of cells containing diffuse nuclear staining with brightly stained spots that may represent intermediates between B and C (Figure 5.7). Some of these 'intermediates' contain a lot of diffuse nuclear L1 staining and might be early in the transition from B to C whilst others have much less diffuse L1 staining and may represent later B-C intermediates (Figure 5.7).

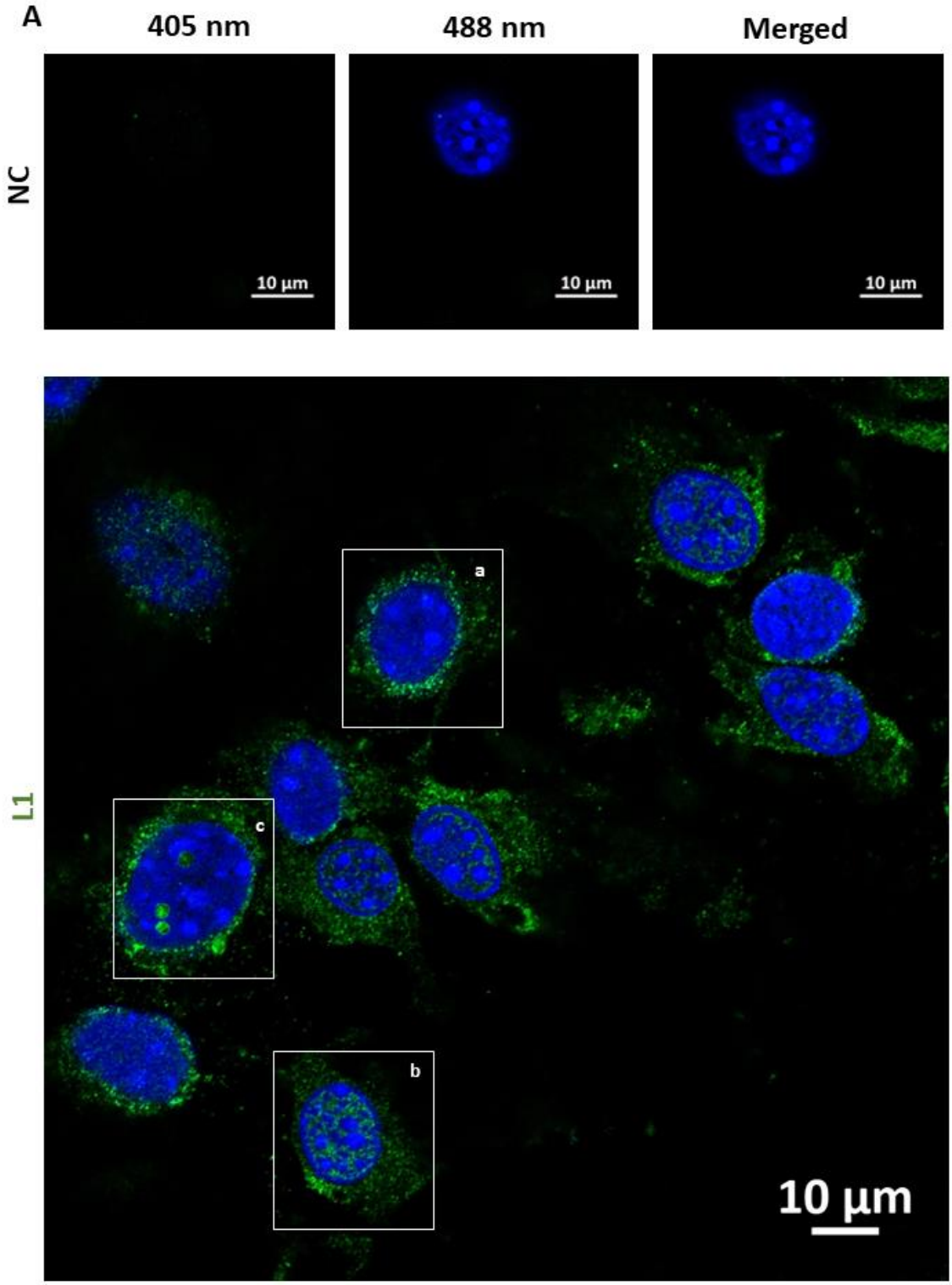
A
405 nm
488 nm
Merged
NC
10 µm
10 µm
10 µm
L1
a
b
c
10 µm

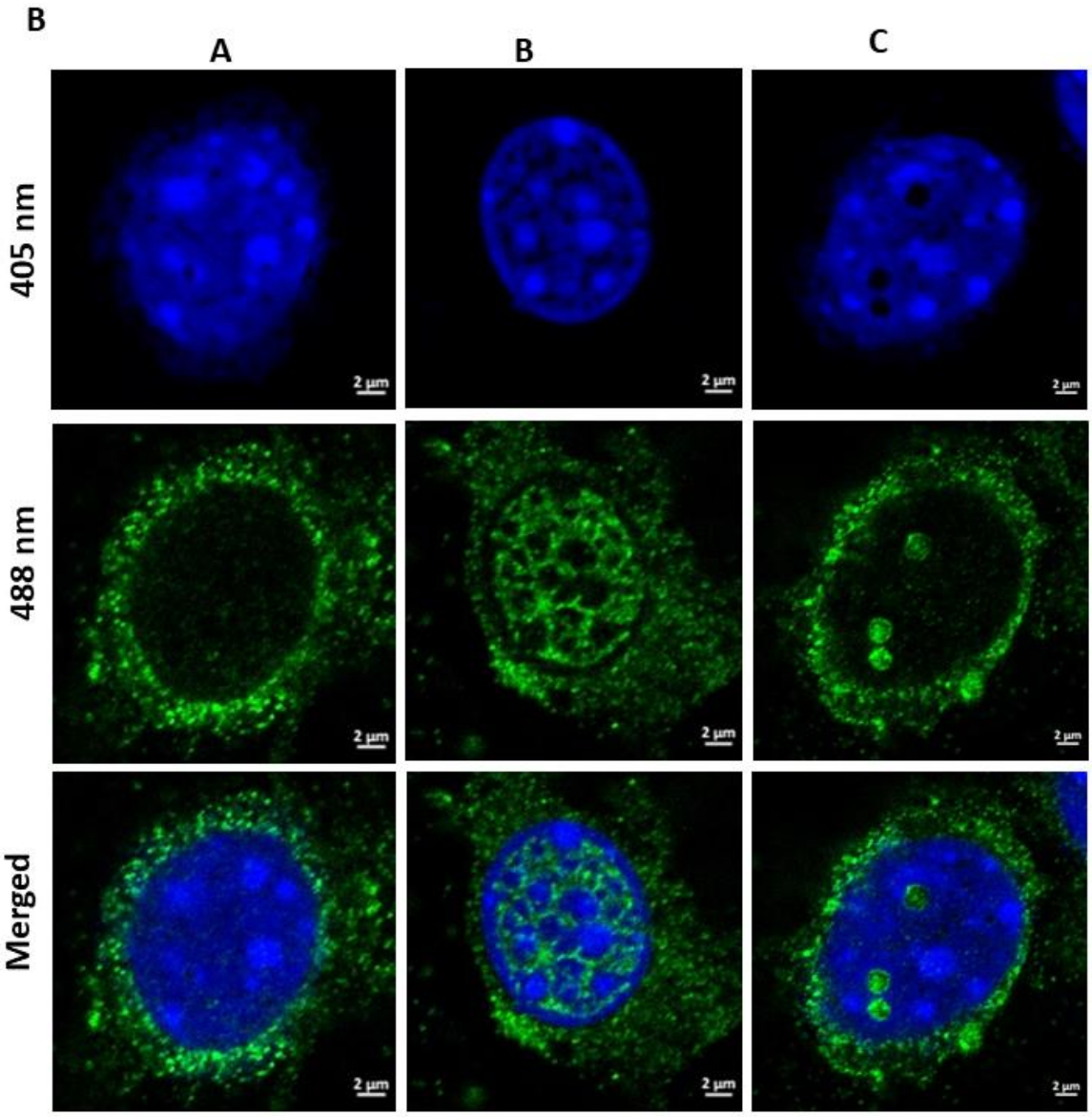
B
A
B
C
405 nm
488 nm
Merged
2 µm

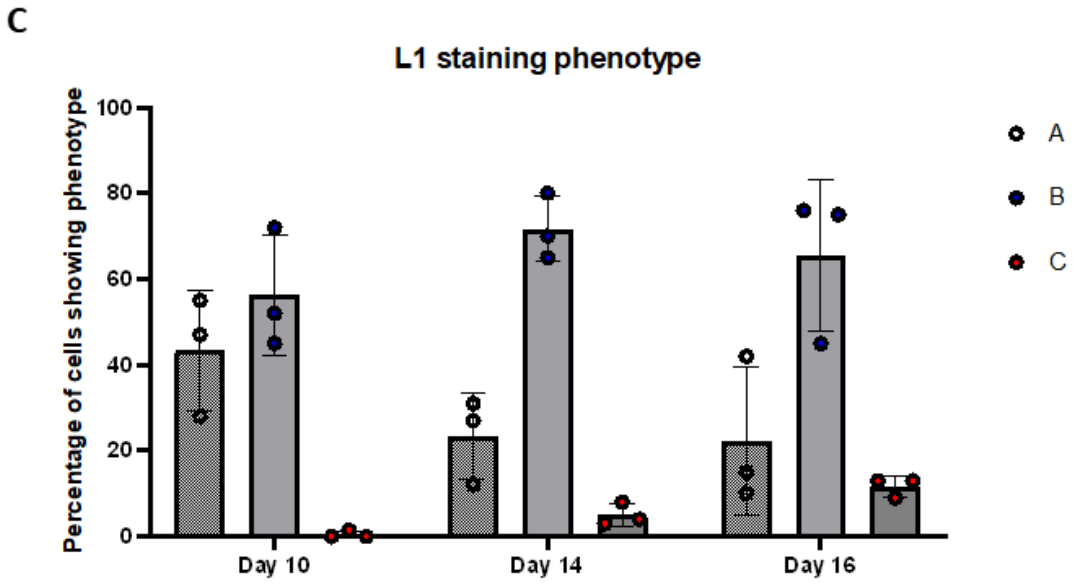

Figure 5.6: Staining pattern of L1 in W12E cells differentiated in 3D changes over time. (A) Immunofluorescent staining of L1 (green, 488 nm) and cell nuclei (blue, 405 nm) in cells derived from the top of W12E organotypic rafts. A no-primary antibody negative control sample was imaged and processed identically (top row). Three phenotypes of L1 staining can be observed, which are shown as zoomed-in images (B): no nuclear staining, diffuse nuclear staining or discrete foci of nuclear staining (denoted phenotypes A, B and C). Scale bars =10 μm and 2 μm for (A) and (B) respectively. (C) Cells derived from the top of rafts grown to day 10, 14 or 16 were stained for L1 and the number of cells in each phenotypic group was quantified. At least one hundred cells were counted for each biological replicate and three individual experiments were carried out. Each dot represents the percentage of cells with that staining pattern from each replicate and the mean and standard deviation are displayed.

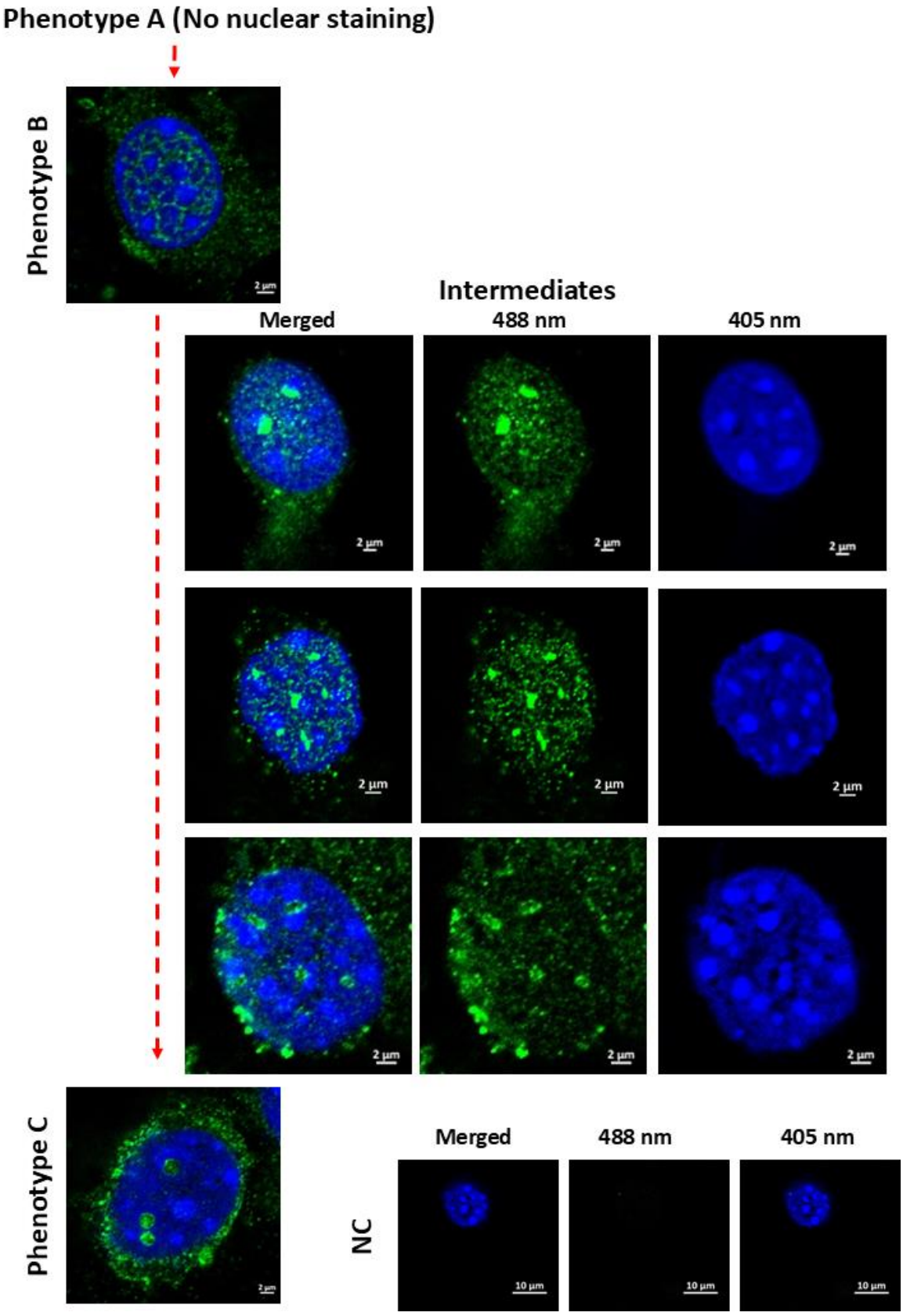

Figure 5.7: Proposed development of L1 nuclear staining over time. Immunofluorescent staining of L1 (green, 488 nm) and cell nuclei (blue, 405 nm) in cells derived from the top of W12E organotypic rafts. We propose that phenotype A progresses to phenotype B as L1 is transported into the nucleus at later times in cell differentiation. Following this and due to the accumulation of cells with phenotype C

and reduction in cells with phenotype B, we propose that as cells terminally differentiate, they may progress from staining phenotype B to C. Staining patterns that appear to be intermediates along this pathway are shown in the panels on the right with L1 (488 nm) and nuclear staining (405 nm) alone or merged. A no-primary antibody negative control sample was imaged and processed identically (bottom right row). Scale bars = 2 μm for all images except NC where scale bars = 10 μm.

5.5 L1 clusters within the nucleus are composed of multiple independent fragments

We wished to gain further detail on the composition of L1 foci within differentiated cells from the top layers of epithelial organotypic rafts to determine if these were structured clusters of L1, such as assembling virions or capsomeres. Full-thickness z-stacks through a cell demonstrating an intermediate between phenotypes B and C that contained L1 foci and some diffuse staining throughout the nucleus were captured using Airyscan to enable high resolution (Figure 5.8A, B). Z-stacks were subsequently rendered using Imaris software to fit a surface over the immunofluorescence data and provide definition to structures within the cell (Supplementary video 1, Figure 5.8C). Clusters of L1 can be observed that fill 'holes' in the nucleus (Figure 5.8C, D). Whilst these appear as one cluster of staining when visualised as a 2D slice through the cell, 3D reconstruction reveals these L1 foci to be comprised of multiple independent staining fragments (Figure 5.8C, D). Two such clusters are shown in detail in the orange and red boxes (Figure 5.8). The remainder of L1 staining outside of these foci appears as smaller clusters and as individually stained molecules. Some L1 staining was also observed outside of the nucleus with some clusters of L1 staining, which were smaller than those within the nucleus. Clusters within the perinuclear space (Figure 5.8C) mirror those seen in Figure 5.6 and may represent the translation of L1 at the polysomes. However, the negative control also contained a small amount of staining outside of the nucleus. This likely represents cellular debris from the top of the tissue, which autofluoresces and may limit the confidence in the cytoplasmic staining observed (Figure 5.8E). However, no nuclear staining was observed in the negative control, so we have confidence that the nuclear L1 staining is true. Overall, the foci of L1 observed in differentiated W12E cells from the top of organotypic rafts contain multiple structures and may represent organised assembly sites.

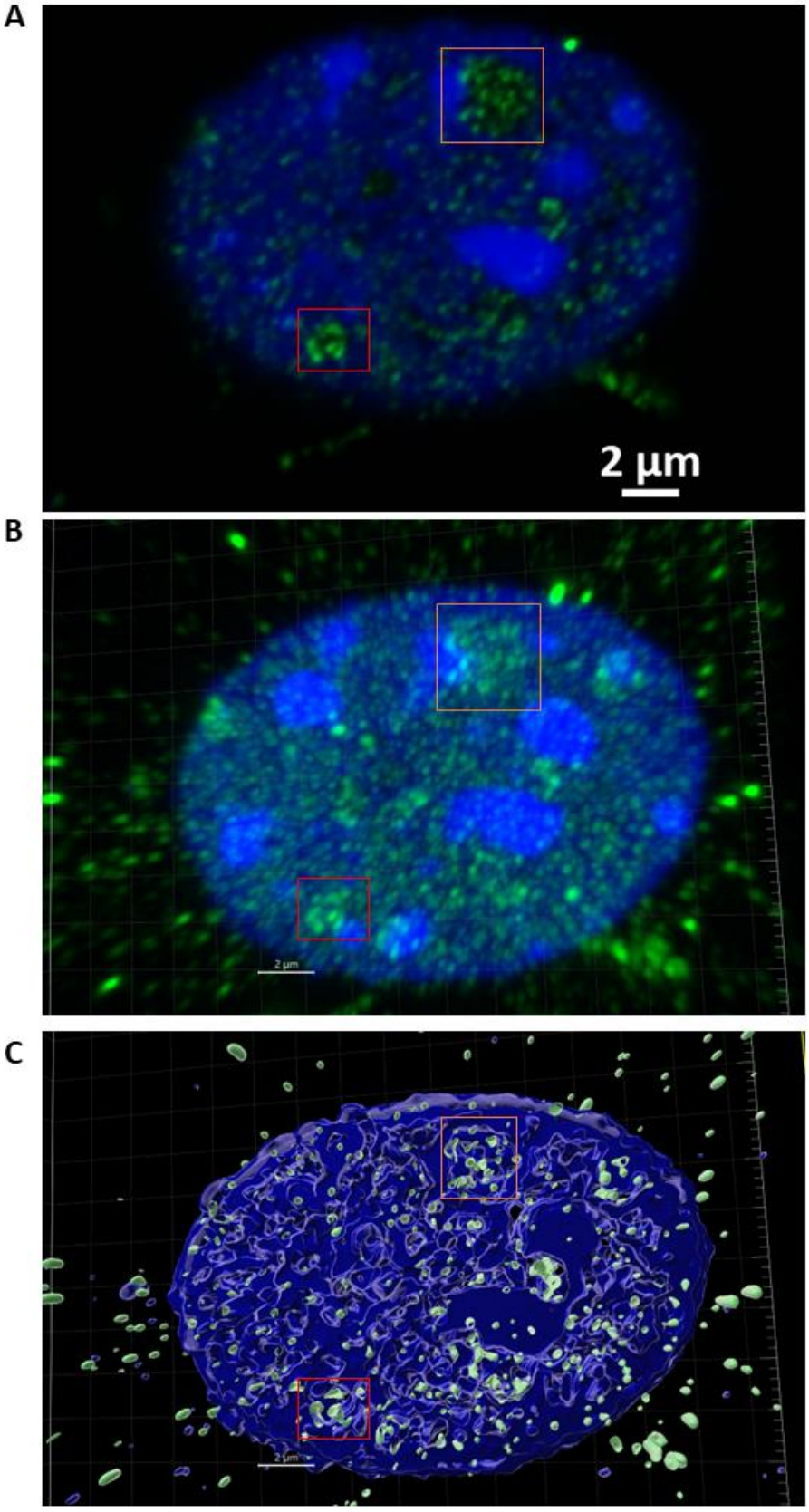
A
2 µm
B
C

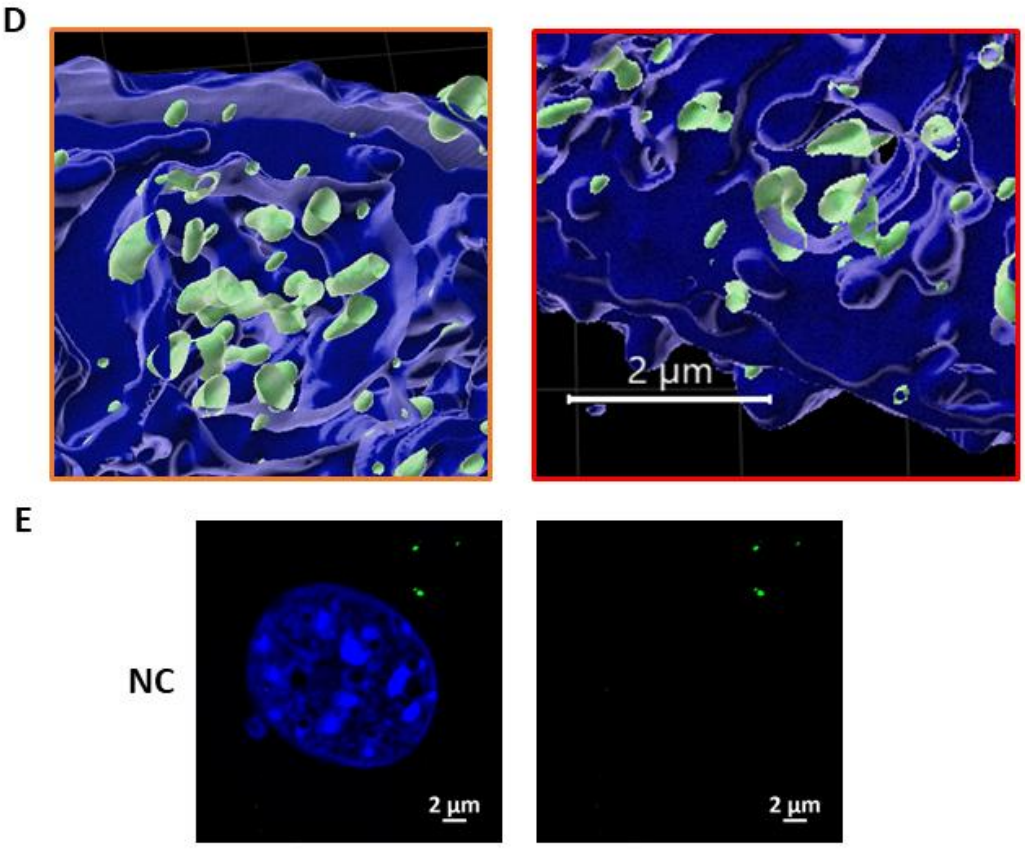

Figure 5.8: Intranuclear foci of L1 are composed of multiple structured particles. Immunofluorescent staining of L1 (green, 488 nm) and cell nuclei (blue, 405 nm) in cells derived from the top of W12E organotypic rafts. A z-stack was collected with images taken every 0.2 µm for 40 slices to capture the full thickness of the nucleus. (A) A 2D image of a single slice through the z-stack. (B) Each slice was compiled to produce a maximum intensity projection (MIP) of the L1 staining throughout the cell. (C) Imaris was used to render a surface over the nucleus and L1 staining, which allows for structures within the cell to be visualized. The orange and red boxed images of foci staining in A, B and C are shown magnified in (D). Here, the surface generated by Imaris shows these foci to be composed of multiple structured particles. (E) A no primary antibody control was imaged and processed identically to the previous images. A small amount of signal can be observed outside of the nucleus, which we propose is due to autofluorescence from debris derived from the top of tissues. Scale bars = 2 µm.

5.6 EM analysis of W12E tissues reveals viral-like particles in the upper layers

To gain further understanding of what each of these observed phenotypes of L1 staining may represent in terms of the viral life cycle and virion assembly, we attempted the CLEM approach described previously for the cells derived from the top of W12E organotypic rafts (Section 5.4) (Hanson *et al.*, 2010). Unfortunately, this approach was unsuccessful, with no cells detected within the resulting resin sections. We suggest that this may be due to not having a high enough confluence of cells that come off during the rafts being inverted onto the coverslip. This makes it difficult to detect adequate cells within the resin when imaging by electron microscopy. Another limitation involved the cell location at the front of the resin face. Some of the face is removed during the polishing steps which may have resulted in the resin containing the cells of interest to have been lost before sections were taken for imaging. Instead, we opted to process whole 3D organotypic raft cultures directly for EM analysis. Small 1 mm^3 sections of tissue were cut from W12E tissues, negatively stained and processed for TEM. Tissues were fixed in resin such that a cross-sectional slice of the tissue (including the collagen layer and then up through the full thickness of the cell layers) could be imaged. This approach was successful and allowed cross-sectional analysis of W12E organotypic raft tissues (Figure 5.9). It was difficult to image the full thickness of the raft as the grid bars of the copper TEM grids occluded some layers (Supplementary Figure 5.2). Nevertheless, layers of undifferentiated and differentiated cells can be visualised in one grid square and cells at the top of the tissue had differentiation phenotypes including flattening of the cell and nucleus, and in some cases nuclear breakdown (Matsui and Amagai, 2015). A dense fibrous network can also be observed within cells in the upper layers of the tissue, with tightly interconnected fibres and the darker appearance of cells in the upper cells compared to the basal and mid-layer cells due to the density of proteins within these cells (Figure 5.9). The W12E cells differentiated in 2D appeared more similar to cells within the mid-layers of the organotypic raft cultures, as they still had intact nuclear membranes and did not contain the dense fibrous network of cells at the top of organotypic rafts (Figure 5.5C, Figure 5.9). This suggests that it is difficult to reproduce the later stages of differentiation that take place within tissues in 2D culture.

Cells within the upper layers of the epithelium contained darkly stained spheres within the nucleus (Figure 5.10). These particles had a diameter between 44 – 55 nm and may represent HPV virions, however, there was some variability in shape and size (Figure 5.10B, D). This variability could be due to differences in the assembly progression of these particles or due to differences in capsid maturation. Disulphide bonds between neighbouring L1 capsomeres are required for the maturation of capsids from relatively unstructured, physically fragile structures to stable, tightly formed capsids (Buck *et al.*, 2005). The redox environment of cells is important for the development of these disulphide bonds and it has been proposed that this process does not take place within the reducing environment of living cells but only within the oxidising environment of cells at the surface of the epithelium (Buck *et al.*, 2005; Wang *et al.*, 2009; Buck, Day and Trus, 2013). Some cells in the upper layers of W12E rafts contained dense clusters of darkly stained material (Figure 5.11A-D). These resemble the aggregates of VLP's observed previously in the literature (Flores *et al.*, 1999) (Figure 5.11E) and could represent the staining phenotype C, with foci of L1 staining limited to discrete areas of the nucleus. It is tempting to speculate that these particles are HPV virions, however, due to the variability in size, it would be important to confirm our observations with immunogold labelling of L1 to determine that these structures are composed of viral proteins.

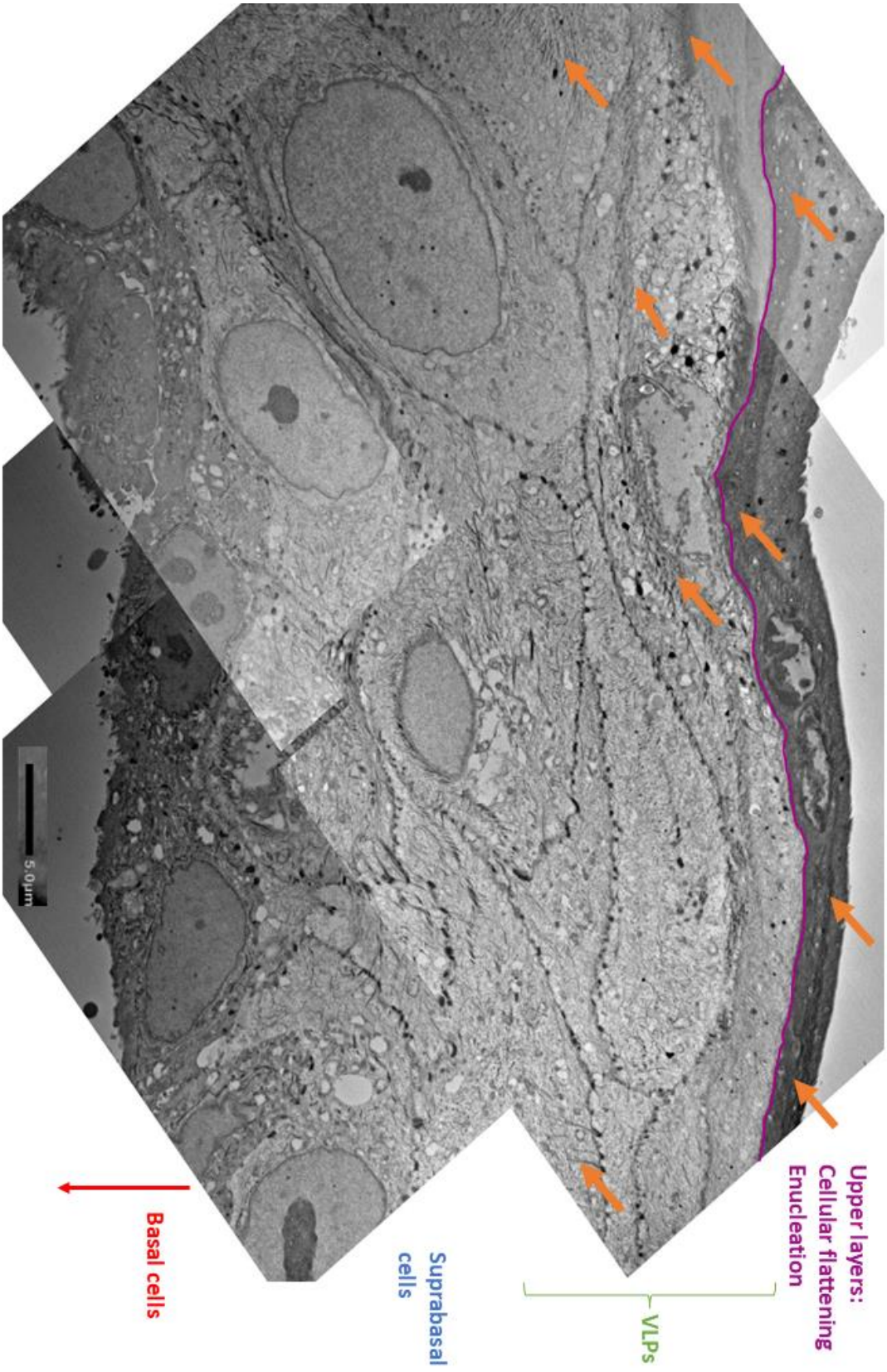

Figure 5.9: Cross-sectional EM analysis of a W12E organotypic raft. W12E organotypic rafts were grown for 14 days at the air-liquid interface, fixed and dissected to produce 1 mm^3 sections of tissue. These tissue blocks were negatively stained and embedded in resin. Thin resin sections were cut and analysed by TEM. The cross-section through part of a raft is shown. The full thickness of the tissue was not visible

due to the gridlines of the copper grids occluding part of the tissue (Supplementary Figure 5.2). The upper differentiated layers are annotated by a purple line. Here, cellular flattening and enucleation can be visualised and a dense fibrous network is formed (with fibres indicated by orange arrows). Below this are the suprabasal cells. The approximate cell layers in which viral-like particles were observed across tissues is indicated by the green brace. The tissue had a small tear, likely due to processing events so the break in the tissue at the bottom of the image does not represent the bottom of the tissue as basal cells and the collagen layer could still be visualised below the copper grid lines (data not shown).

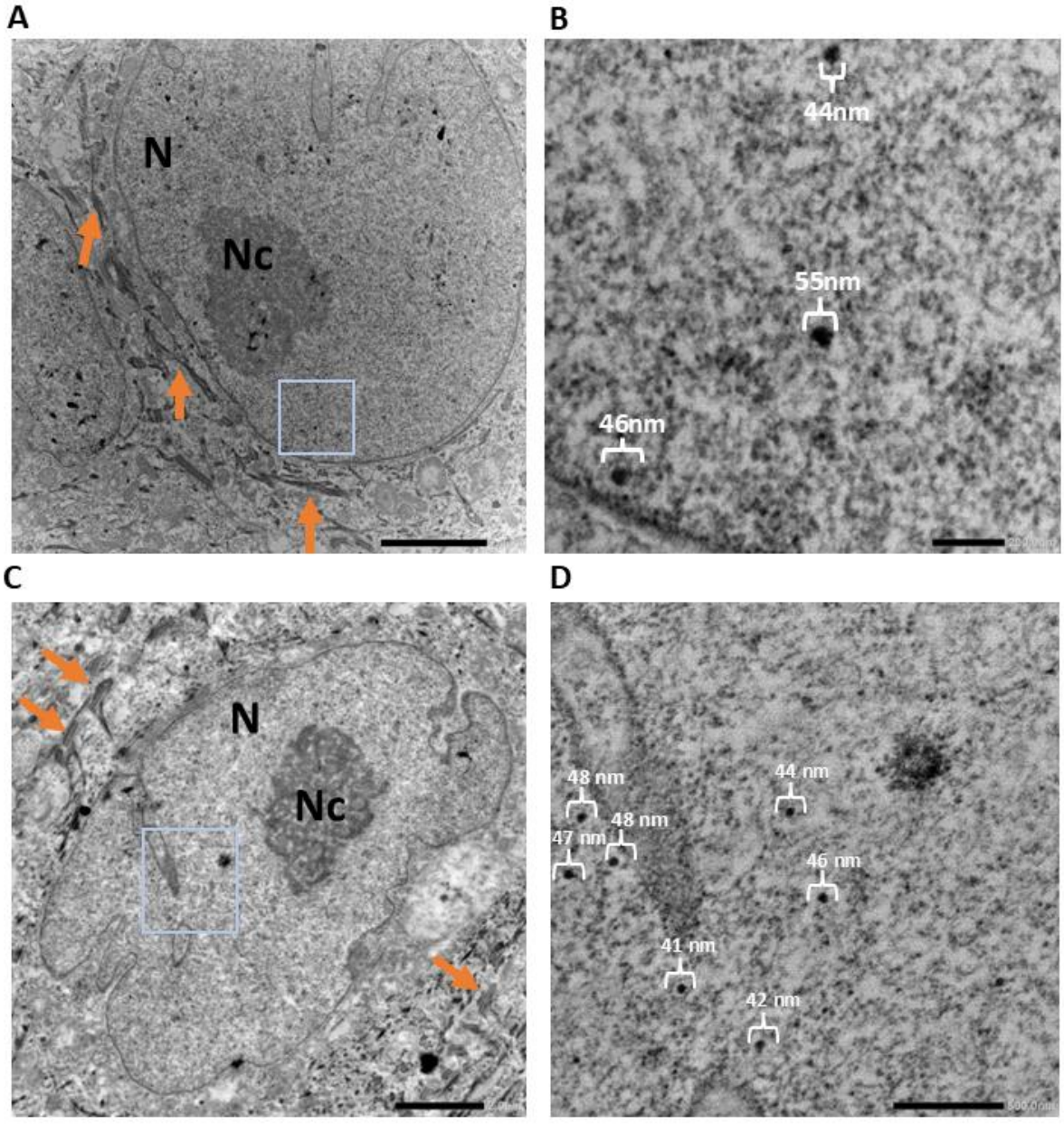

Figure 5.10: Size determination of negatively stained particles within the upper layers of W12E organotypic rafts. EM images of W12E organotypic rafts negatively stained and embedded in resin. (A & C) Cells in the upper epithelial layers contain darkly stained spheres which resemble viral-like particles. These cells still contain intact nuclear membranes and the nucleus and nucleolus are denoted by N and Nc

respectively. Orange arrows show keratin granules which demonstrate these cells are within the upper epithelial layers. The blue boxes are magnified in the right-hand panels. (B & D) Size determination of darkly stained particles within cells in the upper epithelial layers of W12E organotypic rafts. ImageJ was used to determine the diameter of darkly stained particles using the scale bar as a reference. Representative images from two biological replicate W12E rafts. Scale bars = 2 μm (A & C), 200 nm (B) and 500 nm (D).

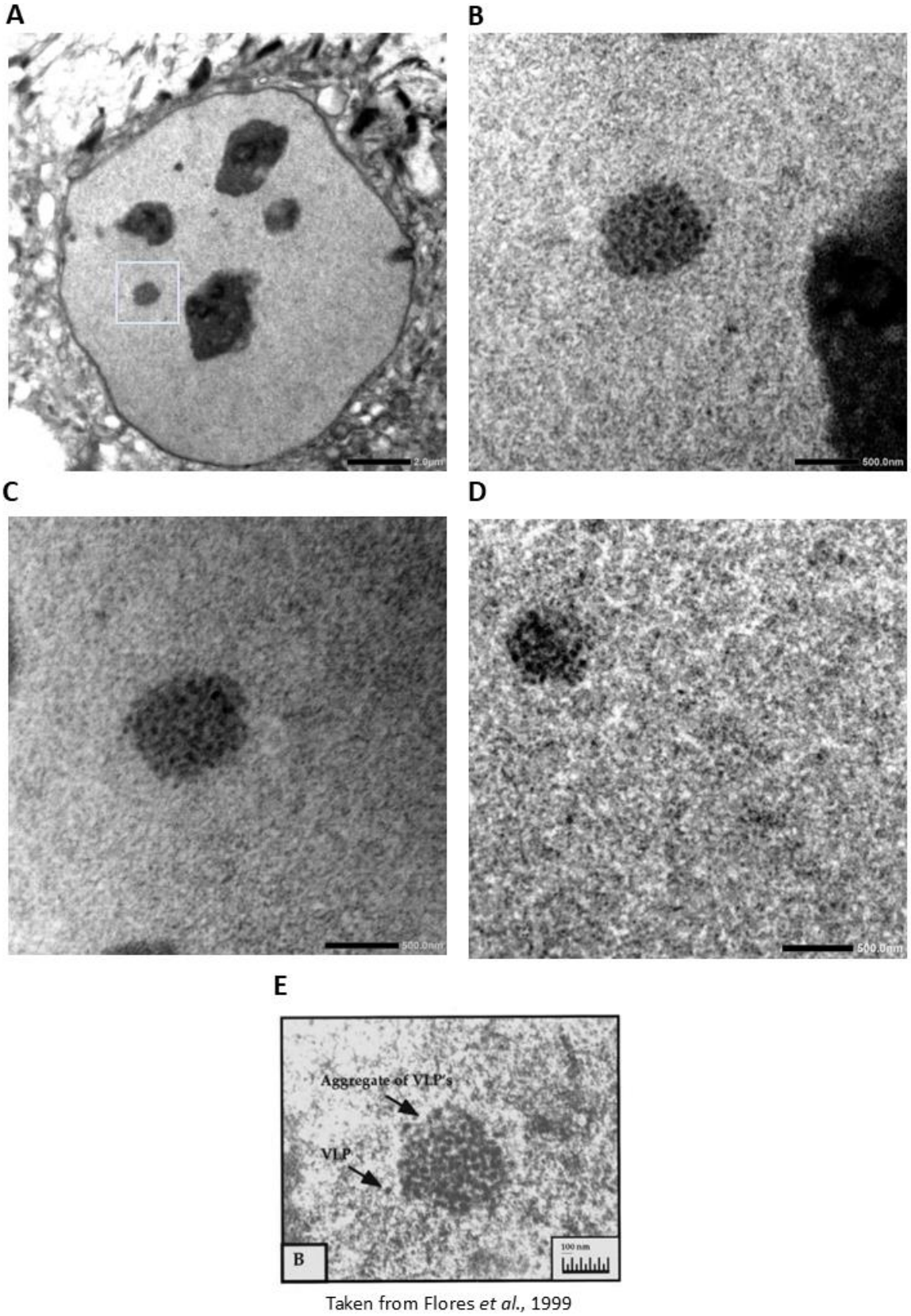

Taken from Flores *et al.*, 1999

Figure 5.11: Aggregates of virus-like particles in the upper layers of W12E organotypic rafts. EM images of W12E organotypic rafts negatively stained and embedded in resin. (A) Differentiated cell in the upper epithelial layers that showed densely stained areas with a different composition to nucleoli. Blue boxed region is zoomed in on the right-hand side (B). (C, D) Similar densely packed, darkly stained aggregates of viral-like particles were observed within biological replicates. These

appear similar to the VLP aggregates shown by Flores and colleagues (E) (Flores *et al.*, 1999). Scale bars = 2 μm (A), 500 nm (B, C &D) and 100 nm (E).

5.7 Microwave treatment reduces L1 nuclear expression

Following our characterisation of L1 expression and localisation within W12E tissues, we aimed to understand how microwave treatment affected this. We repeated the quantification of cells within phenotypes A, B and C following microwave treatment. Rafts were inverted for treatment after 14 days of growth onto gridded glass-bottomed dishes and cells coming off the top of tissues were immediately fixed to provide a 0H time point. Microwave treatment reversed the normal progression of L1 localisation observed during differentiation, as the proportion of cell staining patterns within tissues fixed immediately after treatment (0H) resembled that of mock-treated tissues at day 10 (Figure 5.12). The number of cells with diffuse nuclear staining (pattern B) had reduced in comparison to mock-treated tissues at the same time point (52% from 72%) and the number of cells with no nuclear staining had increased (pattern A) (41% from 23%) (Figure 5.12). Cells derived from the treated area had abnormal looking nuclei with no nuclear L1 staining (Figure 5.13A). Instead, L1 was disorganised around these cells, possibly due to the degradation of nuclear or cellular membranes following microwave treatment (Figure 5.13A). The majority of cells that were derived from the distal sites of treated tissues showed diffuse nuclear staining at 0H post-treatment, similar to mock-treated tissues (Figure 5.13A). Therefore, cells at the site of treatment are responsible for the reduction of phenotype B in tissues 0 hours post-treatment (Figure 5.12, Figure 5.13A).

To create a 16-hour time-point, treated tissues were incubated at 37 °C for 16 hours following treatment and subsequently inverted onto a pre-heated glass-bottomed dish and the cells were fixed. Again, microwave treatment was observed to reverse the changes normally associated with differentiation. Cells derived from 16H treated tissues had continued to lose nuclear L1 staining with 66% of cells classified within phenotype A (from 41% at 0 hours post-treatment) (Figure 5.12). The cells that were derived from the treated areas of rafts had nuclei that were undefined with chromatin condensation evident, which could represent cells committing to apoptosis (Figure

5.13A). Moreover, these cells showed very little L1 staining in either the nucleus or cytoplasm, similar to observations at 0 hours post-treatment. At 16 hours post-treatment, a lot of cells distal from the site of treatment had also lost nuclear L1 staining, which may be responsible for the rise in phenotype A in comparison to 0 hours (Figure 5.12, Figure 5.13A). Overall, microwave treatment not only reduces L1 nuclear localisation within treated cells, likely through nuclear breakdown induced by cell death, but also at sites away from treatment, where nuclei still appear healthy. This represents a reversal to the progression of L1 staining observed during the differentiation of tissues and might therefore help to prevent virion production and assembly.

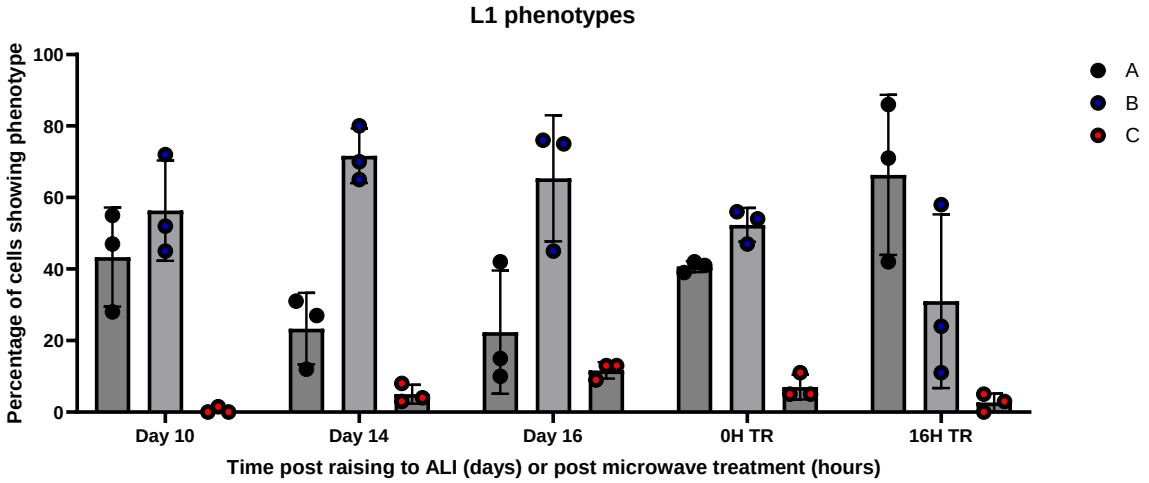

Figure 5.12: L1 staining within treated rafts is reduced and represents a reversal in differentiation. Quantification of IF staining patterns of L1 in mock compared to treated tissues. Cells derived from the top of mock rafts grown to day 10, 14 or 16, or following microwave treatment at 0 and 16 hours, were stained for L1 and the number of cells in each phenotypic group was quantified. At least one hundred cells were counted for each replicate and three individual experiments were carried out. Each dot represents the percentage of cells with that staining pattern from each replicate and the mean and standard deviation are displayed in the graph. The key in the top right-hand corner represents the staining phenotype (as defined in Figure 5.6B).

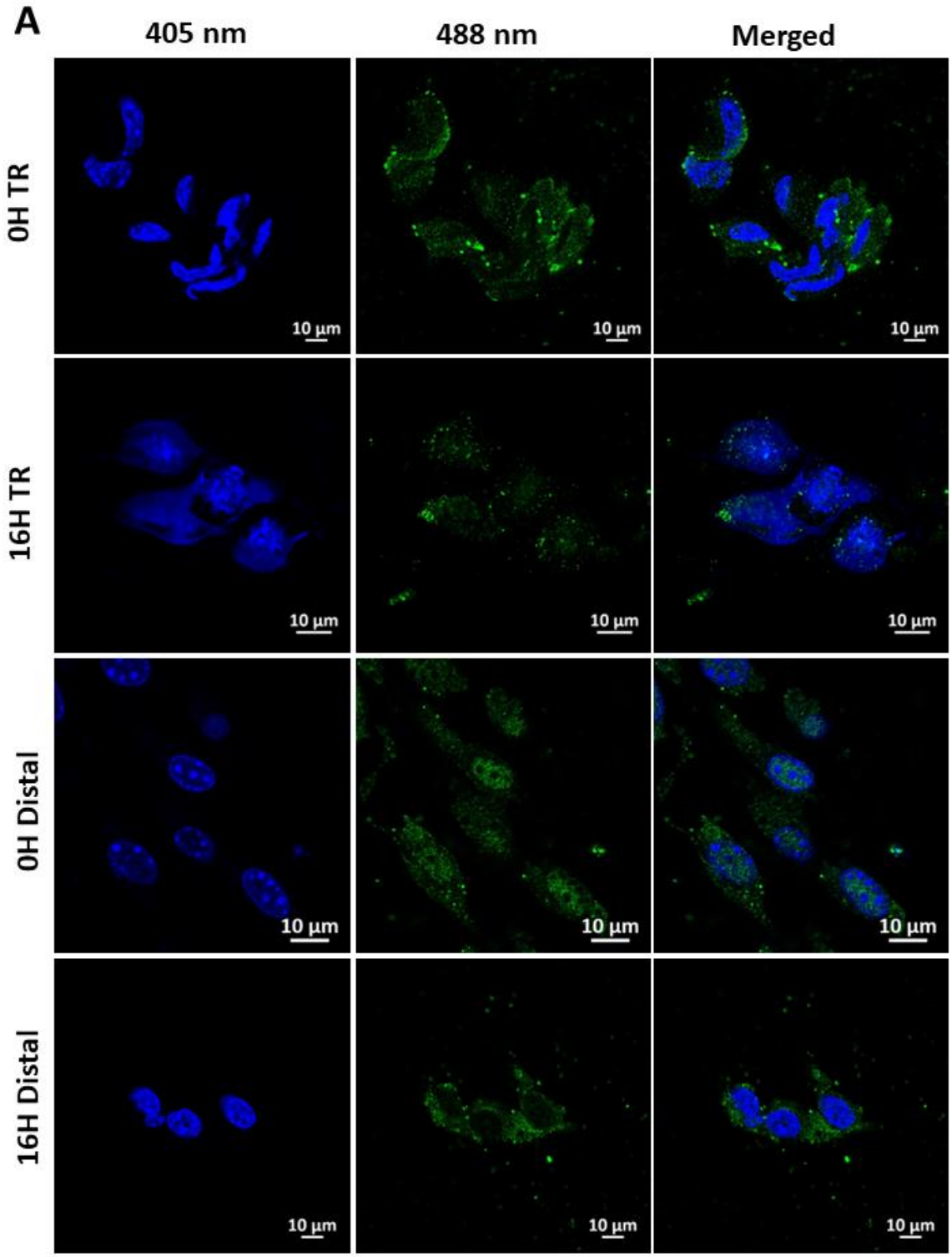
A
405 nm
488 nm
Merged
0H TR
16H TR
0H Distal
16H Distal
10 µm

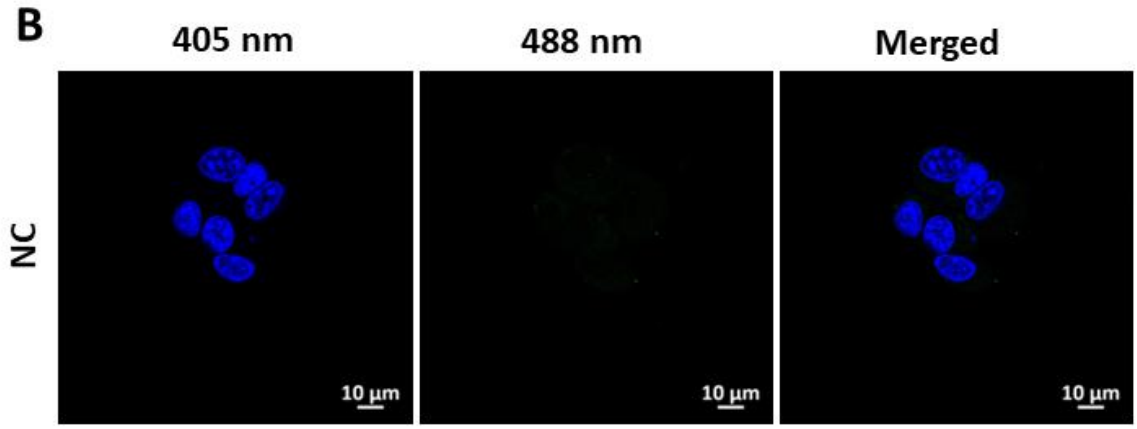

Figure 5.13: Microwave treatment results in L1 disruption at the site of treatment and reduces nuclear L1 staining in the distal sites. Immunofluorescent staining of L1 (green, 488 nm) and cell nuclei (blue, 405 nm) within cells from the top of microwave-treated W12E raft tissues. (A) The staining of L1 in cells directly under the site of treatment and cells at distal sites to treatment is shown at 0 and 16 hours post-treatment. (B) A no-primary antibody control was imaged and processed identically to the previous images. Images are representative of three independent experiments. Scale bars = 10 µm.

5.8 EM analysis of microwave-treated rafts reveals gross morphological changes at the site of treatment

Subsequently, we aimed to determine if changes to virion assembly or cellular morphology could be observed by EM analysis following microwave treatment. Rafts were dissected to create tissue sections that contained either treated or distal tissue. Within the treated areas of rafts 16 hours post-treatment, the tissue structure was markedly disturbed (Figure 5.14B). Cellular and nuclear membranes were disrupted and cell-to-cell attachments within the tissue were lost (Figure 5.14B, C). Interestingly, the upper layers of the tissue appeared less disorganised than the mid and lower layers, possibly due to the tight packing of cells and the dense fibrous networks in these upper layers making them less susceptible to hyperthermia-driven disruption (Figure 5.14B). Large dense aggregates can be observed in the mid and lower layers of the raft which could be due to protein denaturation following exposure to heat (Figure 5.14B, C). The nuclei appear to have shrunk in size, lost their membranes and include densely stained material which could represent condensed chromatin (Figure 5.14C). No viral-like particles or aggregates were observed within the treated areas of treated

tissues, however, these could be occluded by the dense aggregates of other proteins within these cells. Moreover, due to time constraints, we were limited to two biological replicates for analysis.

At distal sites to treatment, the tissue appeared more similar to mock-treated tissue. Here, nuclear and cell membranes were still intact for the majority of cells and no large dense aggregates (likely due to protein denaturation following heat stress) were visualised, due to the linearity of microwave treatment, up to 16 hours post-treatment (Figure 5.15A, B). Some cells had abnormal-looking nuclei, which may represent cells committing to apoptosis, which we have previously reported to be upregulated at distal sites to microwave treatment (Figure 5.15C) (Conley *et al.*, 2023). We observed one aggregate of viral-like particles at distal sites to treatment, similar to those observed in mock-treated tissues and previously published reports (Figure 5.15D, E) (Flores *et al.*, 1999). These observations were made in a tissue section that had been fixed immediately post-treatment (0H) so it is likely that these viral-like particles had assembled prior to microwave treatment. No aggregates of viral-like particles were observed in tissues at distal sites to treatment that were fixed 16 hours post-treatment. However, since aggregates were also a rare observation in mock-treated tissues and we only analysed two biological replicates, we cannot confidently draw comparisons between the quantity of these in mock compared to treated rafts.

Overall, microwave treatment induces large morphological changes at the site of treatment. The temperature increase disrupts cell and nuclear membranes but this effect is limited to the site of treatment, confirming the linearity of microwaves. No viral-like particles could be observed within the treated sites of tissues. Aggregates of viral-like particles, as seen in mock-treated tissues, were evident at sites distal to treatment immediately following treatment, but virus-like particles were absent in distal sites to treatment at 16 hours post-treatment.

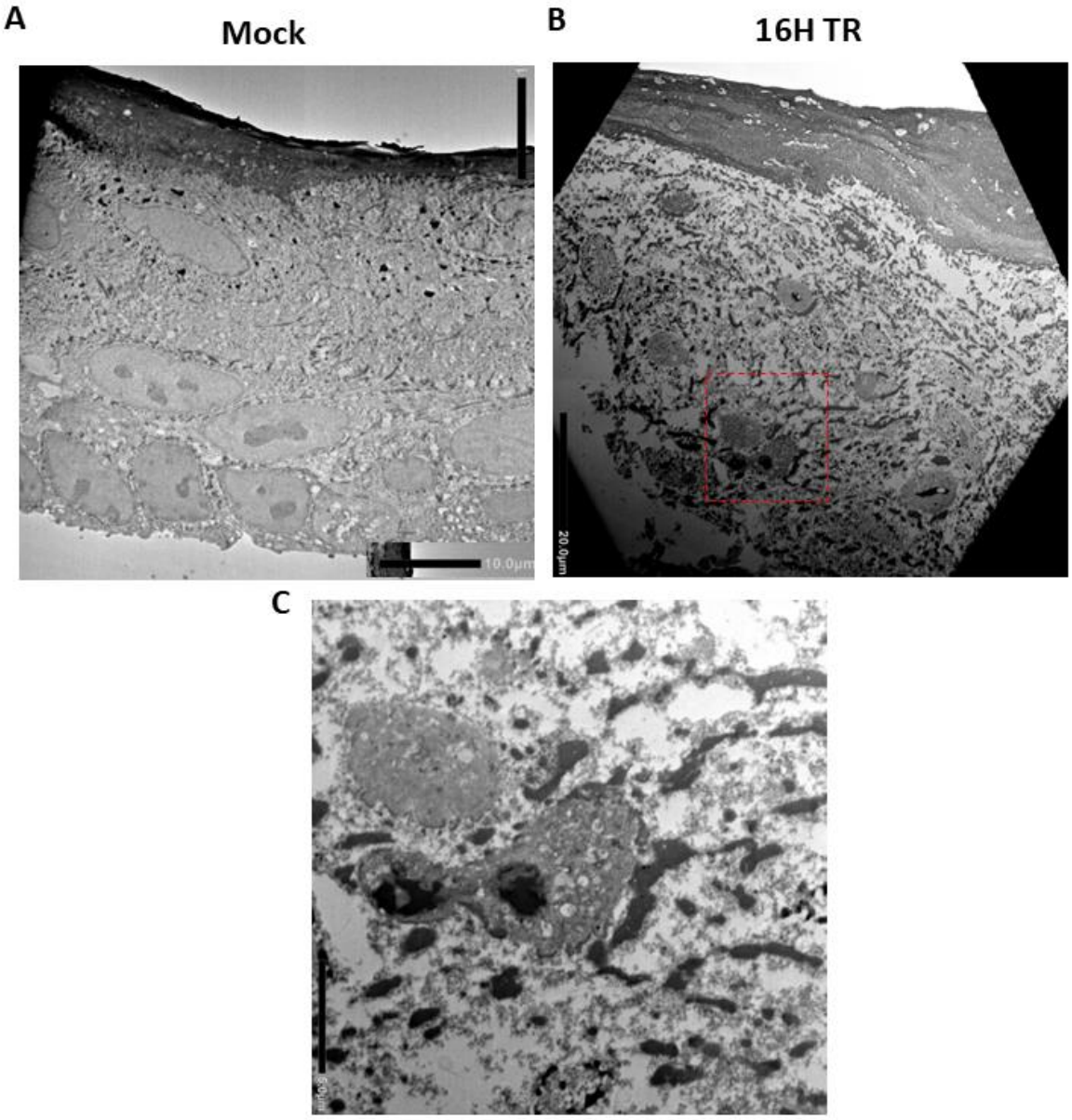

Figure 5.14: Microwave treatment results in gross morphological changes to tissue structures. Microwave-treated and mock W12E tissues were sectioned to produce 1 mm^3 sections of tissues directly at the site of treatment negatively stained and embedded in resin. Thin resin sections were cut and analysed by TEM. (A) Mock-treated W12E tissue for comparison. (B) The treated site of W12E tissues at 16 hours post-treatment showed gross morphological changes. Nuclear and cellular membranes were disrupted and cell-to-cell connections lost. The cells in the red box are magnified in (C). Scale bars = 10 µm (A), 20 µm (B), 5 µm (C).

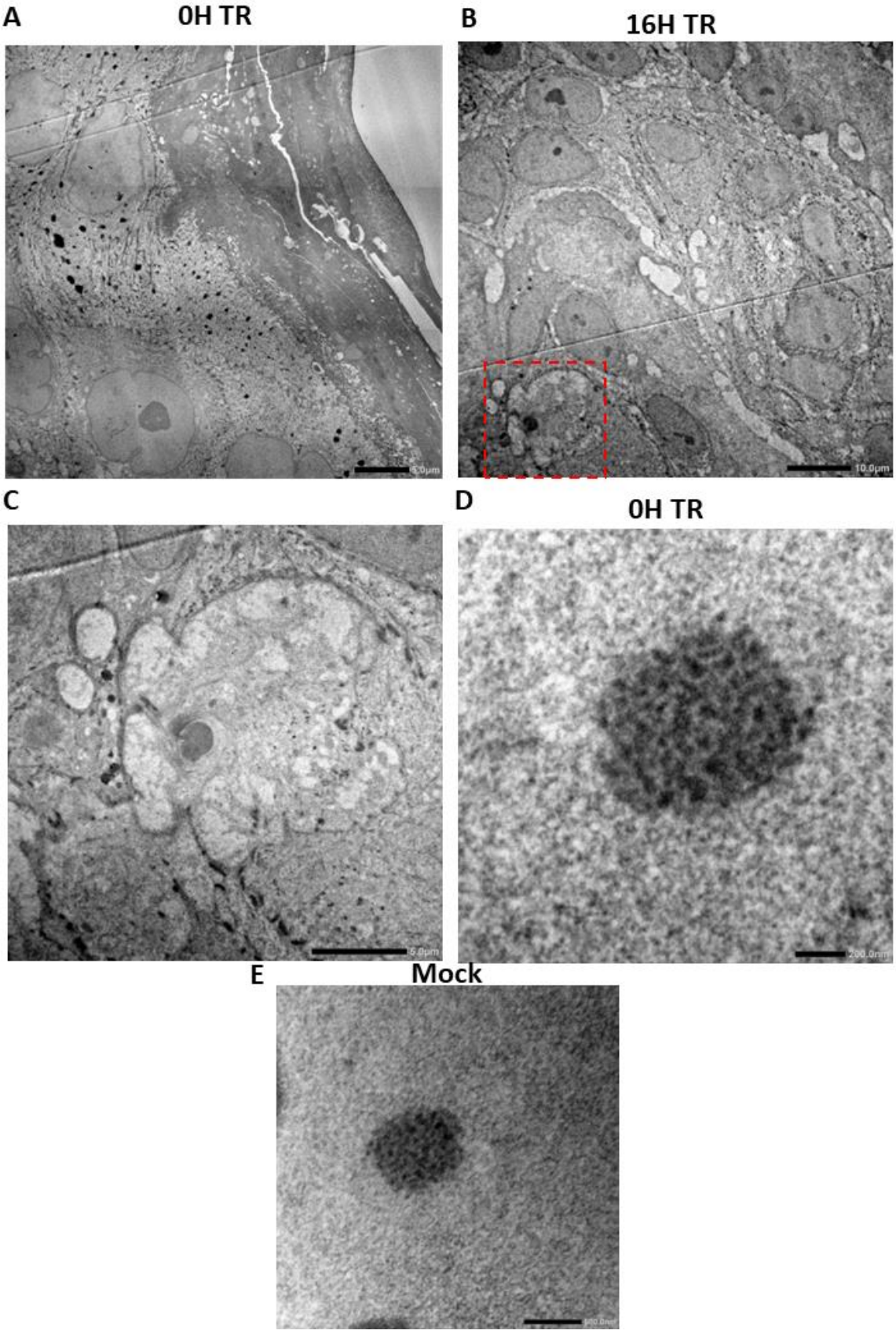

Figure 5.15: Gross morphological changes induced by microwave treatment are limited to the treated sites. Microwave-treated W12E tissues were sectioned to produce 1 mm^3 sections of tissues at distal sites to treatment (> 3 mm from the edge of treated tissue), negatively stained and embedded in resin. Thin resin sections were cut and analysed by TEM. (A, B) Distal sites of treated W12E tissues at 0- and 16-hours

post-treatment. The cellular and nuclear membranes were still present and cellular connection remained. Some cells appear to be undergoing apoptosis, such as the one within the red box, shown magnified in (C). (D, E) Densely stained virus-like particle aggregates observed in distal sites to treatment at 0 hours post-treatment resemble those seen in mock-treated tissues. Scale bars = 5 μm (A, C), 10 μm (B), 5 μm (B), 200 nm (D) and 500 nm (E).

5.9 Discussion

We characterised the localisation of the HPV16 major capsid protein L1 in differentiated W12E cells. These cells were derived from a natural infection and contain HPV episomes, allowing analysis of L1 in the context of the viral genome and production of the other viral proteins, which is a limitation of many previous studies. Initially, we used 2D differentiation models. The majority of cells had exclusively cytoplasmic L1 staining, which is similar to previous reports (Milligan *et al.*, 2007). In differentiated W12E cells grown in 2D, diffuse nuclear staining of L1 was rarely observed and punctate clusters could be visualised at the nuclear boundary using z-stacks. These clusters could represent L1 capsomeres that are imported into the nucleus through the nuclear pores via association with karyopherins (Bird *et al.*, 2008; Nelson, Rose and Moroianu, 2002; Nelson, Rose and Moroianu, 2003; Merle *et al.*, 1999). To our knowledge at the time of writing, no other studies have reported these L1 condensates at the nuclear periphery.

We extended our analysis of L1 localisation to cells in the upper layers of organotypic raft cultures. This involved the development of a protocol for the isolation of these cells and subsequent immunofluorescence staining and imaging to high resolution, which has never previously been attempted in the field. Differentiation phenotypes such as cell flattening and nuclear reorganisation, with larger nucleoli and condensates of chromatin, could be observed in the upper cell layers of tissues analysed by EM (Matsui and Amagai, 2015). Since rafts were inverted onto dishes, we propose that these top cell layers were retained on the glass dishes and analysed by IF and therefore, these cells represent more terminally differentiated stages in comparison to the cells differentiated in 2D. Within cells derived from the upper layers of W12E raft cultures, most cells had diffuse nuclear L1 staining which was excluded

from the nucleoli (phenotype B). This is similar to previous reports of L1 staining patterns using transfection assays (Kieback and Müller, 2006; Siddiqa *et al.*, 2015; Nelson, Rose and Moroianu, 2002). At later time points of raft growth, when more terminal differentiation had taken place, the proportion of cells with L1- staining foci within the nucleus had increased. These foci have similarities to observations by Day and colleagues of L2 recruitment of L1 to nuclear foci, but our observed foci were fewer in number and larger in size than these previous reports (Day *et al.*, 1998). However, the percentage of foci observed in this study was similar to transfection assays using codon-optimised L1 and L2 expressing plasmids (Kieback and Müller, 2006). The authors observed 4% to 13% foci staining of L2 in cell populations when using low and high concentrations of L2 respectively (Kieback and Müller, 2006). L2 was reported to recruit L1 to these nuclear dots, so a similar percentage of L1 foci may be expected (Day *et al.*, 1998; Kieback and Müller, 2006). We observed 1% to 12% of L1 foci staining in cells derived from day 10 and day 16 rafts respectively. The accumulation of L2 in these cells as they continue differentiating over time may drive this increase. This represents a future avenue for research to determine if L1 and L2 colocalise in these cells. Synthesis of L2 is thought to precede L1 expression in terminally differentiating keratinocytes, but a threshold of L2 concentration may be required before relocalisation of the capsid proteins to foci occurs (Florin *et al.*, 2002a; Florin *et al.*, 2002b; Kieback and Müller, 2006). We observed potential intermediates along this pathway which were not observed in previous studies but the transfection assays used in those reports may result in the overexpression of proteins, preventing the visualisation of intermediates (Kieback and Müller, 2006).

We propose that these foci of L1 may represent viral replication or assembly factories. Incoming virions have now been well documented to colocalise with PML-NBs (Day *et al.*, 2004) and previous studies observed L1 colocalisation with PML-NBs when L1 was coexpressed with L2 (Day *et al.*, 1998; Kieback and Müller, 2006). L2 is known to induce the translocation of papillomavirus E2 and the cellular protein PMSP to PML-NBs (Heino, Zhou and F., 2000; Gornemann *et al.*, 2002). This recruitment of E2 may enable the packaging of viral DNA into capsids due to its known ability to bind to episomal papillomavirus genomes (You *et al.*, 2004; McBride, 2013). Viral protein accumulation at PML-NBs may therefore facilitate virion assembly at late times of infection. L2 can

also promote the reorganisation of PML-NBs, with Sp100 release and Daxx concentration (Florin *et al.*, 2002b). Sp100 is a known repressor of viral infection, although it has previously only been implicated in the initial stages of viral establishment, so it is unclear if this function of L2 is necessary at the later assembly stages (Stepp, Meyers and McBride, 2013). Whilst we did not perform colocalisation experiments in this work for L2 or PML-NB components, we predict that due to the full viral genome being present in these cells, L2 expression could direct L1 to PML-NBs, resulting in the foci staining observed. Future experiments should include co-staining of L1 with both L2 and PML-NB components to confirm this hypothesis. The closely related polyomaviruses have been demonstrated to use replication factories within the nucleus which colocalise with PML-NBs, which may represent a shared mechanism between these viruses (Erickson *et al.*, 2012).

Although our CLEM analysis of L1 staining on the upper cells of differentiated W12E rafts was unsuccessful, we were able to image the ultrastructure of cross-sections of W12E organotypic rafts at high resolution. Within the upper layers of these tissues, aggregates of densely stained particles were observed that resembled the VLP aggregates reported by Flores and colleagues (Flores *et al.*, 1999). These were tightly packaged and could represent the foci seen by immunofluorescence, composed of multiple independent structures, suggesting that these foci may be papillomavirus assembly sites. However, to increase our confidence in these findings, it would be important to have correlated data for these cells confirming they show the overlapping foci staining of L1 by both immunofluorescence and EM and/or to use immunogold labelling for L1. We also observed individual viral-like particles in the nuclei of epithelial cells in the upper layers of rafts. These were of a similar size to previous reports of HPV virions in rafts (Pyeon *et al.*, 2005; Wang *et al.*, 2009; Meyers *et al.*, 1992; Song *et al.*, 2010) but the size and shape of these particles varied. Variability in virion size and shape in organotypic raft cultures harbouring HPV16 has previously been reported in the literature (Conway *et al.*, 2009). Virions within raft cultures may therefore have immature capsids. These capsids have previously been demonstrated to have structural flexibility due to the lack of disulphide bonds and appear variable in size and shape by EM analysis (Buck *et al.*, 2005; Buck, Day and Trus, 2013). The development of disulphide bonds in the HPV capsid requires several days during

desquamation and is associated with the oxidising environment of the cell (Buck *et al.*, 2005; Conway *et al.*, 2009). The nuclei of cells in the mid and upper layers of organotypic rafts are largely a reducing environment and the limited growth time of organotypic rafts (14 days) may not allow for the terminally differentiating cell oxidising environment required for virion maturation (Conway *et al.*, 2009). Again, it would be important to carry out L1 immunogold labelling on these viral-like particles observed in the nuclei of the upper epithelial layers of W12E rafts to confirm that these contain viral proteins.

This work progresses the current knowledge of L1 localisation within differentiated cells that mimic natural infection. Although L1 staining had been carried out in tissue sections of organotypic rafts and productive lesions, the resolution limitations prevented spatial analysis of the staining within nuclei (Middleton *et al.*, 2003; Milligan *et al.*, 2007; Wechsler *et al.*, 2012; Song *et al.*, 2010; Ferguson *et al.*, 2021; Laganà *et al.*, 2024). Moreover, current work that discusses L1 localisation within the nucleus was done using transfection or viral vector assays that introduce L1 alone or with L2 (Day *et al.*, 1998; Schafer, Florin and Sapp, 2002; Siddiqa *et al.*, 2015; Nelson, Rose and Moroianu, 2002; Kieback and Müller, 2006). Here, we provide analysis of L1 to high resolution in models that contain the entire viral genome and allow for the full viral lifecycle to take place. Our work shows that the majority of L1 nuclear staining is diffuse. Over time, and possibly accumulation of L2 within these cells, an increase in L1 foci staining was observed which we predict to colocalise with PML-NBs. This confirms previous observations of L1 localisation within transfection and viral vector systems.

Microwave treatment was observed to revert the usual progression of L1 staining in cells during differentiation. Instead, more cells showed no nuclear L1 staining following microwave treatment. This was evident within the treated areas of tissues at 0 hours post-treatment and extended into the distal areas of tissues at 16 hours post-treatment. This contrasts with our previous observations of an increase in epithelial cell differentiation (Chapter 3) (Conley *et al.*, 2023) and L1 transcription following microwave treatment (Chapter 4). Heat shock results in the retention of non-HSP mRNAs in the nucleus where they accumulate (Saavedra *et al.*, 1996; Saavedra *et al.*,

1997; Carmody *et al.*, 2010). Therefore, even with an increase in the transcription of L1, if these transcripts cannot access the cytoplasm to be translated following microwave treatment, L1 protein cannot be transported back into the nucleus for virion assembly. Within the treated areas, we observed cellular and nuclear membrane breakdown which is likely responsible for the loss of nuclear L1 staining following treatment. Moreover, at 16 hours, chromatin condensation was evident in the treated areas, possibly due to apoptosis, and there was very little L1 staining. No viral-like particles or aggregates of viral-like particles could be observed within treated areas. However, this was limited to two biological replicates and condensates of proteins caused by heat shock could obscure these particles. In the distal areas of treated rafts at later time points, the cells appeared healthy, with intact nuclei and cell boundaries visible by confocal microscopy, but nuclear L1 staining was reduced. EM analysis revealed the distal areas of treated rafts to have intact nuclear and cellular membranes. Aggregates of viral-like particles previously observed in mock-treated tissues were present in the distal sites of tissues immediately following microwave treatment but could not be visualised within these sites at 16 hours post-treatment. However, this was limited to two biological replicates and since these aggregates were a rare observation, we cannot confidently conclude they are lost in the distal sites of tissues at later time points post-treatment.

Since virion assembly takes place within the nucleus, the overall reduction in L1 nuclear staining following microwave treatment may act to reduce the production of new virions (Buck, Day and Trus, 2013). In particular, the large reduction in L1 foci staining following treatment, which we propose to represent assembly sites of HPV, may help to prevent the assembly of new virions and subsequent infection. This could help to prevent recurrence of disease from re-infection from an adjacent or distant site, if observations of a lack of viral-like particles at later time points post-treatment are correct (Reuschenbach *et al.*, 2023) (Figure 5.16 Case 2 & 3). However, our work is limited to 16 hours post-treatment so it would be important to determine if these observations were extended to later time points. To investigate this further and the possibility of recurrence from reinfection following microwave treatment, *in vivo* work would be required as the lifetime of organotypic rafts is a limiting factor for this analysis. It would be important to also quantify the virions derived from mock and

microwave-treated tissues, which could make use of previously developed assays to determine viral titres and infectivity (Bodily *et al.*, 2011). Previously, microwaves have been reported to inactivate influenza particles through structure-resonant energy transfer (Yang *et al.*, 2015). The authors hypothesise that microwave photons at frequencies of 8 GHz are capable of physically fracturing virions. Whilst influenza has an envelope and is a different size to HPV, which may result in different resonances of the two viruses, it is an interesting mechanism to consider alongside our observations of no viral-like particles within the treated areas of W12E rafts. Further investigation to determine if this is the case for HPV could involve microwave-treating HPV VLPs or PsVs and analysing virion structures to identify disruption by electron microscopy.

Overall, using high-resolution imaging we have defined the localisation of the major capsid protein of HPV within differentiated epithelial cells harbouring the entire viral genome. Microwave treatment of organotypic rafts reverted the usual progression of L1 staining during differentiation, which resulted in a reduction of cells with L1 nuclear positivity. Since HPV assembles within the nucleus, microwave treatment may prevent virion production and help to prevent recurrence from autoinoculation.

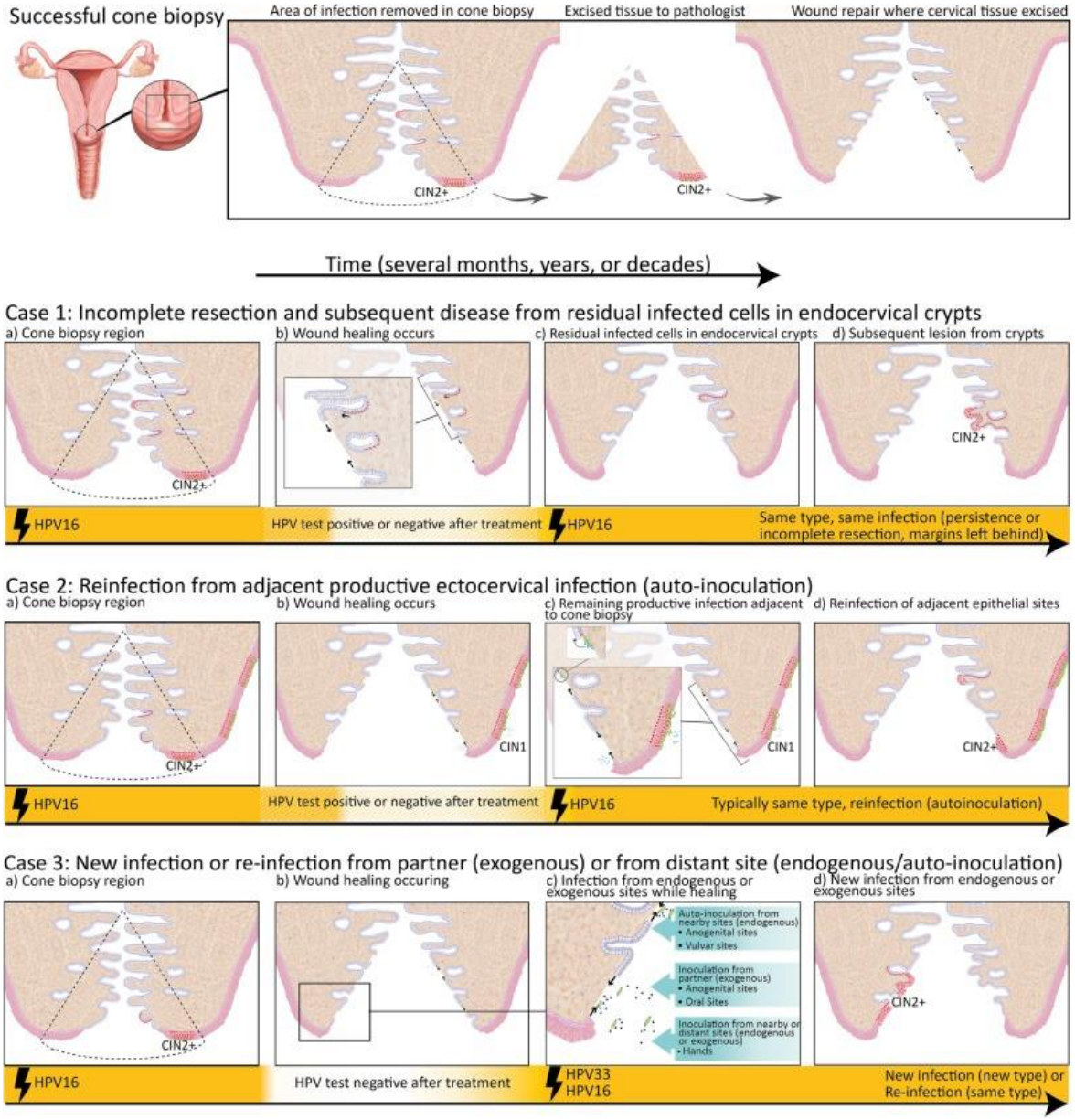

Figure 5.16: Models of recurrence following treatment of CIN2+ lesions. Types of subsequent disease development after excisional treatment of a CIN2+ lesion due to residual cells (Case 1), HPV re-infection due to autoinoculation from an adjacent site (Case 2) or re-infection from a distant site or new infection from a partner (Case 3). Figure made by Caroline Walker and adapted from Reuschenbach *et al.*, 2023.

5.10 Supplementary figures:

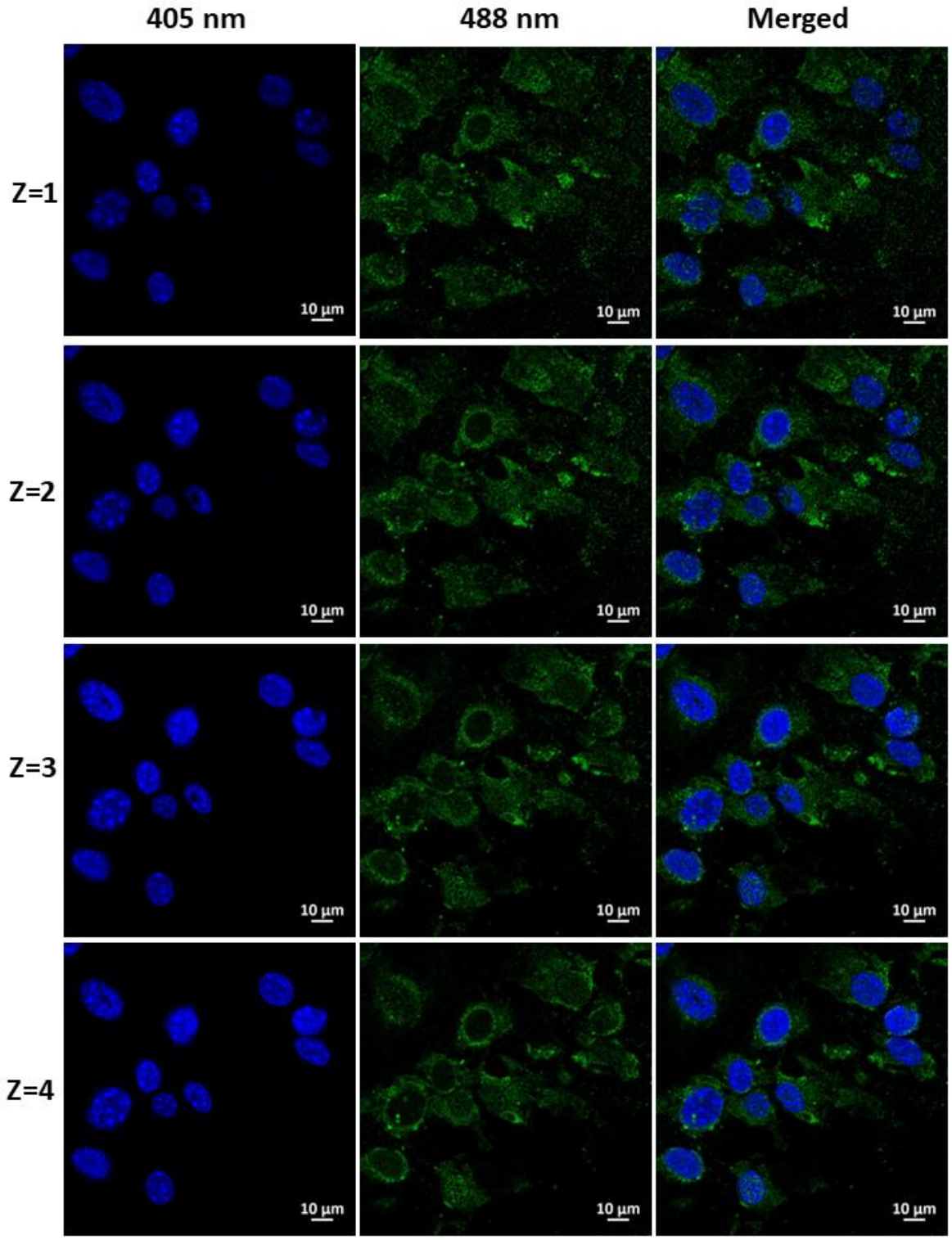

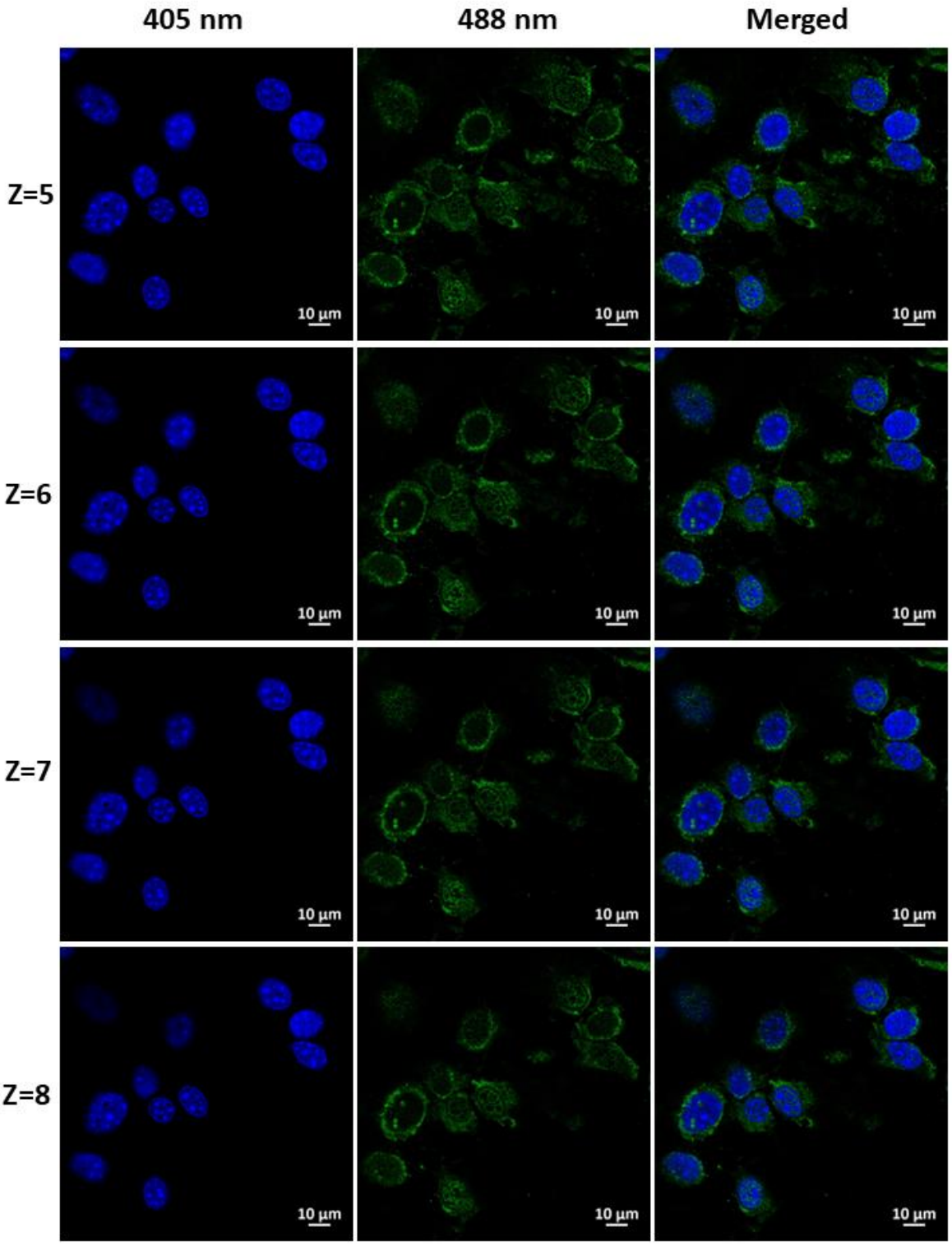
405 nm
488 nm
Merged
Z=5
Z=6
Z=7
Z=8
10 µm

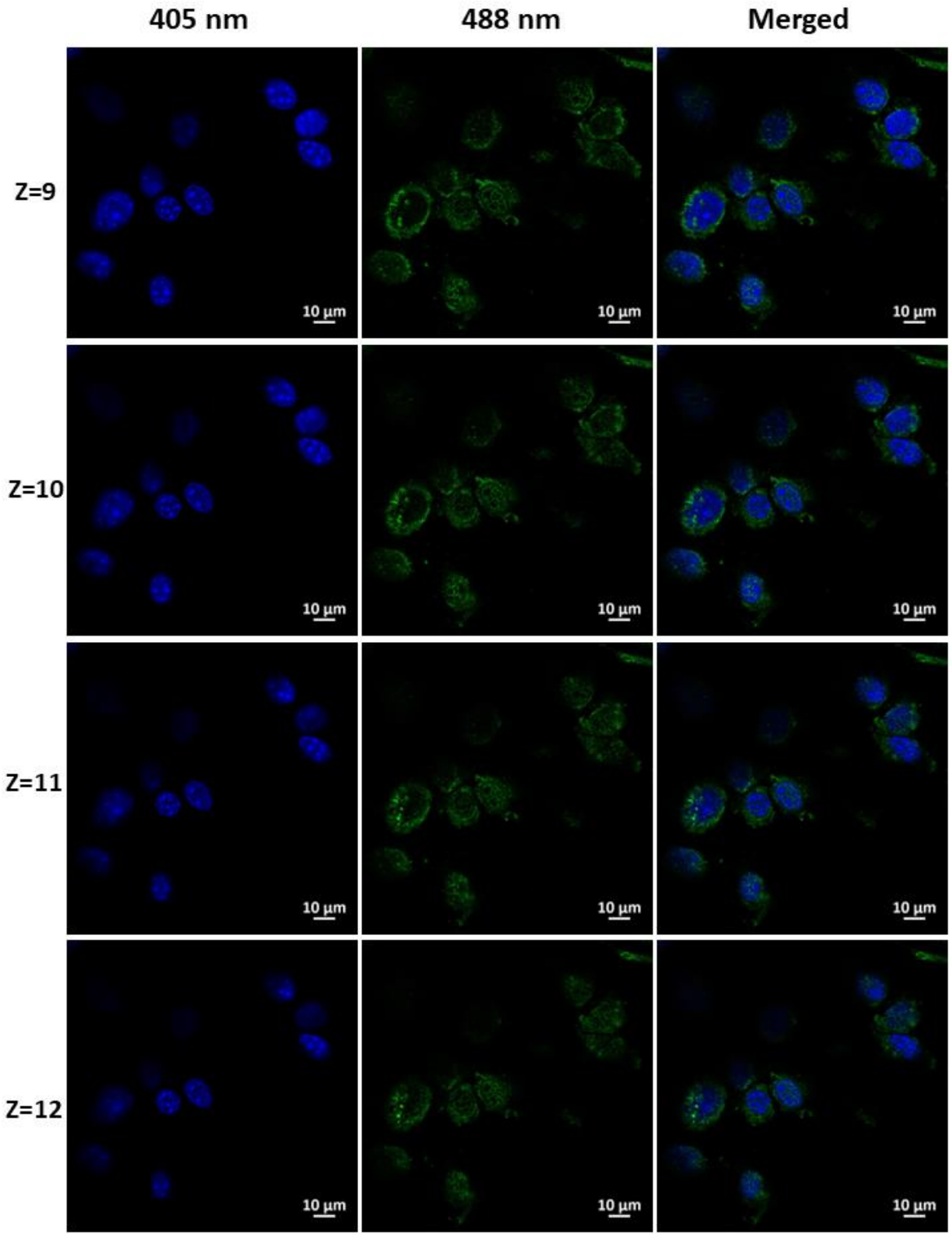
405 nm
488 nm
Merged
Z=9
Z=10
Z=11
Z=12
10 µm

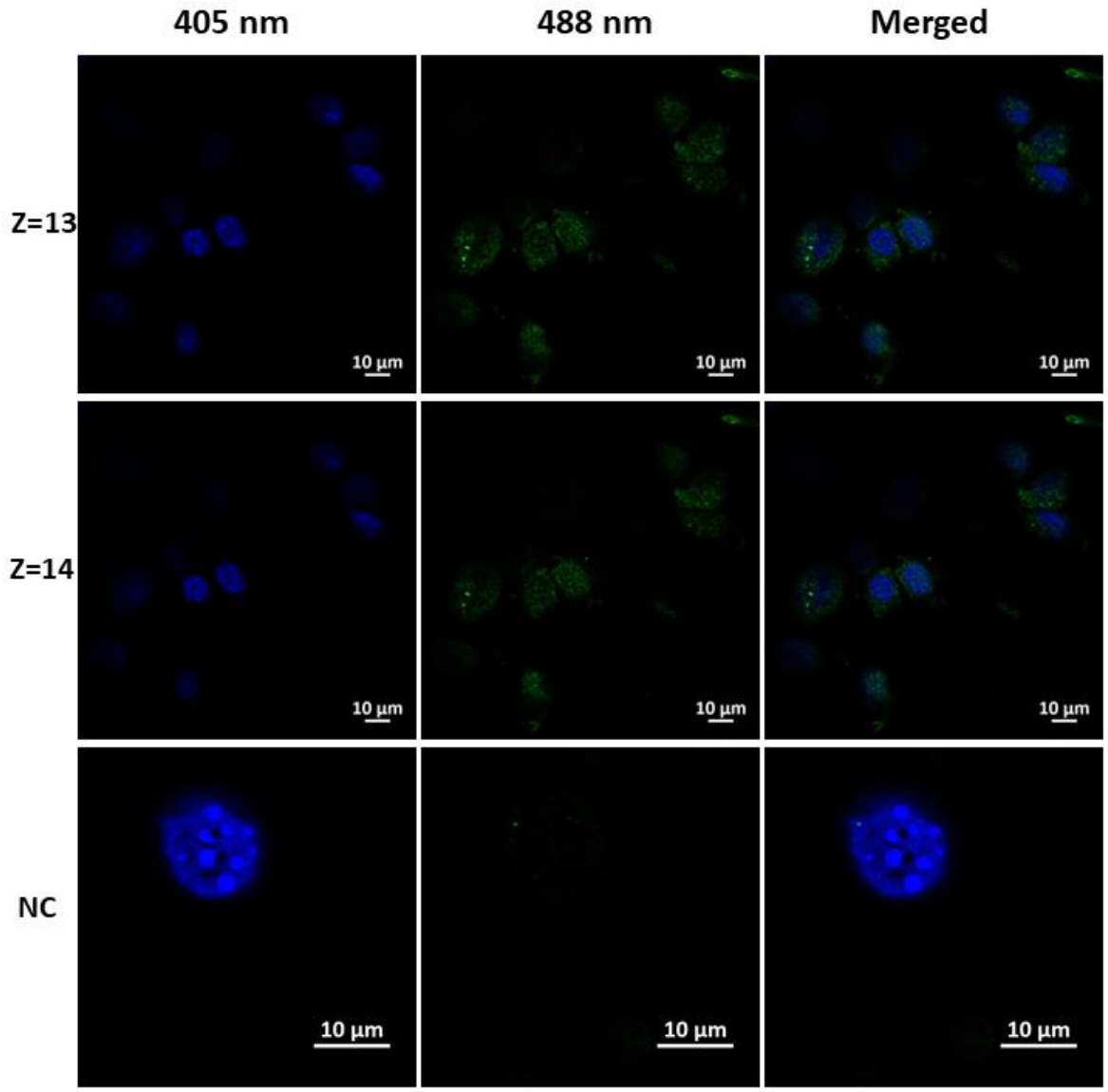

Supplementary Figure 5.1: L1 staining phenotypes do not vary over the thickness of the cell. Immunofluorescent staining of L1 (green, 488 nm) and cell nuclei (blue, 405 nm) in cells derived from the top of W12E organotypic rafts. A z-stack was collected with serial sections (Z=1 to 14) taken along the z-plane every 0.3 µm to show L1 staining throughout the thickness of the nucleus. The L1 staining pattern does not change whilst traversing through the nucleus. A no-primary antibody control was imaged and processed identically to the previous images. Scale bars =10 µm. The same acquisition and processing settings were used as in Figure 5.6.

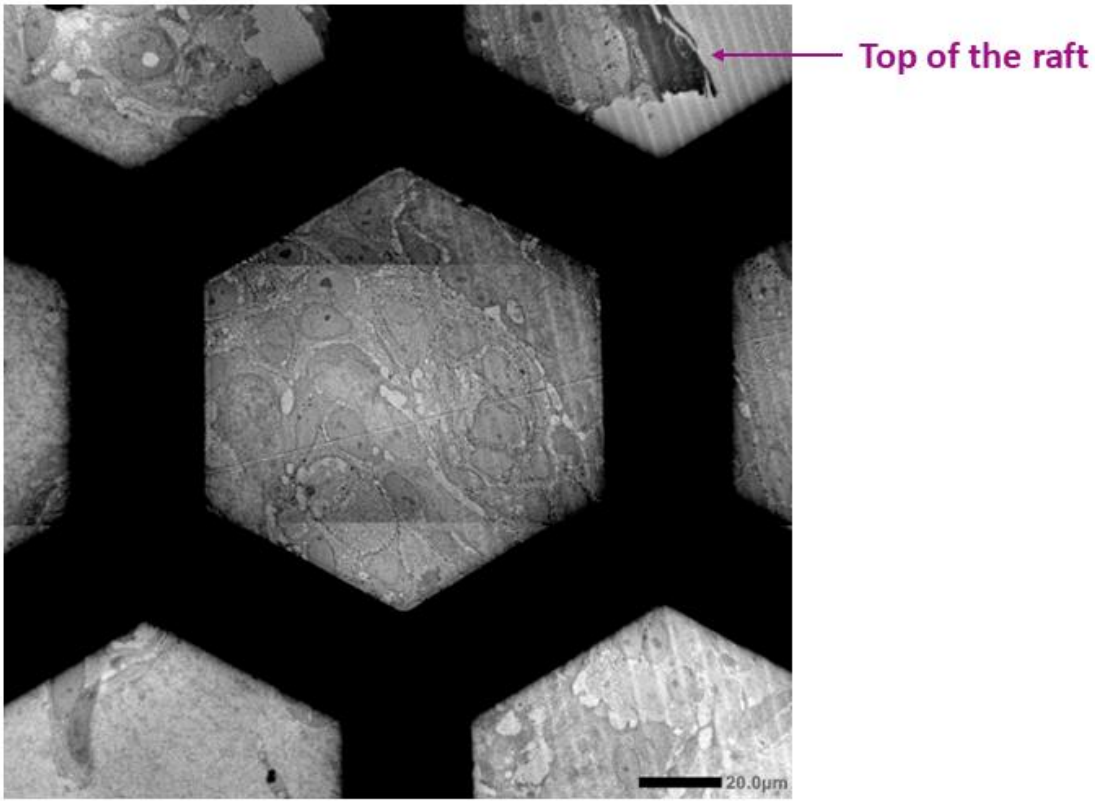

Supplementary Figure 5.2: The thickness of W12E tissue within resin sections extends over the copper gridlines of TEM grids, preventing high magnification image acquisition of the full thickness of the raft tissue.

Chapter 6 Discussion

Human papillomavirus is the most common sexually transmitted viral infection and can result in morbidities in the mucosal epithelium of the anogenital region and other anatomical sites (Bruni *et al.*, 2023). Whilst an effective prophylactic vaccine is now available against many of the most common, disease-causing genotypes of HPV (Frazer, 2019; de Sanjose *et al.*, 2019), the uptake of this vaccine is low in many geographical areas and the vaccine was only introduced in 2006, initially just to adolescent females, leaving several generations unprotected (Bruni *et al.*, 2016). Cervical cancer is the most extensively studied disease arising from HPV infection and whilst the WHO has implemented targets for the eradication of cervical cancer (WHO, 2020), recent models have predicted that the threshold for elimination (less than 4 cases per 100,000 women per annum) will not be reached until 2100, dependent upon a high (90%) vaccination and screening rate (Brisson *et al.*, 2020). Cases of HPV-positive cervical, anal and oropharyngeal cancers are rising (Lechner *et al.*, 2022; Deshmukh *et al.*, 2020; IARC, 2022). Therefore, there is still a large burden of disease caused by HPV, which requires good treatment options, especially in low and middle-income countries (LMIC) where the number of cases is predicted to rise the highest (IARC, 2022). Current treatment options are relatively effective but carry with them significant side effects, potential complications and some carry high rates of recurrence (McCarthy *et al.*, 2016; Prendeville and Sankaranaryanan, 2017; Martin-Hirsch *et al.*, 2013; Kyrgiou *et al.*, 2006). Therefore, we aimed to determine if microwave treatment, which has previously been used for the treatment or co-treatment of selected cancers, may offer an improved option for the treatment of HPV-positive anogenital lesions (Wang *et al.*, 2021; Breen and Lencioni, 2015; Liu *et al.*, 2022). The Swift® is a hand-held device capable of delivering microwaves through a probe applicator tip and has previously been observed to be safe and effective for the treatment of HPV-associated plantar warts and actinic keratoses (Bristow *et al.*, 2017; Jackson *et al.*, 2020). Before extending the Swift® device to the treatment of HPV-positive anogenital lesions, we sought to investigate the molecular mechanisms behind microwave treatment on the life cycle of HPV and the keratinocytes the virus infects.

Before discussing the effects of microwave treatment elucidated in this study, a summary of the novel HPV lifecycle findings in this thesis will be provided. The main aim of Chapter 5 was to determine, to a high resolution, the intracellular localisation of the HPV16 major capsid protein L1. Our analysis used W12E cells which contain the entire viral genome and were differentiated within organotypic rafts, providing a more natural infection model than previous studies (Day *et al.*, 1998; Sun *et al.*, 1995; Schafer, Florin and Sapp, 2002; Siddiqa *et al.*, 2015). We provide new insights into the change of L1 nuclear localisation over time, which had not previously been possible due to limitations in transfection-based or viral vector assays. We observed an accumulation of L1 within the nucleus over raft growth time, which supports the theory of virion assembly in the nucleus of more differentiated cells (Buck, Day and Trus, 2013). Following the nuclear translocation of L1, which was initially diffusely distributed about the nucleus, L1 became localised to tightly stained nuclear foci. The percentage of foci observed is similar to previous studies that used codon-optimised L1 and L2 transfection assays (Kieback and Müller, 2006) and supports the observations of L1 localisation to PML-NBs, first reported by Day and colleagues (Day *et al.*, 1998). We propose that these foci of L1 correlate to aggregates of viral-like particles observed by EM in our work, which mirror those observed by Flores and colleagues (Flores *et al.*, 1999). However, due to a low cell density restricting cellular identification by EM, our correlative approach of the immunofluorescence and EM data was prevented, and further work is required to confidently draw this conclusion. Avenues for future research include immunogold labelling to confirm that the aggregates of viral-like particles contain HPV capsid proteins. Moreover, to overcome the CLEM limitations of a low cell density, it may be possible to use nitrocellulose blotting membranes to retain a confluent layer of cells from the top of organotypic rafts. This strategy has recently been used to preserve a near-uniform coverage of surface cervical keratinocytes, which can subsequently be used for immunofluorescence staining (Shiraz *et al.*, 2022).

The main aim of Chapter 3 was to investigate changes to the keratinocyte transcriptional landscape following microwave treatment. The results indicate that microwave treatment of 3D *in vitro*-grown tissues results in a hyperthermic response, which strengthens our previous observations of HSP70 induction following treatment

(Conley *et al.*, 2023). A comparison of our data with previously published transcriptomes of cells undergoing hyperthermia revealed several shared genes and pathways (Yonezawa and Bono, 2023; Scutigliani *et al.*, 2022; Richter, Haslbeck and Buchner, 2010). This suggests that the temperature reached within tissues rather than the method of heating is most important to the resulting transcriptomic effects within cells, which contrasts with previous observations of different heating methods resulting in differing biological effects (Yang *et al.*, 2016; Whitney, Carswell and Rylander, 2013). Microwave treatment resulted in some transcriptomic changes that haven't previously been reported in other studies on hyperthermia, such as increased differentiation, although this may be characteristic of the keratinocyte model used in this work. We previously observed increased differentiation following microwave treatment through involucrin and keratin 10 staining (Conley *et al.*, 2023). The high degree of variation observed in samples 16 hours post treatment represents a limitation to our sequencing analysis. Subsequent work to increase the number of biological replicates per sample group to enable identification of outliers would improve the confidence in the results.

Microwave treatment also induced immune activation. The role of hyperthermia in immune activation is well-documented (Toraya-Brown and Fiering, 2014) although not extensively reported in previous transcriptome meta-analyses (Yonezawa and Bono, 2023; Scutigliani *et al.*, 2022; Richter, Haslbeck and Buchner, 2010). Innate immunity was activated, at both the mRNA and cytokine level, in HPV-negative and HPV-positive cells following treatment but this increase was greater in HPV-positive cells. We propose that the enhanced immune activation in treated compared to mock HPV-positive cells is through the alleviation of the normal immune evasion tactics used by the virus (Section 1.9.2) (Zhou, Tuong and Frazer, 2019). The viral oncoproteins have multiple functions in inhibiting immune activation (Scarth *et al.*, 2021) and we have previously shown that microwave treatment decreases the expression of E6 and E7 in cervical cancer models (Conley *et al.*, 2023). We provide additional evidence for oncoprotein downregulation following treatment within an earlier disease stage by inferring an indirect decrease in the expression of E6 and E7 through increased expression of their downstream target proteins, p53 and Rb (Figure 4.10, Figure 4.11). Therefore, detection of the virus may be unhindered, resulting in an increased

mounting of the immune response following microwave-delivered hyperthermia. We observed an increase in several Th1 cytokines following microwave treatment in both HPV-negative and HPV-positive cells, which builds on existing evidence of microwave treatment upregulating Th1 immunity (Zhou *et al.*, 2021) and cross-presentation of antigens to CD8+ T cells (Bristow *et al.*, 2017). Therefore, microwave treatment may be capable of driving the Th1/Th2 balance from a Th2 dominant response which enables viral persistence (Alcocer-Gonzalez *et al.*, 2006; Torres-Poveda *et al.*, 2014) to a Th1 dominant response which is responsible for the clearance of HPV (Coleman *et al.*, 1994; Konya and Dillner, 2001; Nakagawa *et al.*, 2002).

Following our observations of microwave treatment altering the host transcriptome, our main aim of Chapter 4 was to investigate if this was also extended to viral transcription. Within models of cervical cancer, the abundance of transcripts encoding the E6 and E7 oncoproteins was decreased in a spatially localised manner, which radiated from the treated to proximal and distal areas following treatment (Conley *et al.*, 2023). In cells that contain HPV16 episomes and resemble an earlier model of disease, microwave treatment caused a significant increase in the expression of the early and late viral transcripts, with a larger magnitude fold change in the late viral transcripts. We hypothesise that the increase in the differentiation status of the keratinocytes following microwave treatment is responsible for this increase (Chapter 3). Following this rise, a decrease in HPV16 mRNA levels was observed at later time points post-treatment, which could be due to immune activation or the cell stress response inhibiting transcription. Previous reports have suggested that non-heat shock protein mRNAs are retained within the nucleus of eukaryotes following hyperthermia, although this has not been confirmed in mammalian cells (Saavedra *et al.*, 1996; Saavedra *et al.*, 1997; Carmody *et al.*, 2010). If mRNAs were transported out of the nucleus, we have previously observed the formation of stress granules in microwave-treated cells which would prohibit translation (Conley *et al.*, 2023; Riggs *et al.*, 2020) Therefore, these mechanisms may prevent the viral transcripts from being translated following treatment. Our results support this as we observed an increase in the expression of p53 and Rb following microwave treatment, which are normally targeted by E6 and E7 respectively for degradation. A greater increase in p53 compared to Rb was observed, likely due to heat

shock-mediated induction of this protein (Jentsch *et al.*, 2020). L1 expression and localisation in microwave-treated cells were also disrupted with reduced nuclear translocation of the protein and very few instances of foci staining in comparison to mock-treated tissues. The production of new virions will be hampered if L1 cannot access the nucleus, the site of virion assembly (Buck, Day and Trus, 2013). In support of this, no viral-like particles were observed by EM within the treated areas of treated rafts, however further investigation is required to confirm this using immunogold labelling. Our EM observations of treated rafts also showed nuclear and cellular membrane breakdown within the treated areas. Nuclear breakdown could expose the viral DNA, which is normally tightly confined to the nucleus, to cytosolic PRRs (Uhlorn *et al.*, 2020; Moody, 2022) whilst cellular breakdown could expose viral antigens to antigen-presenting cells within the epithelium (Stanley, 2006). We also showed that microwave treatment could inhibit viral genome replication (Figure 4.12). Altogether, microwave treatment reduced viral transcription at later time points, inhibited genome amplification and interfered with viral protein production and localisation within the cell representing a restriction of the viral life cycle.

Our data builds on existing evidence that microwaves are a safe and effective form of treatment for HPV-associated lesions (Bristow *et al.*, 2017; Hagon *et al.*, 2023; Jackson *et al.*, 2020). Microwave treatment of *in vitro* models of HPV-positive anogenital lesions ablates the tissue precisely at the site of treatment without grossly disturbing the neighbouring tissue (Conley *et al.*, 2023). Previously, we reported that microwaves could induce HSP70, apoptosis and autophagy, downregulate the HPV oncoproteins and reduce proliferation in cancer models (Conley *et al.*, 2023). The work presented in this thesis has uncovered some of the additional molecular mechanisms behind microwave treatment. We confirmed that microwave treatment results in hyperthermia and our results indicate an induction of immunity and inhibition of the viral life cycle in precancerous models of disease. Alongside ablation of lesions, the immune activation and viral life cycle inhibition driven by microwave treatment may prevent local recurrence and in cases of multifocal disease, may result in the regression of lesions at untreated sites. The importance of immunity in preventing lesion recurrence is evident through studies that have introduced pre or postoperative vaccination for HPV, found to result in a 59% risk reduction for CIN2+ recurrence in a

recent meta-analysis (Jentschke *et al.*, 2020). Larger studies that are currently taking place including the NOVEL, HOPE9, VACCIN and CONVENANT trials will confirm these conclusions and help to determine the optimal point of vaccination. However, due to the expense of vaccination and the requirement for trained personnel for excisional treatment, a treatment option that induces the immune response would be more cost-effective and applicable to LMIC. The low cost of the Swift®, at several thousand pounds, alongside the potential for it to be used without a consistent electricity supply also makes it attractive for use in developing nations.

Microwaves offer a greater depth of penetration in comparison to cryo- or laser therapies (Conley *et al.*, 2023). This is particularly beneficial when considering the hypothesis that the reserve cells, which lie under the basal cells of the epithelium, frequently harbour HPV infection following treatment and can result in recurrence (Doorbar and Griffin, 2019; Reich and Regauer, 2023). No smoke or vapour is produced by the Swift® device, making it safe for virus-positive lesions and different probe sizes could be designed to target lesions at particular anatomical sites. Moreover, the small size of the treated area following microwave treatment may reduce the associated side effects, compared to other treatment options, and the risk of subsequent complications carried by the excisional techniques. Participants in the cutaneous *in vivo* studies using the Swift® device reported pain from microwave treatment, which was bearable and transient and didn't require the use of anaesthesia (Bristow *et al.*, 2017). Whilst treatment of the mucosal epithelium could result in higher pain, local anaesthesia could be administered alongside treatment (as for the excisional therapies), allowing microwave treatment to be used as a part of a 'see and treat approach', which can be particularly efficient in low resource settings (Prendeville and Sankaranaryanan, 2017). Moreover, microwave treatment is quick, which could save clinicians time, and the mild nature of the procedure might allow for sequential treatments to be carried out in quicker succession than those used currently. We propose that the Swift® device could be used to improve the treatment of genital warts and anal, cervical and vulval precancers (AIN, CIN and VIN) and the device has recently been approved for a clinical trial for AIN. Data from the clinical trial will enable an analysis of the pain experienced by individuals undergoing treatment and

determine the requirement for local anaesthesia. Longitudinal studies will also enable the effectiveness and recurrence rates to be determined in mucosal lesions.

Our *in vitro* modelling of tissues that resemble CIN-grade lesions and cervical cancer has allowed us to analyse the molecular mechanisms behind microwave treatment, however, they have some major limitations. We carried out our research exclusively on models containing HPV16. The high-risk HPV types share many similarities in their life cycles and genome organisation, so the findings presented in this thesis likely apply to infections with other high-risk types (Graham, 2017; Doorbar *et al.*, 2012). However, some differences between the high-risk viruses have been proposed, such as the hypothesis that the HPV16 dominance in OPSCC cases is due to differences in the interactions of the high-risk viral proteins with the immune system (Villa *et al.*, 1992; Roberts *et al.*, 2019). NIKS18 are an attractive model for further testing of microwave treatment since, due to the isogenic background of NIKS16 and NIKS18, direct comparisons between HPV16 and HPV18 could be made. The low-risk HPV types share many similarities in their life cycles with the high-risk types with the core proteins (E1, E2, E4, L1 and L2) having conserved roles (Egawa and Doorbar, 2017). Therefore, both the immune activation and the disruptions to the HPV16 life cycle observed in our study (which also took place in HPV-negative cell lines) are likely extendable to lesions containing these lrHPV types.

Another limitation is that these models do not represent the complexity of the tissue structure as they do not contain infiltrating immune cells, such as LCs, or a blood supply. It is also difficult to model lesion regrowth following microwave treatment due to the limited lifespan of these models. Moreover, the nature of heating within tissues is different and optimisation of the treatment parameters would be required before implementing the therapy into each new tissue site. To overcome some of these limitations, *in vivo* animal modelling could be used. Mice infected with the mouse papillomavirus MmuPV1 can form lesions in the vaginal and anal tracts (Cladel *et al.*, 2013; Cladel *et al.*, 2015; Hu *et al.*, 2015). This would provide a model of the anatomical site of interest and could be used to investigate immune cell infiltration and lesion regression. MmuPV1 infection can also induce lesions at the back of mouse tongues, providing models of OPSCC which would allow comparisons between microwave

treatment at different sites within the same model (Cladel *et al.*, 2016). However, differences between MmuPV1 and the high-risk HPV types exist, including differences in the functions of the oncoproteins (Hu *et al.*, 2017; Romero-Masters, Lambert and Munger, 2022). Furthermore, due to the extensive host adaptation of the papillomaviruses (Doorslaer, 2013), there are likely differences in the immune evasion strategies used by MmuPV1 that may limit the extension of these findings to anogenital lesions caused by the high-risk HPV types. An alternative *in vivo* model could be to generate tumours in transgenic mice containing the HPV16 E6 and E7 oncoproteins under the control of the K14 promoter (Song, Pitot and Lambert, 1999; Schaeffer *et al.*, 2004). These mice can develop anal or cervical cancers following treatment with the chemical carcinogen DMBA (Stelzer *et al.*, 2010; Thomas *et al.*, 2011) or exogenous estrogen (Spurgeon *et al.*, 2017) respectively. Similarly to MmuPV1 infection, this would provide a model of disease which would include immune cell communication and could provide a model of lesion regrowth following treatment. Moreover, it would allow confirmation of a reduction in the HPV16 oncoproteins following microwave treatment. However, gene expression is regulated from the K14 promoter rather than the endogenous papillomavirus promoter and since E6 and E7's functions are dependent upon their interaction with several proteins, there may be some differences in these protein-protein interactions in mice. The small size of these murine anogenital lesions would also require alterations to the Swift® probe and microwave energy.

In conclusion, this investigation has shown that microwave treatment induces hyperthermia, which can drive immune activation within keratinocytes. The resulting cytokine release would be predicted to induce a Th1 response which may help to protect against disease recurrence. Microwave treatment inhibits the human papillomavirus life cycle by restricting viral genome amplification and gene expression at later time points post-treatment. We have progressed the current understanding of the localisation of the major capsid protein within a natural model of disease and observed disruption of L1 nuclear placement following microwave treatment, which may prevent virion assembly. Overall, our work has added to the growing body of evidence that microwave treatment is a safe and effective therapy. We have additionally provided evidence for the extension of its use to HPV-driven lesions in the

anogenital region which has contributed to the approval of the Swift® device for clinical trials for the treatment of AIN.

List of references

Abravaya, K., Myers, M. P., Murphy, S. P. and Morimoto, R. I. (1992) 'The human heat shock protein hsp70 interacts with HSF, the transcription factor that regulates heat shock gene expression', *Genes & development,* 6(7).

Adams, T., S. and Mbatani, N., H. (2018) 'Clinical management of women presenting with field effect of HPV and intraepithelial disease', *Best practice & research. Clinical obstetrics & gynaecology,* 47.

Adler, K., Erickson, T. and Bobrow, M. (1997) 'High sensitivity detection of HPV-16 in SiHa and CaSki cells utilizing FISH enhanced by TSA', *Histochemistry and cell biology,* 108(4-5).

Alcocer-Gonzalez, J. M., Berumen, J., Tamez-Guerra, R., Bermudez-Morales, V., Peralta-Zaragoza, O., Hernandez-Pando, R., Moreno, J., Gariglio, P. and Madrid-Marina, V. (2006) 'In vivo expression of immunosuppressive cytokines in human papillomavirus-transformed cervical cancer cells', *Viral immunology,* 19(3).

Allen-Hoffmann, B. L., Schlosser, S. J., Ivarie, C. A., Sattler, C. A., Meisner, L. F. and O'Connor, S. L. (2000) 'Normal growth and differentiation in a spontaneously immortalized near-diploid human keratinocyte cell line, NIKS', *The Journal of investigative dermatology,* 114(3).

Amin, J., Ananthan, J. and Voellmy, R. (1988) 'Key Features of Heat Shock Regulatory Elements', 8(9).

Angel, P. and Karin, M. (1991) 'The role of Jun, Fos and the AP-1 complex in cell-proliferation and transformation', *Biochimica et Biophysica Acta (BBA) - Reviews on Cancer,* 1072(2-3).

Arbyn, M., Kyrgiou, M., Simoens, C., Raifu, A. O., Koliopoulos, G., Martin-Hirsch, P., Prendiville, W. and Paraskevaidis, E. (2008) 'Perinatal mortality and other severe adverse pregnancy outcomes associated with treatment of cervical intraepithelial neoplasia: meta-analysis', *BMJ,* 337(sep18 1).

Ashrafi, G. H., Brown, D. R., Fife, K. H. and Campo, M. S. (2006a) 'Down-regulation of MHC class I is a property common to papillomavirus E5 proteins', *Virus Research,* 120(1-2).

Ashrafi, G. H., Haghshenas, M., Marchetti, B. and Campo, M. S. (2006b) 'E5 protein of human papillomavirus 16 downregulates HLA class I and interacts with the heavy chain via its first hydrophobic domain', *International Journal of Cancer,* 119(9).

Assarzadegan, N., Brooks, E. and Voltaggio, L. (2022) 'HPV-driven anal neoplasia: review and recent developments', *Pathology,* 54(2).

Aydin, I., Weber, S., Snijder, B., Ventayol, P. S., Kühbacher, A., Becker, M., Day, P. M., Schiller, J. T., Kann, M., Pelkmans, L., Helenius, A. and Schelhaas, M. (2014) 'Large Scale RNAi Reveals the Requirement of Nuclear Envelope Breakdown for Nuclear Import of Human Papillomaviruses', *PLOS Pathogens,* 10(5).

Baeuerle, P. and Henkel, T. (1994) 'Function and activation of NF-kappa B in the immune system', *Annual review of immunology,* 12.

Baker, C. P., W. Lindgren, V. Braun, M, Gonda, M. Howley, P. 1987. Structural and transcriptional analysis of human papillomavirus 16 sequences in cervical carcinoma cell lines. Journal of Virology.

Baker, T., S., Newcomb, W., W., Olson, N., H., Cowsert, L., M., Olson, C. and Brown, J., C. (1991) 'Structures of bovine and human papillomaviruses. Analysis by cryoelectron microscopy and three-dimensional image reconstruction', *Biophysical journal,* 60(6).

Bastien, N. and McBride, A. A. (2000) 'Interaction of the papillomavirus E2 protein with mitotic chromosomes', *Virology,* 270(1).

Basu, S., Binder, R., Suto, R., Anderson, K. and Srivastava, P. (2000) 'Necrotic but not apoptotic cell death releases heat shock proteins, which deliver a partial maturation signal to dendritic cells and activate the NF-kappa B pathway', *International immunology,* 12(11).

Basu, S. and Srivastava, P. K. (2003) 'Fever-like temperature induces maturation of dendritic cells through induction of hsp90', *International Immunology,* 15(9).

Bedard, M. C., Chihanga, T., Carlile, A., Jackson, R., Brusadelli, M. G., Lee, D., VonHandorf, A., Rochman, M., Dexheimer, P. J., Chalmers, J., Nuovo, G., Lehn, M., Williams, D. E. J., Kulkarni, A., Carey, M., Jackson, A., Billingsley, C., Tang, A., Zender, C., ... and Wells, S. I. (2023) 'Single cell

transcriptomic analysis of HPV16-infected epithelium identifies a keratinocyte subpopulation implicated in cancer', *Nature Communications,* 14(1), pp. 1-20.
Bedell, M., A., Hudson, J., B., Golub, T., R., Turyk, M., E., Hosken, M., Wilbanks, G., D. and Laimins, L., A. (1991) 'Amplification of human papillomavirus genomes in vitro is dependent on epithelial differentiation', *Journal of virology,* 65(5).
Belleudi, F., Leone, L., Purpura, V., Cannella, F., Scrofani, C., Torrisi, M. R., Belleudi, F., Leone, L., Purpura, V., Cannella, F., Scrofani, C. and Torrisi, M. R. (2011) 'HPV16 E5 affects the KGFR/FGFR2b-mediated epithelial growth through alteration of the receptor expression, signaling and endocytic traffic', *Oncogene 2011 30:50,* 30(50).
Berezutskaya, E., Yu, B., Morozov, A., Raychaudhuri, P. and Bagchi, S. (1997) 'Differential regulation of the pocket domains of the retinoblastoma family proteins by the HPV16 E7 oncoprotein', *Cell growth & differentiation : the molecular biology journal of the American Association for Cancer Research,* 8(12).
Berman, T., A. and Schiller, J., T. (2017) 'Human papillomavirus in cervical cancer and oropharyngeal cancer: One cause, two diseases', *Cancer,* 123(12).
Bermúdez-Morales, V. H., Peralta-Zaragoza, O., Alcocer-González, J., M., Moreno, J. and Madrid-Marina, V. (2011) 'IL-10 expression is regulated by HPV E2 protein in cervical cancer cells', *Molecular Medicine Reports,* 4(2).
Bernard, H.-U. (1994) 'Coevolution of papiliomaviruses with human populations', *Trends in Microbiology,* 2(4).
Bernard, H.-U., Burk, R. D., Chen, Z., van Doorslaer, K., zur Hansen, H. and de Villiers, E.-M. (2010) 'Classification of papillomaviruses (PVs) based on 189 PV types and proposal of taxonomic amendments', *Virology,* 401(1).
Binder, R. J. and Srivastava, P. K. (2005) 'Peptides chaperoned by heat-shock proteins are a necessary and sufficient source of antigen in the cross-priming of CD8+ T cells', *Nature Immunology 2005 6:6,* 6(6).
Bird, G., O'Donnell, M., Moroianu, J. and Garcea, R. L. (2008) 'Possible Role for Cellular Karyopherins in Regulating Polyomavirus and Papillomavirus Capsid Assembly'.
Bodily, J., M., Mehta, K., P., Cruz, L., Meyers, C. and Laimins, L., A. (2011) 'The E7 open reading frame acts in cis and in trans to mediate differentiation-dependent activities in the human papillomavirus type 16 life cycle', *Journal of virology,* 85(17).
Bono, H. and Hirota, K. (2020) 'Meta-Analysis of Hypoxic Transcriptomes from Public Databases', *Biomedicines,* 8(1).
Bordeaux, J., Forte, S., Harding, E., Darshan, M. S., Klucevsek, K. and Moroianu, J. (2006) 'The L2 Minor Capsid Protein of Low-Risk Human Papillomavirus Type 11 Interacts with Host Nuclear Import Receptors and Viral DNA', *Journal of Virology,* 80(16).
Borrego-Soto, G., Ortiz-López, R. and Rojas-Martínez, A. (2015) 'Ionizing radiation-induced DNA injury and damage detection in patients with breast cancer', *Genetics and Molecular Biology,* 38(4).
Bostofte, E., Berget, A., Falck Larsen, J., Hjortkjaer Pedersen, P. and Rank, F. (1986) 'Conization by carbon dioxide laser or cold knife in the treatment of cervical intra-epithelial neoplasia', *Acta obstetricia et gynecologica Scandinavica,* 65(3).
Boukamp, P., Petrussevska , R. T., Breitkreutz , D., Hornung , J., Markham , A. and Fusenig, N. E. (1988) 'Normal keratinization in a spontaneously immortalized aneuploid human keratinocyte cell line', *The Journal of cell biology,* 106(3).
Bourgault, V., I., Moyal Barracco, M., Ziol, M., Chaboissier, A., Barget, N., Berville, S., Paniel, B., Jullian, E., Clerici, T., Maillère, B. and Guillet, J., G. (2004) 'Spontaneous regression of grade 3 vulvar intraepithelial neoplasia associated with human papillomavirus-16-specific CD4(+) and CD8(+) T-cell responses', *Cancer research,* 64(23).
Boyer, S., Wazer, D. and Band, V. (1996) 'E7 protein of human papilloma virus-16 induces degradation of retinoblastoma protein through the ubiquitin-proteasome pathway', *Cancer research,* 56(20).

Brace, C. L. (2009) 'Radiofrequency and microwave ablation of the liver, lung, kidney and bone: What are the differences: "Organ-specific thermal ablation"', *Current problems in diagnostic radiology,* 38(3).
Bravo, I. G. and Alonso, Á. (2007) 'Phylogeny and evolution of papillomaviruses based on the E1 and E2 proteins', *Virus Genes 2006 34:3,* 34(3).
Breasted, J. H. T. E. S. s. p. 1930. Therapeutic Heat and Cold.: Waverley Press.
Breen, D. J. and Lencioni, R. (2015) 'Image-guided ablation of primary liver and renal tumours', *Nature Reviews Clinical Oncology 2015 12:3,* 12(3).
Breen, E., J., Tan, W. and Khan, A. (2016) 'The Statistical Value of Raw Fluorescence Signal in Luminex xMAP Based Multiplex Immunoassays', *Scientific reports,* 6.
Breitburd, F., Croissant, O. and Orth, G. 1987. Expression of human papillomavirus type-1 E4 gene products in warts. Cancer Cells: Cold Spring Harbor Laboratory Press.
Brisson, M., Kim, J. J., Canfell, K., Drolet, M., Gingras, G., Burger, E. A., Martin, D., Simms, K. T., Bénard, É., Boily, M.-C., Sy, S., Regan, C., Keane, A., Caruana, M., Nguyen, D. T. N., Smith, M. A., Laprise, J.-F., Jit, M., Alary, M., ... and Hutubessy, R. (2020) 'Impact of HPV vaccination and cervical screening on cervical cancer elimination: a comparative modelling analysis in 78 low-income and lower-middle-income countries', *The Lancet,* 395(10224).
Bristow, I., Lim, W., C., Lee, A., Holbrook, D., Savelyeva, N., Thomson, P., Webb, C., Polak, M. and Ardern-Jones, M., R. (2017) 'Microwave therapy for cutaneous human papilloma virus infection', *European journal of dermatology : EJD,* 27(5).
Brown, D. R., Kitchin, D., Qadadri, B., Neptune, N., Batteiger, T. and Ermel, A. (2006) 'The human papillomavirus type 11 E1--E4 protein is a transglutaminase 3 substrate and induces abnormalities of the cornified cell envelope', *Virology,* 345(1).
Brown, D. R., Shew, M. L., Qadadri, B., Neptune, N., Vargas, M., Tu, W., Juliar, B. E., Breen, T. E. and Fortenberry, J. D. (2005) 'A Longitudinal Study of Genital Human Papillomavirus Infection in a Cohort of Closely Followed Adolescent Women', *The Journal of Infectious Diseases,* 191(2).
Bruni, L., Albero, G., Serrano, B., Mena, M., Collado, J., Gómez, D., Muñoz, J., Bosch, F. and de Sanjose, S. 2023. Human Papillomavirus and Related Diseases in the World. ICO/IARC Information Centre on HPV and Cancer (HPV Information Centre).
Bruni, L., Diaz, M., Barrionuevo-Rosas, L., Herrero, R., Bray, F., Bosch, F. X., de Sanjose, S. and Castellsague, X. (2016) 'Global estimates of human papillomavirus vaccination coverage by region and income level: a pooled analysis', *The Lancet. Global health,* 4(7).
Bryan, J. T. and Brown, D. R. (2000) 'Association of the human papillomavirus type 11 E1()E4 protein with cornified cell envelopes derived from infected genital epithelium', *Virology,* 277(2).
Bryan, J. T. and Brown, D. R. (2001) 'Transmission of human papillomavirus type 11 infection by desquamated cornified cells', *Virology,* 281(1).
Buck, C. B., Cheng, N., Thompson, C. D., Lowy, D. R., Steven, A. C., Schiller, J. T. and Trus, B. L. (2008) 'Arrangement of L2 within the papillomavirus capsid', *Journal of virology,* 82(11).
Buck, C. B., Day, P. M. and Trus, B. L. (2013) 'The Papillomavirus Major Capsid Protein L1', *Virology,* 445(0).
Buck, C. B., Pastrana, D. V., Lowy, D. R. and Schiller, J. T. (2004) 'Efficient Intracellular Assembly of Papillomaviral Vectors', *Journal of Virology,* 78(2).
Buck, C. B., Thompson, C. D., Pang, Y.-Y. S., Lowy, D. R. and Schiller, J. T. (2005) 'Maturation of Papillomavirus Capsids', *Journal of Virology,* 79(5).
Bulkmans, N., W, J., Berkhof, J., Bulk, S., Bleeker, M., C, G., van Kemenade, F., J., Rozendaal, L., Snijders, P., J, F. and Meijer, C., J, L, M. (2007) 'High-risk HPV type-specific clearance rates in cervical screening', *British Journal of Cancer,* 96(9), pp. 1419-1424.
Burnett, T. S. and Sleeman, J. P. (1984) 'Uneven distribution of methylation sites within the human papillomavirus la genome: possible relevance to viral gene expression', *Nucleic acids research,* 12(23).
Campo, M. S., Graham, S. V., Cortese, M. S., Ashrafi, G. H., Araibi, E. H., Dornan, E. S., Miners, K., Nunes, C. and Man, S. (2010) 'HPV-16 E5 down-regulates expression of surface HLA class I and reduces recognition by CD8 T cells', *Virology,* 407(1).

Cardone, G., Moyer, A. L., Cheng, N., Thompson, C. D., Dvoretzky, I., Lowy, D. R., Schiller, J. T., Steven, A. C., Buck, C. B. and Trus, B. L. (2014) 'Maturation of the Human Papillomavirus 16 Capsid', *mBio,* 5(4).
Carmody, S. R., Tran, E. J., Apponi, L. H., Corbett, A. H. and Wente, S. R. (2010) 'The mitogen-activated protein kinase Slt2 regulates nuclear retention of non-heat shock mRNAs during heat shock-induced stress', *Molecular and cellular biology,* 30(21).
Castle, P. E., Murokora, D., Perez, C., Alvarez, M., Chong Quek, S. and Campbell, C. (2017) 'Treatment of cervical intraepithelial lesions', *International journal of gynaecology and obstetrics: the official organ of the International Federation of Gynaecology and Obstetrics,* 138 Suppl 1(S1).
Cerqueira, C., Liu, Y., Kühling, L., Chai, W., Hafezi, W., Kuppevelt, T. H. v., Kühn, J. E., Feizi, T. and Schelhaas, M. (2013) 'Heparin increases the infectivity of Human Papillomavirus Type 16 independent of cell surface proteoglycans and induces L1 epitope exposure', *Cellular Microbiology,* 15(11).
Cerqueira, C. and Schiller, J., T. (2017) 'Papillomavirus assembly: An overview and perspectives', *Virus research,* 231.
Chambers, G., Millan, D., Cuschieri, K., Cubie, H. A. and Graham, S. V. (2013) 'Assessing the detection of human papillomavirus late mRNA in liquid base cytology samples for risk stratification of cervical disease', *Journal of Medical Virology,* 86(4).
Chang, Y. E., Pena, L., Sen, G. C., Park, J. K. and Laimins, L. A. (2002) 'Long-Term Effect of Interferon on Keratinocytes That Maintain Human Papillomavirus Type 31', *Journal of Virology,* 76(17).
Chen, J., Xue, Y., Poidinger, M., Lim, T., Chew, S., H., Pang, C., L., Abastado, J., P. and Thierry, F. (2014) 'Mapping of HPV transcripts in four human cervical lesions using RNAseq suggests quantitative rearrangements during carcinogenic progression', *Virology,* 462-463.
Chen, T., Guo, J., Yang, M., Zhu, X. and Cao, X. (2011) 'Chemokine-Containing Exosomes Are Released from Heat-Stressed Tumor Cells via Lipid Raft-Dependent Pathway and Act as Efficient Tumor Vaccine', *The Journal of Immunology,* 186(4).
Cheng, W., Hung, C., Chai, C., Hsu, K., He, L., Rice, C., Ling, M. and Wu, T. (2001) 'Enhancement of Sindbis virus self-replicating RNA vaccine potency by linkage of Mycobacterium tuberculosis heat shock protein 70 gene to an antigen gene', *Journal of immunology (Baltimore, Md. : 1950),* 166(10).
Cheng, Y., Weng, S., Yu, L., Zhu, N., Yang, M. and Yuan, Y. (2019) 'The Role of Hyperthermia in the Multidisciplinary Treatment of Malignant Tumors', *Integrative Cancer Therapies,* 18.
Chermnykh, E. S., Alpeeva, E. V. and Vorotelyak, E. A. (2020) 'Transglutaminase 3: The Involvement in Epithelial Differentiation and Cancer', *Cells,* 9(9).
Chesson, H. W., Dunne, E. F., Hariri, S. and Markowitz, L. E. (2014) 'The Estimated Lifetime Probability of Acquiring Human Papillomavirus in the United States', *Sexually transmitted diseases,* 41(11).
Chojnacki, M. and Melendy, T. (2018) 'The human papillomavirus DNA helicase E1 binds, stimulates, and confers processivity to cellular DNA polymerase epsilon', *Nucleic Acids Research,* 46(1).
Chow, L. T. H., H. Nasseri, M. Stoler, M H. Wolinsky, S.M. Chin, M.T. Hirochika, R. Arvan, D. S. Broker, T.R. (1987) *Human papillomavirus gene expression.* Cancer cells: Cold Spring Harbor Laboratory.
Christensen, N. D. (2005) 'Cottontail rabbit papillomavirus (CRPV) model system to test antiviral and immunotherapeutic strategies', *Antiviral chemistry & chemotherapy,* 16(6).
Christie, G. E. and Calendar, R. (2016) 'Bacteriophage P2', *Bacteriophage,* 6(1).
Cicchese, J., Evans, S., Hult, C., Joslyn, L., Wessler, T., Millar, J., Marino, S., Cilfone, N., Mattila, J., Linderman, J. and Kirschner, D. (2018) 'Dynamic balance of pro- and anti-inflammatory signals controls disease and limits pathology', *Immunological reviews,* 285(1).
Cigno, I. L., Calati, F., Borgogna, C., Zevini, A., Albertini, S., Martuscelli, L., Andrea, M. D., Hiscott, J., Landolfo, S. and Gariglio, M. (2019) 'Human Papillomavirus E7 Oncoprotein Subverts Host Innate Immunity via SUV39H1-Mediated Epigenetic Silencing of Immune Sensor Genes', *Journal of Virology*.

Cladel, N. M., Budgeon, L. R., Balogh, K. K., Cooper, T. K., Hu, J. and Christensen, N. D. (2015) 'A Novel Pre-Clinical Murine Model to Study the Life Cycle and Progression of Cervical and Anal Papillomavirus Infections', *PLoS ONE,* 10(3).
Cladel, N. M., Budgeon, L. R., Balogh, K. K., Cooper, T. K., Hu, J. and Christensen, N. D. (2016) 'Mouse papillomavirus MmuPV1 infects oral mucosa and preferentially targets the base of the tongue', *Virology,* 488.
Cladel, N. M., Budgeon, L. R., Cooper, T. K., Balogh, K. K., Hu, J. and Christensen, N. D. (2013) 'Secondary Infections, Expanded Tissue Tropism, and Evidence for Malignant Potential in Immunocompromised Mice Infected with Mus musculus Papillomavirus 1 DNA and Virus', *Journal of Virology*.
Coleman, N., Birley, H. D., Renton, A. M., Hanna, N. F., Ryait, B. K., Byrne, M., Taylor-Robinson, D. and Stanley, M. A. (1994) 'Immunological events in regressing genital warts', *American journal of clinical pathology,* 102(6).
Conley, M., J., Epifano, I., Kirk, A., Stevenson, A. and Graham, S., V. (2023) 'Microwave hyperthermia represses human papillomavirus oncoprotein activity and induces cell death due to cell stress in 3D tissue models of anogenital precancers and cancers', *EBioMedicine,* 91.
Conway, M. J., Alam, S., Ryndock, E. J., Cruz, L., Christensen, N. D., Roden, R. B. S. and Meyers, C. (2009) 'Tissue-Spanning Redox Gradient-Dependent Assembly of Native Human Papillomavirus Type 16 Virions', *Journal of Virology,* 83(20).
Cortese, M., S., Ashrafi, G., H. and Campo, M., S. (2010) 'All 4 di-leucine motifs in the first hydrophobic domain of the E5 oncoprotein of human papillomavirus type 16 are essential for surface MHC class I downregulation activity and E5 endomembrane localization', *International journal of cancer,* 126(7).
Crezee, H., van Leeuwen, C. M., Oei, A. L., Stalpers, L. J., Bel, A., Franken, N. A. and Kok, H. P. (2016) 'Thermoradiotherapy planning: Integration in routine clinical practice', *International journal of hyperthermia : the official journal of European Society for Hyperthermic Oncology, North American Hyperthermia Group,* 32(1).
Crezee, J., Franken, N. A. P. and Oei, A. L. (2021) 'Hyperthermia-Based Anti-Cancer Treatments', *Cancers,* 13(6).
Cricca, M., Venturoli, S., Leo, E., Costa, S., Musiani, M. and Zerbini, M. (2009) 'Molecular analysis of HPV 16 E6I/E6II spliced mRNAs and correlation with the viral physical state and the grade of the cervical lesion', *Journal of medical virology,* 81(7).
Crook, T., Tidy, J. and Vousden, K. (1991) 'Degradation of p53 can be targeted by HPV E6 sequences distinct from those required for p53 binding and trans-activation', *Cell,* 67(3).
Cubie, H. A. (2013) 'Diseases associated with human papillomavirus infection', *Virology,* 445(1-2).
Cumming, S. A., McPhillips, M. G., Veerapraditsin, T., Milligan, S. G. and Graham, S. V. (2003) 'Activity of the Human Papillomavirus Type 16 Late Negative Regulatory Element Is Partly due to Four Weak Consensus 5′ Splice Sites That Bind a U1 snRNP-Like Complex', *Journal of Virology,* 77(9).
Cumming, S. A., Repellin, C. E., McPhillips, M., Radford, J. C., Clements, J. B. and Graham, S. V. (2002) 'The Human Papillomavirus Type 31 Late 3′ Untranslated Region Contains a Complex Bipartite Negative Regulatory Element', *Journal of Virology,* 76(12).
Darshan, M. S., Lucchi, J., Harding, E. and Moroianu, J. (2004) 'The L2 Minor Capsid Protein of Human Papillomavirus Type 16 Interacts with a Network of Nuclear Import Receptors', *Journal of Virology,* 78(22).
Davy, C. E., Jackson, D. J., Wang, Q., Raj, K., Masterson, P. J., Fenner, N. F., Southern, S., Cuthill, S., Millar, J. B. A. and Doorbar, J. (2002) 'Identification of a G2 Arrest Domain in the E1∧E4 Protein of Human Papillomavirus Type 16', *Journal of Virology,* 76(19).
Day, P. M., Baker, C. C., Lowy, D. R. and Schiller, J. T. (2004) 'Establishment of papillomavirus infection is enhanced by promyelocytic leukemia protein (PML) expression', *Proceedings of the National Academy of Sciences,* 101(39).
Day, P. M., Roden, R. B. S., Lowy, D. R. and Schiller, J. T. (1998) 'The Papillomavirus Minor Capsid Protein, L2, Induces Localization of the Major Capsid Protein, L1, and the Viral Transcription/Replication Protein, E2, to PML Oncogenic Domains'.

Day, P. M., Thompson, C. D., Schowalter, R. M., Lowy, D. R. and Schiller, J. T. (2013) 'Identification of a Role for the trans-Golgi Network in Human Papillomavirus 16 Pseudovirus Infection', *Journal of Virology*.
de Berker, D., McGregor, J. M., Mohd Mustapa, M. F., Exton, L. S. and Hughers, B. R. (2017) 'British Association of Dermatologists' guidelines for the care of patients with actinic keratosis 2017', *The British journal of dermatology,* 176(1).
de Boer, P., Hoogenboom, J. P. and Giepmans, B. N. G. (2015) 'Correlated light and electron microscopy: ultrastructure lights up!', *Nature Methods 2015 12:6,* 12(6).
de Jong, A., van der Burg, S. H., Kwappenberg, K. M., van der Hulst, J. M., Franken, K. L., Geluk, A., van Meijgaarden, K. E., Drijfhout, J. W., Kenter, G., Vermeij, P., Melief, C. J. and Offringa, R. 2002. Frequent detection of human papillomavirus 16 E2-specific T-helper immunity in healthy subjects. *Cancer Research*.
De Marco, F. and Marcante, M. (1993) 'HPV-16 E6-E7 differential transcription induced in Siha cervical cancer cell line by interferons', *Journal of biological regulators and homeostatic agents,* 7(1).
de Sanjose, S., Brotons, M., LaMontagne, D. S. and Bruni, L. (2019) 'Human papillomavirus vaccine disease impact beyond expectations', *Current Opinion in Virology,* 39.
de Villiers, E.-M., Fauquet , C., Broker , T. R., Bernard , H.-U. and zur Hausen, H. (2004) 'Classification of papillomaviruses', *Virology,* 324(1).
De Vuyst, H., Lillo, F., Broutet, N. and Smith, J. S. (2008) 'HIV, human papillomavirus, and cervical neoplasia and cancer in the era of highly active antiretroviral therapy', *European journal of cancer prevention : the official journal of the European Cancer Prevention Organisation (ECP),* 17(6).
Del Nonno, F., Pisani, G., Visca, P., Signore, F., Grillo, L. R., Baiocchini, A., Garbuglia, A. R., Sepe, S., Piacentini, M. and Falasca, L. (2011) 'Role and predictive strength of transglutaminase type 2 expression in premalignant lesions of the cervix', *Modern Pathology 2011 24:6,* 24(6).
del Pino, M., Vorsters, A., Joura, E. A., Doorbar, J., Haniszewski, M., Gudina, I. A., Kodjamanova, P., Velicer, C. and Drury, R. (2024) 'Risk factors for human papillomavirus infection and disease: A targeted literature summary', *Journal of Medical Virology,* 96(2).
Denslow, S. A., Rositch, A. F., Firnhaber, C., Ting, J., Smith, J. S. and Sheri A Denslow, A. F. R., Cynthia Firnhaber, Jie Ting, Jennifer S Smith (2013) 'Incidence and progression of cervical lesions in women with HIV: a systematic global review', *International Journal of STD & AIDS,* 25(3).
Deshmukh, A. A., Suk, R., Shiels, M. S., Sonawane, K., Nyitray, A. G., Liu, Y., Gaisa, M. M., Palefsky, J. M. and Sigel, K. (2020) 'Recent Trends in Squamous Cell Carcinoma of the Anus Incidence and Mortality in the United States, 2001-2015', *Journal of the National Cancer Institute,* 112(8).
Dey, P., Gibbs, A., Arnold, D. F., Saleh, N., Hirsch, P. J. and Woodman, C. B. J. (2002) 'Loop diathermy excision compared with cervical laser vaporisation for the treatment of intraepithelial neoplasia: a randomised controlled trial', *BJOG: An International Journal of Obstetrics & Gynaecology,* 109(4).
DiGiuseppe, S., Bienkowska-Haba, M., Guion, L. G. and Sapp, M. (2017) 'Cruising the cellular highways: How human papillomavirus travels from the surface to the nucleus', *Virus Research,* 231.
Doorbar, J. (2005) 'The papillomavirus life cycle', *Journal of clinical virology : the official publication of the Pan American Society for Clinical Virology,* 32 Suppl 1.
Doorbar, J. (2006) 'Molecular biology of human papillomavirus infection and cervical cancer', *Clinical Science,* 110(5).
Doorbar, J. (2013) 'The E4 protein; structure, function and patterns of expression', *Virology,* 445(1-2).
Doorbar, J., Campbell, D., Grand, R. J. and Gallimore, P. H. (1986) 'Identification of the human papilloma virus-1a E4 gene products.', *The EMBO Journal,* 5(2).
Doorbar, J., Elston, R. C., Napthine, S., Raj, K., Medcalf, E., Jackson, D., Coleman, N., Griffin, H. M., Masterson, P., Stacey, S., Mengistu, Y. and Dunlop, J. (2000) 'The E1^E4 Protein of Human Papillomavirus Type 16 Associates with a Putative RNA Helicase through Sequences in Its C Terminus', *Journal of Virology,* 74(21).

Doorbar, J., Foo, C., Coleman, N., Medcalf, L., Hartley, O., Prospero, T., Napthine, S., Sterling, J., Winter, G. and Griffin, H. (1997) 'Characterization of Events during the Late Stages of HPV16 Infectionin VivoUsing High-Affinity Synthetic Fabs to E4', *Virology,* 238(1).
Doorbar, J. and Griffin, H. (2019) 'Refining our understanding of cervical neoplasia and its cellular origins', *Papillomavirus research,* 7.
Doorbar, J., Quint, W., Banks, L., Bravo, I. G., Stoler, M., Broker, T. R. and Stanley, M. A. (2012) 'The biology and life-cycle of human papillomaviruses', *Vaccine,* 30 Suppl 5.
Doorslaer, K. V. (2013) 'Evolution of the Papillomaviridae', *Virology,* 445(1-2).
Doorslaer, K. V., Chen, Z., Bernard, H.-U., Chan, P. K. S., DeSalle, R., Dillner, J., Forslund, O., Haga, T., McBride, A. A., Villa, L. L., Burk, R. D. and Consortium, I. R. (2018) 'ICTV Virus Taxonomy Profile: Papillomaviridae', *The Journal of General Virology,* 99(8).
Duan, T.-L., Jiao, H., He, G.-J., Yan, Y.-B., Duan, T.-L., Jiao, H., He, G.-J. and Yan, Y.-B. (2020) 'Translation Efficiency and Degradation of ER-Associated mRNAs Modulated by ER-Anchored poly(A)-Specific Ribonuclease (PARN)', *Cells 2020, Vol. 9, Page 162,* 9(1).
Duensing, S. and Münger, K. (2004) 'Mechanisms of genomic instability in human cancer: Insights from studies with human papillomavirus oncoproteins', *International Journal of Cancer,* 109(2).
Duman, R. S., Adams, D. H. and Simen, B. B. (2005) 'Transcription factors as modulators of stress responsivity', *Handbook of Stress and the Brain - Part 1: The Neurobiology of Stress,* 15.
Duncan, I. (1983) 'The Semm cold coagulator in the management of cervical intraepithelial neoplasia', *Clinical obstetrics and gynecology,* 26(4).
Dupuy, C., Buzoni-Gatel, D., Touze, A., Le Cann, P., Bout, D. and Coursaget, P. (1997) 'Cell mediated immunity induced in mice by HPV 16 L1 virus-like particles', *Microbial pathogenesis,* 22(4).
Eckert, R., L., Sturniolo, M., T., Broome, A., M., Ruse, M. and Rorke, E., A. (2005) 'Transglutaminase function in epidermis', *The Journal of investigative dermatology,* 124(3).
Eferl, R. and Wagner, E. F. (2003) 'AP-1: a double-edged sword in tumorigenesis', *Nature Reviews Cancer 2003 3:11,* 3(11).
Egawa, K. (2003) 'Do human papillomaviruses target epidermal stem cells?', *Dermatology,* 207(3).
Egawa, N. and Doorbar, J. (2017) 'The low-risk papillomaviruses', *Virus Research,* 231.
Egawa, N., Egawa, K., Griffin, H. and Doorbar, J. (2015) 'Human Papillomaviruses; Epithelial Tropisms, and the Development of Neoplasia', *Viruses,* 7(7), pp. 3863-3890.
El Awady, M., K, Kaplan, J., B., O'Brien, S., J. and Burk, R., D. (1987) 'Molecular analysis of integrated human papillomavirus 16 sequences in the cervical cancer cell line SiHa', *Virology,* 159(2).
Elming, P. B., Sørensen, B. S., Oei, A. L., Franken, N. A. P., Crezee, J., Overgaard, J. and Horsman, M. R. (2019) 'Hyperthermia: The Optimal Treatment to Overcome Radiation Resistant Hypoxia', *Cancers,* 11(1).
Erickson, K. D., Bouchet-Marquis, C., Heiser, K., Szomolanyi-Tsuda, E., Mishra, R., Lamothe, B., Hoenger, A. and Garcea, R. L. (2012) 'Virion assembly factories in the nucleus of polyomavirus-infected cells', *PLoS pathogens,* 8(4).
Facciorusso, A., Aziz, M. A. A. E., Tartaglia, N., Ramai, D., Mohan, B. P., Cotsoglou, C., Pusceddu, S., Giacomelli, L., Ambrosi, A. and Sacco, R. (2020) 'Microwave Ablation Versus Radiofrequency Ablation for Treatment of Hepatocellular Carcinoma: A Meta-Analysis of Randomized Controlled Trials', *Cancers 2020, Vol. 12, Page 3796,* 12(12).
Feder, M. and Hofmann, G. (1999) 'Heat-shock proteins, molecular chaperones, and the stress response: evolutionary and ecological physiology', *Annual review of physiology,* 61.
Femino, A., Fay, F., Fogarty, K. and Singer, R. (1998) 'Visualization of single RNA transcripts in situ', *Science (New York, N.Y.),* 280(5363).
Ferguson, J., Campos-León, K., Pentland, I., Stockton, J., D., Günther, T., Beggs, A., D., Grundhoff, A., Roberts, S., Noyvert, B. and Parish, J., L. (2021) 'The chromatin insulator CTCF regulates HPV18 transcript splicing and differentiation-dependent late gene expression', *PLoS pathogens,* 17(11).
Filippova, M., Parkhurst, L. and Duerksen-Hughes, P. J. (2004) 'The human papillomavirus 16 E6 protein binds to Fas-associated death domain and protects cells from Fas-triggered apoptosis', *The Journal of biological chemistry,* 279(24).

Filippova, M., Song, H., Connolly, J. L., Dermody, T. S. and Duerksen-Hughes, P. J. (2002) 'The human papillomavirus 16 E6 protein binds to tumor necrosis factor (TNF) R1 and protects cells from TNF-induced apoptosis', *The Journal of biological chemistry,* 277(24).
Flores, E., R., Allen-Hoffmann, B., L., Lee, D., Sattler, C., A. and Lambert, P., F. (1999) 'Establishment of the human papillomavirus type 16 (HPV-16) life cycle in an immortalized human foreskin keratinocyte cell line', *Virology,* 262(2).
Florin, L., Sapp, C., Streeck, R. E. and Sapp, M. (2002a) 'Assembly and translocation of papillomavirus capsid proteins', *Journal of Virology,* 76(19).
Florin, L., Schafer, F., Sotlar, K., Streeck, R. E. and Sapp, M. (2002b) 'Reorganization of nuclear domain 10 induced by papillomavirus capsid protein L2', *Virology,* 295(1).
Franckena, M. (2012) 'Review of radiotherapy and hyperthermia in primary cervical cancer', *International journal of hyperthermia : the official journal of European Society for Hyperthermic Oncology, North American Hyperthermia Group,* 28(6).
Franckena, M., Stalpers, L. J., Koper, P. C. M., Wiggenraad, R. G. J., Hoogenraad, W. J., van Dijk, J. D. P., Warlam-Rodenhuis, C. C., Jobsen, J. J., van Rhoon, G. C. and van der Zee, J. (2008) 'Long-term improvement in treatment outcome after radiotherapy and hyperthermia in locoregionally advanced cervix cancer: an update of the Dutch Deep Hyperthermia Trial', *International journal of radiation oncology, biology, physics,* 70(4).
Franco, E. L., Villa, L. L., Sobrinho, J. P., Prado, J. M., Rousseau, M. C., Desy, M. and Rohan, T. E. (1999) 'Epidemiology of acquisition and clearance of cervical human papillomavirus infection in women from a high-risk area for cervical cancer', *The Journal of infectious diseases,* 180(5).
Frazer, I. H. (2019) 'The HPV Vaccine Story', *ACS Pharmacology & Translational Science,* 2(3).
Friedl, F., Kimura, I., Osato, T. and Ito, Y. (1970) 'Studies on a New Human Cell Line (SiHa) Derived from Carcinoma of Uterus. I. Its Establishment and Morphology1', *Proceedings of the Society for Experimental Biology and Medicine,* 135(2).
Fruchter, R. G., Maiman, M., Sedlis, A., Bartley, L., Camilien, L. and Arrastia, C. D. (1996) 'Multiple recurrences of cervical intraepithelial neoplasia in women with the human immunodeficiency virus', *Obstetrics and gynecology,* 87(3).
Fuchs, E. and Green, H. (1980) 'Changes in keratin gene expression during terminal differentiation of the keratinocyte', *Cell,* 19(4).
Garzetti, G. G., Ciavattini, A., Goteri, G., De Nictolis, M., Menso, S., Muzzioli, M. and Fabris, N. (1995) 'HPV DNA positivity and natural killer cell activity in the clinical outcome of mild cervical dysplasia: integration between virus and immune system', *Gynecologic and obstetric investigation,* 39(2).
Gheit, T. (2019) 'Mucosal and Cutaneous Human Papillomavirus Infections and Cancer Biology', *Frontiers in oncology,* 9.
Ghim, S., Newsome, J., Bell, J., Sundberg, J. P., Schlegel, R. and Jenson, A. B. (2000) 'Spontaneously regressing oral papillomas induce systemic antibodies that neutralize canine oral papillomavirus', *Experimental and molecular pathology,* 68(3).
Giuliano, A. R., Harris, R., Sedjo, R. L., Baldwin, S., Roe, D., Papenfuss, M. R., Abrahamsen, M., Inserra, P., Olvera, S. and Hatch, K. (2002) 'Incidence, Prevalence, and Clearance of Type-Specific Human Papillomavirus Infections: The Young Women's Health Study', *The Journal of Infectious Diseases,* 186(4).
Goetschius, D. J., Hartmann, S. R., Subramanian, S., Bator, C. M., Christensen, N. D. and Hafenstein, S. L. (2021) 'High resolution cryo EM analysis of HPV16 identifies minor structural protein L2 and describes capsid flexibility', *Scientific Reports,* 11(1), pp. 1-15.
Gomez-Pastor, R., Burchfiel, E. and Thiele, D. (2018) 'Regulation of heat shock transcription factors and their roles in physiology and disease', *Nature reviews. Molecular cell biology,* 19(1).
Goon, P., Sonnex, C., Jani, P., Stanley, M., Sudhoff, H., Goon, P., Sonnex, C., Jani, P., Stanley, M. and Sudhoff, H. (2007) 'Recurrent respiratory papillomatosis: an overview of current thinking and treatment', *European Archives of Oto-Rhino-Laryngology 2007 265:2,* 265(2).
Gornemann, J., Hofmann, T. G., Will, H. and Muller, M. (2002) 'Interaction of Human Papillomavirus Type 16 L2 with Cellular Proteins: Identification of Novel Nuclear Body-Associated Proteins', *Virology,* 303(1).

Graham, S., V. (2010) 'Human papillomavirus: gene expression, regulation and prospects for novel diagnostic methods and antiviral therapies', *Future microbiology,* 5(10).
Graham, S. V. (2017) 'The human papillomavirus replication cycle, and its links to cancer progression: a comprehensive review', *Clinical science (London, England : 1979),* 131(17).
Graham, S. V. (2024) 'HPV and RNA Binding Proteins: What We Know and What Remains to Be Discovered', *Viruses,* 16(5), pp. 783.
Graham, S. V. and Faizo, A. A. A. (2017) 'Control of human papillomavirus gene expression by alternative splicing', *Virus Research,* 231.
Gravitt, P., E. (2011) 'The known unknowns of HPV natural history', *The Journal of clinical investigation,* 121(12).
Gruener, M., Bravo, I. G., Momburg, F., Alonso, A., Tomakidi, P., Gruener, M., Bravo, I. G., Momburg, F., Alonso, A. and Tomakidi, P. (2007) 'The E5 protein of the human papillomavirus type 16 down-regulates HLA-I surface expression in calnexin-expressing but not in calnexin-deficient cells', *Virology Journal 2007 4:1,* 4(1).
Grulich, A., E., Poynten, I., M., Machalek, D., A., Jin, F., Templeton, D., J. and Hillman, R., J. (2012) 'The epidemiology of anal cancer', *Sexual health,* 9(6).
Guion, L. G. and Sapp, M. (2020) 'The Role of Promyelocytic Leukemia Nuclear Bodies During HPV Infection', *Frontiers in Cellular and Infection Microbiology,* 10.
Gunasekharan, V., Haché, G. and Laimins, L. (2012) 'Differentiation-dependent changes in levels of C/EBPβ repressors and activators regulate human papillomavirus type 31 late gene expression', *Journal of virology,* 86(9).
Gunasekharan, V., Li, Y., Andrade, J. and Laimins, L. (2016) 'Post-Transcriptional Regulation of KLF4 by High-Risk Human Papillomaviruses Is Necessary for the Differentiation-Dependent Viral Life Cycle', *PLoS pathogens,* 12(7).
Guo, Y., Guettouche, T., Fenna, M., Boellmann, F., Pratt, W. B., Toft, D. O., Smith, D. F. and Voellmy, R. (2001) 'Evidence for a Mechanism of Repression of Heat Shock Factor 1 Transcriptional Activity by a Multichaperone Complex', *Journal of Biological Chemistry,* 276(49).
Habiger, C., Jäger, G., Walter, M., Iftner, T. and Stubenrauch, F. (2015) 'Interferon Kappa Inhibits Human Papillomavirus 31 Transcription by Inducing Sp100 Proteins', *Journal of Virology,* 90(2).
Hagon, W., Hagon, J., Noble, G., Brenton-Rule, A., Stewart, S. and Bristow, I. (2023) 'Microwave therapy for the treatment of plantar warts', *Journal of Foot and Ankle Research 2023 16:1,* 16(1).
Han, H., Shim, H., Shin, D., Shim, J. E., Ko, Y., Shin, J., Kim, H., Cho, A., Kim, E., Lee, T., Kim, H., Kim, K., Yang, S., Bae, D., Yun, A., Kim, S., Kim, C. Y., Cho, H. J., Kang, B., ... and Lee, I. (2015) 'TRRUST: a reference database of human transcriptional regulatory interactions', *Scientific Reports,* 5(1), pp. 1-11.
Hanson, H. H., Reilly, J. E., Lee, R., Janssen, W. G. and Phillip, G. R. (2010) 'Streamlined embedding of cell monolayers on gridded glass-bottom imaging dishes for correlative light and electron microscopy', *Microscopy and microanalysis : the official journal of Microscopy Society of America, Microbeam Analysis Society, Microscopical Society of Canada,* 16(6).
Hartl, F., Bracher, A. and Hayer-Hartl, M. (2011) 'Molecular chaperones in protein folding and proteostasis', *Nature,* 475(7356).
Hasan, U. (2014) 'Human papillomavirus (HPV) deregulation of Toll-like receptor 9', *Oncoimmunology,* 3.
Hasan, U. A., Zannetti, C., Parroche, P., Goutagny, N., Malfroy, M., Roblot, G., Carreira, C., Hussain, I., Muller, M., Taylor-Papadimitriou, J., Picard, D., Sylla, B. S., Trinchieri, G., Medzhitov, R. and Tommasino, M. (2013) 'The human papillomavirus type 16 E7 oncoprotein induces a transcriptional repressor complex on the Toll-like receptor 9 promoter', *The Journal of experimental medicine,* 210(7).
Hasday, J. D., Thompson, C. and Singh, I. S. (2014) 'Fever, Immunity, and Molecular Adaptations', *Comprehensive Physiology,* 4.
Hayden, M., West, A. and Ghosh, S. (2006) 'NF-kappaB and the immune response', *Oncogene,* 25(51).
Heck, D., Yee, C., Howley, P. and Münger, K. (1992) 'Efficiency of binding the retinoblastoma protein correlates with the transforming capacity of the E7 oncoproteins of the human

papillomaviruses', *Proceedings of the National Academy of Sciences of the United States of America,* 89(10).
Heino, P., Zhou, J. and F., L. P. (2000) 'Interaction of the Papillomavirus Transcription/Replication Factor, E2, and the Viral Capsid Protein, L2', *Virology,* 276(2).
Heled, Y., Fleischmann, C. and Epstein, Y. (2013) 'Cytokines and their role in hyperthermia and heat stroke', *Journal of basic and clinical physiology and pharmacology,* 24(2).
Hemmi, H., Takeuchi, O., Kawai, T., Kaisho, T., Sato, S., Sanjo, H., Matsumoto, M., Hoshino, K., Wagner, H., Takeda, K., Akira, S., Hemmi, H., Takeuchi, O., Kawai, T., Kaisho, T., Sato, S., Sanjo, H., Matsumoto, M., Hoshino, K., ... and Akira, S. (2000) 'A Toll-like receptor recognizes bacterial DNA', *Nature 2000 408:6813,* 408(6813).
Herdman, T., M., Pett, M. R., Roberts, I., Alazawi, W. O. F., Teschendorff, A. E., Zhang, X.-Y., Stanley, M. A. and Coleman, N. (2006) 'Interferon-β treatment of cervical keratinocytes naturally infected with human papillomavirus 16 episomes promotes rapid reduction in episome numbers and emergence of latent integrants', *Carcinogenesis,* 27(11), pp. 2341-2353.
Higgins, R. V., van Nagell, J. R., Donaldson, E. S., Gallion, H. H., Pavlik, E. J. and Kryscio, R. J. (1990) 'The efficacy of laser therapy in the treatment of cervical intraepithelial neoplasia', *Gynecologic Oncology,* 36(1).
Hoffmann, R., Hirt, B., Bechtold, V., Beard, P. and Raj, K. (2006) 'Different modes of human papillomavirus DNA replication during maintenance', *Journal of virology,* 80(9).
Hong, S., Mehta, K., P. and Laimins, L., A. (2011) 'Suppression of STAT-1 expression by human papillomaviruses is necessary for differentiation-dependent genome amplification and plasmid maintenance', *Journal of virology,* 85(18).
Hu, C., Yang, J., Qi, Z., Wu, H., Wang, B., Zou, F., Mei, H., Liu, J., Wang, W. and Liu, Q. (2022) 'Heat shock proteins: Biological functions, pathological roles, and therapeutic opportunities', *MedComm,* 3(3).
Hu, J., Budgeon, L. R., Cladel, N. M., Balogh, K., Myers, R., Cooper, T. K. and Christensen, N. D. (2015) 'Tracking vaginal, anal and oral infection in a mouse papillomavirus infection model', *The Journal of General Virology,* 96(Pt 12).
Hu, J., Cladel, N. M., Budgeon, L. R., Balogh, K. K. and Christensen, N. D. (2017) 'The Mouse Papillomavirus Infection Model', *Viruses,* 9(9).
Hufbauer, M. and Akgül, B. (2017) 'Molecular Mechanisms of Human Papillomavirus Induced Skin Carcinogenesis', *Viruses 2017, Vol. 9, Page 187,* 9(7).
Hummel, M., Hudson, J., B. and Laimins, L., A. (1992) 'Differentiation-induced and constitutive transcription of human papillomavirus type 31b in cell lines containing viral episomes', *Journal of virology,* 66(10).
IARC (2012) 'Biological agents', *IARC monographs on the evaluation of carcinogenic risks to humans,* 100(Pt B).
IARC 2022. Cervical cancer screening. IARC Handbooks of cancer prevention.
IARC. (2007) 'Human Papillomavirus (HPV) Infection'.
Ihara, M., Takeshita, S., Okaichi, K., Okumura, Y. and Ohnishi, T. (2014) 'Heat exposure enhances radiosensitivity by depressing DNA-PK kinase activity during double strand break repair'.
Ilves, I., Kivi, S. and Ustav, M. (1999) 'Long-Term Episomal Maintenance of Bovine Papillomavirus Type 1 Plasmids Is Determined by Attachment to Host Chromosomes, Which Is Mediated by the Viral E2 Protein and Its Binding Sites', *Journal of Virology*.
Iost, I. and Dreyfus, M. (1994) 'mRNAs can be stabilized by DEAD-box proteins', *Nature,* 372(6502).
Israr, M., Rosenthal, D., Frejo-Navarro, L., DeVoti, J., Meyers, C., Bonagura, V. R., Israr, M., Rosenthal, D., Frejo-Navarro, L., DeVoti, J., Meyers, C. and Bonagura, V. R. (2018) 'Microarray analysis of human keratinocytes from different anatomic sites reveals site-specific immune signaling and responses to human papillomavirus type 16 transfection', *Molecular Medicine 2018 24:1,* 24(1).
Ito, A., Tanaka, K., Kondo, K., Shinkai, M., Honda, H., Matsumoto, K., Saida, T. and Kobayashi, T. (2003) 'Tumor regression by combined immunotherapy and hyperthermia using magnetic nanoparticles in an experimental subcutaneous murine melanoma', *Cancer Science,* 94(3).

Jablonska, S., Orth, G., Obalek, S. and Croissant, O. (1985) 'Cutaneous warts clinical, histologic, and virologic correlations', *Clinics in Dermatology,* 3(4).
Jackson, D. N., Hogarth, F. J., Sutherland, D., Holmes, E. M., Donnan, P. T. and Proby, C. M. (2020) 'A feasibility study of microwave therapy for precancerous actinic keratosis', *British Journal of Dermatology,* 183(2).
Jain, S., Moore, R. A., Anderson, D. M., Gough, G. W. and Stanley, M. A. (2006) 'Cell-mediated immune responses to COPV early proteins', *Virology,* 356(1-2).
Jentsch, M., Snyder, P., Sheng, C., Cristiano, E. and Loewer, A. (2020) 'p53 dynamics in single cells are temperature-sensitive', *Scientific reports,* 10(1).
Jentschke, M., Kampers, J., Becker, J., Sibbertsen, P. and Hillemanns, P. (2020) 'Prophylactic HPV vaccination after conization: A systematic review and meta-analysis', *Vaccine,* 38(41).
Johansson, C. and Schwartz, S. (2013) 'Regulation of human papillomavirus gene expression by splicing and polyadenylation', *Nature reviews. Microbiology,* 11(4).
Joyce, J. G., Tung, J. S., Przysiecki, C. T., Cook, J. C., Lehman, E. D., Sands, J. A., Jansen, K. U. and Keller, P. M. (1999) 'The L1 major capsid protein of human papillomavirus type 11 recombinant virus-like particles interacts with heparin and cell-surface glycosaminoglycans on human keratinocytes', *The Journal of biological chemistry,* 274(9).
Kadish, A. S., Ho, G. Y., Burk, R. D., Wang, Y., Romney, S. L., Ledwidge, R. and Angeletti, R. H. (1997) 'Lymphoproliferative responses to human papillomavirus (HPV) type 16 proteins E6 and E7: outcome of HPV infection and associated neoplasia', *Journal of the National Cancer Institute,* 89(17).
Kajitani, N. and Schwartz, S. (2022) 'The role of RNA-binding proteins in the processing of mRNAs produced by carcinogenic papillomaviruses', *Seminars in Cancer Biology,* 86.
Kalabusheva, E., Shtompel, A., Rippa, A., Ulianov, S., Razin, S. and Vorotelyak, E. (2023) 'A Kaleidoscope of Keratin Gene Expression and the Mosaic of Its Regulatory Mechanisms', *International journal of molecular sciences,* 24(6).
Kalantari, M., Osann, K., Calleja-Macias, I., E., S., K., Yan, B., Jordan, S., Chase, D., M., Tewari, K., S. and Bernard, H., U. (2014) 'Methylation of human papillomavirus 16, 18, 31, and 45 L2 and L1 genes and the cellular DAPK gene: Considerations for use as biomarkers of the progression of cervical neoplasia', *Virology,* 448.
Kang, S. D., Chatterjee, S., Alam, S., Salzberg, A. C., Milici, J., van der Burg, S. H. and Meyers, C. (2018) 'Effect of Productive Human Papillomavirus 16 Infection on Global Gene Expression in Cervical Epithelium', *Journal of Virology,* 92(20).
Karim, R., Meyers, C., Backendorf, C., Ludigs, K., Offringa, R., Ommen, G.-J. B. v., Melief, C. J. M., Burg, S. H. v. d. and Boer, J. M. (2011) 'Human Papillomavirus Deregulates the Response of a Cellular Network Comprising of Chemotactic and Proinflammatory Genes', *PLOS ONE,* 6(3).
Karin, M., Liu, Z. g. and Zandi, E. (1997) 'AP-1 function and regulation', *Current opinion in cell biology,* 9(2).
Karstensen, B., Poppelreuther, S., Bonin, M., Walter, M., Iftner, T. and Stubenrauch, F. (2006) 'Gene expression profiles reveal an upregulation of E2F and downregulation of interferon targets by HPV18 but no changes between keratinocytes with integrated or episomal viral genomes', *Virology,* 353(1).
Kennedy, I. M., Haddow, J. K. and Clements, J. B. (1990) 'Analysis of human papillomavirus type 16 late mRNA 3' processing signals in vitro and in vivo'.
Kennedy, I. M., Haddow, J. K. and Clements, J. B. (1991) 'A negative regulatory element in the human papillomavirus type 16 genome acts at the level of late mRNA stability', *Journal of Virology*.
Kieback, E. and Müller, M. (2006) 'Factors influencing subcellular localization of the human papillomavirus L2 minor structural protein', *Virology,* 345(1).
Kim, D., Langmead, B., Salzberg, S. L., Kim, D., Langmead, B. and Salzberg, S. L. (2015) 'HISAT: a fast spliced aligner with low memory requirements', *Nature Methods 2015 12:4,* 12(4).
Kim, K. H., Greenfield, W. W., Cannon, M. J., Coleman, H. N., Spencer, H. J. and Nakagawa, M. (2012) 'CD4+ T-cell response against human papillomavirus type 16 E6 protein is associated with a favorable clinical trend', *Cancer immunology, immunotherapy : CII,* 61(1).

Kim, Y., Lee, J., Kim, E. T., Shin, H. J., Gu, S. Y., Seol, H. S., Ling, P. D., Lee, C. H. and Ahn, J. (2011) 'Human Cytomegalovirus Infection Causes Degradation of Sp100 Proteins That Suppress Viral Gene Expression', *Journal of Virology*.
Kines, R. C., Thompson, C. D., Lowy, D. R., T Schiller, J. T. and Day, P. M. (2009) 'The initial steps leading to papillomavirus infection occur on the basement membrane prior to cell surface binding', *Proceedings of the National Academy of Sciences of the United States of America,* 106(48).
Kirk, A. and Graham, S., V. (2024) 'The human papillomavirus late life cycle and links to keratinocyte differentiation', *Journal of medical virology,* 96(2).
Kirnbauer, R. B., F. Cheng, N. Lowy, D, R. Schiller, J, T. (1992) 'Papillomavirus L1 major capsid protein self-assembles into virus-like particles that are highly immunogenic. | Proceedings of the National Academy of Sciences'.
Kiyono, T., Hiraiwa, A., Fujita, M., Hayashi, Y., Akiyama, T. and Ishibashi, M. (1997) 'Binding of high-risk human papillomavirus E6 oncoproteins to the human homologue of the Drosophila discs large tumor suppressor protein', *Proceedings of the National Academy of Sciences of the United States of America,* 94(21).
Kjær, S. K., Trung Nam, T., Sparen, P., Tryggvadottir, L., Munk, C., Dasbach, E., Liaw, K.-L., Nygård, J. and Nygård, M. (2007) 'The Burden of Genital Warts: A Study of Nearly 70,000 Women from the General Female Population in the 4 Nordic Countries', *The Journal of Infectious Diseases,* 196(10).
Klagge, I. M. and Schneider-Schaulies, S. (1999) 'Virus interactions with dendritic cells', *Journal of General Virology,* 80(4).
Klug, A. and Finch, J. T. (1965) 'Structure of viruses of the papilloma-polyoma type I human wart virus', *Journal of molecular biology,* 11(2).
Klymenko, T., Gu, Q., Herbert, I., Stevenson, A., Iliev, V., Watkins, G., Pollock, C., Bhatia, R., Cuschieri, K., Herzyk, P., Gatherer, D. and Graham, S. (2017) 'RNA-Seq Analysis of Differentiated Keratinocytes Reveals a Massive Response to Late Events during Human Papillomavirus 16 Infection, Including Loss of Epithelial Barrier Function', *Journal of virology,* 91(24).
Klymenko, T., Hernandez-Lopez, H., MacDonald, A. I., Bodily, J. M. and Graham, S. V. (2016) 'Human Papillomavirus E2 Regulates SRSF3 (SRp20) To Promote Capsid Protein Expression in Infected Differentiated Keratinocytes', *Journal of Virology,* 90(10).
Koffa, M. D., Graham, S. V., Takagaki, Y., Manley, J. L. and Clements, J. B. (2000) 'The human papillomavirus type 16 negative regulatory RNA element interacts with three proteins that act at different posttranscriptional levels', *Proceedings of the National Academy of Sciences,* 97(9).
Kong, G., Braun, D. R. and Dewhirst, M. W. 2001. Characterization of the effect of hyperthermia on nanoparticle extravasation from tumor vasculature. *Cancer Research*.
Konya, J. and Dillner, J. (2001) 'Immunity to oncogenic human papillomaviruses', *Advances in cancer research,* 82.
Kozak, M. (1991) 'An analysis of vertebrate mRNA sequences: intimations of translational control', *The Journal of cell biology,* 115(4).
Kozak, M. (2002) 'Pushing the limits of the scanning mechanism for initiation of translation', *Gene,* 299(1-2).
Krump, N. A., You, J., Krump, N. A. and You, J. (2018) 'Molecular mechanisms of viral oncogenesis in humans', *Nature Reviews Microbiology 2018 16:11,* 16(11).
Krzywinski, M., Schein, J., Birol, İ., Connors, J., Gascoyne, R., Horsman, D., Jones, S. J. and Marra, M. A. (2009) 'Circos: An information aesthetic for comparative genomics', *Genome Research,* 19(9).
Kuehner, F. and Stubenrauch, F. (2022) 'Functions of Papillomavirus E8^E2 Proteins in Tissue Culture and In Vivo', *Viruses,* 14(5), pp. 953.
Kumari, S. and Bhor, V. M. (2022) 'A literature review on correlation between HPV coinfection with C. trachomatis and cervical neoplasia - coinfection mediated cellular transformation', *Microbial Pathogenesis,* 168.
Kwok, C. S., Holland, R. and Gibbs, S. (2011) 'Efficacy of topical treatments for cutaneous warts: a meta-analysis and pooled analysis of randomized controlled trials - Kwok - 2011 - British Journal of Dermatology', *British Journal of Dermatology*.

Kyrgiou, M., Koliopoulos, G., Martin-Hirsch, P., Arbyn, M., Prendiville, W. and Paraskevaidis, E. (2006) 'Obstetric outcomes after conservative treatment for intraepithelial or early invasive cervical lesions: systematic review and meta-analysis', *Lancet (London, England),* 367(9509).
Lace, M., J., Anson, J., R., Turek, L., P. and Haugen, T., H. (2008a) 'Functional mapping of the human papillomavirus type 16 E1 cistron', *Journal of virology,* 82(21).
Lace, M. J., Anson, J. R., Thomas, G. S., Turek, L. P. and Haugen, T. H. (2008b) 'The E8--E2 gene product of human papillomavirus type 16 represses early transcription and replication but is dispensable for viral plasmid persistence in keratinocytes', *Journal of virology,* 82(21).
Laganà, M., Margolles, G., Jaracz-Ros, A., Mercier-Nomé, F., Roingeard, P., Lambert, P., Schlecht-Louf, G. and Bachelerie, F. (2024) 'Optimized protocol for 3D epithelial cultures supporting human papillomavirus replication', *STAR protocols,* 5(1).
Lambert, P. F. (1991) 'Papillomavirus DNA replication', *Journal of virology,* 65(7).
Lang, B. J., Prince, T. L., Okusha, Y., Bunch, H. and Calderwood, S. K. (2022) 'Heat shock proteins in cell signaling and cancer', *Biochimica et Biophysica Acta (BBA) - Molecular Cell Research,* 1869(3).
Larsson, G. 1983. Conization for preinvasive and early invasive carcinoma of the uterine cervix. Acta Obstet Gynecol Scand Suppl.
Lau, L., Gray, E. E., Brunette, R. L. and Stetson, D. B. (2015) 'DNA tumor virus oncogenes antagonize the cGAS-STING DNA-sensing pathway', *Science (New York, N.Y.),* 350(6260).
Lazear, H. M., Schoggins, J. W. and Diamond, M. S. (2019) 'Shared and Distinct Functions of Type I and Type III Interferons', *Immunity,* 50(4).
Lechner, M., Liu, J., Masterson, L., Fenton, T. R., Lechner, M., Liu, J., Masterson, L. and Fenton, T. R. (2022) 'HPV-associated oropharyngeal cancer: epidemiology, molecular biology and clinical management', *Nature Reviews Clinical Oncology 2022 19:5,* 19(5).
Leeson, S., Alalade, R., Singh, N., Nieminen, P., Cruickshank, M., Carcopino, X. and Bergeron, C. (2021) 'Options for triage and implications for colposcopists within European HPV-based cervical screening programmes', *European journal of obstetrics, gynecology, and reproductive biology,* 258.
Lehman, C. W. and Botchan, M. R. (1998) 'Segregation of viral plasmids depends on tethering to chromosomes and is regulated by phosphorylation', *Proceedings of the National Academy of Sciences,* 95(8).
Li, N., Franceschi, S., Howell-Jones, R., Snijders, P. and Clifford, G. (2011) 'Human papillomavirus type distribution in 30,848 invasive cervical cancers worldwide: Variation by geographical region, histological type and year of publication', *International journal of cancer,* 128(4).
Li, W., Thompson, C. H., Cossart, Y. E., O'Brien, C. J., Liu, J., Scolyer, R. A., Carter, J. R., Dalrymple, C. and Rose, B. R. (2004) 'The site of infection and ethnicity of the patient influence the biological pathways to HPV-induced mucosal cancer', *Modern Pathology 2004 17:9,* 17(9).
Li, X., Gao, X., Jin, L., Wang, Y., Hong, Y., McHepange, U., Wang, X., Jiang, Y., Wei, H. and Chen, H. (2009) 'Local hyperthermia could induce migrational maturation of Langerhans cells in condyloma acuminatum', *Journal of dermatological science,* 54(2).
Liao, Y., Smyth, G. K. and Shi, W. (2014) 'featureCounts: an efficient general purpose program for assigning sequence reads to genomic features', *Bioinformatics,* 30(7).
Lipovsky, A., Popa, A., Pimienta, G., Wyler, M., Bhan, A., Kuruvilla, L., Guie, M.-A., Poffenberger, A. C., Nelson, C. D. S., Atwood, W. J. and DiMaio, D. (2013) 'Genome-wide siRNA screen identifies the retromer as a cellular entry factor for human papillomavirus', *Proceedings of the National Academy of Sciences,* 110(18).
Liu, G., Sharma, M., Tan, N. and Barnabas, R. V. (2018) 'HIV-positive women have higher risk of human papilloma virus infection, precancerous lesions, and cervical cancer', *AIDS,* 32(6).
Liu, S., Cai, W., Luo, Y., Dou, J., Wu, J., Wu, H., Han, Z., Yu, J. and Liang, P. (2022) 'CEUS Versus MRI in Evaluation of the Effect of Microwave Ablation of Breast Cancer', *Ultrasound in medicine & biology,* 48(4).
Liu, T., Zhang, L., Joo, D. and Sun, S. (2017) 'NF-κB signaling in inflammation', *Signal transduction and targeted therapy,* 2.
Livak, K., J. and Schmittgen, T., D. (2001) 'Analysis of relative gene expression data using real-time quantitative PCR and the 2(-Delta Delta C(T)) Method', *Methods (San Diego, Calif.),* 25(4).

Love, M. I., Huber, W., Anders, S., Love, M. I., Huber, W. and Anders, S. (2014) 'Moderated estimation of fold change and dispersion for RNA-seq data with DESeq2', *Genome Biology 2014 15:12,* 15(12).
Lutgens, L., Zee, J. v. d., Ruysscher, D. K. M. D., Lambin, P. and Platt, J. (2010) 'Combined use of hyperthermia and (chemo)radiation therapy for treating locally advanced cervix carcinoma', *Cochrane Database of Systematic Reviews,* 2021(3).
Mace, T. A., Zhong, L., Kokolus, K. M. and Repasky, E. A. (2012) 'Effector CD8+ T cell IFN-γ production and cytotoxicity are enhanced by mild hyperthermia', *International Journal of Hyperthermia,* 28(1).
Maglennon, G., A., McIntosh, P. and Doorbar, J. (2011) 'Persistence of viral DNA in the epithelial basal layer suggests a model for papillomavirus latency following immune regression', *Virology,* 414(2).
Mahat, D. B., Salamanca, H. H., Duarte, F. B., Danko, C. G. and Lis, J. T. (2016) 'Mammalian Heat Shock Response and Mechanisms Underlying Its Genome-wide Transcriptional Regulation', *Molecular Cell,* 62(1).
Malagón, T., Franco, E. L., Tejada, R., Vaccarella, S., Malagón, T., Franco, E. L., Tejada, R. and Vaccarella, S. (2024) 'Epidemiology of HPV-associated cancers past, present and future: towards prevention and elimination', *Nature Reviews Clinical Oncology 2024 21:7,* 21(7).
Mantso, T., Goussetis, G., Franco, R., Botaitis, S., Pappa, A. and Panayiotidis, M. (2016) 'Effects of hyperthermia as a mitigation strategy in DNA damage-based cancer therapies', *Seminars in Cancer Biology,* 37-38.
Marion, J. B. (1981) 'ELECTROMAGNETIC RADIATION', *Physics in the Modern World*, pp. 377-397.
Marks, R., Rennie, G. and Selwood, T. S. (1988) 'Malignant transformation of solar keratoses to squamous cell carcinoma', *Lancet,* 1(8589).
Martin-Hirsch, P. P. L., Paraskevaidis, E., Bryant, A. and Dickinson, H. O. (2013) 'Surgery for cervical intraepithelial neoplasia', *The Cochrane database of systematic reviews,* 2013(12).
Martinez-Zapien, D., Ruiz, F. X., Poirson, J., Mitschler, A., Ramirez, J., Forster, A., Cousido-Siah, A., Masson, M., Pol, S. V., Podjarny, A., Travé, G., Zanier, K., Martinez-Zapien, D., Ruiz, F. X., Poirson, J., Mitschler, A., Ramirez, J., Forster, A., Cousido-Siah, A., ... and Zanier, K. (2016) 'Structure of the E6/E6AP/p53 complex required for HPV-mediated degradation of p53', *Nature 2016 529:7587,* 529(7587).
Matsui, T. and Amagai, M. (2015) 'Dissecting the formation, structure and barrier function of the stratum corneum', *International Immunology,* 27(6).
Matsumoto, H., Takahashi, A., Wang, X., Ohnishi, K. and Ohnishi, T. (1997) 'Transfection of p53-knockout mouse fibroblasts with wild-type p53 increases the thermosensitivity and stimulates apoptosis induced by heat stress', *International Journal of Radiation Oncology*Biology*Physics,* 38(5).
Mayer, M. and Bukau, B. (2005) 'Hsp70 chaperones: cellular functions and molecular mechanism', *Cellular and molecular life sciences : CMLS,* 62(6).
Maza, M., Schocken, C. M., Bergman, K. L., Randall, T. C. and Cremer, M. L. (2016) 'Cervical Precancer Treatment in Low- and Middle-Income Countries: A Technology Overview', *Journal of global oncology,* 3(4).
McBride, A. A. (2013) 'The Papillomavirus E2 proteins', *Virology,* 445(1-2).
McBride, A. A. (2017) 'Oncogenic human papillomaviruses', *Philosophical Transactions of the Royal Society B: Biological Sciences,* 372(1732).
McBride, A. A. and Warburton, A. (2017) 'The role of integration in oncogenic progression of HPV-associated cancers', *PLoS pathogens,* 13(4).
McCarthy, C. M., Ramphul, M., Madden, M. and Hickey, K. (2016) 'The use and success of cold coagulation for the treatment of high grade squamous cervical intra-epithelial neoplasia: a retrospective review', *European journal of obstetrics, gynecology, and reproductive biology,* 203.
McCredie, M. R. E., Sharples, K. J., Paul, C., Baranyai, J., Medley, G., Jones, R. W. and Skegg, D. C. G. (2008) 'Natural history of cervical neoplasia and risk of invasive cancer in women with cervical intraepithelial neoplasia 3: a retrospective cohort study', *The Lancet Oncology,* 9(5).

McFarlane, M., MacDonald, A. I., Stevenson, A. and Graham, S. V. (2015) 'Human Papillomavirus 16 Oncoprotein Expression Is Controlled by the Cellular Splicing Factor SRSF2 (SC35)', *Journal of Virology,* 89(10).
McIntosh, P. B., Laskey, P., Sullivan, K., Davy, C., Wang, Q., Jackson, D. J., Griffin, H. M. and Doorbar, J. (2010) 'E1^E4-mediated keratin phosphorylation and ubiquitylation: a mechanism for keratin depletion in HPV16-infected epithelium', *Journal of Cell Science,* 123(16).
McKinney, C. C., Hussmann, K. L. and McBride, A. A. (2015) 'The Role of the DNA Damage Response throughout the Papillomavirus Life Cycle', *Viruses 2015, Vol. 7, Pages 2450-2469,* 7(5).
McPhillips, M. G., Veerapraditsin, T., Cumming, S. A., Karali, D., Milligan, S. G., Boner, W., Morgan, I. M. and Graham, S. V. (2004) 'SF2/ASF Binds the Human Papillomavirus Type 16 Late RNA Control Element and Is Regulated during Differentiation of Virus-Infected Epithelial Cells', *Journal of Virology,* 78(19).
Meehan, G. R., Herder, V., Allan, J., Huang, X., Kerr, K., Mendonca, D. C., Ilia, G., Wright, D. W., Nomikou, K., Gu, Q., Arias, S. M., Hansmann, F., Hardas, A., Attipa, C., Lorenzo, G. D., Cowton, V., Upfold, N., Palmalux, N., Brown, J. C., ... and Palmarini, M. (2023) 'Phenotyping the virulence of SARS-CoV-2 variants in hamsters by digital pathology and machine learning', *PLOS Pathogens,* 19(11).
Megill, C. and Wilkin, T. (2017) 'Topical therapies for the treatment of anal high-grade squamous intraepithelial lesions', *Seminars in colon & rectal surgery,* 28(2).
Melnikow, J., McGahan, C., Sawaya, G. F., Ehlen, T. and Coldman, A. (2009) 'Cervical Intraepithelial Neoplasia Outcomes After Treatment: Long-term Follow-up From the British Columbia Cohort Study', *JNCI Journal of the National Cancer Institute,* 101(10).
Merle, E., Rose, R. C., LeRoux, L. and Moroianu, J. 1999. Nuclear import of HPV11 L1 capsid protein is mediated by karyopherin alpha2beta1 heterodimers. J Cell Biochem.
Meyer, R. E., Braun, R. D., Rosner, G. L. and Dewhirst, M. W. (2000) 'Local 42°C Hyperthermia Improves Vascular Conductance of the R3230Ac Rat Mammary Adenocarcinoma during Sodium Nitroprusside Infusion', *Radiation Research,* 154(2).
Meyers, C., Frattini, M. G., Hudson, J. B. and Laimins, L. A. (1992) 'Biosynthesis of Human Papillomavirus from a Continuous Cell Line Upon Epithelial Differentiation'.
Meyers, C. and Laimins, L. A. (1994) 'In Vitro Systems for the Study and Propagation of Human Papillomavirus', *Current Topics in Microbiology and Immunology*.
Michel, S., Bernerd, F., Jetten, A., M., Floyd, E., E., Shroot, B. and Reichert, U. (1992) 'Expression of keratinocyte transglutamine mRNA revealed by in situ hybridization', *The Journal of investigative dermatology,* 98(3).
Middleton, K. 2002. Analysis of papillomavirus E1^E4 expression with respect to epithelial proliferation and differentiation in productive and neoplastic papillomavirus lesions. Doctoral thesis, University of London.
Middleton, K., Peh, W., Southern, S., Griffin, H., Sotlar, K., Nakahara, T., El-Sherif, A., Morris, L., Seth, R., Hibma, M., Jenkins, D., Lambert, P., Coleman, N. and Doorbar, J. (2003) 'Organization of Human Papillomavirus Productive Cycle during Neoplastic Progression Provides a Basis for Selection of Diagnostic Markers', *Journal of Virology,* 77(19).
Milligan, S., G., Veerapraditsin, T., Ahamet, B., Mole, S. and Graham, S., V. (2007) 'Analysis of novel human papillomavirus type 16 late mRNAs in differentiated W12 cervical epithelial cells', *Virology,* 360(1).
Mirabello, L., Schiffman, M., Ghosh, A., Rodriguez, A. C., Vasiljevic, N., Wentzensen, N., Herrero, R., Hildesdheim, A., Wacholder, S., Scibior-Bentowska, D., Burk, R. D. and Lorincz, A. T. (2013) 'Elevated methylation of HPV16 DNA is associated with the development of high grade cervical intraepithelial neoplasia', *International journal of cancer,* 132(6).
Mirabello, L., Sun, C., Ghosh, A., Rodriguez, A. C., Schiffman, M., Wentzensen, N., Hildesheim, A., Herrero, R., Wacholder, S., Lorincz, A. and Burk, R. D. (2012) 'Methylation of human papillomavirus type 16 genome and risk of cervical precancer in a Costa Rican population', *Journal of the National Cancer Institute,* 104(7).

Mishra, R. R. and Sharma, A. K. (2016) 'Microwave–material interaction phenomena: Heating mechanisms, challenges and opportunities in material processing', *Composites Part A: Applied Science and Manufacturing,* 81.
Miura, S., Kawana, K., Schust, D. J., Fujii, T., Yokoyama, T., Iwasawa, Y., Nagamatsu, T., Adachi, K., Tomoi, A., Tomoi, K., Kojima, S., Yasugi, T., Kozuma, S. and Taketani, Y. (2010) 'CD1d, a sentinel molecule bridging innate and adaptive immunity, is downregulated by the human papillomavirus (HPV) E5 protein: a possible mechanism for immune evasion by HPV', *Journal of virology,* 84(22).
Moll, R., Divo, M. and Langbein, L. (2008) 'The human keratins: biology and pathology', *Histochemistry and cell biology,* 129(6).
Moody, C. (2017) 'Mechanisms by which HPV Induces a Replication Competent Environment in Differentiating Keratinocytes', *Viruses,* 9(9), pp. 261.
Moody, C., A. and Laimins, L., A. (2009) 'Human papillomaviruses activate the ATM DNA damage pathway for viral genome amplification upon differentiation', *PLoS pathogens,* 5(10).
Moody, C. A. (2022) 'Regulation of the Innate Immune Response during the Human Papillomavirus Life Cycle', *Viruses 2022, Vol. 14, Page 1797,* 14(8).
Moore, S., Rady, P. and Tyring, S. (2022) 'Acquired epidermodysplasia verruciformis: clinical presentation and treatment update', *International journal of dermatology,* 61(11).
Moore, W. (2011) 'The Edwin Smith papyrus', *BMJ,* 342(mar16 3).
Moussa, A. M., Ziv, E., Solomon, S. B. and Camacho, J. C. (2019) 'Ablative Therapy: Part 1: Microwave Ablation in Primary Lung Malignancies', *Seminars in Interventional Radiology,* 36(4).
Müller, H., Moroni, M., Vigo, E., Petersen, B., Bartek, J. and Helin, K. (1997) 'Induction of S-phase entry by E2F transcription factors depends on their nuclear localization', *Molecular and cellular biology,* 17(9).
Nakagawa, M., Viscidi, R., Deshmukh, I., Costa, M. D., Palefsky, J. M., Farhat, S. and Moscicki, A.-B. (2002) 'Time Course of Humoral and Cell-Mediated Immune Responses to Human Papillomavirus Type 16 in Infected Women', *Clinical and Vaccine Immunology,* 9(4).
Negorev, D. G., Vladimirova, O. V., Ivanov, A., Rauscher, F. and Maul, G. G. (2006) 'Differential Role of Sp100 Isoforms in Interferon-Mediated Repression of Herpes Simplex Virus Type 1 Immediate-Early Protein Expression', *Journal of Virology,* 80(16).
Nelson, C. W. and Mirabello, L. (2023) 'Human papillomavirus genomics: Understanding carcinogenicity', *Tumour Virus Research,* 15.
Nelson, L. M., Rose, R. C. and Moroianu, J. (2002) 'Nuclear Import Strategies of High Risk HPV16 L1 Major Capsid Protein', *Journal of Biological Chemistry,* 277(26), pp. 23958-23964.
Nelson, L. M., Rose, R. C. and Moroianu, J. (2003) 'The L1 major capsid protein of human papillomavirus type 11 interacts with Kap beta2 and Kap beta3 nuclear import receptors', *Virology,* 306(1).
Nestle, F. O., Di Meglio, P., Qin, J.-Z., Nickoloff, B. J., Nestle, F. O., Di Meglio, P., Qin, J.-Z. and Nickoloff, B. J. (2009) 'Skin immune sentinels in health and disease', *Nature Reviews Immunology 2009 9:10,* 9(10).
Newton, J., Flores-Arredondo, J., Suki, S., Ware, M., Krzykawska-Serda, M., Agha, M., Law, J., Sikora, A., Curley, S. and Corr, S. (2018) 'Non-Invasive Radiofrequency Field Treatment of 4T1 Breast Tumors Induces T-cell Dependent Inflammatory Response', *Scientific reports,* 8(1).
Nicholls, P. K., Moore, P. F., Anderson, D. M., Moore, R. A., Parry, N. R., Gough, G. W. and Stanley, M. A. (2001) 'Regression of canine oral papillomas is associated with infiltration of CD4+ and CD8+ lymphocytes', *Virology,* 283(1).
Nieland, T., Tan, M., Monne-van Muijen, M., Koning, F., Kruisbeek, A. and van Bleek, G. (1996) 'Isolation of an immunodominant viral peptide that is endogenously bound to the stress protein GP96/GRP94', *Proceedings of the National Academy of Sciences of the United States of America,* 93(12).
Nuñez, J. R., Anderton, C. R. and Renslow, R. S. (2018) 'Optimizing colormaps with consideration for color vision deficiency to enable accurate interpretation of scientific data', *PLOS ONE,* 13(7).
O'Connor, M., Chan, S.-Y. and Bernard, H.-U. 1995. Transcription Factor Binding Sites in the Long Control Region of Genital HPVs. The Human Papillomavirus Compendium III-21:40.

Oeckinghaus, A. and Ghosh, S. (2009) 'The NF-kappaB family of transcription factors and its regulation', *Cold Spring Harbor perspectives in biology,* 1(4).
Oei, A., L., van Leeuwen, C., M., ten Cate, R., Rodermond, H., M., Buist, M., R., Stalpers, L., J., Crezee, J., Kok, H., P., Medema, J., P. and Franken, N., A. (2015a) 'Hyperthermia Selectively Targets Human Papillomavirus in Cervical Tumors via p53-Dependent Apoptosis', *Cancer research,* 75(23).
Oei, A. L., Vriend, L. E. M., Crezee, J., Franken, N. A. P. and Krawczyk, P. M. (2015b) 'Effects of hyperthermia on DNA repair pathways: one treatment to inhibit them all', *Radiation Oncology,* 10(1), pp. 1-13.
Oh, S. T., Kyo, S. and Laimins, L. A. (2001) 'Telomerase Activation by Human Papillomavirus Type 16 E6 Protein: Induction of Human Telomerase Reverse Transcriptase Expression through Myc and GC-Rich Sp1 Binding Sites', *Journal of Virology,* 75(12).
Ong, C. K., Chan, S. Y., Campo, M. S., Fujinaga, K., Mavromara-Nazos, P., Labropoulou, V., Pfister, H., Tay, S. K., Meulen, J. t. and Villa, L. L. (1993) 'Evolution of human papillomavirus type 18: an ancient phylogenetic root in Africa and intratype diversity reflect coevolution with human ethnic groups', *Journal of Virology,* 67(11).
Orth, G. (1987) 'Epidermodysplasia Verruciformis', *The Papovaviridae*.
Orth, G., Favre, M. and Croissant, O. (1977) 'Characterization of a New Type of Human Papillomavirus That Causes Skin Warts', *Journal of Virology,* 24(1).
Orth, G., Jablonska, S., Favre, M., Croissant, O., Jarzabek-Chorzelska, M., Rzesa, G., Orth, G., Jablonska, S., Favre, M., Croissant, O., Jarzabek-Chorzelska, M. and Rzesa, G. (1978) 'Characterization of two types of human papillomaviruses in lesions of epidermodysplasia verruciformis', *Proceedings of the National Academy of Sciences,* 75(3).
Ostberg, J. R., Dayanc, B. E., Yuan, M., Oflazoglu, E. and Repasky, E. A. (2007) 'Enhancement of natural killer (NK) cell cytotoxicity by fever-range thermal stress is dependent on NKG2D function and is associated with plasma membrane NKG2D clustering and increased expression of MICA on target cells', *Journal of Leukocyte Biology,* 82(5).
Ozbun, M. A. (2002) 'Infectious human papillomavirus type 31b: purification and infection of an immortalized human keratinocyte cell line', *Journal of General Virology,* 83(11).
Ozbun, M. A. and Meyers, C. (1997) 'Characterization of late gene transcripts expressed during vegetative replication of human papillomavirus type 31b', *Journal of Virology,* 71(7).
Ozbun, M. A. and Meyers, C. (1998) 'Temporal Usage of Multiple Promoters during the Life Cycle of Human Papillomavirus Type 31b', *Journal of Virology*.
Paris, C., Pentland, I., Groves, I., Roberts, D. C., Powis, S. J., Coleman, N., Roberts, S. and Parish, J. L. (2015) 'CCCTC-Binding Factor Recruitment to the Early Region of the Human Papillomavirus 18 Genome Regulates Viral Oncogene Expression', *Journal of Virology,* 89(9).
Pentland, I., Campos-León, K., Cotic, M., Davies, K., J., Wood, C., D., Groves, I., J., Burley, M., Coleman, N., Stockton, J., D., Noyvert, B., Beggs, A., D., West, M., J., Roberts, S. and Parish, J., L. (2018) 'Disruption of CTCF-YY1-dependent looping of the human papillomavirus genome activates differentiation-induced viral oncogene transcription', *PLoS biology,* 16(10).
Popa, A., Zhang, W., Harrison, M., Goodner, K., Kazakov, T., Goodwin, E., Lipovsky, A., Burd, C. and DiMaio, D. (2015) 'Direct binding of retromer to human papillomavirus type 16 minor capsid protein L2 mediates endosome exit during viral infection', *PLoS pathogens,* 11(2).
Prendeville, W. and Sankaranaryanan, R. 2017. Colposcopy and Treatment of Cervical Precancer. IARC Technical Report.
Prescott, E. L., Brimacombe, C. L., Hartley, H., Bell, I., Graham, S. and Roberts, S. (2014) 'Human Papillomavirus Type 1 E1^E4 Protein Is a Potent Inhibitor of the Serine-Arginine (SR) Protein Kinase SRPK1 and Inhibits Phosphorylation of Host SR Proteins and of the Viral Transcription and Replication Regulator E2', *Journal of Virology,* 88(21).
Proksch, E., Brandner, J. M. and Jensen, J. (2008) 'The skin: an indispensable barrier', *Experimental dermatology,* 17(12).
Pyeon, D., Lambert, P. F., Ahlquist, P., Pyeon, D., Lambert, P. F. and Ahlquist, P. (2005) 'Production of infectious human papillomavirus independently of viral replication and epithelial cell differentiation', *Proceedings of the National Academy of Sciences,* 102(26).

Pyeon, D., Pearce, S. M., Lank, S. M., Ahlquist, P. and Lambert, P. F. (2009) 'Establishment of human papillomavirus infection requires cell cycle progression', *PLoS pathogens,* 5(2).
Ramoz, N., Rueda, L.-A., Bouadjar, B., Montoya, L.-S., Orth, G., Favre, M., Ramoz, N., Rueda, L.-A., Bouadjar, B., Montoya, L.-S., Orth, G. and Favre, M. (2002) 'Mutations in two adjacent novel genes are associated with epidermodysplasia verruciformis', *Nature Genetics 2002 32:4,* 32(4).
Rapp, B., Pawellek, A., Kraetzer, F., Schaefer, M., May, C., Purdie, K., Grassmann, K. and Iftner, T. (1997) 'Cell-type-specific separate regulation of the E6 and E7 promoters of human papillomavirus type 6a by the viral transcription factor E2', *Journal of virology,* 71(9).
Ray, P. (1999) 'Stress genes and species survival', *Molecular and cellular biochemistry,* 196(1-2).
Rector, A., Lemey, P., Tachezy, R., Mostmans, S., Ghim, S.-J., Van Doorslaer, K., Roelke, M., Bush, M., Montali, R. J., Joslin, J., Burk, R. D., Jenson, A. B., Sundberg, J. P., Shapiro, B. and Van Ranst, M. (2007) 'Ancient papillomavirus-host co-speciation in Felidae', *Genome Biology 2007 8:4,* 8(4).
Regad, T., . and Chelbi-Alix, M. K. (2001) 'Role and fate of PML nuclear bodies in response to interferon and viral infections', *Oncogene 2001 20:49,* 20(49).
Reich, O. and Regauer, S. (2023) 'Elimination of reserve cells for prevention of HPV-associated cervical cancer', *Virus research,* 329.
Reich, O., Regauer, S., McCluggage, W. G., Bergeron, C. and Redman, C. (2017) 'Defining the Cervical Transformation Zone and Squamocolumnar Junction: Can We Reach a Common Colposcopic and Histologic Definition?', *International journal of gynecological pathology : official journal of the International Society of Gynecological Pathologists,* 36(6).
Reiser, J., Hurst, J., Voges, M., Krauss, P., Münch, P., Iftner, T. and Stubenrauch, F. (2011) 'High-Risk Human Papillomaviruses Repress Constitutive Kappa Interferon Transcription via E6 To Prevent Pathogen Recognition Receptor and Antiviral-Gene Expression', *Journal of Virology,* 85(21).
Reuschenbach, M., Doorbar, J., del Pino, M., Joura, E. A., Walker, C., Drury, R., Rauscher, A. and Saah, A. J. (2023) 'Prophylactic HPV vaccines in patients with HPV-associated diseases and cancer', *Vaccine,* 41(42).
Richards, K. H., Wasson, C. W., Watherston, O., Doble, R., Eric Blair, G., Wittmann, M. and Macdonald, A. (2015) 'The human papillomavirus (HPV) E7 protein antagonises an Imiquimod-induced inflammatory pathway in primary human keratinocytes', *Scientific Reports 2015 5:1,* 5(1).
Richards, R. M., Lowy, D. R., Schiller, J. T. and Day, P. M. (2006) 'Cleavage of the papillomavirus minor capsid protein, L2, at a furin consensus site is necessary for infection', *Proceedings of the National Academy of Sciences of the United States of America,* 103(5).
Richter, K., Haslbeck, M. and Buchner, J. (2010) 'The heat shock response: life on the verge of death', *Molecular cell,* 40(2).
Riggs, C. L., Kedersha, N., Ivanov, P. and Anderson, P. (2020) 'Mammalian stress granules and P bodies at a glance', *Journal of Cell Science,* 133(16).
Rincon-Orozco, B., Halec, G., Rosenberger, S., Muschik, D., Nindl, I., Bachmann, A., Ritter, T. M., Dondog, B., Ly, R., Bosch, F. X., Zawatzky, R. and Rösl, F. (2009) 'Epigenetic Silencing of Interferon-κ in Human Papillomavirus Type 16–Positive Cells', *Cancer Research,* 69(22).
Roberts, S., Evans, D., Mehanna, H. and Parish, J. L. (2019) 'Modelling human papillomavirus biology in oropharyngeal keratinocytes', *Philosophical Transactions of the Royal Society B: Biological Sciences,* 374(1773).
Rodríguez, A. C., Schiffman, M., Herrero, R., Wacholder, S., Hildesheim, A., Castle, P. E., Solomon, D. and Burk, R. (2008) 'Rapid Clearance of Human Papillomavirus and Implications for Clinical Focus on Persistent Infections', *JNCI: Journal of the National Cancer Institute,* 100(7).
Romero-Masters, J. C., Lambert, P. F. and Munger, K. (2022) 'Molecular Mechanisms of MmuPV1 E6 and E7 and Implications for Human Disease', *Viruses,* 14(10).
Ronco, L. V., Karpova, A. Y., Vidal, M. and Howley, P. M. (1998) 'Human papillomavirus 16 E6 oncoprotein binds to interferon regulatory factor-3 and inhibits its transcriptional activity', *Genes & development,* 12(13).
Roth-Carter, Q. R., Koetsier, J. L., Broussard, J. A. and Green, K. J. (2022) 'Organotypic Human Skin Cultures Incorporating Primary Melanocytes', *Current Protocols,* 2(9).

Rowlands, V., Rutkowski, A. J., Meuser, E., Carr, T. H., Harrington, E. A. and Barrett, J. C. (2019) 'Optimisation of robust singleplex and multiplex droplet digital PCR assays for high confidence mutation detection in circulating tumour DNA', *Scientific Reports,* 9(1), pp. 1-13.
Ruesch, M., Stubenrauch, F. and Laimins, L. (1998) 'Activation of papillomavirus late gene transcription and genome amplification upon differentiation in semisolid medium is coincident with expression of involucrin and transglutaminase but not keratin-10', *Journal of virology,* 72(6).
Ryabchenko, B., Šroller, V., Horníková, L., Lovtsov, A., Forstová, J. and Huérfano, S. (2023) 'The interactions between PML nuclear bodies and small and medium size DNA viruses', *Virology Journal,* 20(1).
Rösl, F., Arab, A., Klevenz, B. and zur Hausen, H. (1993) 'The effect of DNA methylation on gene regulation of human papillomaviruses', *The Journal of general virology,* 74 (Pt 5)(5).
Rösl, F., Dürst, M. and zur Hausen, H. (1988) 'Selective suppression of human papillomavirus transcription in non-tumorigenic cells by 5-azacytidine', *The EMBO journal,* 7(5).
Saavedra, C., Tung, K. S., Amberg, D. C., Hopper, A. K. and Cole, C. N. (1996) 'Regulation of mRNA export in response to stress in Saccharomyces cerevisiae', *Genes & development,* 10(13).
Saavedra, C. A., Hammell, C. M., Heath, C. V. and Cole, C. N. (1997) 'Yeast heat shock mRNAs are exported through a distinct pathway defined by Rip1p', *Genes & development,* 11(21).
Saikia, P., Fensterl, V. and Sen, G., C. (2010) 'The inhibitory action of P56 on select functions of E1 mediates interferon's effect on human papillomavirus DNA replication', *Journal of virology,* 84(24).
Sand, F., L., Frederiksen, K. and Kjaer, S., K. (2022) 'Risk of recurrent disease following conization of cervical intraepithelial neoplasia grade 3 according to post-conization HPV status and surgical margins', *Gynecologic oncology,* 165(3).
Sanders, C. M. and Stenlund, A. (1998) 'Recruitment and loading of the E1 initiator protein: an ATP-dependent process catalysed by a transcription factor.', *The EMBO Journal,* 17(23).
Sanders, C. M. and Stenlund, A. (2000) 'Transcription factor-dependent loading of the E1 initiator reveals modular assembly of the papillomavirus origin melting complex', *The Journal of biological chemistry,* 275(5).
Santoro, M. (2000) 'Heat shock factors and the control of the stress response', *Biochemical pharmacology,* 59(1).
Scarth, J. A., Patterson, M. R., Morgan, E. L. and Macdonald, A. (2021) 'The human papillomavirus oncoproteins: a review of the host pathways targeted on the road to transformation', *The Journal of General Virology,* 102(3).
Schaeffer, A. J., Nguyen, M., Liem, A., Lee, D., Montagna, C., Lambert, P. F., Ried, T. and Difilippantonio, M. J. (2004) 'E6 and E7 Oncoproteins Induce Distinct Patterns of Chromosomal Aneuploidy in Skin Tumors from Transgenic Mice', *Cancer Research,* 64(2).
Schafer, F., Florin, L. and Sapp, M. (2002) 'DNA Binding of L1 Is Required for Human Papillomavirus Morphogenesis in Vivo', *Virology,* 295(1).
Schelhaas, M., Shah, B., Holzer, M., Blattmann, P., Kühling, L., Day, P. M., Schiller, J. T. and Helenius, A. (2012) 'Entry of Human Papillomavirus Type 16 by Actin-Dependent, Clathrin- and Lipid Raft-Independent Endocytosis', *PLOS Pathogens,* 8(4).
Schiffman, M., Castle, P., E., Jeronimo, J., Rodriguez, A. and C. Wacholder, S. (2007) 'Human papillomavirus and cervical cancer', *Lancet (London, England),* 370(9590).
Schiffman, M. and Rodriguez, A. C. (2008) 'Heterogeneity in CIN3 diagnosis', *The Lancet Oncology,* 9(5).
Schiffman, M., Wentzensen, N., Wacholder, S., Kinney, W., Gage, J. C. and Castle, P. E. (2011) 'Human Papillomavirus Testing in the Prevention of Cervical Cancer', *JNCI Journal of the National Cancer Institute,* 103(5).
Schiffman, M. C., P, E. Jeronimo, J. Rodriguez, A, C. Wacholder, S. (2007) 'Human papillomavirus and cervical cancer', *Lancet (London, England),* 370(9590).
Schmitt, M., Dalstein, V., Waterboer, T., Clavel, C., Gissmann, L. and Pawlita, M. (2010) 'Diagnosing Cervical Cancer and High-Grade Precursors by HPV16 Transcription Patterns'.

Schreiner, S., Bürck, C., Glass, M., Groitl, P., Wimmer, P., Kinkley, S., Mund, A., Everett, R. D. and Dobner, T. (2013) 'Control of human adenovirus type 5 gene expression by cellular Daxx/ATRX chromatin-associated complexes', *Nucleic Acids Research,* 41(6).
Schwartz, S. (2013) 'Papillomavirus transcripts and posttranscriptional regulation', *Virology,* 445(1-2).
Scott, M., Nakagawa, M. and Moscicki, A.-B. (2001) 'Cell-Mediated Immune Response to Human Papillomavirus Infection', *Clinical Diagnostic Laboratory Immunology,* 8(2).
Scott, M., Stites, D. P. and Moscicki, A. B. (1999) 'Th1 cytokine patterns in cervical human papillomavirus infection', *Clinical and diagnostic laboratory immunology,* 6(5).
Scott, M. L., Woodby, B. L., Ulicny, J., Raikhy, G., Orr, A. W., Songock, W. K. and Bodily, J. M. (2020) 'Human Papillomavirus 16 E5 Inhibits Interferon Signaling and Supports Episomal Viral Maintenance', *Journal of Virology,* 94(2).
Scutigliani, E., Lobo-Cerna, F., Mingo Barba, S., Scheidegger, S. and Krawczyk, P. (2022) 'The Effects of Heat Stress on the Transcriptome of Human Cancer Cells: A Meta-Analysis', *Cancers,* 15(1).
Selinka, H., Giroglou, T., Nowak, T., Christensen, N. D. and Sapp, M. (2003) 'Further Evidence that Papillomavirus Capsids Exist inTwo DistinctConformations', *Journal of Virology,* 77(24).
Selinka, H. C., Giroglou, T. and Sapp, M. (2002) 'Analysis of the infectious entry pathway of human papillomavirus type 33 pseudovirions', *Virology,* 299(2).
Sen, G., Boxer, L., Webster, D., Bussat, R., Qu, K., Zarnegar, B., Johnston, D., Siprashvili, Z. and Khavari, P. (2012) 'ZNF750 is a p63 target gene that induces KLF4 to drive terminal epidermal differentiation', *Developmental cell,* 22(3).
Shah, S. D., Doorbar, J. and Goldstein, R. A. (2010) 'Analysis of Host–Parasite Incongruence in Papillomavirus Evolution Using Importance Sampling', *Molecular Biology and Evolution,* 27(6).
Sharma, K., Machalek, D. A., Toh, Z. Q., Amenu, D., Muchengeti, M., Ndlovu, A. K., Mremi, A., Mchome, B., Vallely, A. J., Denny, L., Rees, H. and Garland, S. M. (2023) 'No woman left behind: achieving cervical cancer elimination among women living with HIV', *The Lancet HIV,* 10(6).
Shaulian, E., Schreiber , M., Piu , F., Beeche , M., Wagner , E. F. and Karin, M. (2000) 'The mammalian UV response: c-Jun induction is required for exit from p53-imposed growth arrest', *Cell,* 103(6).
Shiraz, A., Egawa, N., Pelt, D. M., Crawford, R., Nicholas, A. K., Romashova, V., Sasieni, P., Griffin, H. and Doorbar, J. (2022) 'Cervical cell lift: A novel triage method for the spatial mapping and grading of precancerous cervical lesions', *eBioMedicine,* 82.
Siddharthan, R. V., Lanciault, C. and Tsikitis, V. L. (2019) 'Anal intraepithelial neoplasia: diagnosis, screening, and treatment', *Annals of gastroenterology,* 32(3).
Siddiqa, A., Léon, K., C., James, C., D., Bhatti, M., F., Roberts, S. and Parish, J., L. (2015) 'The human papillomavirus type 16 L1 protein directly interacts with E2 and enhances E2-dependent replication and transcription activation', *The Journal of general virology,* 96(8).
Silins, I., Ryd, W., Strand, A., Wadell, G., Törnberg, S., Hansson, B. G., Wang, X., Arnheim, L., Dahl, V., Bremell, D., Persson, K., Dillner, J. and Rylander, E. (2005) 'Chlamydia trachomatis infection and persistence of human papillomavirus', *International journal of cancer,* 116(1).
Singh, I., Gupta, A., Nagarsekar, A., Cooper, Z., Manka, C., Hester, L., Benjamin, I., He, J. and Hasday, J. (2008) 'Heat shock co-activates interleukin-8 transcription', *American journal of respiratory cell and molecular biology,* 39(2).
Sivéry, A., Courtade, E. and Thommen, Q. (2016) 'A minimal titration model of the mammalian dynamical heat shock response', *Physical biology,* 13(6).
Smith, J. L., Campos, S. K., Wandinger-Ness, A. and Ozbun, M. A. (2008) 'Caveolin-1-Dependent Infectious Entry of Human Papillomavirus Type 31 in Human Keratinocytes Proceeds to the Endosomal Pathway for pH-Dependent Uncoating', *Journal of Virology,* 82(19).
Song, C. W., Shakil, A., Griffin, R. J. and Okajima, K. 1997. Improvement of tumor oxygenation status by mild temperature hyperthermia alone or in combination with carbogen. Semin Oncol.
Song, H., Moseley, P. L., Lowe, S. L. and Ozbun, M. A. (2010) 'Inducible heat shock protein 70 enhances HPV31 viral genome replication and virion production during the differentiation-dependent life cycle in human keratinocytes', *Virus research,* 147(1).

Song, S., Pitot, H. C. and Lambert, P. F. (1999) 'The Human Papillomavirus Type 16 E6 Gene Alone Is Sufficient To Induce Carcinomas in Transgenic Animals', *Journal of Virology,* 73(7).
Spanos, W., Hoover, A., Harris, G., Wu, S., Strand, G., Anderson, M., Klingelhutz, A., Hendriks, W., Bossler, A. and Lee, J. (2008) 'The PDZ binding motif of human papillomavirus type 16 E6 induces PTPN13 loss, which allows anchorage-independent growth and synergizes with ras for invasive growth', *Journal of virology,* 82(5).
Sperling, T., Ołdak, M., Walch-Rückheim, B., Wickenhauser, C., Doorbar, J., Pfister, H., Malejczyk, M., Majewski, S., Keates, A. C. and Smola, S. (2012) 'Human Papillomavirus Type 8 Interferes with a Novel C/EBPβ-Mediated Mechanism of Keratinocyte CCL20 Chemokine Expression and Langerhans Cell Migration', *PLOS Pathogens,* 8(7).
Spoden, G., Freitag, K., Husmann, M., Boller, K., Sapp, M., Lambert, C. and Florin, L. (2008) 'Clathrin- and Caveolin-Independent Entry of Human Papillomavirus Type 16—Involvement of Tetraspanin-Enriched Microdomains (TEMs)', *PLOS ONE,* 3(10).
Spurgeon, M. E., den Boon, J. A., Horswill, M., Barthakur, S., Forouzan, O., Rader, J. S., Beebe, D. J., Roopra, A., Ahlquist, P. and Lambert, P. F. (2017) 'Human papillomavirus oncogenes reprogram the cervical cancer microenvironment independently of and synergistically with estrogen', *Proceedings of the National Academy of Sciences,* 114(43).
Srivastava, P. (2002) 'Roles of heat-shock proteins in innate and adaptive immunity', *Nature Reviews Immunology,* 2(3), pp. 185-194.
Stanley, M. (2006) 'Immune responses to human papillomavirus', *Vaccine,* 24 Suppl 1.
Stanley, M., Browne, H., Appleby, M. and Minson, A. (1989) 'Properties of a non-tumorigenic human cervical keratinocyte cell line', *International journal of cancer,* 43(4).
Stanley, M. A. (2012) 'Epithelial Cell Responses to Infection with Human Papillomavirus', *Clinical Microbiology Reviews,* 25(2).
Stauffer, Y., Raj, K., Masternak, K. and Beard, P. (1998) 'Infectious human papillomavirus type 18 pseudovirions', *Journal of molecular biology,* 283(3).
Steger, G. and Corbach, S. (1997) 'Dose-dependent regulation of the early promoter of human papillomavirus type 18 by the viral E2 protein', *Journal of virology,* 71(1).
Stelzer, M. K., Pitot, H. C., Liem, A., Schweizer, J., Mahoney, C. and Lambert, P. F. (2010) 'A Mouse Model for Human Anal Cancer', *Cancer prevention research (Philadelphia, Pa.),* 3(12).
Stepp, W. H., Meyers, J. M. and McBride, A. A. (2013) 'Sp100 Provides Intrinsic Immunity against Human Papillomavirus Infection', *mBio,* 4(6).
Stevenson, A., Wakeham, K., Pan, J., Kavanagh, K., Millan, D., Bell, S., McLellan, D., Graham, S. and K, C. (2020) 'Droplet digital PCR quantification suggests that higher viral load correlates with improved survival in HPV-positive oropharyngeal tumours', *Journal of clinical virology : the official publication of the Pan American Society for Clinical Virology,* 129.
Storm, K. F. (1983) *Hyperthermia in Cancer Therapy.* Hall Medical Publishers.
Straub, E., Fertey, J., Dreer, M., Iftner, T. and Stubenrauch, F. (2015) 'Characterization of the Human Papillomavirus 16 E8 Promoter', *Journal of virology,* 89(14).
Stubenrauch, F., Hummel, M., Iftner, T. and Laimins, L. A. (2000) 'The E8^E2C Protein, a Negative Regulator of Viral Transcription and Replication, Is Required for Extrachromosomal Maintenance of Human Papillomavirus Type 31 in Keratinocytes', *Journal of Virology,* 74(3).
Stubenrauch, F. and Laimins, L. A. (1999) 'Human papillomavirus life cycle: active and latent phases', *Seminars in cancer biology,* 9(6).
Stubenrauch, F., Lim, H. B. and Laimins, L. A. (1998) 'Differential requirements for conserved E2 binding sites in the life cycle of oncogenic human papillomavirus type 31', *Journal of virology,* 72(2).
Sun, C., Reimers, L. L. and Burk, R. D. (2011) 'Methylation of HPV16 genome CpG sites is associated with cervix precancer and cancer', *Gynecologic oncology,* 121(1).
Sun, X. Y., Frazer, I., Muller, M., Gissmann, L. and Zhou, J. (1995) 'Sequences required for the nuclear targeting and accumulation of human papillomavirus type 6B L2 protein', *Virology,* 213(2).
Suto, R. and Srivastava, P. K. (1995) 'A Mechanism for the Specific Immunogenicity of Heat Shock Protein-Chaperoned Peptides', *Science,* 269(5230).

Suzue, K., Zhou, X., Eisen, H. and Young, R. (1997) 'Heat shock fusion proteins as vehicles for antigen delivery into the major histocompatibility complex class I presentation pathway', *Proceedings of the National Academy of Sciences of the United States of America,* 94(24).
Swain, S. L. (1995) 'T-Cell Subsets: Who does the polarizing?', *Current Biology,* 5(8).
Taberna, M., Mena, M., Pavón, M. A., Alemany, L., Gillison, M. L. and Mesía, R. (2017) 'Human papillomavirus-related oropharyngeal cancer', *Annals of Oncology,* 28(10).
Tainio, K., Athansiou, A., Tikkinen, K. A. O., Aaltonen, R., Cardenas, J., Glazer-Livson, S., Jakobsson, M., Joronen, K., Kiviharju, M., Louvanto, K., Oksjoki, S., Tahtinen, R., Virtanen, S., Nieminen, P., Kyrgio, M. and Kallialal, I. (2018) 'Clinical course of untreated cervical intraepithelial neoplasia grade 2 under active surveillance: systematic review and meta-analysis', *BMJ (Clinical research ed.),* 360.
Tamura, Y., Peng, P., Liu, K., Daou, M. and Srivastava, P. (1997) 'Immunotherapy of tumors with autologous tumor-derived heat shock protein preparations', *Science (New York, N.Y.),* 278(5335).
Taub, D., Anver, M., Oppenheim, J., Longo, D. and Murphy, W. (1996) 'T lymphocyte recruitment by interleukin-8 (IL-8). IL-8-induced degranulation of neutrophils releases potent chemoattractants for human T lymphocytes both in vitro and in vivo', *The Journal of clinical investigation,* 97(8).
Terenzi, F., Saikia, P. and Sen, G., C. (2008) 'Interferon-inducible protein, P56, inhibits HPV DNA replication by binding to the viral protein E1', *The EMBO journal,* 27(24).
Thomas, M. K., Pitot, H. C., Liem, A. and Lambert, P. F. (2011) 'Dominant Role of HPV16 E7 in Anal Carcinogenesis', *Virology,* 421(2).
Thompson, M. R., Kaminski, J. J., Kurt-Jones, E. A., Fitzgerald, K. A., Thompson, M. R., Kaminski, J. J., Kurt-Jones, E. A. and Fitzgerald, K. A. (2011) 'Pattern Recognition Receptors and the Innate Immune Response to Viral Infection', *Viruses 2011, Vol. 3, Pages 920-940,* 3(6).
Toraya-Brown, S. and Fiering, S. (2014) 'Local tumour hyperthermia as immunotherapy for metastatic cancer', *International journal of hyperthermia : the official journal of European Society for Hyperthermic Oncology, North American Hyperthermia Group,* 30(8).
Torres-Poveda, K., Bahena-Román, M., Madrid-González, C., Burguete-García, A. I., Bermúdez-Morales, V. H., Peralta-Zaragoza, O. and Madrid-Marina, V. (2014) 'Role of IL-10 and TGF-β1 in local immunosuppression in HPV-associated cervical neoplasia', *World Journal of Clinical Oncology,* 5(4).
Trefná, H., Crezee, H., Schmidt, M., Marder, D., Lamprecht, U., Ehmann, M., Hartmann, J., Nadobny, J., Gellermann, J., van Holthe, N., Ghadjar, P., Lomax, N., Abdel-Rahman, S., Bert, C., Bakker, A., Hurwitz, M. D., Diederich, C. J., Stauffer, P. R. and van Rhoon, G. C. (2017) 'Quality assurance guidelines for superficial hyperthermia clinical trials: I. Clinical requirements', *International journal of hyperthermia : the official journal of European Society for Hyperthermic Oncology, North American Hyperthermia Group,* 33(4).
Trinklein, N., Murray, J., Hartman, S., Botstein, D. and Myers, R. (2004) 'The role of heat shock transcription factor 1 in the genome-wide regulation of the mammalian heat shock response', *Molecular biology of the cell,* 15(3).
Trus, B. L., Roden, R. B., Greenstone, H. L., Vrhel, M., Schiller, J. T. and Booy, F. P. (1997) 'Novel structural features of bovine papillomavirus capsid revealed by a three-dimensional reconstruction to 9 A resolution', *Nature structural biology,* 4(5).
Tulapurkar, M., Almutairy, E., Shah, N., He, J., Puche, A., Shapiro, P., Singh, I. and Hasday, J. (2012) 'Febrile-range hyperthermia modifies endothelial and neutrophilic functions to promote extravasation', *American journal of respiratory cell and molecular biology,* 46(6).
Udono, H. and Srivastava, P. (1993) 'Heat shock protein 70-associated peptides elicit specific cancer immunity', *The Journal of experimental medicine,* 178(4).
Uhlorn, B. L., Jackson, R., Li, S., Bratton, S. M., Doorslaer, K. V. and Campos, S. K. (2020) 'Vesicular trafficking permits evasion of cGAS/STING surveillance during initial human papillomavirus infection', *PLOS Pathogens,* 16(11).
Upadhyay, M. and Vivekanandan, P. (2015) 'Depletion of CpG Dinucleotides in Papillomaviruses and Polyomaviruses: A Role for Divergent Evolutionary Pressures', *PLOS ONE,* 10(11).

van der Zee, J., Gonzalez, D. G., van Rhoon, G. C., van Dijk, J. D., van Putten, W. L. and Hart, A. A. (2000) 'Comparison of radiotherapy alone with radiotherapy plus hyperthermia in locally advanced pelvic tumours: a prospective, randomised, multicentre trial. Dutch Deep Hyperthermia Group', *Lancet (London, England),* 355(9210).
Van Doorslaer, K., Li, Z., Xirasagar, S., Maes, P., Kaminsky, D., Liou, D., Sun, Q., Kaur, R., Huyen, Y. and McBride, A. A. (2017) 'The Papillomavirus Episteme: a major update to the papillomavirus sequence database', *Nucleic Acids Research,* 45(D1).
Veerapraditsin, T. 2004. Interaction between the HPV-16 Negative Regulatory Element and Cellular Proteins during Epithelial Cell Differentiation. Doctoral thesis, University of Glasgow.
Veitch, D., Kravvas, G. and Al-Niaimi, F. (2017) 'Pulsed Dye Laser Therapy in the Treatment of Warts: A Review of the Literature', *Dermatologic surgery : official publication for American Society for Dermatologic Surgery [et al.],* 43(4).
Velichko, A. K., Petrova, N. V., Kantidze, O. L. and Razin, S. V. (2012) 'Dual effect of heat shock on DNA replication and genome integrity', *Molecular Biology of the Cell,* 23(17).
Vihervaara, A., Mahat, D. B., Guertin, M. J., Chu, T., Danko, C. G., Lis, J. T., Sistonen, L., Vihervaara, A., Mahat, D. B., Guertin, M. J., Chu, T., Danko, C. G., Lis, J. T. and Sistonen, L. (2017) 'Transcriptional response to stress is pre-wired by promoter and enhancer architecture', *Nature Communications 2017 8:1,* 8(1).
Villa, L. L., Vieira, K. B. L., Pei, X.-F. and Schlegel, R. (1992) 'Differential effect of tumor necrosis factor on proliferation of primary human keratinocytes and cell lines containing human papillomavirus types 16 and 18', *Molecular Carcinogenesis,* 6(1).
Voellmy, R. (1996) 'Sensing stress and responding to stress', *EXS,* 77.
Wang, F., Flanagan, J., Su, N., Wang, L., C., Bui, S., Nielson, A., Wu, X., Vo, H., T., Ma, X., J. and Luo, Y. (2012) 'RNAscope: a novel in situ RNA analysis platform for formalin-fixed, paraffin-embedded tissues', *The Journal of molecular diagnostics : JMD,* 14(1).
Wang, H.-K., Duffy, A. A., Broker, T. R. and Chow, L. T. (2009) 'Robust production and passaging of infectious HPV in squamous epithelium of primary human keratinocytes', *Genes & Development,* 23(2).
Wang, J. W. and Roden, R. B. S. (2013) 'L2, the minor capsid protein of papillomavirus', *Virology,* 445(0).
Wang, K., Wang, C., Jiang, H., Zhang, Y., Lin, W., Mo, J. and Jin, C. (2021) 'Combination of Ablation and Immunotherapy for Hepatocellular Carcinoma: Where We Are and Where to Go', *Frontiers in Immunology,* 12.
Wang, Q., Griffin, H., Southern, S., Jackson, D., Martin, A., McIntosh, P., Davy, C., Masterson, P. J., Walker, P. A., Laskey, P., Omary, M. B. and Doorbar, J. (2004) 'Functional analysis of the human papillomavirus type 16 E1=E4 protein provides a mechanism for in vivo and in vitro keratin filament reorganization', *Journal of virology,* 78(2).
Wang, X., Liu, H., Ge, H., Ajiro, M., Sharma, N. R., Meyers, C., Morozov, P., Tuschl, T., Klar, A., Court, D. and Zheng, Z.-M. (2017) 'Viral DNA Replication Orientation and hnRNPs Regulate Transcription of the Human Papillomavirus 18 Late Promoter', *mBio,* 8(3).
Wang, Y., Guan, J., Wang, H., Wang, Y., Leeper, D. and Iliakis, G. (2001) 'Regulation of DNA replication after heat shock by replication protein a-nucleolin interactions', *The Journal of biological chemistry,* 276(23).
Wasson, C. W., Morgan, E. L., Müller, M., Ross, R. L., Hartley, M., Roberts, S. and Macdonald, A. (2017) 'Human papillomavirus type 18 E5 oncogene supports cell cycle progression and impairs epithelial differentiation by modulating growth factor receptor signalling during the virus life cycle', *Oncotarget,* 8(61).
Wechsler, E. I., Wang, Q., Roberts, I., Pagliarulo, E., Jackson, D., Untersperger, C., Coleman, N., Griffin, H. and Doorbar, J. (2012) 'Reconstruction of Human Papillomavirus Type 16-Mediated Early-Stage Neoplasia Implicates E6/E7 Deregulation and the Loss of Contact Inhibition in Neoplastic Progression'.
Wei-Chun, K., Yee-Fan, L., Yi-Chang, C., Ning, C., Yu-Sen, H., Yao-Hui, T., Jang-Ming, L., Hsao-Hsun, H., Jin-Shing, C. and Yeun-Chung, C. (2016) 'CT-guided percutaneous microwave ablation of pulmonary malignant tumors', *Journal of Thoracic Disease,* 8(Suppl 9).

Weintraub, S. J., Prater, C. A. and Dean, D. C. (1992) 'Retinoblastoma protein switches the E2F site from positive to negative element', *Nature,* 358(6383), pp. 259-261.
Westrich, J. A., Warren, C. J. and Pyeon, D. (2017) 'Evasion of Host Immune Defenses by Human Papillomavirus', *Virus research,* 231.
Whitney, J., Carswell, W. and Rylander, N. (2013) 'Arrhenius parameter determination as a function of heating method and cellular microenvironment based on spatial cell viability analysis', *International Journal of Hyperthermia*.
WHO 2020. Global strategy to accelerate the elimination of cervical cancer as a public health problem. https://www.who.int/publications/i/item/9789240014107.
WHO 2024. Cervical cancer. https://www.who.int/news-room/fact-sheets/detail/cervical-cancer.
Woodhall, S., Ramsey, T., Cai, C., Crouch, S., Jit, M., Birks, Y., Edmunds, W. J., Newton, R. and Lacey, C. J. N. (2008) 'Estimation of the impact of genital warts on health-related quality of life', *Sexually Transmitted Infections,* 84(3).
Wust, P., Hildebrandt, B., Sreenivasa, G., Rau, B., Gellermann, J., Riess, H., Felix, R. and Schlag, P. M. (2002) 'Hyperthermia in combined treatment of cancer', *The Lancet. Oncology,* 3(8).
Xu, X., Han, Z., Ruan, Y., Liu, M., Cao, G., Li, C. and Li, F. (2021) 'HPV16-LINC00393 Integration Alters Local 3D Genome Architecture in Cervical Cancer Cells', *Frontiers in cellular and infection microbiology,* 11.
Yang, K., Huang, C., Chi, M., Chiang, H., Wang, Y., Hsia, C., Andocs, G., Wang, H. and Chi, K. (2016) 'In vitro comparison of conventional hyperthermia and modulated electro-hyperthermia', *Oncotarget,* 7(51).
Yang, S.-C., Lin, H.-C., Liu, T.-M., Lu, J.-T., Hung, W.-T., Huang, Y.-R., Tsai, Y.-C., Kao, C.-L., Chen, S.-Y. and Sun, C.-K. (2015) 'Efficient Structure Resonance Energy Transfer from Microwaves to Confined Acoustic Vibrations in Viruses', *Scientific Reports,* 5(1), pp. 1-10.
Yang, Y., Zhang, L., Zhang, Y., Huo, W., Qi, R., Guo, H., Li, X., Wu, X., Bai, F., Liu, K., Qiao, Y., Piguet, V., Croitoru, D., Chen, H., D. and Gao, X., H. (2021) 'Local Hyperthermia at 44°C Is Effective in Clearing Cervical High-Risk Human Papillomaviruses: A Proof-of-Concept, Randomized Controlled Clinical Trial', *Clinical infectious diseases : an official publication of the Infectious Diseases Society of America,* 73(9).
Yonezawa, S. and Bono, H. (2023) 'Meta-Analysis of Heat-Stressed Transcriptomes Using the Public Gene Expression Database from Human and Mouse Samples', *International journal of molecular sciences,* 24(17).
You, J., Croyle, J. L., Nishimura, A., Ozato, K. and Howley, P. M. (2004) 'Interaction of the Bovine Papillomavirus E2 Protein with Brd4 Tethers the Viral DNA to Host Mitotic Chromosomes', *Cell,* 117(3).
Youssefian, L., Vahidnezhad, H., Mahmoudi, H., Saeidian, A. H., Daneshpazhooh, M., Hesari, K. K., Zeinali, S., de Jong, S. J., Orth, G., Blanchet-Bardot, C., Jouanguy, E., Casanova, J. and Uitto, J. (2019) 'Epidermodysplasia Verruciformis: Genetic Heterogeneity and EVER1 and EVER2 Mutations Revealed by Genome-Wide Analysis', *The Journal of investigative dermatology,* 139(1).
Yu, L., Majerciak, V. and Zheng, Z.-M. (2022) 'HPV16 and HPV18 Genome Structure, Expression, and Post-Transcriptional Regulation', *International Journal of Molecular Sciences,* 23(9), pp. 4943.
Yu, M., Pan, H., Che, N., Li, L., Wang, C., Wang, Y., Ma, G., Qian, M., Liu, J., Zheng, M., Xie, H., Ling, L., Zhao, Y., Guan, X., Ding, Q., Zhou, W., Wang, S., Yu, M., Pan, H., ... and Wang, S. (2020) 'Microwave ablation of primary breast cancer inhibits metastatic progression in model mice via activation of natural killer cells', *Cellular & Molecular Immunology 2020 18:9,* 18(9).
Zanna, M., Yasmin, A., Omar, A., Arshad, S., Mariatulqabtiah, A., Nur-Fazila, S. and Mahiza, M. (2021) 'Review of Dendritic Cells, Their Role in Clinical Immunology, and Distribution in Various Animal Species', *International journal of molecular sciences,* 22(15).
Zhang, B., Li, P., Wang, E., Brahmi, Z., Dunn, K. W., Blum, J. S. and Roman, A. (2003) 'The E5 protein of human papillomavirus type 16 perturbs MHC class II antigen maturation in human foreskin keratinocytes treated with interferon-gamma', *Virology,* 310(1).
Zheng, H., Benjamin, I. J., Basu, S. and Li, Z. (2003) 'Heat shock factor 1-independent activation of dendritic cells by heat shock: implication for the uncoupling of heat-mediated immunoregulation from the heat shock response', *European Journal of Immunology,* 33(6).

Zhou, C., Tuong, Z. K. and Frazer, I. H. (2019) 'Papillomavirus Immune Evasion Strategies Target the Infected Cell and the Local Immune System', *Frontiers in Oncology,* 9.
Zhou, J., Doorbar, D., Sun, X. Y., Crawford, L. V., McLean, C. S. and Frazer, I. H. (1991) 'Identification of the nuclear localization signal of human papillomavirus type 16 L1 protein', *Virology,* 185(2).
Zhou, W., Jiang, Y., Chen, L., Ling, L., Liang, M., Pan, H., Wang, S., Ding, Q., Liu, X. and Wang, S. (2014) 'Image and pathological changes after microwave ablation of breast cancer: a pilot study', *European journal of radiology,* 83(10).
Zhou, W., Yu, M., Pan, H., Qiu, W., Wang, H., Qian, M., Che, N., Zhang, K., Mao, X., Li, L., Wang, R., Xie, H., Ling, L., Zhao, Y., Liu, X., Wang, C., Ding, Q. and Wang, S. (2021) 'Microwave ablation induces Th1-type immune response with activation of ICOS pathway in early-stage breast cancer', *Journal for ImmunoTherapy of Cancer,* 9(4).
Zhou, W., Zha, X., Liu, X., Ding, Q., Chen, L., Ni, Y., Zhang, Y., Xu, Y., Chen, L. and Wang, S. (2012) 'US-guided percutaneous microwave coagulation of small breast cancers: a clinical study', *Radiology,* 263(2).
Zhou, Y., Zhou, B., Pache, L., Chang, M., Khodabakhshi, A., Tanaseichuk, O., Benner, C. and Chanda, S. (2019) 'Metascape provides a biologist-oriented resource for the analysis of systems-level datasets', *Nature communications,* 10(1).
Zobel, T., Iftner, T. and Stubenrauch, F. (2003) 'The Papillomavirus E8ΛE2C Protein Represses DNA Replication from Extrachromosomal Origins', *Molecular and Cellular Biology,* 23(22).
Zou, J., Guo, Y., Guettouche, T., Smith, D. F. and Voellmy, R. (1998) 'Repression of Heat Shock Transcription Factor HSF1 Activation by HSP90 (HSP90 Complex) that Forms a Stress-Sensitive Complex with HSF1', *Cell,* 94(4).

Appendix

Primer efficiencies for RT-qPCR

To calculate the primer efficiencies for any unpublished primer probe sets (HSP70, IL-1β, TNF-α and TGT), six ten-fold dilution series of cDNA were run in triplicate by RT-qPCR using the primer-probe sets. A simple linear regression was carried out on the resulting C_T values and log (Dilution factors). The slope of the line was then used to calculate the qPCR Efficiency, using the ThermoFisher online qPCR Efficiency Calculator. All efficiencies were within 90 – 110% and considered acceptable. Work performed by Andrew Stevenson.

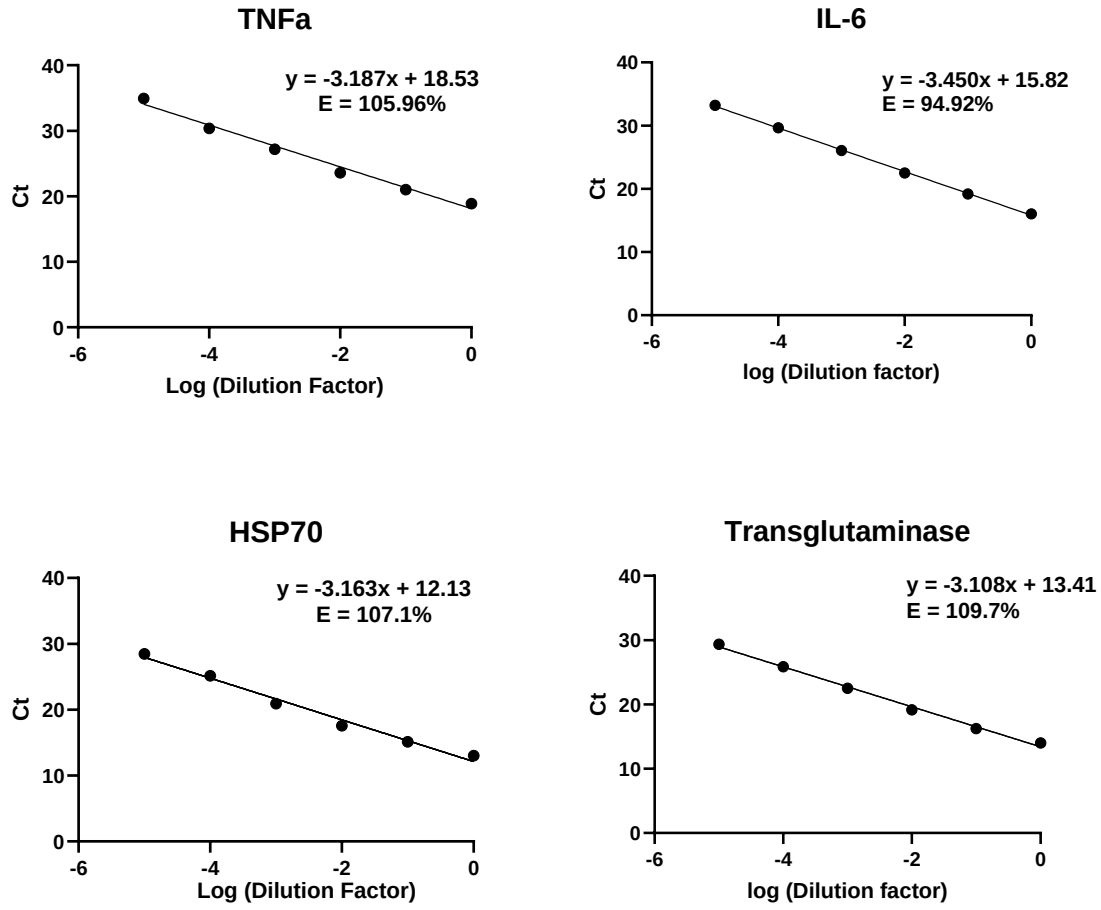

Supplementary Figure 1: Primer efficiencies for RT-qPCR. A cDNA sample was serially diluted (using 10-fold dilutions) and run by RT-qPCR using primer-probe sets for TNF-α, IL-6, HSP70 and Transglutaminase. Samples were run in triplicate and a semi-log plot shows the resulting C_T value against the dilution factor. A simple linear regression was used to calculate the slope of the line and this was used to estimate the efficiency of the reaction (E) using the ThermoFisher online qPCR Efficiency Calculator.